

**Interannual and seasonal climatic variability  
recorded by reef corals, Plio/Pleistocene (Florida)  
and Mio/Pliocene (Dominican Republic)**

Von der Fakultät für Physik und Geowissenschaften  
der Universität Leipzig  
genehmigte

D I S S E R T A T I O N

zur Erlangung des akademischen Grades

Doktor der Naturwissenschaften

Dr. rer. nat.

vorgelegt

von Diplom-Geologe Aron Böcker

geboren am 12. September 1983 in Jena

Gutachter: Prof. Dr. Thomas Brachert  
Prof. Dr. Adrian Immenhauser

Tag der Verleihung: 16.04.2014

**Bibliographische Beschreibung:**

Böcker, Aron

*Interannual and seasonal climatic variability recorded by reef corals, Plio/Pleistocene (Florida) and Mio/Pliocene (Dominican Republic)*

Universität Leipzig, Dissertation

141 S., 182 Lit., 65 Abb., 4 Tab., 6 Anlagen

## Referat:

In this study reef corals from two Caribbean and adjacent regions in different periods were investigated. Sclerochronological records of corals from well preserved Miocene to Pleistocene reefs were used to document potential changes in seasonal and interannual climate associated with CAS uplift and closure. In southern Florida the Plio/Pleistocene Caloosahatchee Formation is cropping out. During the deposition of this stacked shallow marine sediments at the Plio/Pleistocene Florida carbonate platform, a rich coral fauna existed. Corals from the Caloosahatchee Formation were investigated herein, regarding to reveal high resolution (bimonthly) climatic archives in their skeletons. The second region investigated herein is the Cibao Valley in the Dominican Republic, where sediments of the Neogene Yaque Group are outcropping. Corals from the Late Miocene Cercado Formation and the Mio/Pliocene Gurabo Formation (both upper part of the Yaque Group) are discussed here. Both formations are mixed carbonate-siliciclastic deposits of the prograding inner-shelf and contain a well preserved faunal record. Sclerochronological methods are used to identify seasonal and interannual climatic variability. Especially radiography, stable isotope analysis and laser ablation measurements (LA-ICP-MS) were used and discussed with a special focus on the pristine preservation of the analysed coralline material.

# Contents

<b>1</b>	<b>Introduction</b>	<b>8</b>
1.1	Coral Growth . . . . .	8
1.2	Coral Calcification . . . . .	9
1.3	Isotopic Disequilibrium . . . . .	11
1.4	Paleoceanography . . . . .	15
1.4.1	Florida . . . . .	15
1.4.2	Dominican Republic . . . . .	16
1.5	Climatic setting of the study area . . . . .	17
1.5.1	Overview about the global climatic features (Ocean gateways, El Nino Southern Oscillation, AMO, NAO) . . . . .	17
1.5.2	Climatic setting of Florida . . . . .	21
1.5.3	Climatic setting of the Dominican Republic . . . . .	23
1.6	Geologic setting . . . . .	24
1.6.1	Geologic setting of southern Florida . . . . .	24
1.6.2	Geologic setting of the Cibao Valley . . . . .	26
<b>2</b>	<b>Materials and Methods and Analytical Procedures</b>	<b>32</b>
2.1	Collection of Corals in the Field . . . . .	32
2.1.1	Outcrops Florida . . . . .	32
2.1.2	Outcrops Dominican Republic . . . . .	34
2.2	Diagenesis . . . . .	38
2.3	Technical sample preparation for geochemical analyses . . . . .	38
2.4	X-ray diffraction (XRD) . . . . .	38
2.5	Scanning Electron Microscopy (SEM) . . . . .	39
2.6	Microsampling for stable isotope measurements . . . . .	39
2.7	Oxygen and carbon isotope measurements . . . . .	40
2.8	Coral densitometry . . . . .	40
2.9	Resampling, rescaling and splicing of transects . . . . .	41
2.10	Laser ablation ICP mass spectrometry . . . . .	42
2.11	Spectral Analyses . . . . .	43
<b>3</b>	<b>Results</b>	<b>44</b>
3.1	452K1 <i>Solenastrea</i> Hennessy Airport Quarry, DeSoto, Florida . . . . .	44
3.1.1	Preservation . . . . .	44
3.1.2	Oxygen and Carbon Stable Isotope Composition . . . . .	46
3.1.3	Main and Trace Element Composition . . . . .	46
3.1.4	X-radiography/Coral densitometry . . . . .	52
3.2	452K14 <i>Solenastrea</i> Hennessy Airport Quarry, DeSoto, Florida . . . . .	54
3.2.1	Preservation . . . . .	54
3.2.2	X-radiography/Coral densitometry . . . . .	54
3.3	509A <i>Solenastrea</i> from an abandoned pit, Florida . . . . .	55
3.3.1	Preservation . . . . .	55
3.3.2	Oxygen and Carbon Stable Isotope Composition . . . . .	57
3.3.3	X-radiography/Coral densitometry . . . . .	57
3.4	455C <i>Montastrea</i> Dominican Republic . . . . .	58
3.4.1	Preservation . . . . .	59
3.4.2	Oxygen and Carbon Stable Isotope Composition . . . . .	61
3.4.3	X-radiography/Coral densitometry . . . . .	62
3.5	464C <i>Stephanocoenia</i> Dominican Republic . . . . .	63

3.5.1	Preservation . . . . .	63
3.5.2	Oxygen and Carbon Stable Isotope Composition . . . . .	65
3.5.3	Main and Trace Element Composition . . . . .	66
3.5.4	X-radiography/Coral densitometry . . . . .	68
3.6	X-radiography of other corals . . . . .	69
3.6.1	Plio/Pleistocene Florida . . . . .	69
3.6.2	Miocene Cercado Formation and Mio/Pliocene Gurabo Formation, Dominican Republic . . . . .	71
<b>4</b>	<b>Discussion</b>	<b>78</b>
4.1	Florida . . . . .	78
4.1.1	Outcrop 452 . . . . .	78
4.1.2	Outcrop 509 . . . . .	84
4.1.3	Skeletal growth parameters of Plio/Pleistocene Corals from Florida .	89
4.2	Dominican Republic . . . . .	91
4.2.1	Outcrop 455 . . . . .	91
4.2.2	Outcrop 464 . . . . .	92
4.2.3	Skeletal growth parameters of all Mio/Pliocene Corals from Domini- can Republic . . . . .	96
<b>5</b>	<b>Conclusion</b>	<b>97</b>
5.1	Growth rates . . . . .	97
5.2	Proxies Florida, 452 and 509 . . . . .	98
5.3	Proxies Dominican Republic, 455 and 464 (and 503) . . . . .	98
	<b>References</b>	<b>101</b>

## List of Figures

1	Calcification rate . . . . .	10
2	HDB-Formation after the Worum-Model . . . . .	11
3	Isotopic composition of various groups of calcareous organisms . . . . .	12
4	Temperature dependency of oxygen isotope fractionation . . . . .	13
5	Kinetic effect in corals . . . . .	14
6	Surface circulation features in the North Atlantic . . . . .	15
7	Caribbean circulation patterns today and before the closure of CAS . . . . .	16
8	Caribbean SST . . . . .	18
9	Caribbean SSS . . . . .	19
10	AMO index . . . . .	20
11	NAO pattern . . . . .	21
12	Climatological data for Tampa, Florida from 1961-1990 . . . . .	22
13	Climatological data for Santiago, Dominican Republic from 1961-1990 . . . . .	24
14	Generalized stratigraphic column for Pliocene and Pleistocene of the Everglades . . . . .	25
15	Florida Peninsula during the early Calabrian Pleistocene . . . . .	26
16	Location of the island of Hispaniola and Cibao Valley in the northern Dominican Republic . . . . .	27
17	Relationship between Neogene sections on Rio Cana and Rio Gurabo . . . . .	28
18	Summary of the Stratigraphy of the Outcrops in the Cibao Valley . . . . .	29
19	cross section of the sediment wedge along the southern flank of Cibao Basin . . . . .	30
20	Stratigraphic positions of the samples from the Cibao Valley . . . . .	31
21	Overview of sample locations in southern Florida, USA . . . . .	32
22	Overview of sample locations at the island of Hispaniola . . . . .	33
23	Cibao Valley and Rio Yaque del Norte with its tributaries . . . . .	35
24	Sample locations in the tributary rivers Rio Gurabo, Arroyo Bellaco and Rio Cana/Cañada de Zamba . . . . .	36
25	XRD standard measurements . . . . .	39
26	Calibration of the X-Ray system for coral densitometry . . . . .	41
27	Splicing of transects . . . . .	42
28	Scanning electron microscopy images from <i>Solenastrea</i> 452K1 . . . . .	45
29	Stable isotope data <i>Solenastrea</i> 452K1 . . . . .	46
30	Positions of sampling transects in different slabs of <i>Solenastrea</i> 452K1 . . . . .	48
31	Comparison of selected element/calcium-ratios and stable isotope values in <i>Solenastrea</i> 452K1 . . . . .	50
32	REE <i>Solenastrea</i> 452K1 . . . . .	51
33	Line-measurement in <i>Solenastrea</i> 452K1 . . . . .	52
34	X-radiograph and visible light image of <i>Solenastrea</i> 452K1 . . . . .	53
35	Visible light, X-ray and density in <i>Solenastrea</i> 452K14 . . . . .	54
36	Scanning electron microscopy images from <i>Solenastrea</i> 509A . . . . .	56
37	Cross Correlation of $\delta^{18}O$ and $\delta^{13}C$ in <i>Solenastrea</i> 509A S1 . . . . .	57
38	Visible light and X-radiograph image of 509A S1 <i>Solenastrea</i> coral slab. . . . .	58
39	Scanning electron microscopy images from <i>Montastrea</i> 455C S2 . . . . .	60
40	Visual light and X-radiograph of <i>Montastrea</i> 455C S2 . . . . .	61
41	Stable isotope data and skeletal density <i>Montastrea</i> 455C Transect A . . . . .	62
42	Stable isotope data and skeletal density <i>Montastrea</i> 455C Transect C . . . . .	62
43	Scanning electron microscopy images of <i>Stephanocoenia</i> 464C . . . . .	64
44	Cross-correlation of $\delta^{18}O$ and $\delta^{13}C$ for <i>Stephanocoenia</i> 464C S2 . . . . .	65
45	Visual light, X-radiograph and measured parameter for <i>Stephanocoenia</i> 464C S2 . . . . .	66

46	Comparison of selected element/calcium-ratios and stable isotope values in <i>Stephanocoenia</i> 464C . . . . .	67
47	REE <i>Stephanocoenia</i> . . . . .	68
48	Relationship between coral density and thickness of all X-radiographed corals	69
49	Extension rate and density for all <i>Solenastrea</i> Florida . . . . .	70
50	Density and growth rates of corals from the Cibao Valley, Dominican Republic	72
51	X-radiographs of coral slabs from Plio/Pleistocene of South Florida . . . . .	74
52	X-radiographs of coral slabs from Gurabo Formation, Dominican Republic .	75
53	X-radiographs of coral slabs from Cercado Formation, Dominican Republic	76
54	X-radiographs of coral slabs from Gurabo Formation and from Holocene Lago Enriquillo, Dominican Republic . . . . .	77
55	Classification of HDBs (X-ray) . . . . .	79
56	Classification of HDBs ( $\delta^{18}O$ ) . . . . .	79
57	SST changes in the younger Neogene of Florida . . . . .	81
58	Spectral analyses <i>Solenastrea</i> 452K1 . . . . .	83
59	Correlation of X-radiograph and stable isotope data in 509A . . . . .	85
60	Isotopic ranges . . . . .	87
61	Spectral analyses <i>Solenastrea</i> 509A . . . . .	89
62	Calcification Rate and Growth Rate all <i>Solenastrea</i> Florida . . . . .	90
63	HDB formation in <i>Stephanocoenia</i> 464C . . . . .	94
64	<i>Stephanocoenia</i> 464C HDBs and geochemical data . . . . .	96
65	Spectral analyses <i>Stephanocoenia</i> 464C . . . . .	97

## List of Tables

2	Correlation coefficients for selected Metall/Calcium ratios and stable isotopes for <i>Stephanocoenia</i> 464C . . . . .	68
3	Mean skeletal extension rates, skeletal densities and calcification rates for corals from Florida . . . . .	70
4	Mean skeletal extension rates, skeletal densities and calcification rates for corals from the Dominican Republic . . . . .	72
5	Theoretical damping of SST seasonality with low sampling frequency . . . .	86

## Acronyms

$\rho$	Density
KV	Kilovolt
SSS	Sea Surface Salinity
SST	Sea Surface Temperature
BEI	Backscatter Electron Image
SLP	Sea Level Pressure
$T_{opt}$	Optimal Temperature for Coral Growth
$T_{min}$	Minimum Temperature for Coral Growth
$T_{max}$	Maximum Temperature for Coral Growth
CAS	Central American Seaway
LDB	Low Density Band
EDX	Energy Dispersive X-ray Spectroscopy
SEM	Scanning Electron Microscopy
HDB	High Density Band
XRD	X-Ray diffraction
NAO	North Atlantic Oscillation
AWP	Atlantic Warm Pool
COC	Center Of Calcification
GBR	Great Barrier Reef, Australia
AMO	Atlantic Multidecadal Oscillation
ITCZ	Intertropical Convergence Zone
USVI	United States Virgin Islands
ENSO	El Niño Southern Oscillation
dHDB	double High Density Band



# 1 Introduction

## 1.1 Coral Growth

Many studies about carbonate secreting organisms exist and show the importance of scientific findings in this field. This is especially the case since benthic carbonate producing organisms play an essential role in the global budget of  $CO_3^{2-}$  and  $CO_2$  and shallow-water reefs seem to be the protagonists in this process (*Dullo, 2005*). Reef corals produce, as all skeletal carbonate producers, biotically controlled precipitates whereby the organism determines the setting (location, beginning, end, composition, crystallography) of the process (*Schlager, 2003*). Within the phylum Cnidaria both the class Hydrozoa and the class Anthozoa have members that build up tropical coral reefs (*Johnston, 1980*). In this work only anthozoan corals are studied, so-called “stony corals” in the subclass Zoantharia (Hexacorallia) which are members of the order Scleractinia (Madreporaria) (*Wells, 1956*). All Scleractinia have massive, compact exoskeletons which consist of aragonitic calcium carbonate and are divided further in the hermatypic (reef-building) corals and ahermatypic (non-reef-building) corals (*Johnston, 1980*). All hermatypic corals have incorporated in their endodermal tissue endosymbiotic, unicellular, dinoflagellate algae (called zooxanthellae) and are capable of the fastest rates of skeletogenesis – necessary for the formation and maintenance of reef structures (*Johnston, 1980*). Reef corals only occur in the belt of tropical carbonate sediments that currently surrounds the globe between 30°N and 30°S (*Schlager, 2003*). A tropical climate is needed because the mean temperature of the coldest month in the year should not fall below 18-19 °C and not exceed 30-32 °C (*Yonge, 1973; Jokiel and Coles, 1977; Johnston, 1980*). Ideal conditions for reef building corals is a sea surface temperature in the between 25-29 °C with a normal salinity, depending on the species (*Weber and Woodhead, 1970; Druffel, 1997*). Further the water should be clear and the depth less than 50 m (*Weber and Woodhead, 1970*). As *Johnston (1980)* figures out, “at their interface with the ocean, coral reefs are extremely dynamic structures, experiencing a delicate balance between biological and chemical mineral accretion on the one hand, and biological, chemical and physical erosional processes on the other” (*Johnston, 1980*). Corals are, as all Coelenterates, primitive animals characterized by a body wall consisting of two layers of cells: an outer ectoderm and an inner endoderm (*Weber and Woodhead, 1970*). Between those layers is situated the mesoglea, a gelatinous matrix primarily structureless of varying thickness (*Weber and Woodhead, 1970*). The carbonate skeleton secreted by the corals tissues (coenenchyme) is either aragonitic or calcitic in its crystallography (*Weber and Woodhead, 1970*). All of the specimens analyzed in this study precipitate aragonitic skeletons consisting of the coralline basic unit sclerodermites, which are acicular crystals (trabeculae) arranged radial around “centers of calcification” (COC) (*Weber and Woodhead, 1970*). Since reef corals live in symbiosis with zooxanthellae (“z-corals”), which are photo-autotrophic organisms that generate organic matter from dissolved substances and sunlight (*Schlager, 2003*), they have to live in light saturated shallow water. Within endodermal cells, zooxanthellae are efficient primary producers which provide oxygen and fix carbon (*Johnston, 1980*). Corals occur in different growth forms, such as ramose, encrusting, foliose and massive (*Swart, 1983*). Reef corals build up a continuous skeleton (*Knutson et al., 1972*), which consists of distinct growth bands of alternate dense and less dense aragonite as an annual phenomenon (*Knutson et al., 1972; Dodge et al., 1974; Highsmith, 1979; Swart, 1983*). Although a coral skeleton is considered to be an exoskeleton, it is not in direct contact with seawater environment (*Weber and Woodhead, 1970*). This skeleton is not precipitated in isotopic equilibrium with seawater, the living coenosarc is an effective barrier to equilibrium exchange between skeleton and seawater (*Epstein and Mayeda, 1953; Weber and Woodhead, 1970*). The stable isotope

ratios are controlled both vital and inorganic environmental factors (*Weber and Woodhead, 1970; Swart, 1983*) and elect reef corals as miscellaneous climatic archives.

## 1.2 Coral Calcification

Massive corals secrete a skeleton composed of sclerodermite. The sclerodermites are the basic unit of coral skeletal microstructure and comprise centers of calcification from which radiate bundles of acicular aragonite crystals (*Wells, 1956*). The coral skeleton consists of distinct growth bands of alternate dense and less dense aragonite which can be visualized with X-radiography (e.g. (*Knutson et al., 1972; Dodge et al., 1974; Highsmith, 1979; Swart, 1983; Lough and Barnes, 1990; Worum et al., 2007; Lough and Cooper, 2011*)). This density banding is observable in all here published corals and further are termed the areas of high skeletal density “high density bands” (HDBs) and areas of low skeletal density “low density bands” (LDBs). Beside a changing density in space and time also the rate of skeletal extension (growth rate) is changing in the most massive grown corals. As *Dodge and Brass (1984)* mention, HDBs have a less extension than LDBs but a greater density. These and other studies (*Hudson et al., 1976; Stearn et al., 1977*) conclude that “HDBs form over a very short period, their extension and calcification rates may be significantly higher than those of LDBs” (*Dodge and Brass, 1984*). *Barnes and Lough (1993)* carve out “reports of seasonality associated with sub-annual bands largely separate into those which conclude that dense bands are formed in summer, or periods of warmest water, and those which conclude that they are formed in winter”, so that a couple of one HDB and one LDB is supposed to be one year. Additionally, sub-annual HDBs (“stress bands”) can form in response to discrete environmental perturbations (*Hudson et al., 1976; Barnes and Lough, 1993*). It has been also shown, that the timing of high density band formation differs among taxa and regions (*Lough and Barnes, 1990*). Coral calcification is the product of the skeletal growth rate within a given time and the skeletal density in the same given time (Equation 1) (*Dodge and Brass, 1984*):

$$C\left[\frac{g}{cm^2 \times yr}\right] = G\left[\frac{cm}{yr}\right] \times \rho\left[\frac{g}{cm^3}\right] \quad (1)$$

Where C is the calcification rate, G the growth rate and  $\rho$  the skeletal density. If any two of the three parameters are known, the third can be calculated (*Dodge and Brass, 1984*). *Bosscher (1993)* found for *Montastrea annularis*, from Curacao, Netherlands Antilles an inverse relationship between extension rate and skeletal density. Calcification rates in experimental studies also seem to have higher values at optimum temperatures (Fig. 1) (*Carricart-Ganivet, 2004; Marshall and Clode, 2004; Worum et al., 2007*), even if it’s not fully understand how zooxanthellea enhance calcification or not (*Marshall, 1996*). Calcification rate of *Montastrea annularis* increases by  $0.57 g/cm^2/year$  for each  $1.0^\circ C$  increase in SST and the effect of lower temperatures is one limiting factor of the distribution of *Montastrea annularis* to the north (*Carricart-Ganivet, 2004*).

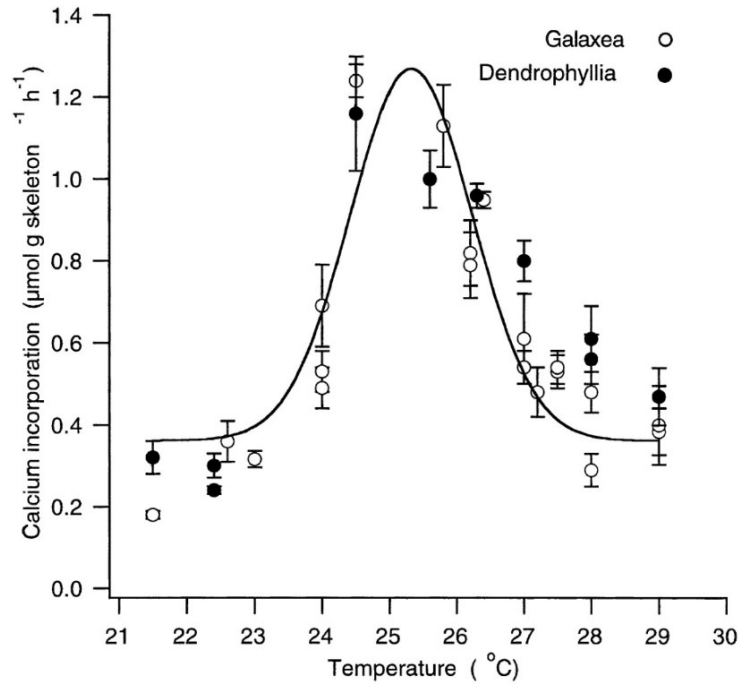


Figure 1: Calcification rate (y-axis) relative to temperature in *Galaxea fascicularis* and *Dendrophyllia* sp. with a Gaussian curve fitted to the *Galaxea* data. From *Marshall and Clode* (2004).

To determine how an increase in SST might affect annual density banding, *Worum et al.* (2007) invoked a simple SST increase where the mean-annual ocean temperature linearly increased by 2.5 °C over 20 yr (Fig. 2) (*Worum et al.*, 2007). The formation of the HDBs is considered to take place in the warmest months of the year (summer). With an increasing mean SST, the calcification rate reaches its maximum at an optimal temperature which is crossed twice a year, in spring and in autumn. Both, in summer and winter the SST is above or below calcification optimum temperature. Between these two extremes in temperature, an annual “HDB doublet” (dHDB) occurs in which two relatively narrow HDBs are formed (*Worum et al.*, 2007; *Brachert et al.*, 2013a). If the mean SST increases more, the calcification optimum temperature is crossed only in winter, so that the formation of the HDB takes place in the coldest months of the year (Fig. 2) (*Worum et al.*, 2007). This X-ray pattern suggested by *Worum et al.* (2007) is not easy to distinguish from the normal, annual formed couples of HDBs and LDBs and in some places  $\delta^{18}O$  values are needed to delimit one year from the next.

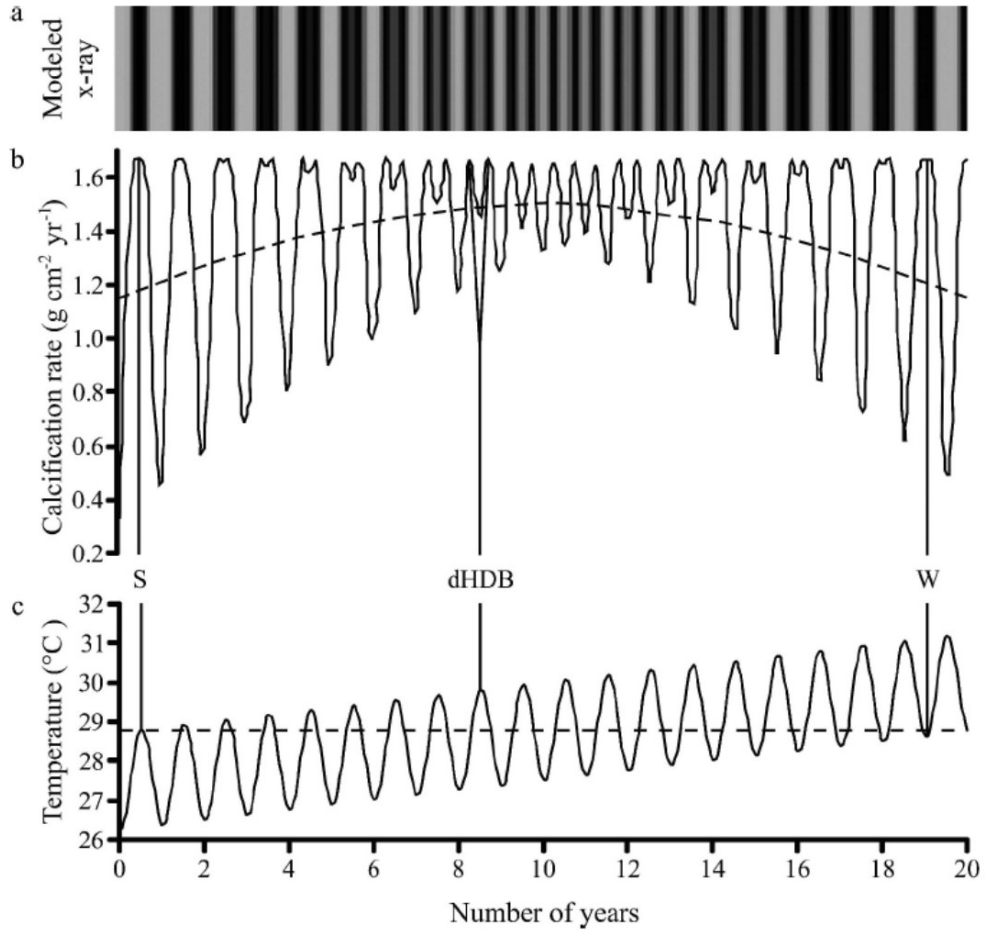
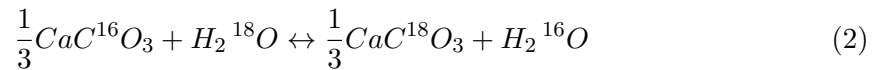


Figure 2: Modeled density banding pattern from *Worum et al. (2007)* in *Montastrea* for a SST increase. (a) Modeled X-ray of density banding pattern; W = HDB formation in winter, S = HDB formation in summer. Double HDBs when the optimal temperature for this species is crossed twice within one year. (b) Calculated calcification rate. (c) SST increase of 2.5 °C within 20 yrs. Dashed line is  $T_{opt}$  for *Montastrea* growing in the Mexican Caribbean. From *Worum et al. (2007)*

### 1.3 Isotopic Disequilibrium

In a normal, slowly precipitation of  $CaCO_3$  from a solution, thermodynamics dictate the partitioning of oxygen and carbon isotopes between the solution and the solid phase (*O'Neil et al., 1969*). In this case, the oxygen isotope exchange reaction for example can be (*O'Neil et al., 1969*):



while the fractionation factor is:

$$\alpha = \frac{\left(\frac{^{18}O}{^{16}O}\right)_{CaCO_3}}{\left(\frac{^{18}O}{^{16}O}\right)_{H_2O}} \quad (3)$$

Several experimental studies of oxygen fractionation between solids and water over wide temperature ranges showed that the fractionation factor over the range 0-500°C is represented by an equation of the form:

$$\ln \alpha = AT^{-2} + B \quad (4)$$

where A and B are constants, so that the fractionation is strictly proportional to  $T^{-2}$  (O'Neil *et al.*, 1969). Non-equilibrium isotope partitioning is often observed during biological calcification (Weber and Woodhead, 1970; McConnaughey, 1989a,b), such as coral growth. The heavy isotopes of oxygen and carbon are consistently depleted in the coral skeleton relative to equilibrium (Weber and Woodhead, 1970, 1972). This offset from equilibrium is constant within a given coral genus and termed isotopic "vital effect" (Weber and Woodhead, 1972). Both, hermatypic and ahermatypic corals precipitate their skeletons in isotopic disequilibrium with seawater, but hermatypic corals have a much more narrow range of values  $\delta^{18}O$  and  $\delta^{13}C$  than ahermatypic (Fig. 3) (Swart, 1983). This is indicating a connection between the activity of the zooxanthellae and the fractionation of the isotopes Swart (1983).

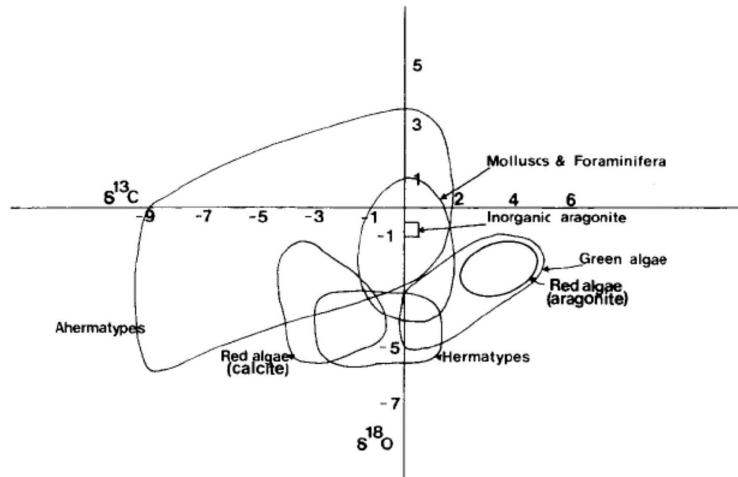
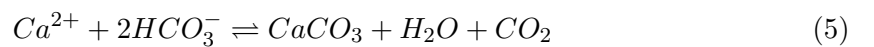


Figure 3: Isotopic composition of various groups of calcareous organisms. From (Swart, 1983)

As Swart (1983) figures out, several theories about the influence of the zooxanthellae on coral skeleton formation vary from the (1) removing of  $CO_2$  by the zooxanthellae, (2) photosynthates used for matrix formation, (3) providing of energy for the active transport of  $Ca^{2+}$  and  $HCO_3^-$  and (4) removing crystal poisons such as phosphate by the zooxanthellae. Undoubted is that zooxanthellae do photosynthesis and use  $CO_2$  for this. In the following equation for  $CaCO_3$  precipitation the equilibrium is shifted to the right and with this to the formation of  $CaCO_3$  (Swart, 1983):



Since  $CO_2$  is the active carbon species for the photosynthesis, it is liable to fractionation while being fixed. The fractionation accompanying this step is approximately 27 % (Swart, 1983).

If carbonates are precipitated slowly, the isotopic composition is governed by the temperature-dependent thermodynamic isotope fractionation factors (McCrea, 1950) and the isotopic composition of the fluid (Aharon, 1991). For paleoclimatic investigations the carbonate is the recorder of the ambient environment. “Isotope offsets” can be determined by comparing experimental equilibrium isotope fractionations with isotope determinations from reef skeletal material deposited over the temperature range of 20-30 °C (Fig. 4)(Aharon, 1991).

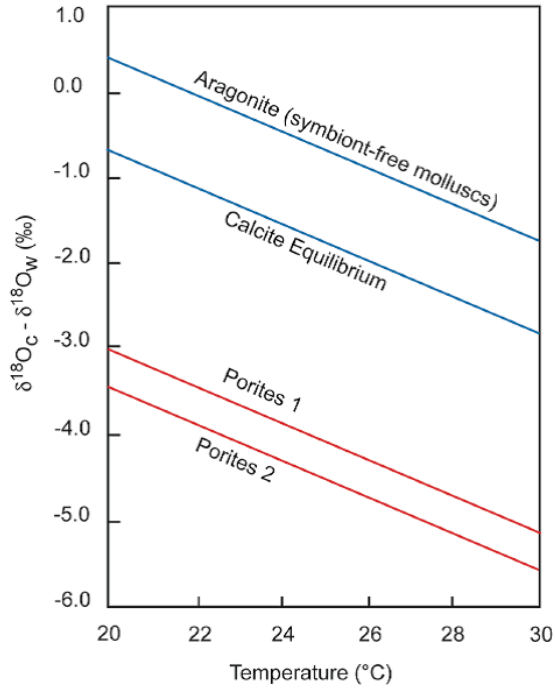


Figure 4: Temperature dependency of oxygen isotope fractionation over the temperature range from 20-30°C for selected biogenic aragonites and equilibrium calcite. Shown coral  $\delta^{18}O$  offsets occur between coral specimens from the same genus (*Porites*). From Hetzinger (2007) redrawn after Aharon (1991)

Isotopic disequilibria which lead to this offsets are divided into two patterns: the “kinetic” and the “metabolic” effect (McConnaughey, 1989a). Contemporaneous depletion of  $^{18}O$  and  $^{13}C$  isotopes is attributed to kinetic isotope effect and considered to be a result of a slower reaction kinetics for molecules with the heavy isotopes ( $^{18}O$  and  $^{13}C$ ) during important processes in biological calcification (McConnaughey, 1989a,b; Aharon, 1991). This effect is associated with rapid calcification and tends to be constant in the rapid growing parts of a coral skeleton (Fig. 5). It is related to the equilibrium isotope partitioning by the equation

$$\delta^{18}O_{coral} = \delta^{18}O_{equ} + \delta^{18}O_{offset} \quad (6)$$

where  $\delta^{18}O_{offset}$  is constant with respect to temperature for individual coral colonies and varies among coral taxa (Weber and Woodhead, 1972; Aharon, 1991). In carbonates which are showing mainly the kinetic pattern, a linear correlation between skeletal  $\delta^{18}O$  and  $\delta^{13}C$

is common (McConnaughey, 1989a). In different skeletal extension rates at one specimen, a bias in the environmental signal is possible (Hetzinger, 2007).

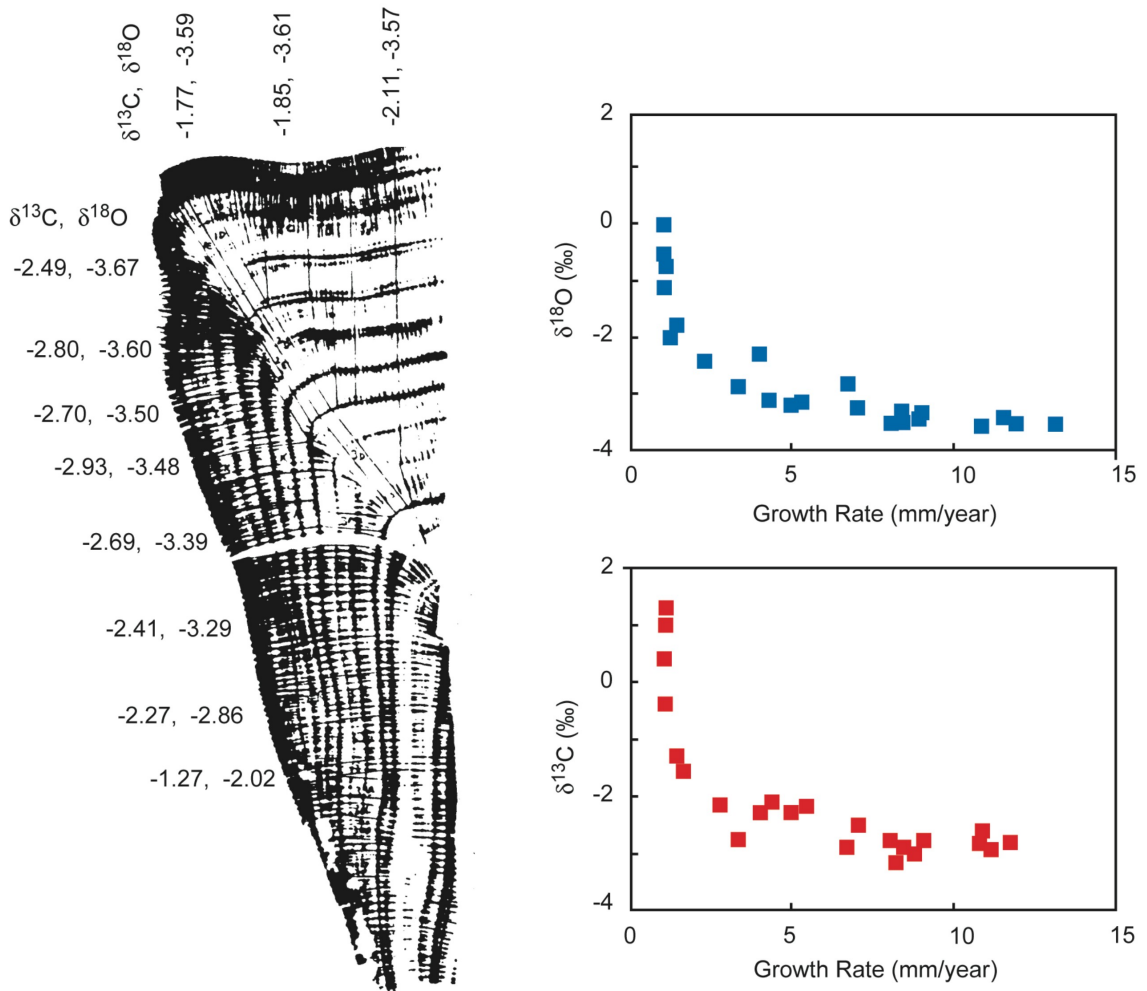


Figure 5: Left: X-radiography and skeletal isotopic composition of a portion of a horizontally sampled *Pavona clavus* coral head retrieved off Punta Pitt, San Cristobal Island (Galápagos). Each pair of numbers represents the carbon/oxygen isotopic ratio ( $\delta^{13}\text{C}$ ,  $\delta^{18}\text{O}$ ) for skeletal material deposited over the interval 1979-1982. The upper surface of the coral head received more sunshine than the lateral surfaces, hence grew faster, and was relatively depleted in  $^{18}\text{O}$ . Right: Correlations between skeletal  $\delta^{18}\text{O}$  (top) and  $\delta^{13}\text{C}$  (bottom) and skeletal extension (growth) rate for horizontally sampled *Pavona clavus* heads. From Hetzinger (2007) redrawn after McConnaughey (1989a)

The metabolic effect involves an additional positive or negative modulation of skeletal  $\delta^{13}\text{C}$ . This run away of the skeletal  $\delta^{13}\text{C}$  from the linear correlation to the skeletal  $\delta^{18}\text{O}$  reflects changes in the  $\delta^{13}\text{C}$  of dissolved inorganic carbon, caused mainly by photosynthesis (positive excursion in skeletal  $\delta^{13}\text{C}$ ) or respiration (negative excursion in skeletal  $\delta^{13}\text{C}$ ) (McConnaughey, 1989a). The skeletal  $\delta^{18}\text{O}$  is not directly affected by photosynthesis (McConnaughey, 1989a). However vital effects manipulate coral  $\delta^{18}\text{O}$  in different degrees, this offsets seem to be stable over time as long as the maximum growth axis within a coral colony is sampled and so a well calibrated oxygen isotope paleotemperature equation is available for corals (Epstein and Mayeda, 1953; McConnaughey, 1989a,b; Druffel, 1997; Gagan et al., 2000; Hetzinger, 2007). The slope of this equation 0.22 ‰ per 1 °C decrease in SST predicted by the temperature-dependent aragonite-water fractionation factor. This

slope is the same as that defined for the equilibrium precipitation of calcite (*Epstein and Mayeda, 1953; Weber and Woodhead, 1972; Druffel, 1997*).

## 1.4 Paleooceanography

### 1.4.1 Florida

The Peninsula of Florida is surrounded by the Gulf of Mexico in the west and the North Atlantic Ocean in the east. Therefore different oceanic currents influence the shelf of the Florida Platform. In the Gulf of Mexico the clockwise flowing Loop Current is variable in position. From the Yucatan Peninsula it can move 900 km to north and has a strong impact on the Florida Current (Fig. 6). After circulation clockwise in the Gulf of Mexico the Loop Current is moving in southern direction off the Florida shelf margin and partly there upon. South of Florida the Loop Current becomes together with the Antilles Current the Florida Current, which flows at the south and eastern margin of the Florida shelf from the Florida Straits to Cape Hatteras. The Florida Current has been shown to move in mean 30 Sv and is subject to both seasonal and interannual variability with a difference of up to 10 Sv (*Schott et al., 1988*).

In the Pliocene during warm stages the global sea level was around 20 m higher than today and shallow water covered large areas of the flat Florida peninsula (e.g. (*Cronin, 1991; Crowley, 1991; Petuch, 2003, 2007*)) (Fig. 7). A high diverse and abundant molluscan fauna of the Florida Platform during the middle Pliocene (3.5 – 2.5 Ma) suggest that the oceanic productivity was higher than in the Pleistocene and recent (*Allmon, 1993*). The cause of this enhanced productivity is still debated and there are two major hypothesis: (1) enhanced upwelling (*Jones and Allmon, 1995; Allmon et al., 1996*) or (2) input of

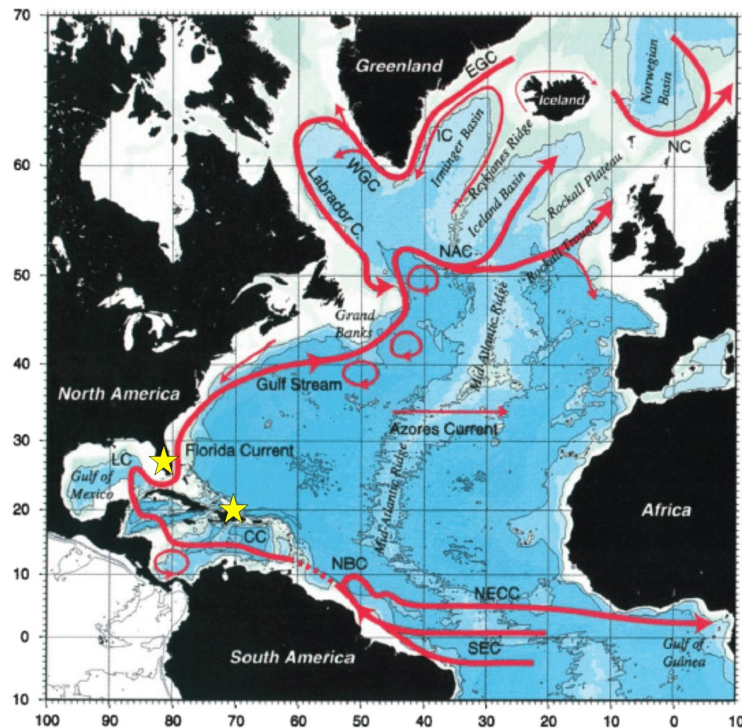


Figure 6: Recent most significant surface circulation features in the North Atlantic. Gulf of Mexico Loop Current( LC); Caribbean Current (CC); Irminger Current (IC), Norwegian Current (NC), East and West Greenland Currents (EGC and WGC). From *Fratantoni (2001)* with yellow stars marking the two regions observed here.



nutrient-rich freshwater (*Tao and Grossman, 2010*).

### 1.4.2 Dominican Republic

The modern Caribbean Sea is a semi-enclosed basin in the Atlantic west of Central America between North America and South America. It is divided by the Antilles Islands from the Atlantic Ocean. The main inflow of Atlantic water masses into the Caribbean Sea is through the Grenada, St. Vincent and St. Lucia passages in the southeast (*Wüst, 1963; Gordon, 1967*). This water masses then continues as the Caribbean Current and between the Yucatan peninsula and Jamaica entering the Gulf of Mexico where it becomes the Gulf Loop Current (Fig. 7)(*Fratantoni, 2001*). Today it is the source area of warm water masses flowing to the high latitudes, the trans-equatorial heat transfer to higher latitudes. Major oceanographic features changed in the geologic past and had several impacts on climate and the biosphere belonging to this regions. North of the Antilles Islands in the southern North Atlantic the Antilles Current flows westward. It is contributing to the Florida Current. Since the Neogene deposits in the Cibao Basin are shelf sediments many authors studied these and identified sequence boundaries (e.g. (*Vaughan et al., 1921; Saunders et al., 1986; Budd and Johnson, 1999; Klaus et al., 2011; McNeill et al., 2012*)). The sedimentary infill into the Cibao Basin was asymmetric because the majority was delivered by the Cordillera Central in the south. The Basin itself consisted of a broad shelf a long the northern margin of the Cordillera Central which was sloping northward to the (probably shallow marine or lowland and not yet uplifted) Cordillera Septentrional (*McNeill et al., 2012*). This environment provided coral growth despite of the high sediment influx (*Saunders et al., 1986; McNeill et al., 2012*). During the early Pliocene of the Cibao Basin in the Dominican Republic the annual mean SSTs increased to  $\sim 28-29^{\circ}\text{C}$  and the SSS also increased, as observable in the planctonic foraminifera distribution of the Cercado and Lower Gurabo Formation (*Steph et al., 2006; Lutz et al., 2008*). These changes around 4.8 Ma are most

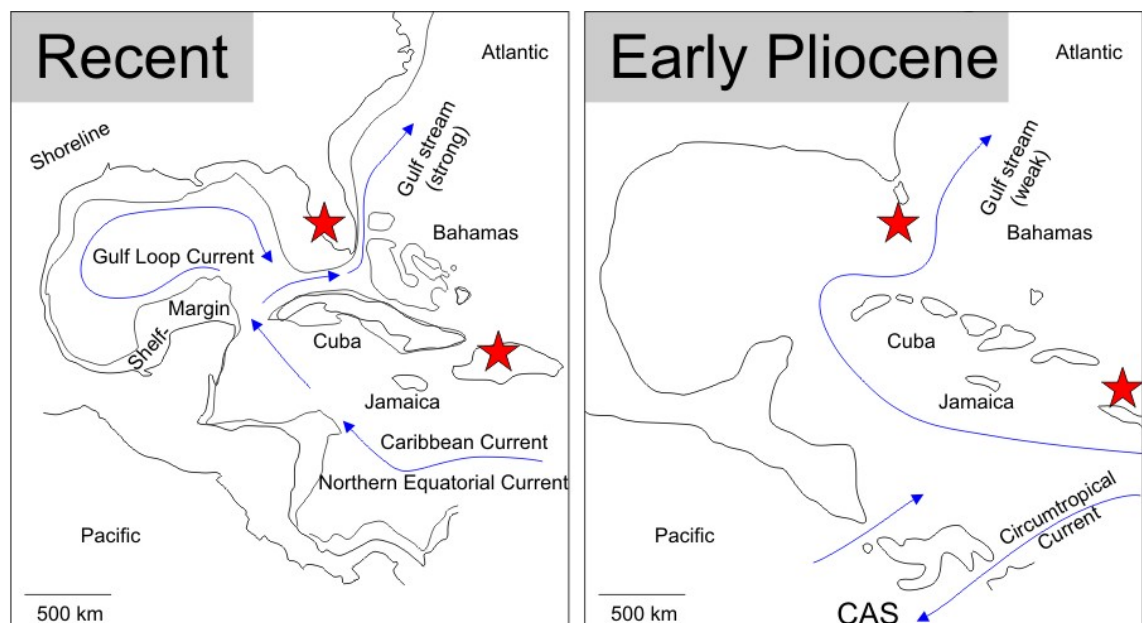


Figure 7: Caribbean circulation patterns today and before the closure of the Central American Seaway (CAS). The warm water from the Caribbean entered via the Circumtropical Current in the Early Pliocene the equatorial Pacific and not as recent the North Atlantic via a strong Gulf Stream. Red Stars show the sample areas of the corals in this study. Illustration redrawn after *Lutz et al. (2008)*

likely related to the major oceanographic event in the early Pliocene, the tectonic uplift of Central America which restricted the exchange of water masses between the Pacific and the Atlantic ocean via the Central American Seaway (CAS) (Fig. 7). This blocking of the flow of warm and saline waters into the Pacific led to an increase of SST and SSS in the Cibao Valley (*Lutz et al.*, 2008). The main questions of the interruption of the surface water exchange between the Caribbean Sea and the Pacific Ocean are still is there a causal relationship between the closure of the CAS and the onset of the Northern Hemispheric Glaciation (NHG) and also a precise timing for the final closure is still missing (*Duque-Caro*, 1990; *Haug and Tiedemann*, 1998; *Bartoli et al.*, 2005; *Lunt et al.*, 2008; *Montes et al.*, 2012). However, the closure of the CAS introduced more warm water masses via the Gulf Stream in the northern hemisphere (Fig. 7). The flow direction through the CAS may have changed from westward net transport before Late Miocene to an eastward upper ocean transport through the CAS after the strengthening of the formation of North Atlantic Deep Water during the late Miocene approaching modern values around 6 Ma (*Steph et al.*, 2006). In the early and middle Pliocene the rate of thermohaline overturn in the North Atlantic allowed a net eastward transport through the CAS (*Nof and Van Gorder*, 2003).

## 1.5 Climatic setting of the study area

### 1.5.1 Overview about the global climatic features (Ocean gateways, El Nino Southern Oscillation, AMO, NAO)

Since South America became attached to North America during the collision of the Caribbean and the South American plate around 3.5 million years ago the Isthmus of Panama formed and closed the Central American Seaway (CAS), major global changes in climate, ocean currents and biologic composition of both Americas happened (*Lutz et al.*, 2008) (Fig. 7). A great mixing between the Atlantic and Pacific Ocean was interrupted and the Circumtropical Current, which transported parts of the modern source of the Gulf Stream from the Atlantic into the Pacific, ebbed. In the Pliocene the Gulf Stream was not an important source of warm water in the northern latitudes and therefore the gradient of SST along the equatorial Pacific was quite lower than recently (*Steph et al.*, 2006; *Fedorov et al.*, 2006). The mean SST in the east was substantially higher than today but similar in the west. This condition of a large reduction in the east-west temperature gradient along the equator in the Pacific is called a permanent El Nino state (*Molnar and Cane*, 2002; *Fedorov et al.*, 2006). Since 3 Ma until today this gradient is intermittent and is reduced strongly during El Nino events. The mechanisms which control the regional SST (Fig. 8) in the tropical Atlantic are dominated by climate variabilities emanating from other oceans like the El Nino Southern Oscillation (ENSO) (*Giannini et al.*, 2000; *Hastenrath et al.*, 1984). Observed anomalously dry summers accompanied by lower sea level pressure (SLP) and higher SST in the equatorial Pacific are the unmistakable signature of an ongoing warm ENSO event (*Hastenrath et al.*, 1984). The tropical Atlantic was at the same time characterized by higher SLP and lower SST (*Giannini et al.*, 2000). SST variability in the Caribbean is linked mainly to sea level pressure variations by changing surface winds (*Giry et al.*, 2012). These surface winds affect also the Atlantic Warm Pool (AWP), a large body of water with temperature above 28.5 °C. It is modulated in seasonal, interannual and multidecadal timescales (*Wang and Enfield*, 2003; *Wang et al.*, 2006, 2007, 2008a,b). During the boreal summer, the AWP is maximal extended and effects summer climate of the western hemisphere. Strong influence on interannual and multidecadal modulations has the El Nino Southern Oscillation (ENSO) and the Atlantic Multidecadal Oscillation (AMO).

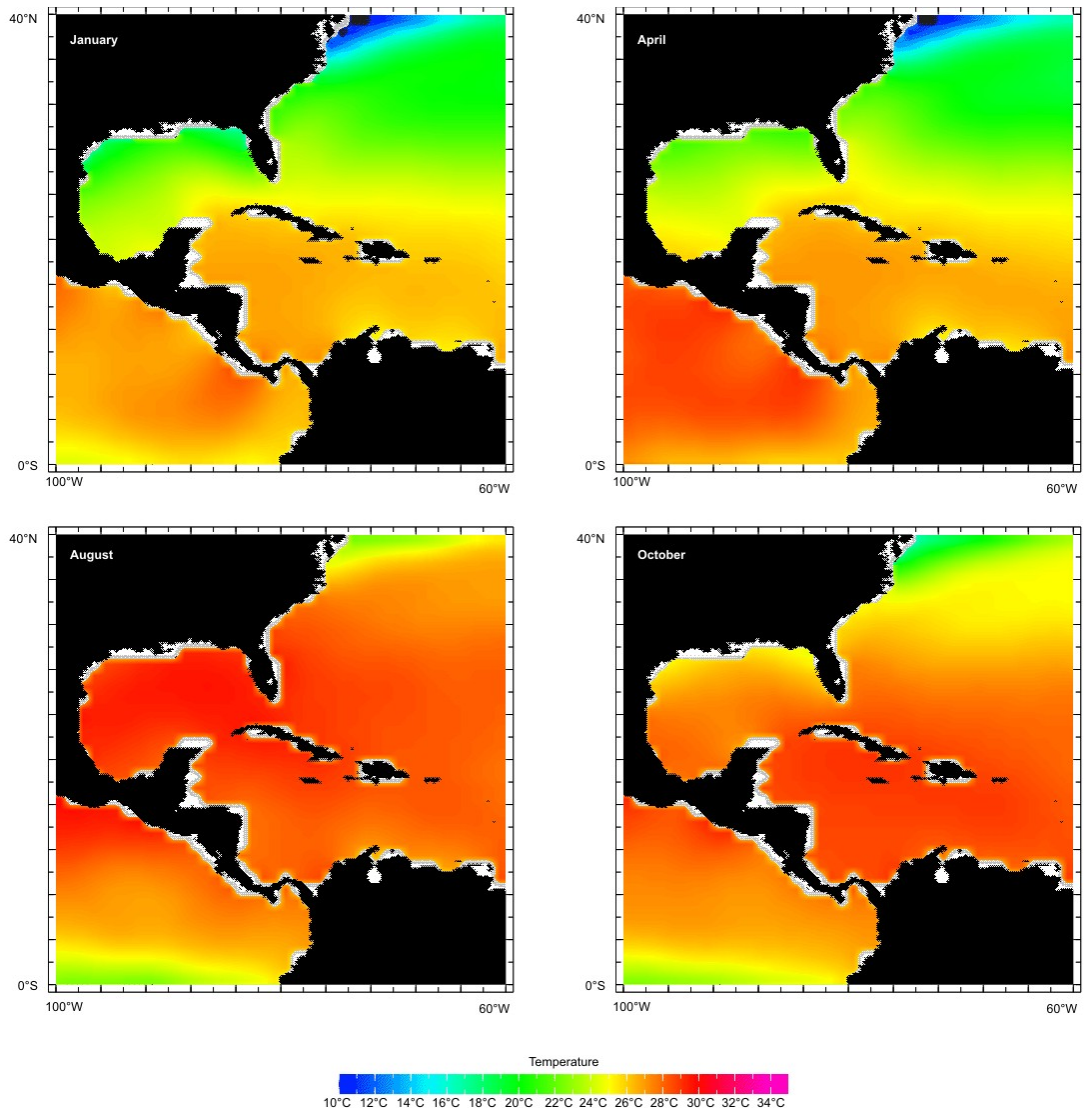


Figure 8: Recent Sea Surface Temperature (SST) within a year in the Caribbean region. Data source Levitus94: World Ocean Atlas 1994 (*Levitus and Boyer, 1994b*)

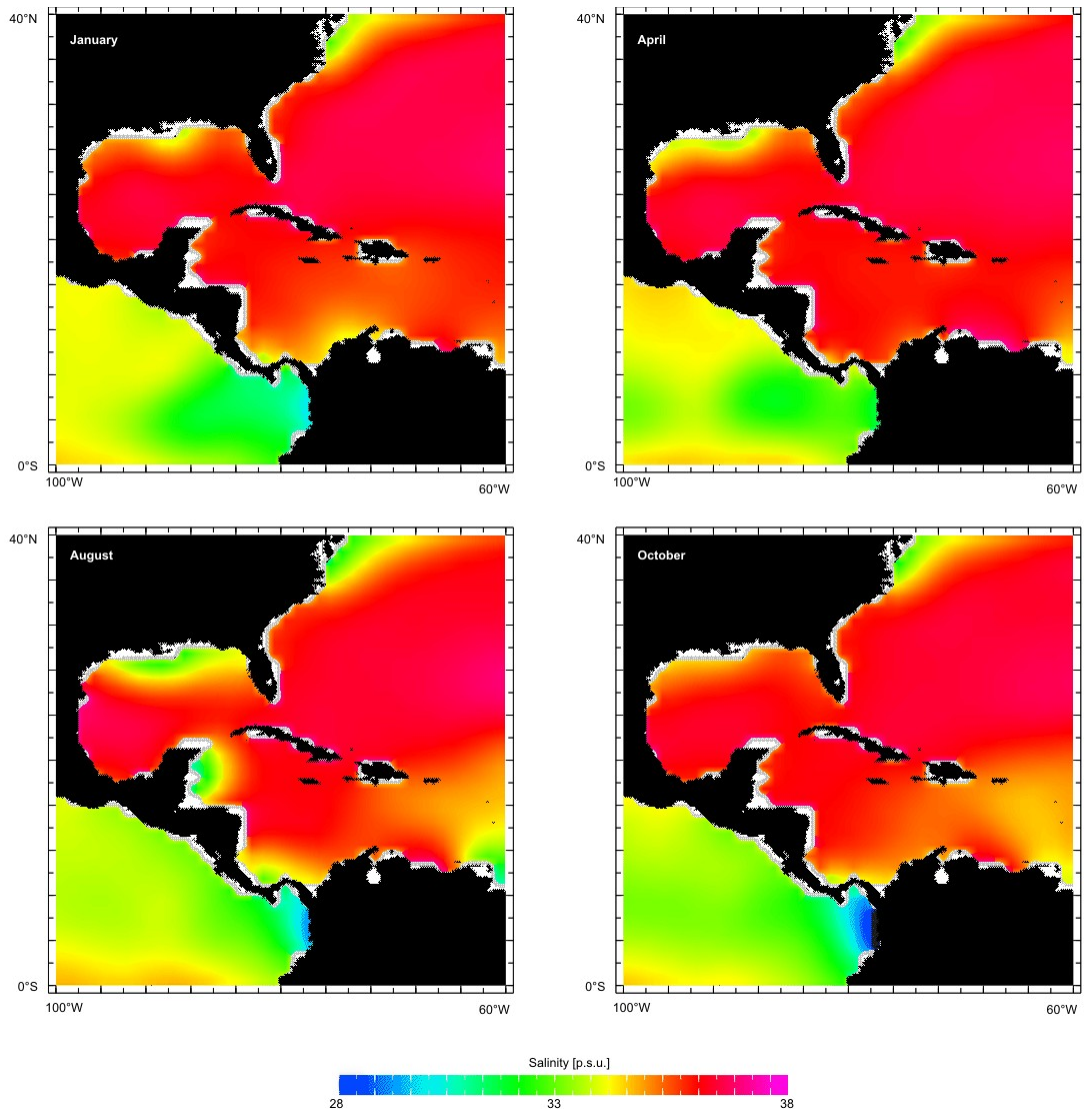


Figure 9: Recent Sea Surface Salinities (SSS) within a year in the Caribbean region. Data source Levitus94: World Ocean Atlas 1994 (*Levitus and Boyer, 1994a*)

The AMO is a 50 - 80 year climate signal in the northern hemisphere with particular presence in the North Atlantic (Fig. 10)(*Wyatt et al., 2012*). Models indicate, that AMO cycles invoke changes in the south-to-north circulation and overturning of water and heat in the Atlantic Ocean. This has a strong effect on south Florida where in a warm AMO-phase more rainfall occurs and the Lake Okeechobee inflow increases significant up to 40 % between AMO extremes (NOAA).

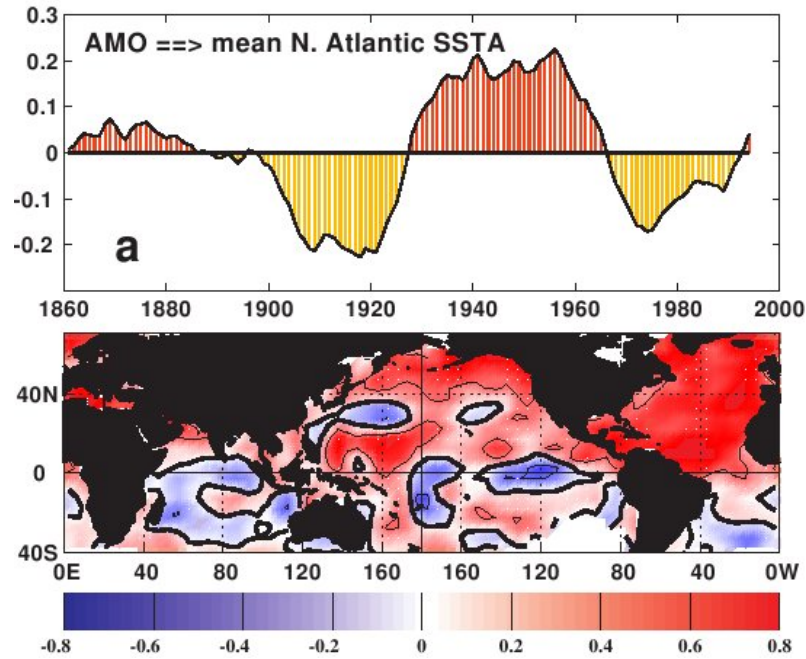


Figure 10: Upper panel: AMO index: the ten-year running mean of detrended Atlantic sea surface temperature anomaly (SSTA, °C) north of the equator. Lower panel: Correlation of the AMO index with gridded SSTA over the world ocean (all seasons). The thick contour is zero and thin contours denote the 95 % significance level. Source: NOAA<sup>1</sup>, AOML

The most prominent teleconnection pattern is the North Atlantic Oscillation (NAO) (Barnston and Livezey, 1987). It consists of a north-south dipole of anomalies, centered over Greenland and between 35-40°N in the central North Atlantic. A positive NAO-phase is characterized by below-normal heights and pressure in the high latitudes of the North Atlantic and above-normal heights and pressure over the central North Atlantic, western Europe and the eastern United States. The negative NAO-phase works the other way around. Swinging from one phase to another, the NAO produces large changes in surface air temperature, winds, storminess and precipitation over the Atlantic and neighboring continents (Hurrell and Deser, 2009). As there is no preferred timescale for the variability of the NAO, large changes can occur between two winters and also in a decade (Hurrell and Deser, 2009). In general a strong positive phase of the NAO is associated with above-average temperatures in northern Europe and eastern United States as well as below-average temperatures in Greenland, southern Europe and the Middle East (Figure 4). Negative phases of the NAO result in opposite temperature and precipitation patterns.

<sup>1</sup>NOAA ([www.nws.noaa.gov](http://www.nws.noaa.gov))

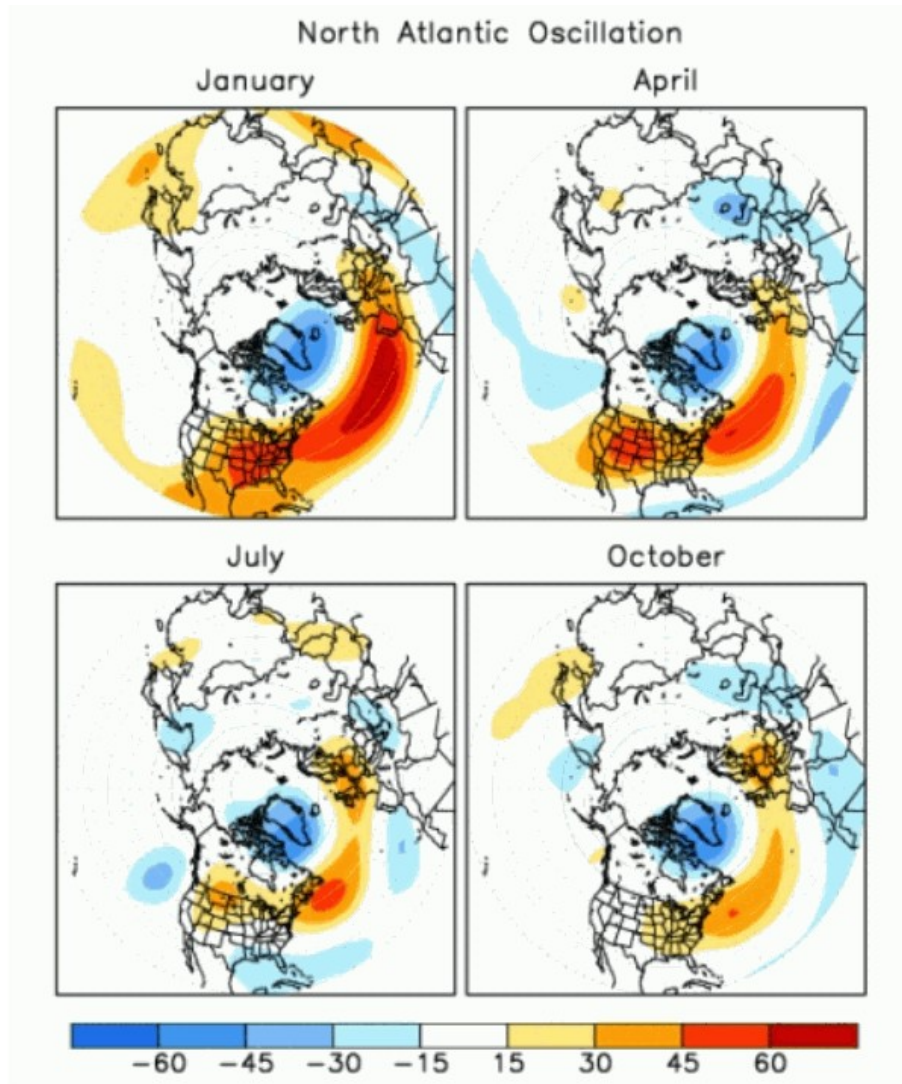


Figure 11: Map of a positive phase of the NAO. The loading patterns for January, April, July, and October, are displayed so that the plotted value at each grid point represents the temporal correlation between the monthly standardized height anomalies at that point and the teleconnection pattern time series valid for the specified month. Source: NOAA<sup>2</sup>

### 1.5.2 Climatic setting of Florida

**Plio/Pleistocene** The late Messinian Miocene was characterized by extreme climatic degeneration with severe cold periods and major eustatic lows. This caused a one million years lasting emerging of the North American paleoceanographic basins from 5.5 Ma to 4.5 Ma (*Petuch, 2007*). This situation changed in the early Zanclean Pliocene with a sea level rise that re-flooded the Okeechobean Sea (*Petuch, 2007*). In the Piacenzian Pliocene the Okeechobean Sea was occupied by the Tamiami Subsea, a return to tropical and subtropical conditions. Sea levels were at their highest and the invertebrate faunas were the richest in North America. Short before the Plio-Pleistocene boundary a short period of cooling and accompanying sea level drop occurred with the extinction of many key Caloosahatchee taxa. After this cooling event a warm period and another climatic degeneration took place at the Plio-Pleistocene boundary, coming along with extinctions

<sup>2</sup>NOAA ([www.nws.noaa.gov](http://www.nws.noaa.gov))

and a general impoverishment of the northern faunas (*Petuch, 2007*). In the Calabrian Age warm time in the early Pleistocene which followed the the marine climate returned to late Piacenzian conditions. With the end of the Calabrian, a lagoonal environment extended from South Carolina to southern Florida (Nashua Lagoon System) and only the landlocked Okeechobean Sea (Caloosahatchee Subsea) contained tropical marine environment (Fig. 2 chapter Stratigraphy of southern Florida)(*Petuch, 2007*). The Nebraskan time is mostly a rapid climatic degeneration and the lowest sea level since the last three million years means the end of all subseas (Nebraskan Glacial Stage) and only the Okeechobean Sea remained intact because of its deeper basinal structure. In the Aftonian Interglacial Stage, in the Yarmouthian Interglacial Stage and in the Sangamonian Interglacial Stage the Okeechobean Sea was flooded while it has been emerged in the glacial times of the Pleistocene

**Recent** The modern climate regime in southern Florida is tropical wet and dry (southeast Florida, Florida Keys, Köppen Aw) and humid subtropical for the northern parts (Köppen Cfa). There is a defined rainy season from June to September (*Kottek et al., 2006*). The dryer season is from October to May (Fig. 12). When an El Nino climate cycle in winter happens, rainfall is mostly increased and the temperatures are cooler in Florida, but an exact correlation does not exist. The six strongest El Nino events between 1950 and 1998 increased the rainfall in average to 150 % of the amount typically expected with a large variability (85 - 213 %) (South Florida Water Management District). Easterly winds streaming from the warm Gulf Stream which is surrounding southern Florida keep the temperatures moderate all the year (Fig. 12). In southern Florida the winter temperatures (January) range at their average lowest points from 18 °C (Key West), 11 °C (Tampa) and 15 °C (Miami) and at their average highest points from 24 °C (Key West), 21 °C (Tampa) and 24 °C (Miami). In summer (August) the temperature range at their average lowest points from 26 °C (Key West), 24 °C (Tampa) and 25 °C (Miami) and at their average highest points from 32 °C (Key West), 32 °C (Tampa) and 32 °C (Miami) (Florida Climate Center). Within the summer months the risk of landfalling tropical cyclones is the highest. Annual precipitation averages from 1948-2012 in southern Florida range between 1011 mm (Key West), 1137 mm (Tampa) and 1523 mm (Miami) (Florida Climate Center)<sup>3</sup>.

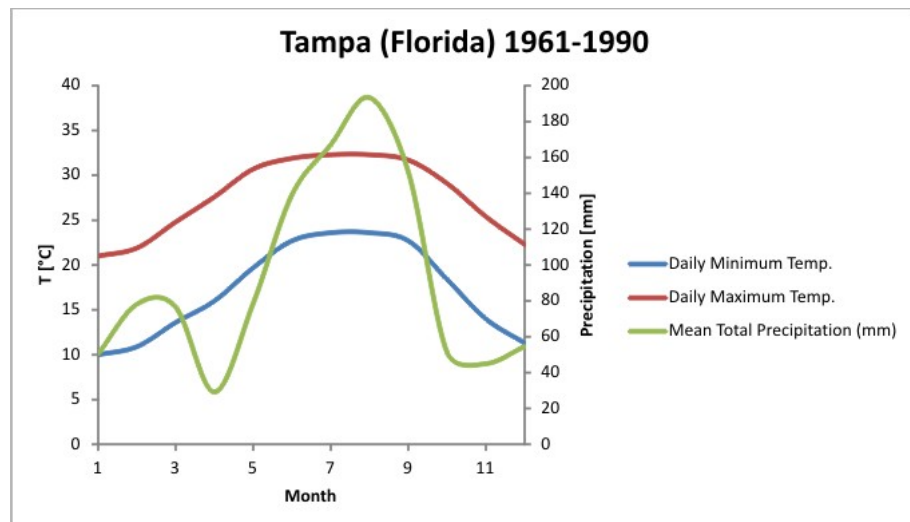


Figure 12: Climatological data for Tampa, Florida from 1961-1990. Data source: WMO<sup>4</sup>

<sup>3</sup>© 2007 Southeast Regional Climate Center, SERCC (<http://www.sercc.com>)

<sup>4</sup>World Meteorological Organization (<http://www.wmo.int>)

### 1.5.3 Climatic setting of the Dominican Republic

**Miocene** The formation of the modern Caribbean reef-coral fauna happened in a geologic short time. Between 4.0 Ma and 1.5 Ma 80 % of the Mio-Pliocene corals got extinct and 60 % of the recent species originated (*Budd et al.*, 1996; *Budd and Johnson*, 1997, 1999). Probably strong environmental changes lead to this development which are supposed to be the uplift of the Central American Isthmus (3.5-3.0 Ma) and the onset of the Northern Hemisphere Glaciation (2.5-1.0 Ma) (*Jackson and Budd*, 1996; *Jackson and Johnson*, 2000). The circulation pattern before the closure of the CAS allowed an intermediate-water exchange via the CAS which was gradually barred as early as 4.5-4.0 Ma until 3.4-3.3 Ma (*Haug and Tiedemann*, 1998; *Steph et al.*, 2006). Low saline Pacific water entered the Caribbean and weakened the North Atlantic salt transport until the final closure of the Panama Strait, which resulted in an irreversible “climate crash” (*Bartoli et al.*, 2005; *Steph et al.*, 2006). The tropical rain belt was shifted in the late Miocene to early Pliocene. This movement to the recent 6 °N of the ITCZ should have an imprint on SSS in the tropical Caribbean, although it is unclear in which direction the ITCZ was shifted (e.g. (*Flohn*, 1981; *Steph et al.*, 2006)). Thus the mid- to early Pliocene climate was warmer than today and less variable than during the late Pliocene and Pleistocene with its large fluctuations in global ice volume (*Crowley*, 1991). SSTs in mid- to high latitudes are supposed to have been 3-7 °C higher and in the tropics was no significant temperature difference (*Dowsett et al.*, 1996). Seasonality was also decreased compared to recent (*Zubakov and Borzenkova*, 1988). Early to mid-Pliocene climate may have also been characterized by a “permanent El Niño-like state” (*Molnar and Cane*, 2002; *Philander and Fedorov*, 2003), which does not exclude a long-term ENSO climate variability forced by the precession (*Huber and Caballero*, 2003). In the Pleistocene the climate is impressed by a succession of glacial-to-interglacial cycles controlled by orbital forcing (*Bartoli et al.*, 2005). This typical pattern appears since the Late Miocene (~3.2 Ma) when the reorganization of the ocean-climate system took place.

**Recent** The island of Hispaniola is located between 18 - 20 °N and is influenced by tropical, subtropical and extratropical climate dynamics. Due to the tropical location of Hispaniola, temperatures range less than 5.5 °C and average between 24 °C (winter) and 28 °C (summer) and it is located at the interface between the seasonally shifting tropical rainy climates and the dry tropical doldrums (Fig. 13) (*Horst*, 1992). The northeasterly trade winds deliver tropical Atlantic moisture and are a dominant feature on Hispaniola (*Lane et al.*, 2009). The modern climate in the Caribbean varies mostly in rainfall activity (*Ross et al.*, 2007). Periods of wet years are followed by periods of dry years and are strongly influenced by combined effects of El Niño Southern Oscillation (ENSO) and the North Atlantic Oscillation (NAO) (*Giannini et al.*, 2000).

Rainfall in the Caribbean is separated in a winter dry season with its center in January-March and a wet season in summer with a first small maximum in May-June and a second large maximum in September-October (Fig. 13) (*Horst*, 1992; *Ross et al.*, 2007). This is due to the movement of the Intertropical Convergence Zone (ITCZ) at its northernmost point during the boreal summer – somewhat south off the Hispaniola (*Lane et al.*, 2009). This ITCZ-doldrums causes a weakening of the trade winds and air pressure (*Kennedy et al.*, 2006; *Lane et al.*, 2009). During the winter (January-March), subtropical high pressure defines dry, stable conditions (*Kennedy et al.*, 2006). Tropical storms and hurricanes can produce heavy rainfalls and from 1871-1991, the Dominican Republic was struck every 3.6 yrs on average (*Horst*, 1992).



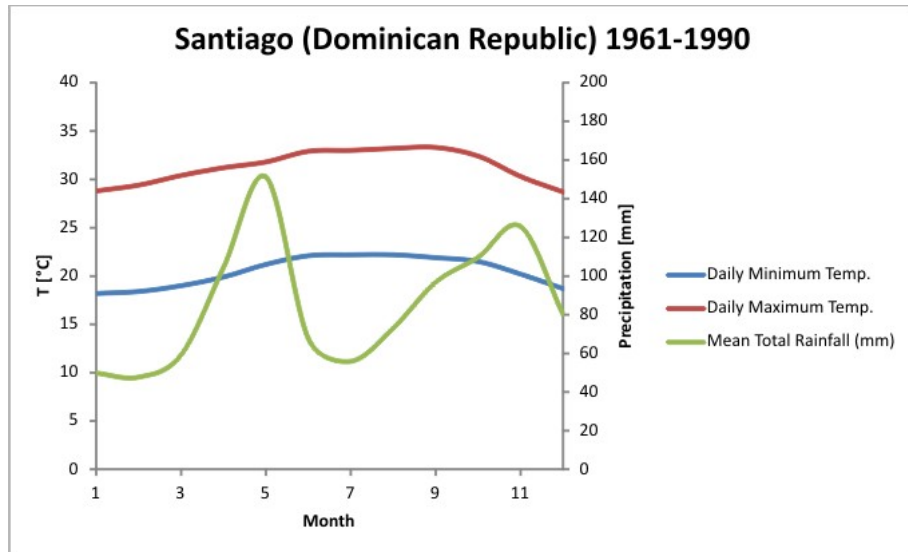


Figure 13: Climatological data for Santiago, Dominican Republic from 1961-1990. Data source: WMO<sup>5</sup>

## 1.6 Geologic setting

### 1.6.1 Geologic setting of southern Florida

The modern Florida is divided in the northern continental region, the Florida Panhandle and the southern Florida peninsula. Surrounded by the Atlantic Ocean in the east, the Gulf of Mexico in the west and the Strait of Florida in the south and with the highest natural elevation 105 m a.s.l. (Britton Hill, close to the border of Georgia at the Florida Panhandle) the geologic history of Florida seems to be basically influenced by the marine realm. A further interest for the geologic past of the southern part of the Florida peninsula exist since the investigated species are from the Plio-Pleistocene Okeechobee Group in southern Florida. The southern part of Florida was divided by a seaway from the continental part. It has been a shallow carbonate platform which has been covered by the Okeechobee Sea. This Okeechobee basin was covered several times by water due to global warm phases. Each flooding event lead to new characteristic marine conditions and is called “Subseas”. The upper 330 m sediment of southern Florida span from the upper Eocene to the Holocene and are divided in four geologic groups, 18 formations and 23 units. Three different depositional regimes are represented in these four groups (*Petuch, 2007*). The first depositional regime adjusted 40 Ma ago as “Carbonate Platform Depositional Episode”. In this time Florida was a flat carbonate platform (Ocala Bank) which was dipping toward the Florida Strait and had a mean depth of 200-300 m in the Everglades area. Due to the Suwanee Strait which separated the Ocala Bank from the continent, very few siliciclastic sediments were deposited on this carbonate platform. Carbonate was accreted and covered with lots of coral islands which grew together and formed Orange Island. These sediments build up the Ocala Group (*Petuch, 2007*). The second depositional regime lasted from the late Oligocene until the early Pliocene as „Upwelling-Deltaic Depositional Episode“. Dramatic changes in deposition occurred because of intense upwelling off west Florida with accompanying decreasing SSTs and higher productivity and planctonic blooms. Another reason was the progradation of huge deltas from the DeSoto plain highlands (former Orange Island). In this time of the Okeechobee Sea terrigenous sediments composed of clay, quartz sand and

<sup>5</sup>World Meteorological Organization (<http://www.wmo.int>)

phosphorites were accumulated (*Petuch, 2007*). The “Pseudoatoll Depositional Episode” is the third and last episode which began 4 Ma before present present in the middle Pliocene and forms the precursor of the modern Everglades. In the Pliocene-Pleistocene transition within the Okeechobee Subsea phase the Caloosahatchee Formation was deposited (Fig. 14) from which most of my samples come from (*Petuch, 2007*).

**Plio-Pleistocene** In this period a ring-shaped reef structure without any subsidence (“Pseudoatoll”) existed and sudden sea level fluctuations together with a climatic cooling at the end of the Pliocene ended the deposition of the Tamiami Formation. The Okeechobee Sea Basin shoaled until freshwater lakes could exist. At 2.2 Ma, the Plio-Pleistocene transition, a transgression lead to a salty Okeechobee Sea covered with mangroves (*Lloyd, 1969; Petuch, 2007; Tao and Grossman, 2010*). This new marine Caloosahatchee Sea (Fig. 15) enabled the deposition of the Caloosahatchee Formation which is separated in four members, from which is only the Fordville Member deposited in the Pliocene (Fig. 14). The three Pleistocene members are the Fort Denaud Member, the Bee Branch Member and the Ayer’s Landing Member. The samples from this epoch cannot distinguished between the four members (see chapter 2 for reasons). North of the Caloosahatchee Strait and the Loxahatchee Strait cooler water conditions prevailed, while the Caloosahatchee Subsea remained as a shallow marine and tropical warm environment). Major paleogeographic features in the Caloosahatchee Subsea were Immokalee Island on the Hendry Platform and the Cape Sable Bank. In the southeast bordered the Miami Archipelago the Caloosahatchee Subsea. At the eastern Hendry Platform existed Miccosukee Island which was covered by mangroves and attached to the deep Loxahatchee Trough with coral reefs between (Fig. 15)(*Petuch, 2007*). The Caloosahatchee marl was deposited under a large range of environmental conditions (*DuBar, 1958; Lloyd, 1969*). Most specimen lived in the presence of isotopically enriched water and therefore under conditions of restricted circulation and

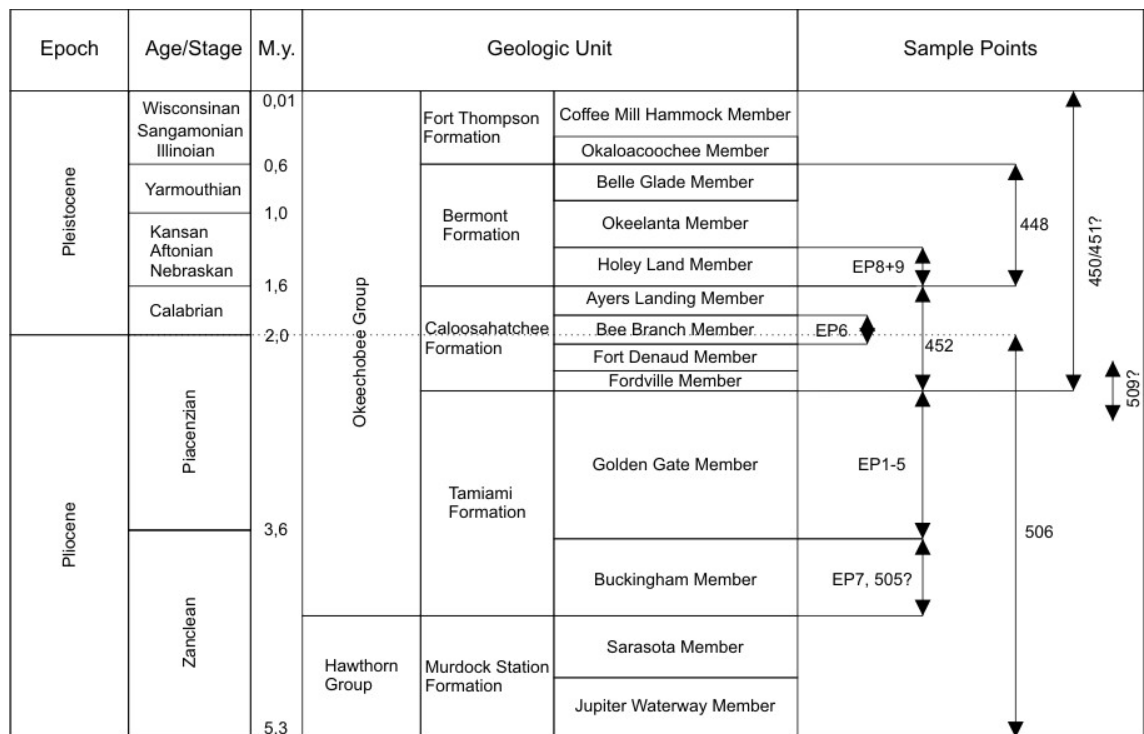


Figure 14: Generalized stratigraphic column for Pliocene and Pleistocene of the Everglades and adjacent areas with correlated sample points. Redrawn after (*Petuch, 2007*)

high evaporation (*Lloyd, 1969*). Reconstructed paleotemperatures of the Caloosahatchee Formation are respectively  $25.1 \pm 1.4^\circ\text{C}$  and  $22.4 \pm 0.5^\circ\text{C}$  and slightly lower than modern SSTs in the Sarasota Bay which are  $24.5 \pm 0.4^\circ\text{C}$  (*Tao and Grossman, 2010*). Climatic conditions are supposed to be the same as modern with higher precipitation in winter and spring and drought in summer (*Lloyd, 1969; Tao and Grossman, 2010*). These conditions are found today in the recent Florida Bay. This is a large ( $20\,000\text{ km}^2$ ) shallow body of water between the peninsula of Florida and the Florida Keys. The main water sources beside precipitation are the Everglades and the attaching seas Gulf of Mexico and Strait of Florida. There is also a restricted circulation and exchange with the open ocean which leads to a  $\delta^{18}\text{O}$  enrichment in the drought period due to strong evaporation, which causes typical patterns within the  $\delta^{18}\text{O}$  values and the salinity of the seawater (*Swart et al., 1989, 1996, 1999; Hudson et al., 1989; Halley and Roulier, 1999; Kelble et al., 2007*).

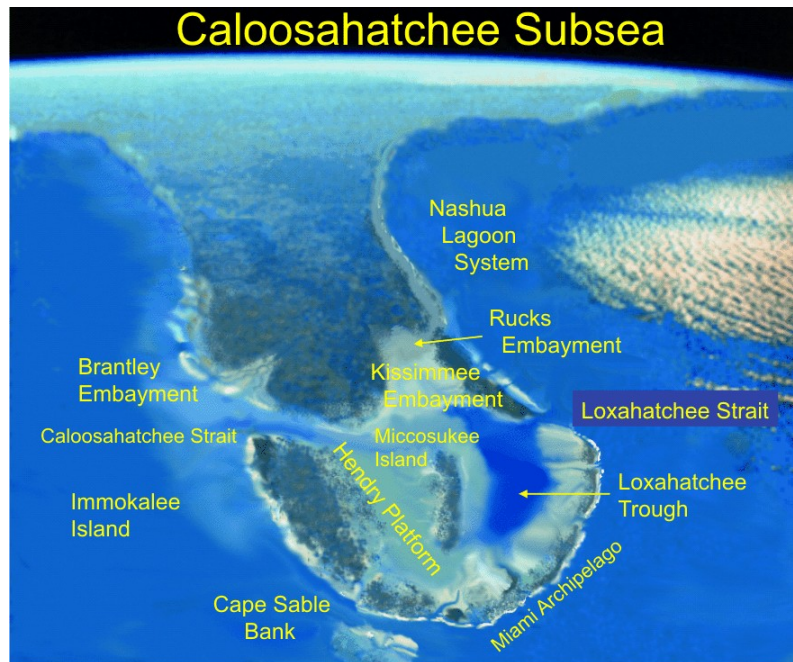


Figure 15: Simulated space shuttle image of the Florida Peninsula during the early Calabrian Pleistocene, showing the possible appearance of the Caloosahatchee Subsea of the Okeechobee Sea and some of its principal geomorphologic features. From (*Petuch, 2007*)

### 1.6.2 Geologic setting of the Cibao Valley

The Neogene deposits of the Dominican Republic with its rich Cenozoic Faunas have attracted many scientists for several decades (*Saunders et al., 1986*). There were beside studies about Cretaceous and Paleogene history major paleontological projects (*Vaughan et al., 1921; Saunders et al., 1986*) (*Klaus and Budd, 2003; McNeill et al., 2012*). The Cibao Basin has composed in the last 10 million years on a combination of strike-slip motion and transpression linked to the interaction between the Caribbean plate and North American plate (*Draper et al., 1994*). The plate-boundary processes, producing an island-arc in intra oceanic setting (*Mann et al., 1991*) of which the Hispaniola Island is part, are still in process and causing stress in the plate. The Island of Hispaniola consists of four northwest-southeast-trending mountain ranges, which are separated by three valleys trending in the same direction. The northernmost of this valleys is the Cibao Valley in the northern part of Hispaniola Island in the Dominican Republic (*Saunders et al., 1986*) (Fig. 16). The Cibao Valley is 230 km long and 30 km wide and is surrounded by the

moderate slope of the Cordillera Central (CC) in the south and the Cordillera Septentrional (CS) in the north, the Rio Yaque del Norte with its minor rivers is crossing the valley in northeastern direction (*Erikson et al.*, 1998). It is lying within the deformed belt that marks the northern border of the Caribbean Plate which is still today an area of shallow earthquake activity (*Saunders et al.*, 1986).



Figure 16: Location of the island of Hispaniola and Cibao Valley in the northern Dominican Republic. From *McNeill et al.* (2012)

The Cordillera Central is part of the Greater Antilles magmatic arc which formed from mid-Cretaceous to Paleogene time. The Cordillera Septentrional is underlain by pre-Eocene subduction complex (*Nagle, 1974; Draper and Nagle, 1991*) and makes it most probable that the Cibao Valley was sat in a fore-arc tectonic setting (*Lewis, 1980; Erikson et al., 1998*). In the late Miocene northern Hispaniola has collided with and overridden parts of the Bahama bank (*Sykes et al., 1982*). The modern Cibao Valley is nearly coincident with the Neogene Cibao Basin (*Draper and Lewis, 1990*) and represents a large synclinal structure with its axis nearly parallel to the valley (Fig. 16) (*Mann et al., 1990*). In the Neogene, the Cibao Valley was a sea filled-graben which was bordered by the Cordillera Central in the south and the Cordillera Septentrional in the north (*Saunders et al., 1986; Nehm, 2005*). During the deposition there was an active down-to-the-basin faulting which steepened the southern edge of the Cibao Valley trough (*Saunders et al., 1986*). Clastic material which was delivered from the Cordillera Central was deposited as shallow marine sequences with a northward progradation of a sedimentary wedge (Fig. 17) (*Saunders et al., 1986; McNeill et al., 2012*). Many of the sediments delivered (especially conglomerates) are reworked material from older conglomerates (*Saunders et al., 1986*). The source area of the sediments from the Rio Gurabo outcrops seem to lack brackish water swamps along the coast because of the domination of ferns and palms backed by quickly rising ground covered with a savanna vegetation and no heavy forest covering (*Saunders et al., 1986*). The delivered sediments further are not being deposited on a stable shelf but rather transported periodically into deeper water down an appreciable slope (*Saunders et al., 1986*). This fact prevented a broad reef development, even if the clear water allowed coral growth (*Saunders*

*et al.*, 1986).

**Oligocene to Miocene rocks** *Saunders et al.* (1986) studied intensive the deposits of the Cibao Valley and created a chronology with heights where later studies are commonly also referenced to (e.g. *Denniston et al.*, 2008; *Lutz et al.*, 2008; *McNeill et al.*, 2012). This sub-chapter is based upon *Saunders et al.* (1986) descriptions too. The oldest sedimentary rocks outcropping in the Cibao Basin are those of the Oligocene Tabera Group. It's including several sedimentary lithologies and a varying degree of folding and planation (*Saunders et al.*, 1986). The contact to Miocene and younger sediments is an unconformity. In some areas of the Cibao Basin the Baitoa Formation is intercalated between the Oligocene or Early Miocene deposits and the Cercado Formation, the oldest part of the Neogene Yaque Group (Fig. 18). The age of the Baitoa Formation is considered to be basal Miocene to late Miocene (*Saunders et al.*, 1986). The earliest beds above the basal unconformity in the Rio Gurabo are of shallow marine origin with brackish influence. Contrasting this, the first beds in the Rio Cana above the unconformity are unfossiliferous and eventually non-marine. Further upward in the Rio Cana are deposited shallow marine beds succeeded by the *Arca* beds. The *Arca* beds are a series of sand and silts containing several shells of the claim *Arca*. In the Rio Gurabo these *Arca* beds are represented by the cross-bedded *Amphistegina* sands. A possible explanation for this is the erosion of the *Arca* beds in the Rio Gurabo by the overlying basal conglomerate of the Gurabo Formation (*Saunders et al.*, 1986).

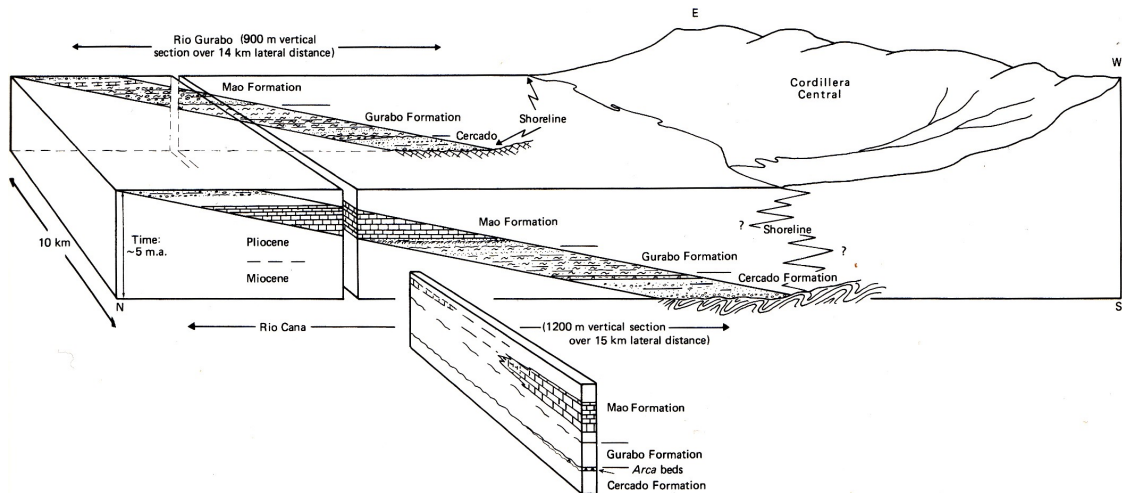


Figure 17: Relationship between Neogene sections on Rio Cana and Rio Gurabo from *Saunders et al.* (1986). Modern depositional interpretation evidences three clinoformal shelf deposits for Mao, Gurabo and Cercado Formation (See Fig. 19). Block diagram from *Saunders et al.* (1986)

**The Neogene Yaque Group** Neogene deposits in the Cibao Valley are mainly part of the Yaque Group (*Erikson et al.*, 1998), which consists of the Cercado, Gurabo and Mao formations. As *Denniston et al.* (2008) figures out “the Cibao Valley of the Dominican Republic contains an ~3 m.y.-long record of well-preserved fossil taxa that existed in the Caribbean prior to final closure of the Central American Seaway”. The Rio Yaque del Norte is flowing through the Cibao Valley along its east-west axis supplied by its five south-to-north oriented tributaries (from west to east Rio Amina, Rio Mao, Rio Gurabo, Rio Cana, Rio Guayubin). These rivers incise the Neogene wedge-shaped basin sedimentary sequences and expose them in a series of dip-oriented sections (*McNeill et al.*, 2012). These sectioned Mio/Pliocene rocks are approximately 5000 m thick and structurally undisturbed

(Mann *et al.*, 1990). The Miocene to Pliocene Yaque Group comprises the three fossil rich deposits of the Cercado, Gurabo and Mao Formation with the underlying spatially discontinuous early to middle Miocene Baitoa Formation (Fig. 18) (McNeill *et al.*, 2012). The ages of the formations have widely varied (e.g. Saunders *et al.*, 1986) and are in the most recent times new refined by Denniston *et al.* (2008) and McNeill *et al.* (2012) (Fig. 18).

<i>Epoch</i>	<i>Stage</i>	<i>Stratigraphic nomenclature</i>	
Pleistocene		Alluvium	
Pliocene	Late	Piacenzian	Yaque Group
	Early	Zanclean	
Miocene	Late	Messinian	Cercado Formation
		Tortonian	Cercado Sandst. Mbr. Bulla Conglom. Mbr. ? Hiatus ?
	Mid.	Serravallian	Baitoa Formation
	Early		? ? Hiatus
Oligo.		Tabera Formation	

Figure 18: Summary of the Stratigraphy of the Outcrops in the Cibao Valley after Saunders *et al.* (1986). From (McNeill *et al.*, 2012)

Recent investigations by Donald McNeill and James Klaus from Miami modified the depositional interpretation of the Neogene formations of the Yaque Group. In difference to the depositional model of Saunders *et al.* (1986, Fig. 17), the three formations which build-up the sedimentary wedge at the south-side of the Cibao Valley represent different depositional stratigraphic sequences which are even correlated to sediment accumulations of the Great Bahama Bank basin (McNeill *et al.*, 2012). These sequences are related to three major sea-level events and form a series of clinoformal shelf deposits (Fig. 19). All three formations vary in thickness at the different sections Rio Cana section and Rio Gurabo section (20) due to the highly dynamic system of a prograding deltaic environment onto the shelf (at least in the Rio Cana section). In general the sediments are sandy and muddy detritus from the bordering mountain ranges and are combined with in situ biogenic carbonate production such as corals, molluscs, red algae, bryozoa, benthic foraminifera and other skeletal fragments (McNeill *et al.*, 2012).

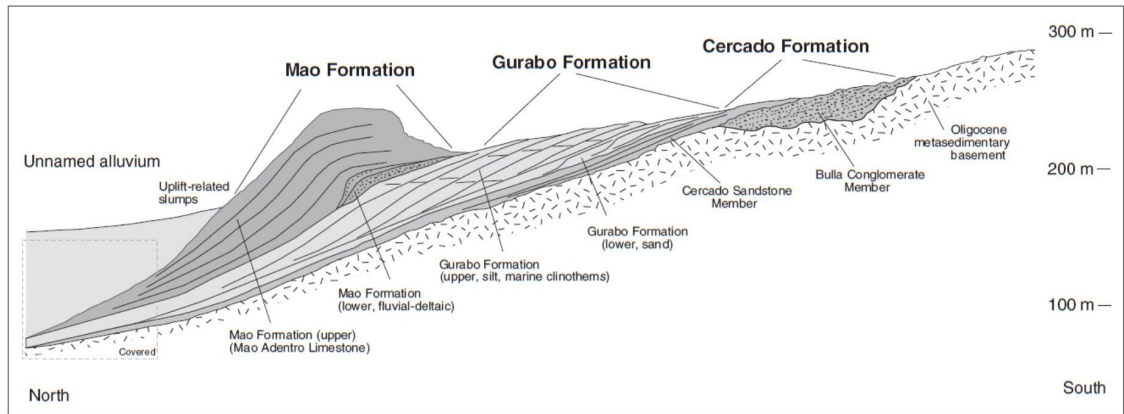


Figure 19: Generalized cross section of the sediment wedge along the southern flank of Cibao Basin. From (McNeill *et al.*, 2012)

**Cercado Formation** The thickness of the Cercado Formation is significant higher in the Cana Section (232 m) than in the Gurabo Section (158 m)(Fig. 20). The Cercado Formation is composed mostly of Sandstones. Minor lithologies are pebble stringers and beds of conglomerate, silt and lignite. Additional rhodolith and coral debris is found (Saunders *et al.*, 1986; McNeill *et al.*, 2012). The Two main lithofacies are (1) laterally discontinuous conglomerates (Bulla Conglomerate Member) and (2) more dominant marine sandstone facies (Cercado Sandstone Member) (McNeill *et al.*, 2012). Saunders *et al.* (1986) found the calcareous nannofossil zone NN11 at the base of the Cercado Formation which gives an age range of 8.6–5.6 Ma. McNeill *et al.* (2012) confirmed this ages with Sr isotope ages, key first occurrences of planctonic foraminifera and magnetic polarity to around 6 Ma.

**Gurabo Formation** The Gurabo Formation is very well exposed along the Rio Gurabo, called the Gurabo Section. In this section the most thickness is observable, probably due to greater water depths at Rio Gurabo (McNeill *et al.*, 2012)(Fig. 20). It is composed of approximately 400 m weakly compacted fine-grained sediment with intervals corals and coral debris with changing fractions. Corals from the middle Gurabo were transported downslope and rapidly buried by sediment. This sediment is dense, low permeable and clayey and so perfect for coral preservation (Evans, 1986; Saunders *et al.*, 1986; Erikson *et al.*, 1998; Denniston *et al.*, 2008). The most samples from the Dominican Republic are picked in the Gurabo Formation. It's age is constrained by a U/Pb measurement to  $5.52 \pm 0.15$  Ma (Denniston *et al.*, 2008) and also by ostracodes and nannofossils (van den Bold, 1975; McNeill *et al.*, 2012). Magnetostratigraphic measurements show a lower interval of reverse polarity and an upper interval of normal polarity. The lower interval was correlated to the lower Gilbert chron C3r (5.89- 5.23 Ma) and the upper interval was correlated to the lowermost subchron in the Gilbert chron C3n.4n (5.23–4.98 Ma, McNeill *et al.*, 2012). This and Sr isotope ages localize the Gurabo Formation in the Miocene around 5 Ma with an unconformity at 4 Ma capping the sequence and introducing the Mao Formation (McNeill *et al.*, 2012).

**Mao Formation** The Mao Formation consists of the two members Mao Adentro Limestone and the Mao Clay (Evans, 1986; McNeill *et al.*, 2012). Thicknesses of the Mao Formation are also significant different in the Gurabo and Cana section (Fig. 20). Highest thickness is due to shallower water and better coral growth conditions in the Cana section

observable. The two members consist of four different lithofacies which are bedded siltstones, conglomerates, interbedded limestone-siltstones and clean siltstones (*Evans, 1986*). All beddings dip more or less steep from 6-13° (*Evans, 1986*) and seem to form clinotherm foresets (*McNeill et al., 2012*). The age estimate for the deposits of the Mao Formation ranges between 4.0 and 3.5 Ma and is made with key biostratigraphic markers, Sr-isotope ratios and magnetic polarity (*Saunders et al., 1986; Lutz et al., 2008; McNeill et al., 2012*).

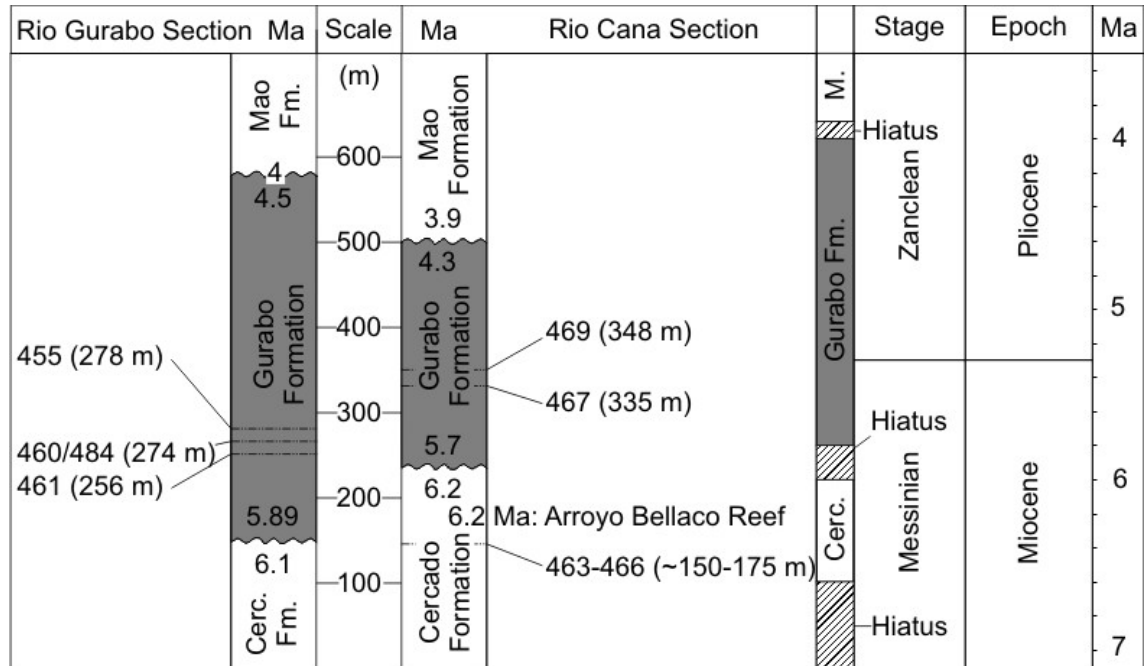


Figure 20: Stratigraphic positions of the samples from the Cibao Valley. Stratigraphy based on *Saunders et al. (1986)*, *McNeill et al. (2012)* and age of the Arroyo Bellaco reef from *Maier et al. (2007)*.



## 2 Materials and Methods and Analytical Procedures

### 2.1 Collection of Corals in the Field

All specimen described were taken from outcrops during two field trips in 2010 and 2012. The field trip in august and September 2010 to Florida and the Dominican Republic produced samples from the outcrops 448 to 474 (Fig. 21). First aim of this journey was to sample as much as possible coral heads with a pristine preservation of the coral skeleton. Such field properties are a low weight, a bright color and a highly porous and visible intern structure of the corallites. Specimens with obvious secondary diagenetic alteration effects like cements or discoloration were discarded.

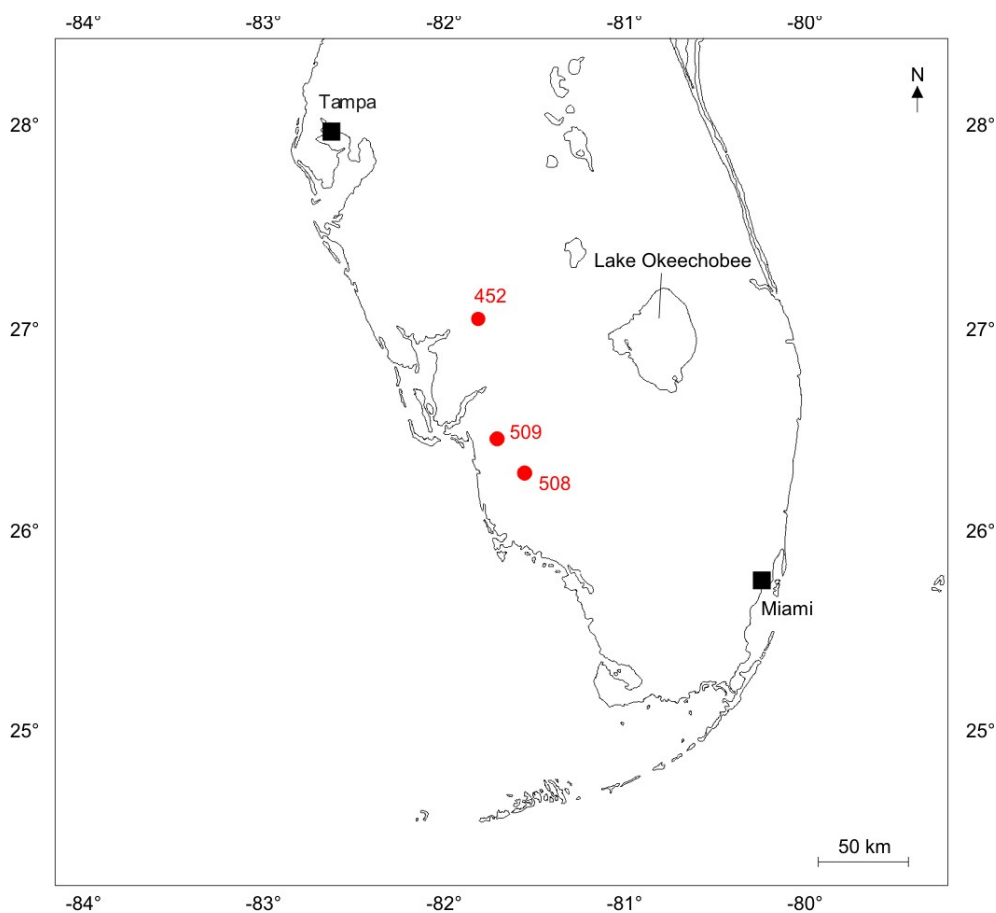


Figure 21: Overview of sample locations in southern Florida, USA

The second field trip to the Dominican Republic and Florida in February 2012 was mostly to check the stratigraphic classification and lithologies of samples that have been taken during the first field trip. Additionally samples from the already visited outcrops (448-474) and other outcrops in the numbers 488 to 513 (Fig. 22) were taken, checking for pristine preservation in the same manner as in the first field trip.

#### 2.1.1 Outcrops Florida

Due to the very flat and low morphology of the southern Florida peninsula natural limestone outcrops are not present. Most of the peninsula is covered by swamps and agricultural areas. The outcrops studied were working or abandoned pits. In consideration of active mining it was not possible to visit the mining front. In abandoned mines it was also not

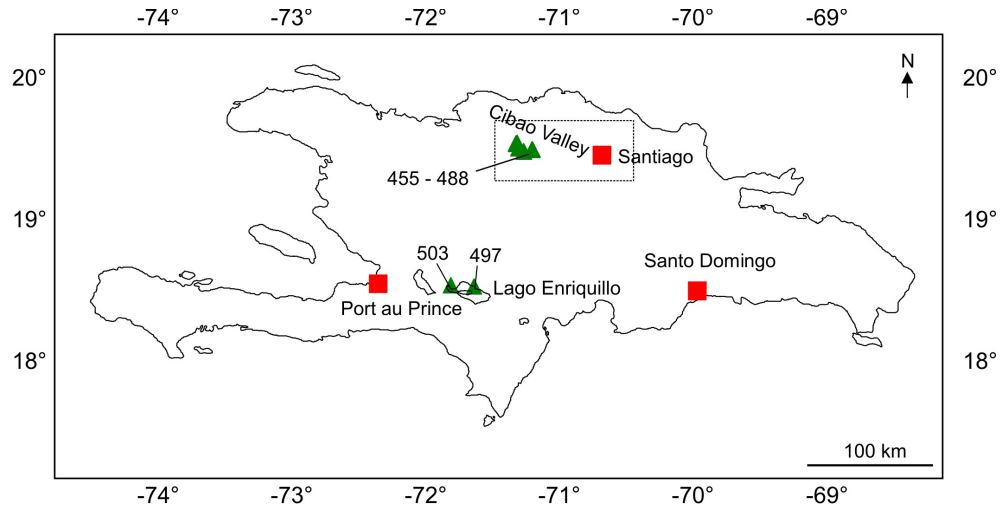


Figure 22: Overview of sample locations at the island of Hispaniola. Cibao Valley outcrops from 455-488, Lago Enriquillo outcrops 497 and 503

possible to visit the vertical face because all holes in the ground are filled with groundwater. Places where could sampled were the pre-sorted pillars of the working or abandoned pits. The spoils of those quarrys were mostly grain-size sorted and consisting of a broad mixture of different species like bivalves, gastropods and corals from a depth of up to 20 m below ground level. Collected samples from these outcrops (outcrops 448-452, 505-513, EP 1-9) always have a questionable stratigraphic correlation because of the lack of primary geologic bedding. For the stratigraphic classification geological maps and biostratigraphic classification with the help of local experts (e.g. Edward Petuch, James Klaus, Donald McNeill) were used. Taken samples were packed and shipped via airmail to Leipzig.

**452** Outcrop 452 is located in the abandoned pit "Hennessy Airport Quarry" from DeSoto Sand & Shell LLC close to Arcadia, Florida (Latitude: 27.0597833; Longitude: -81.7937833; Fig. 21). The geologic map for the state of Florida marks the surface of this area as Plio/Pleistocene Caloosahatchee formation. All samples come from an artificial dumped soil pillars from unknown depth. The distribution of species inside the pillar suggests also Caloosahatchee formation, as local experts confirm. The pre-sorted pillars have a maximal grain size of 10 cm and contain a broad diversity of species of corals, bivalves, gastropods oysters, worms and bone fragments. Approximately a few hundred meters beside the pillar some dm-thick carbonate beds are artificial stored which show sedimentary structures like alternating hardgrounds and tempestite layers which are mostly made up of bivalve shells and sometimes show an imbrication and sometimes are still two-valved. In some of the beds all primary aragonitic shells are dissolved and in some no dissolution effects are existent with all gradual steps in between. The most pristine shells show exactly one borehole.

**508** Outcrop 508 is located at an artificial canal and covered by farm land close to Sarasota, Florida (Latitude: 26.2841667; Longitude: -81.5622000; Fig. 21). The geologic map for the state of Florida marks the surface of this area as Plio/Pleistocene Caloosahatchee formation. The samples come from outcropping beds at the canal. This outcrop was also described as part of the Pliocene fossil reef as stop 6, where it is the only reported Pliocene reef crest from the entire Caribbean region (Meeder, 1979). There can be found 50 different coral species and many different reef facies (Meeder, 1979). One large *Solenastrea* was sampled here (508 A).

**509** Outcrop 509 is located at an abandoned pit close to Sarasota, Florida (Latitude: 26.2841667; Longitude: -81.5622000; Fig. 21). The geologic map for the state of Florida marks the surface of this area as Plio/Pleistocene Caloosahatchee formation. Only artificial soil pillars were existent here and a large diversity of species could be found within them. Carbonate crusts with land snails upon are observable too. This outcrop was also described as part of the Pliocene fossil reef as stop 11 where the large boulders are identified as reef rocks and highly indurated shelly muds (*Meeder, 1979*). Some corals were sampled here (509A).

### 2.1.2 Outcrops Dominican Republic

In the Dominican Republic only natural outcrops were studied. Most of the field work took place in the Cibao Valley, located in the northern part of the Dominican Republic. The Cibao Valley is nerved by the Rio Yaque del Norte and its tributarys. Important tributarys are the Rio Gurabo (outcrop 455-461, 484), Rio Mao and the Rio Cana (outcrops 471-474) with it's creeks Arroyo Bellaco (467-469, 488) and Cañada de Zamba (outcrops 463-466; Fig. 23, Fig. 24). These tributarys cut a Mio/Pliocene reef system in the south of Cibao Valley which has been lifted up around 100-200m since deposition. Named after the incising rivers, the Gurabo Formation, Mao Formation and Cercado Formation are outcropping in these river valleys. During field work, the river valleys were walked and sampled for well preserved corals from silty sediment exposed at the valley flanks. These samples where first checked for diagenetic alteration and then packed and shipped to Leipzig for further study. Second sampling site in the Dominican Republic is the northern shore of Lago Enriquillo (Fig. 22). The waterlevel in the lake changed since the uplift of a barrier in the south separated it from the Caribbean sea. The present water level is -40m below sealevel due to a negative water balance (*Mann et al., 1984*). At the northern shore of Lago Enriquillo is a well preserved Holocene reef about 20-40m above lakelevel, which was build up when the lake was connected to the Caribbean Sea and corals grew in the shallow water (*Greer et al., 2009*). This dry reef is incised by little creeks and roads and also because of the rising shore topography good accessible (*Reuter et al., 2013*).

**455** Outcrop 455 is located in Cibao Valley, Dominican Republic in the river valley of the Rio Gurabo at (Latitude: 19.5000167; Longitude: -71.1811333; Fig. 24). Within the commonly used stratigraphic column of the Panama Paleontology Project from *Saunders, Jung, and Biju-Duval* (1986) it is located in the height of 278m and therefore Gurabo Formation (Fig. 20).

The outcrop consists of slightly dipping beds (approximately some degrees) along an ENE-WSW trending wall. At the base above the Rio Gurabo an approximately 1m thick bed without any internal bedding is visible (coral 455C is from the upper part of this bed). The bed is composed of mostly silty and grey sediment. Embedded are many branches of *Porites* ( $\varnothing 3 - 10\text{ mm}$ ) as well as some azooxanthellate corals and some plates of *Agarithia* not in life position. Additional few bivalves, gastropods and oysters occur. Below this bed until the river-surface begins (ca. 1m), a progradational pattern of parallel dipping dm-thick beds which consist of small lenses of a length of maximal some meters and fine material between is outcropping. The material of the lenses is harder than the material between, due to more carbonate cementation. Above the bed with coral 455 C a large trough of approximately 10-20m width occurs. The thickness of the trough trices in the middle compared to the borders. Inside a clear bedding towards the roof of the trough is visible.

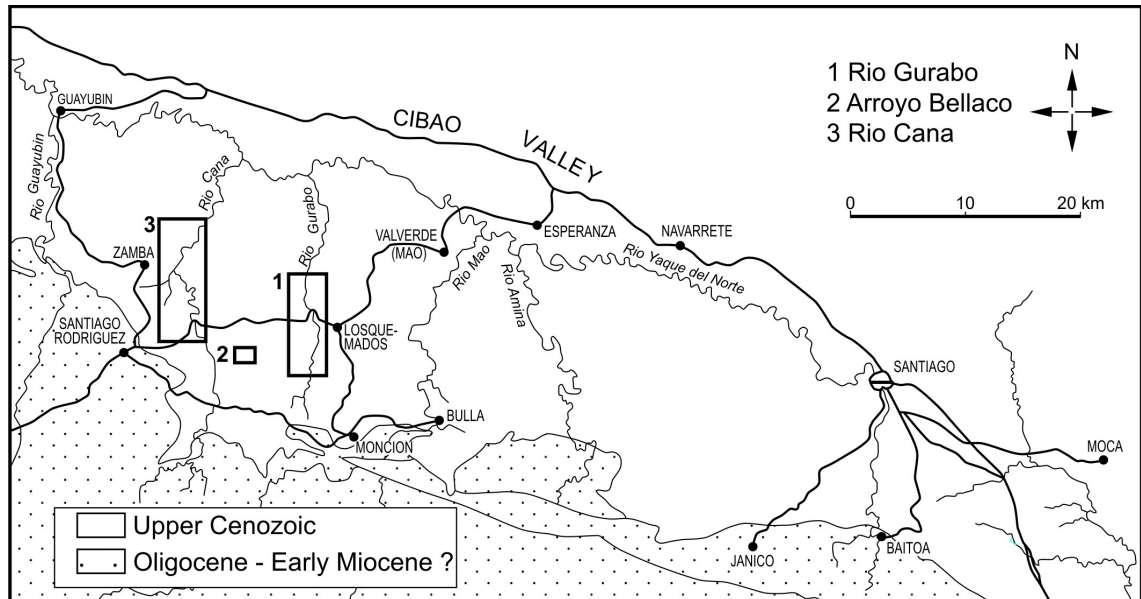


Figure 23: Cibao Valley and Rio Yaque del Norte with its tributaries Rio Gurabo (1), Arroyo Bellaco (2) and Rio Cana/Cañada de Zamba (3). For detailed information see Fig. 24. Modified from *Saunders et al.* (1986).

**460** Outcrop 460 is located in Cibao Valley, Dominican Republic in the river valley of the Rio Gurabo at (Latitude: 19.4989167; Longitude: -71.1809833; Fig. 24). Within the commonly used stratigraphic column of the Panama Paleontology Project from *Saunders, Jung, and Biju-Duval* (1986) it is located in the height of 274 m and therefore Gurabo Formation (Fig. 20).

The outcrop is only some hundred meters beside 455 and there was no fault visible between both. An approximately 1 m thick bed consisting of fine, laminated sand is becoming thinner at this outcrop and finally being replaced by a mixture of massive corals with diameters up to 1 m. Between them coral debris is located. All corals are overturn and show no traces referring to boring organisms. Above this corals beds with some dm thickness are deposited, containing massive corals in life position.

**461** Outcrop 461 is located in Cibao Valley, Dominican Republic in the river valley of the Rio Gurabo at (Latitude: 19.4959000; Longitude: -71.1790500; Fig. 24). Within the commonly used stratigraphic column of the Panama Paleontology Project from *Saunders, Jung, and Biju-Duval* (1986) it is located in the height of 256 m and therefore Gurabo Formation (Fig. 20).

This outcrop is the valley rim of the Rio Gurabo. The lower accessible area is characterized by two clay horizons in a distance of 1.5 m and a thickness of 2-3 cm. Between, above and below this clay horizons is a grey and silty mudstone with single coral heads embedded ( $\varnothing$  20 cm). Coral 461 A was sampled 1 m below the lower clay horizon, coral 461 B was sampled 10 cm above this clay layer.

**463 and 464** Outcrop 463 is located in Cibao Valley, Dominican Republic in the river valley of the Arroyo Bellaco, a tributary of the Rio Cana (Latitude: 19.4846000 ; Longitude: -71.2466833; Fig. 24). Neighboring outcrop 464 is located within the same stratigraphic units approximately 100 m northeastern (Latitude: 19.4854667; Longitude: -71.2465500; Fig. 24). Within the commonly used stratigraphic column of the Panama Paleontology Project from *Saunders, Jung, and Biju-Duval* (1986) they are located in the height of

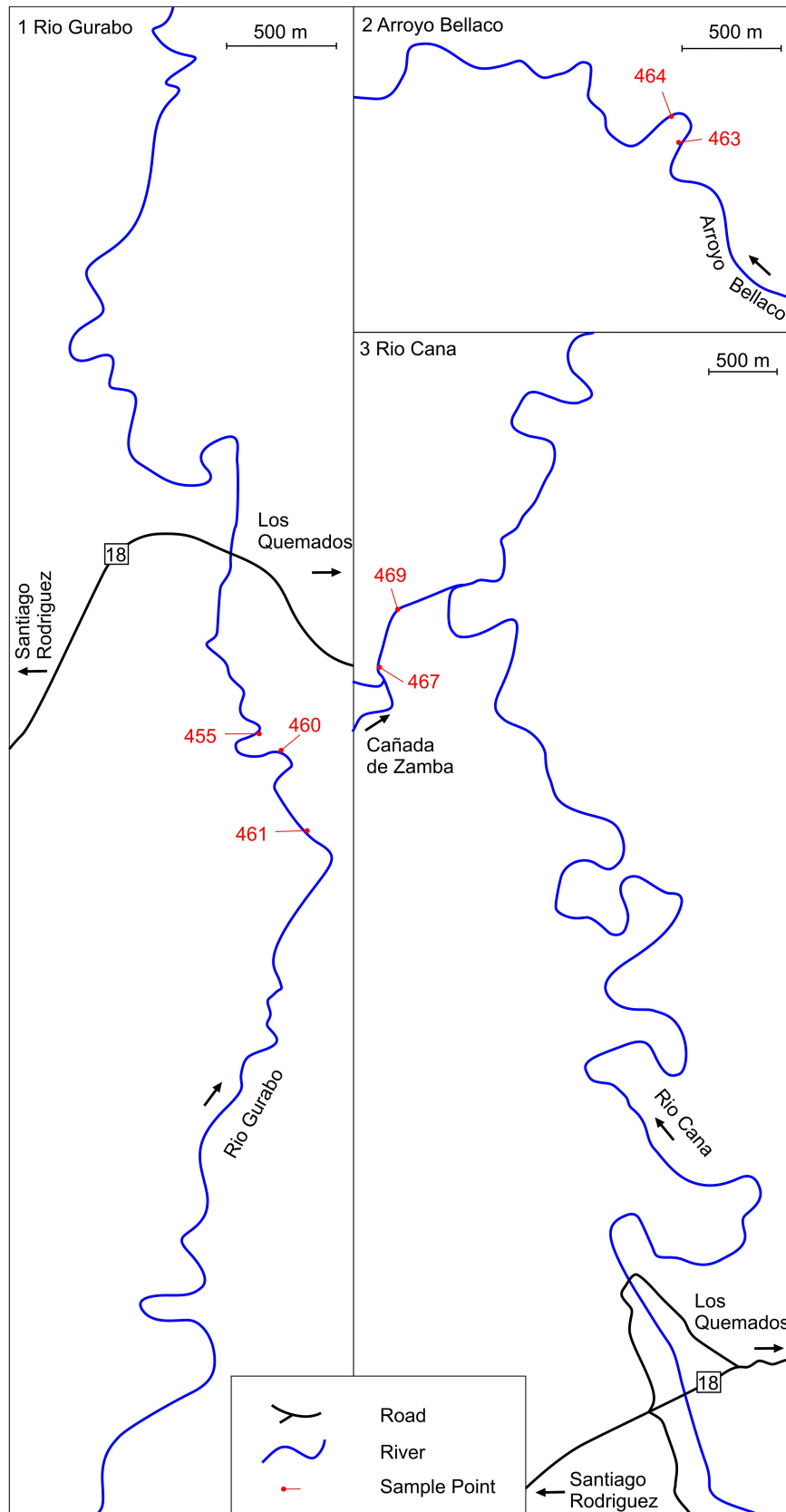


Figure 24: Sample locations in the tributary rivers Rio Gurabo (1), Arroyo Bellaco (2) and Rio Cana/Cañada de Zamba (3) in the Cibao Valley from Fig. 23

150-175 m and therefore belonging to the Cercado Formation (Fig. 20). A *Pocillopora* reef from this outcrop is also described (Reuter *et al.*, 2011).

At the base of the outcrop above the water level is a bed of at least 1.5 m thickness which consists in the lower part of branching corals (*Pocillopora*) with diameters of up to 10 cm and lengths of some dm with a fine silty and grey sediment between. In the upper 20 cm of this bank, also large amounts of branching corals occur but much smaller with lengths of approximately some cm to dm and diameters of only a few cm than in the lower part. The small branching corals are *Porites* and *Acropora*. The sediment between the corals is hard and carbonatic cemented. This bed is overlain by a fine silty sediment bed with a thickness of approximately one meter. It is characterized by a low abundance of biota and contains some bioturbation and lamination. At the contact of the lower *Pocillopora* bed and the upper fine silty sediment bed several massive grown corals (diameters up to 1 m) are deposited, from which some smaller were sampled (463 K1-K4). The fine layer is covered by some degrees north dipping sedimentary structures with sizes of some dm thickness and lengths of several meters. These seem to onlap on lower bed. This overlapping beds are composed of branches of *Pocillopora* and silty grey sediment between. Approximately 100 m down the river a *Pocillopora* reef (outcrop 464) is located (Reuter *et al.*, 2011). The branches there have lengths of up to a few meters and a thickness of approximately 10 cm. Between these sausage-like branches some other corals occur and were sampled (464 A, C and E).

**467** Outcrop 467 is located in Cibao Valley, Dominican Republic in the river valley of the Canada de Zamba, a tributary of the Rio Cana (Latitude: 19.5361000; Longitude: -71.3036667; Fig. 24). Within the commonly used stratigraphic column of the Panama Paleontology Project *Saunders, Jung, and Biju-Duval* (1986) it is located in the height of 335 m and therefore Gurabo Formation (Fig. 20).

The outcrop is an approximately 10 m tall flank of the river valley and the lower 2 m consist of a fine silty and grey sediment. Embedded are many fossils such as bivalves, gastropods, azooxanthellate corals, massive corals, foraminifera. Several corals (467 K1) and bivalves were sampled here.

**469** Outcrop 469 is located in Cibao Valley, Dominican Republic in the river valley of the Canada de Zamba, a tributary of the Rio Cana (Latitude: 19.5411333; Longitude: -71.3027667; Fig. 24). Within the commonly used stratigraphic column of the Panama Paleontology Project from *Saunders, Jung, and Biju-Duval* (1986) it is located in the height of 348 m and therefore Gurabo Formation (Fig. 20).

The outcrop is located some hundred meters beside outcrop 467 and here in the same stratigraphic unit, the fine silty sediment. The sediment is dipping some degrees toward north. Above this bed, yellow silty and sandy sediments with a minimum thickness of 10 m appear. Massive corals occur here condensed to a reef within an approximately 4 m large boulder within the lower fine silty layer. The corals are probably pseudo in-situ and different preserved so that it was decided to sample only some well preserved small corals (corals 469 A, M, N and R).

**503** Outcrop 503 is located at the northern shore of Lago Enriquillo, Dominican Republic (Latitude: 18.5399167; Longitude: -71.7905500; Fig. 22). It is a Holocene reef system which is dried out due to a decrease of the lake level.

Outcropping is a perfect preserved reef of several hundred meters length and approximately 100 m visible width and several meters thickness. The uppermost corals are all altered by boring organisms and covered by layer, bivalve bearing sediments.

## 2.2 Diagenesis

Only a pristine aragonitic coral skeleton is suitable to reveal environmental parameters during the life time of the organism. It is easy to distinguish coral heads with a strong diagenetic influence from those with a small or no influence of diagenetic processes. Heavy recrystallization, higher density, overgrown or even totally filled porespace and an unnatural X-radiograph are typical hints for diagenetic alterations (e.g. *McGregor and Abram, 2008*). This is mostly due to the recrystallization of aragonite into calcite, both  $CaCO_3$ -crystals which can only be distinguished by their inter-atomic spacing (D-value). Not so easy is to separate small diagenetic influence from almost no diagenetic influence, because the sophisticated coral skeleton is almost intact.

Corals and coral slabs were investigated using different analytical methods in order to prove the preservation. Since coral skeletons form cyclic variations in density (growth bands), it is possible to visualize them in X-radiographs (*Knutson et al., 1972; Buddemeier et al., 1974*). Possible diagenetic changes in a large scale are visible in the X-radiographs as regions of higher density (precipitation or sedimentary infill) or lower density (dissolution). X-ray diffraction (XRD) was used to distinguish between the aragonitic and calcitic phase of the  $CaCO_3$ -skeleton. Any hints for calcitic content in the coralline skeleton is evidence for more or less intensive diagenetic alteration (e.g. (*Nothdurft and Webb, 2009; Griffiths et al., 2013*)). Additional scanning electron microscopy (SEM) was carried out to identify possible diagenetic precipitations, microbial activity or dissolution effects in smaller scales than the XRD detection limit.

## 2.3 Technical sample preparation for geochemical analyses

The coral heads were cleaned with fresh water. Covered and infiltrated sediment was retained for future micropaleontologic investigation. Thereafter the coral heads were cut along the axis of maximum growth parallel to the corallites. Slabs of equal thickness between 3 and 10 mm were cut. After cleaning the slabs, they were rinsed with deionized water and ultrasonicated in deionized water for 15 min each side downward to remove the saw dust. After drying for at least 24 hours at room temperature slabs were X-rayed in a SHR 50KV digital X-ray cabinet to visualize annual density couplets, growth perturbations and diagenetic alteration. These informations are important for the planning of the microsampling transects.

Internal chronologies were created by counting the annual density bands, distinguishable through the high density bands (HDB) and low density bands (LDB) which together form one annual couple of density bands (*Knutson et al., 1972*). With the X-ray images it is possible to measure annual skeletal growth rates and skeletal density (see chapter coral densitometry)

## 2.4 X-ray diffraction (XRD)

For powder X-ray diffraction sampling spots were selected at random and drilled with a Proxxon dental rose driller ( $\varnothing 3\text{ mm}$ ) to receive approximately 100 mg coral skeleton powder. Micro samples were used and as micro sample holders served aluminum discs with a diameter of 23 mm and a thickness of 1.5 mm. For small sample volumes, the disc has a cylindrical hole with a diameter of 6.8 mm and a depth of 0.75 mm. Coral powder was filled after grinding in an opaline mortar by hand for few minutes into the micro sample holders and pressed with a glass panel to receive a plain surface. The samples were measured with Rigaku MiniFlex diffractometer with a  $Co - K_{\alpha}$  tube (Phillips PW22XX 30 kV, 15 mA, fixed) with a vertical goniometer with  $2\Theta$  range of  $2 - 150^{\circ}$ . Most samples were measured due to a shorter measurement time from  $28 - 42^{\circ}$  ( $2\Theta$ ), at a step width of  $0.1^{\circ}$  and a preset

time of 1.0 s to reduce measurement time. Within these angle the 100 % intensity reflection angle of aragonite (3.396 Å;  $2\Theta = 30.54^\circ$ ) and calcite (3.035 Å;  $2\Theta = 34.28^\circ$ ) are located (Fig. 25). Prior to this method, some samples were measured over the full angle from 2-140° ( $2\Theta$ ) with a step width of 0.05° and a preset time of 1.0 s to test the significance of the small angle range measurement. The detection limit for calcite is 1%. Standards with known concentrations of aragonite and calcite were measured to compare the results.

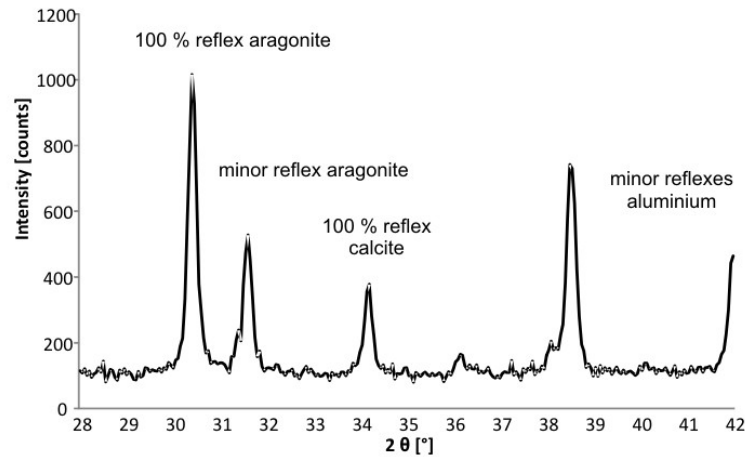


Figure 25: X-ray diffractogram of a powder standard composed of 95 % of Aragonite and 5 % of Calcite measured with aluminium micro sample holder as described in the text. Calcite and Aragonite are well distinguishable.

## 2.5 Scanning Electron Microscopy (SEM)

For scanning electron microscopy samples were broken out of the coral head with a pair of tongs to achieve a fracture. Samples were affixed with a graphite covered polycarbonate upon a sample holder with a diameter of 12 mm which defined maximum sample size. The samples were gold coated until a thickness of 30 nm gold coverage was reached. For microscopy of the samples a CamScan Electron Optics with a range of 5-40 kV and a Nova NanoLab 200 with a range of 0.2-30 kV were used. The Nova is equipped with a Nova 200 132-10 EDX-detector. Samples were measured with 5 kV and mainly secondary electrons were detected for gathering topographic information (Secondary Electron Images (SEI)). Some pictures also show backscatter electron images, which are calculated by detecting emitted electrons which are reflected by the samples' surface and called Backscattered Electron Images (BEI).

## 2.6 Microsampling for stable isotope measurements

Samples for  $\delta^{18}O$  and  $\delta^{13}C$  Isotope Ratio Mass Spectrometry (IR-MS) analysis were taken using a Proxxon micro drill which is fixed to a Proxxon x-y-z-drill table with the possibility to move the sample versus the driller in x-, y- and z-direction with an error of less than 0.05 mm. Before sampling, septae in the corallites chosen for microsampling were removed using a Proxxon dental drill equipped with a rose-head bur. The exposed theca-wall of the corallite was drilled with the Proxxon micro drill equipped with a 0.8 mm diameter driller in a distance of 0.7 mm to avoid pillars between the boreholes which would mean a loss of resolution. The penetration depth of the micro-boreholes in the theca wall was 0.5 mm. The emerging coral powder was sucked up with a disposable pipette and decanted into a vial. Total amount of sample powder for each sample was between 20 – 50  $\mu g$ . Before the



next sample was drilled, the coral skeleton was cleaned with compressed air to remove all powder from the preceding sample.

## 2.7 Oxygen and carbon isotope measurements

Carbonate powder samples for  $\delta^{18}O$  and  $\delta^{13}C$  isotope ratios were measured at the Institut für Geophysik und Geologie, University Leipzig, at the Geozentrum Nordbayern, Friedrich-Alexander University Erlangen-Nürnberg and Institute of Geology and Mineralogy, University Cologne. In Leipzig the carbonate powder in glass vials were reacted with 105 % phosphoric acid at 70 °C using a Kiel IV carbonate preparation line connected to a MAT 253 mass spectrometer. In Erlangen carbonate powder was reacted with 100 % phosphoric acid at 75 °C using a Kiel III carbonate preparation line connected online to a ThermoFinnigan 252 mass spectrometer. In Köln carbonate powder was reacted with 100 % phosphoric acid at 75 °C using a Kiel IV carbonate preparation line connected online to a ThermoFinnigan 253 mass spectrometer. All values are reported in permil relative to V-PDB by assigning a  $\delta^{13}C$  value of +1.95 ‰ and a  $\delta^{18}O$  value of -2.20 ‰ to NBS 19. Reproducibility was checked by replicate analyses of laboratory standards and is better than  $\pm 0.04$  ‰ for  $\delta^{13}C$  and better than  $\pm 0.08$  ‰ for  $\delta^{18}O$  in Leipzig. Reproducibility of analyses of laboratory standards in Erlangen is better than  $\pm 0.03$  ‰ for  $\delta^{13}C$  and better than  $\pm 0.06$  ‰ for  $\delta^{18}O$ . The standard deviation of the standards in Köln was better than  $\pm 0.05$  ‰ for  $\delta^{13}C$  and better than  $\pm 0.12$  ‰ for  $\delta^{18}O$ .

The isotopic data are expressed in delta notation relative to the Vienna Pee Dee Belemnite standard  $CO_2$  (V-PDB).  $\delta$  is the per mil isotopic ratio enrichment in a sample relative to the standard as described by the following equations (*Craig, 1953*):

For oxygen isotopes:

$$\delta^{18}O \text{ [‰]} = \frac{(\delta^{18}O/\delta^{16}O)_{sample} - (\delta^{18}O/\delta^{16}O)_{standard}}{(\delta^{18}O/\delta^{16}O)_{standard}} \times 1000 \quad (7)$$

And for carbon isotopes:

$$\delta^{13}C \text{ [‰]} = \frac{(\delta^{13}C/\delta^{12}C)_{sample} - (\delta^{13}C/\delta^{12}C)_{standard}}{(\delta^{13}C/\delta^{12}C)_{standard}} \times 1000 \quad (8)$$

Negative values for  $\delta$  indicates that the sample is enriched with lighter isotopes ( $^{16}O$  or  $^{12}C$ ) compared to the standard gas. Positive values stand for a sample enriched with heavier isotopes ( $^{18}O$  or  $^{13}C$ ) compared to the standard gas. All values represent relative abundance variations only (*Craig, 1953*).

## 2.8 Coral densitometry

For measurements of coral skeletal densities, the described coral slabs were radiographed using a set of different exposure conditions (25-50 kV, 250-900  $\mu$ A, 60 s). The digital images could display only a field with an diameter of 10 cm. Within this field the x-rays are not equally intensive and make it necessary to use only the inner 5 cm of the images. For larger coral slabs (like 452K1 S6) several pictures were taken under the same conditions and weld together in a graphic program and analyzed with the software CoralXDS 3.0 (Coral X-radiograph Densitometry System from *Helmle et al., 2002*). To calculate density

values from the grey values of the coral images it is necessary to calibrate the software. For this calibration a wedge of aluminium has to be X-rayed under the same conditions as the coral slab and also an aluminium plate with the same thickness as the coral slab has to be radiographed and used as background image, welded together exactly like the coral slab image if necessary (Fig. 26). Because of the quadratic decreasing of X-rays with an increasing thickness of a material and the known ratio of aragonite and aluminium in the X-ray absorption this calibration needs to be performed for every coral slab thickness. The accuracy of the thickness for coral slabs and the aluminium plates is  $\pm 0.05$  mm, for the aluminium wedge  $\pm 0.01$  mm.

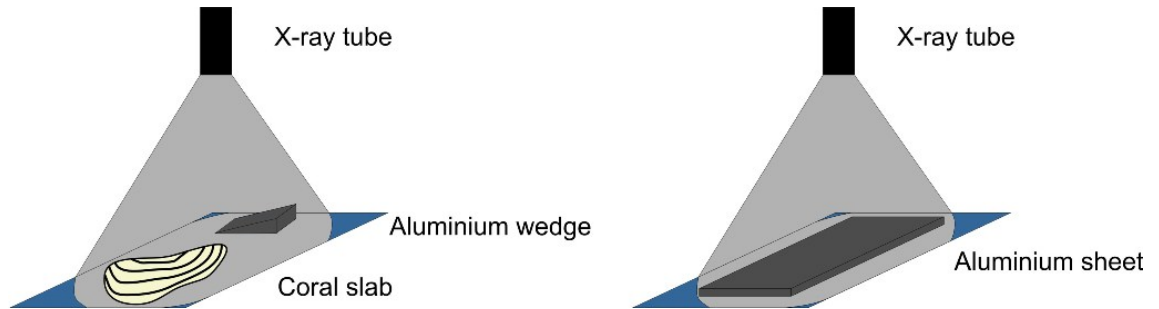


Figure 26: Calibration procedure of the X-ray system for coral densitometry. Aluminium wedge and aluminium sheet in the same thickness as the coral slab are required to calculate skeletal densities.

## 2.9 Resampling, rescaling and splicing of transects

Usually one coral slab with its HDBs and LDBs is represented by several parallel corallites which are cut along their axis of maximum growth. Due to slight changes of the direction of growth which occur in all coral colonies, single corallites are cropping out of the slab's surface and other corallites are dipping into the slab's surface – nearly never one corallite is cut along the coral slab continuous from the base to the colony surface. Therefore, to achieve a continuous  $\delta^{18}O$  record of the life-time of the coral colony, parallel corallites which are overlapping are sampled and the  $\delta^{18}O$  results are spliced together for an integrated time record of the whole coral slab (Fig. 27).

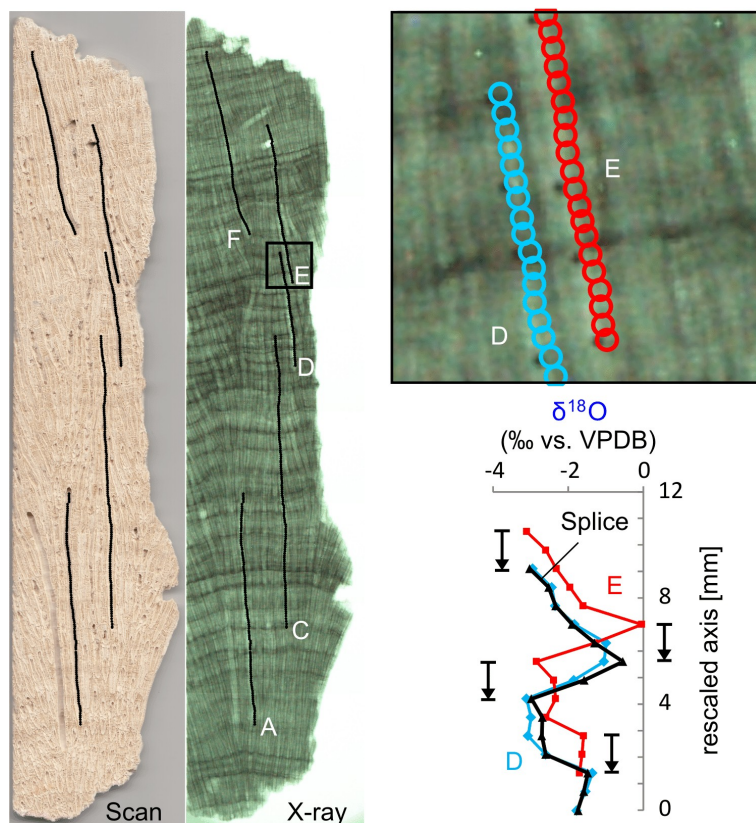


Figure 27: Example for sampling of different overlapping transects (A-F) in visual light and x-radiation in coral slab 452K1 S6. Data in overlapping areas are spliced together as described in text.

For splicing coral  $\delta^{18}O$  records the software AnalySeries (Paillard *et al.*, 1996) was used. Prior to splicing together, transect  $\delta^{18}O$  data were resampled at equal distances (settings: interpolation type - integrational; function type - linear) in the same resolution as they were before. Thereafter, equal distant transects were rescaled using the first transect as reference and rescale the other transects while allocating the  $\delta^{18}O$ -minima and maxima from two overlapping transects (Fig. 27). AnalySeries calculates a new scale for the distorted transects progression to the reference transect (rescaled axis). This step was repeated for every following transect with the use of the anterior transect as reference for rescaling. To eliminate an overlapping but still fragmented  $\delta^{18}O$  transect for the whole coral slab, the average of every overlapping couple of  $\delta^{18}O$ -values was calculated.

## 2.10 Laser ablation ICP mass spectrometry

Samples for Laser Ablation Inductively Coupled Plasma Mass Spectrometry (LA-ICP-MS) were taken from the theca wall of a neighboring corallite parallel to the corallites from the  $\delta^{18}O$  and  $\delta^{13}C$  measurements. Laser ablation measurements were carried out at the Max Planck Institute for Chemistry in Mainz. Targets for laser ablation were predefined in a distance of 0.5 mm using a spot diameter of 80  $\mu\text{m}$ . Laser ablation analyses were done using a 213 nm Nd:YAG laser (NewWave UP 213 Laser Ablation System), where ablation in the New Wave Large Format Cell was carried out in a helium atmosphere (approximately 0.65 l/min). Ablated material was immediately flushed away by the helium flow and introduced into a coupled ThermoFisher Element2 ICP-MS where a plasma torch ionized the sample-gas and deflect it by magnetic fields for normal mass spectrometry. Blanks (20 s) were measured prior to each single-spot analysis and used for correcting the

measured sample ion intensities. The dwell-time was set to 70 s. The isotopes measured were  $^{11}\text{B}$ ,  $^{25}\text{Mg}$ ,  $^{29}\text{Si}$ ,  $^{43}\text{Ca}$ ,  $^{66}\text{Zn}$ ,  $^{88}\text{Sr}$ ,  $^{85}\text{Rb}$ ,  $^{89}\text{Y}$ ,  $^{90}\text{Zr}$ ,  $^{95}\text{Mo}$ ,  $^{111}\text{Cd}$ ,  $^{137}\text{Ba}$ ,  $^{139}\text{La}$ ,  $^{140}\text{Ce}$ ,  $^{141}\text{Pr}$ ,  $^{146}\text{Nd}$ ,  $^{147}\text{Sm}$ ,  $^{151}\text{Eu}$ ,  $^{157}\text{Gd}$ ,  $^{159}\text{Tb}$ ,  $^{163}\text{Dy}$ ,  $^{165}\text{Ho}$ ,  $^{167}\text{Er}$ ,  $^{169}\text{Tm}$ ,  $^{173}\text{Yb}$ ,  $^{175}\text{Lu}$ ,  $^{208}\text{Pb}$ ,  $^{232}\text{Th}$  and  $^{238}\text{U}$ . Laser spots with a diameter of  $80\ \mu\text{m}$  were produced at an energy density (fluence) of  $\sim 12.5\ \text{J} \times \text{cm}^{-2}$  using a repetition rate of 10 Hz. Detection time per isotope was 0.002 s with counting mode and analog mode. Mass window was 10 % and  $^{43}\text{Ca}$  was used for internal standardization. For calibration the reference glass NIST 612 (Jochum *et al.*, 2011) was used and measured twice at the beginning, every 30 laser spots and at the end.

## 2.11 Spectral Analyses

Spectral analyses were performed using the software Past (Hammer *et al.*, 2001). Prior to analysis, data sets were transformed using regular interpolation to achieve equidistant values. Sample positions without values (not enough sample powder and outliers) were ignored and linear interpolation method was used. The new sample number was held constant with the original or was downgraded to have comparable values between data sets with a different spatial resolution. For the REDFIT spectral analyses of the stable isotopes and skeletal density were the settings as follows: oversample at 2, segments at 3 and window at rectangle. Additionally the  $\delta^{18}\text{O}$  signals were short-time Fourier transformed with the window set to multitaper 5.

### 3 Results

Stable Isotope ratios of oxygen and carbon ( $\delta^{18}O$  and  $\delta^{13}C$ ) were measured at two corals of the genus *Solenastrea* from southern Florida which derive from the sample points 452 and 509. In addition, two corals from the Dominican Republic were investigated. One *Monstastrea* from the Gurabo Formation (site 455) and one *Stephanocoenia* from the Cercado Formation (site 464).

#### 3.1 452K1 *Solenastrea* Hennessy Airport Quarry, DeSoto, Florida

From outcrop 452 a coral of the genus *Solenastrea* was collected. The stratigraphic unit is the Caloosahatchee Formation.

##### 3.1.1 Preservation

The preservation of the coral was tested using the methods described in chapter Materials and Methods. According to XRD, only aragonite and no calcite was detected. The preservation investigations with X-ray diffraction to test the coral slabs for diagenetic influence show in two measured areas in the coral 452K1 only the aragonite phase and no detectable calcite. Under the scanning electron microscope (SEM) is observable a mainly pristine skeleton in the *Solenastrea* 452K1 (Fig. 28). In some pore spaces of the coenosteum are isolated patches of (secondary) acicular aragonite covering the primary aragonite with sizes of approximately one  $\mu\text{m}$  in width and up to 50  $\mu\text{m}$  in length. In one single pore space blocky magnesium-carbonate is present (Fig. 28) (*Schroeder and Purser, 1986*). All these are common shallow-marine reef cements (*MacIntyre, 1977; Nothdurft and Webb, 2009*). The coral heads outer margin is approximately 3 mm in thickness bleached. This somehow altered rim of the coral head was also investigated and still showed a pristine skeleton but with the surface covered completely by fibrous aragonite rod cements of some micrometers in thickness. Also some clusters of framboidal pyrite with a constant diameter of 10  $\mu\text{m}$  show up coeval and/or after the secondary aragonite fibres, as EDX detected Fe and S. Even if XRD suggests 100 % aragonite it is not necessary to have this all as pristine aragonite. It is also possible that secondary aragonite is precipitated on the skeletons surface (*McGregor and Abram, 2008; Sayani et al., 2011*).

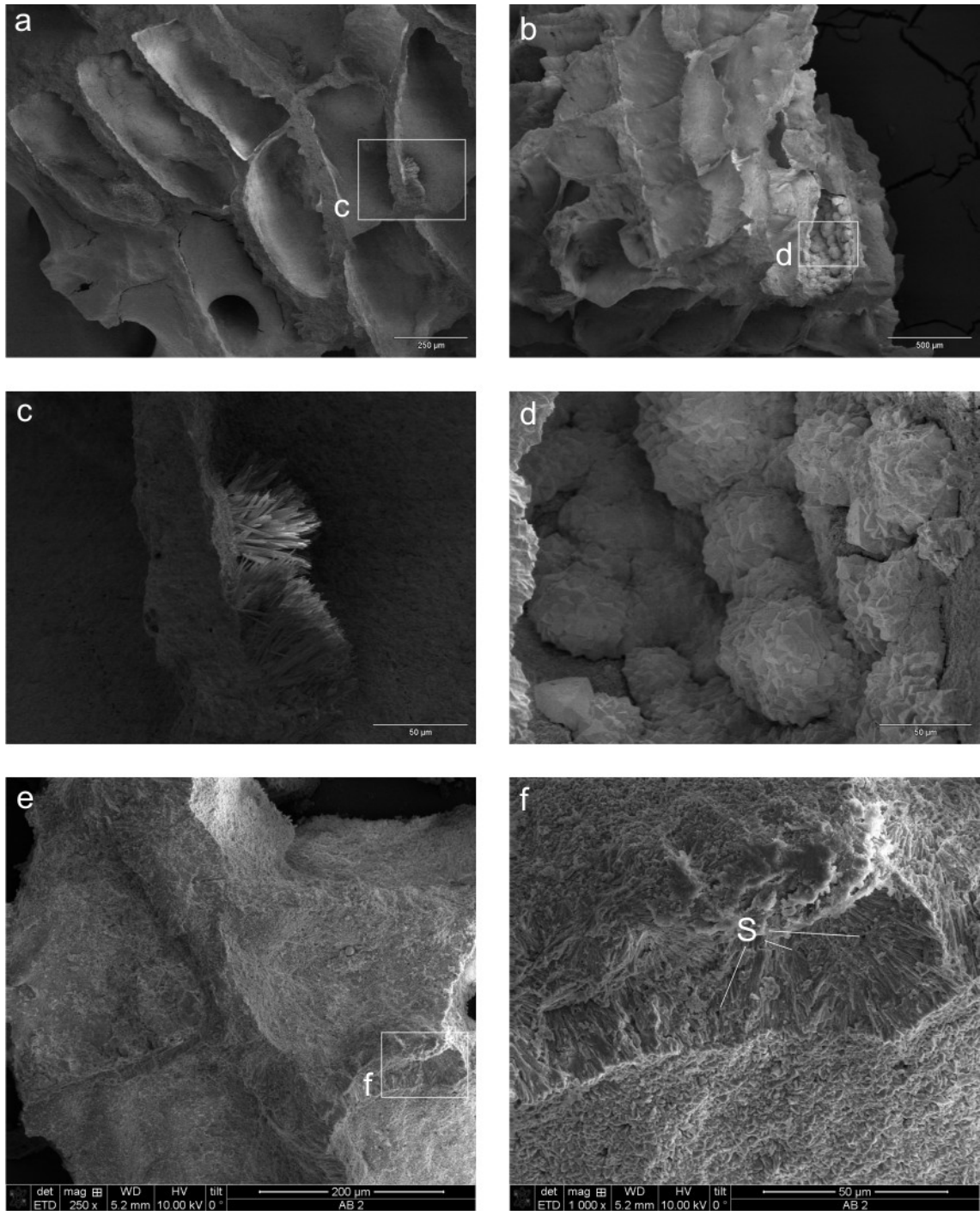


Figure 28: Scanning electron microscopy images from two areas within *Solenastrea* 452K1. Pictures a-d are taken from inner parts of the coral head, pictures e and f are taken from the outer rim of the coral head. The coral skeleton is in wide areas free of diagenetic overgrowth and dissolution (a and b). Close-ups show minor volumes of secondary acicular aragonite (c) and blocky magnesium-carbonate (d). (e) Fractured dissepiment showing sclerodermites (f) Enlargement of the sclerodermites and hardly visible solution effects (S).

From locality 452 six corals were investigated for diagenetic alteration and all are found similar diagenetic textures. All skeletal structures are preserved and in a few pore spaces some cements are found.

### 3.1.2 Oxygen and Carbon Stable Isotope Composition

In the *Solenastrea* 452K1 S6 five transects were sampled along the direction of maximum growth. In total 432 samples for  $\delta^{18}O$  and  $\delta^{13}C$  were measured in this coral. The  $\delta^{18}O$  values range from  $-4.36\text{‰}$  to  $0.65\text{‰}$ , which is a range of  $5.01\text{‰}$ . The mean is  $-2.24 \pm 0.84\text{‰}$  (median:  $-2.37\text{‰}$ ). The  $\delta^{13}C$  values range between  $-4.14\text{‰}$  and  $-0.26\text{‰}$ , which is a range of  $3.9\text{‰}$ . The mean is  $-1.69 \pm 0.56\text{‰}$  (median:  $-1.67\text{‰}$ ). After resampling and splicing the transects together to one masterseries, a total of 316 recalculated sample points remain (see chapter 2 for details). The spliced  $\delta^{18}O$  signal is oscillating with uniform frequency with 36 minima and maxima. The  $\delta^{18}O$  minima have a quite constant and broad valley with little interruptions by smaller maxima (usually one). The maxima are sharp and thin, which produces a pattern like church-windows (Fig. 29). The average values of these 35 minima are  $-3.1 \pm 0.28\text{‰}$  (median  $-3.06\text{‰}$ ). The range of the minima is  $1.4\text{‰}$  from  $-3.84$  to  $-2.44\text{‰}$ . The average value of the 36 maxima are  $-1.02 \pm 0.46\text{‰}$  (median  $-1.08\text{‰}$ ) and the range of the maxima is from  $-1.74\text{‰}$  to  $0.05\text{‰}$  (range of  $1.79\text{‰}$ ). The  $\delta^{13}C$  signal does not show a harmonic oscillation but is rather erratic. A correlation to the  $\delta^{18}O$  signal is not existent ( $r = -0.04$ ). In the same samples as the  $\delta^{18}O$  values the  $\delta^{13}C$  values spread around the mean without a clear correlation to the  $\delta^{18}O$  values within the cycles. In the  $\delta^{18}O$  minima, the  $\delta^{13}C$  ranges from  $-3.29\text{‰}$  to  $-0.72\text{‰}$  (total range  $2.57\text{‰}$ ) and the average of the 35  $\delta^{13}C$  values is  $-1.82 \pm 0.61\text{‰}$  (median:  $-1.76\text{‰}$ ). At the  $\delta^{18}O$  maxima, the 36  $\delta^{13}C$  values average at  $-1.70 \pm 0.44\text{‰}$  (median:  $-1.7\text{‰}$ ) and range from  $-2.81$  to  $-0.61\text{‰}$  (total range:  $2.2\text{‰}$ ). Both average  $\delta^{13}C$  values are less spread than the  $\delta^{18}O$  average values in respect to the range ( $\delta^{18}O$  averages difference:  $(-3.1\text{‰}) - (-1.02\text{‰}) = -2.09\text{‰}$ ;  $\delta^{13}C$  averages difference:  $(-1.7\text{‰}) - (-1.82\text{‰}) = -0.11\text{‰}$ ). Compared to the great range of  $\delta^{13}C$  values is there no statistically significant difference between the periodic averages.

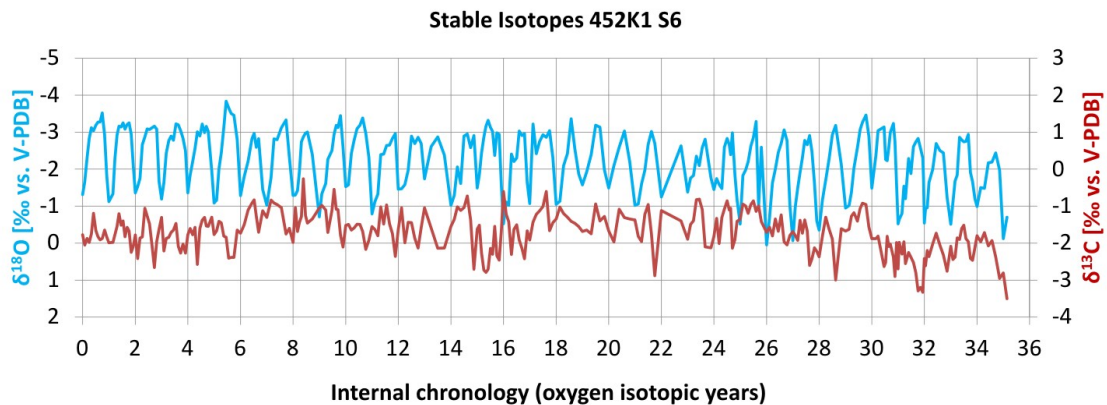


Figure 29: Masterchronology of stable isotope data for *Solenastrea* 452K1 from Florida.  $\delta^{18}O$  (blue) data oscillating while  $\delta^{13}C$  (red) is not correlating with former ( $r = -0.04$ ).

### 3.1.3 Main and Trace Element Composition

For LA-ICP-MS analyses, a 6 mm thick coral slab parallel to the coral slab which was previously sampled for  $\delta^{18}O$ -analyses (452K1 S6) was formatted to  $100 \times 50 \times 5\text{ mm}$  to fit into the sample chamber of the laser ablation system. The X-ray image of both coral slabs are compatible. The LA-ICP-MS track was oriented parallel to the  $\delta^{18}O$  sampling track in the axis of maximum growth, but not covering the whole distance as the  $\delta^{18}O$  transects (Fig. 30). The laser spots were aimed to hit the perpendicular cut theca wall of the truncated corallite. A full penetration of the theca wall in the coenchym beyond happened

in some samples and the theca wall could not always clearly identified as such during targeting the laser spots because of the uneven slabs surface which causes a defocussation in the small section. A spatial resolution of  $500\ \mu\text{m}$  corresponds to six to eighteen samples per year at an average annual growth rate of  $\sim 6\ \text{mm}$ . One laser ablation profile (AB) represents 116 laser spots within 8 years (HDBs) in the older part of the coral. In total the length of this transect is  $57.5\ \text{mm}$ . A second laser ablation profile (CD) with 30 laser spots was created for checking the reproducibility of the measured values parallel (ca.  $1\ \text{cm}$  aside) to the first laser ablation profile (AB) in a spatial resolution of  $0.5\ \text{mm}$  between the spots and a total length of  $15\ \text{mm}$ . Two other profiles were measured in the younger part of the coral. Profile EF consists of 65 laser spots in a spatial resolution of  $0.5\ \text{mm}$  and a length of  $33\ \text{mm}$  and adjacent profile GH with 140 laser spots because of the dipping of the EF-corallite, also  $0.5\ \text{mm}$  distance and a total length of  $70\ \text{mm}$  (Fig. 30). An age model was created on the basis of  $\delta^{18}\text{O}$  data together with annual density banding to provide an internally consistent time series for the laser ablation element transect. An additional line-measurement with a length of  $11\ \text{mm}$  was done with a change of diameter to  $40\ \mu\text{m}$  and a scan speed of  $10\ \mu\text{m}/\text{s}$ .

The measured values for the different isotopes vary for each isotope. The minor elements are calculated as Metall/Calcium ratio for being comparable to literature data. Selected element calcium ratios are plotted in Figure 31.

Since the laser ablation profiles AB and CD belong to the older part of the coral 452K1 and the profiles EF and GH belong to the younger part, the attached descriptions of the profiles are devised between those.

### Older part of the Coral 452K1 (Profiles AB & CD)

**Sr/Ca** The Sr/Ca signal in the coral slab 452K1 S5 shows a more or less cyclic pattern (Fig. 31). The values spread between  $7.3 - 8.7\ \text{mmol}/\text{mol}$  and average at  $7.94 \pm 0.27\ \text{mmol}/\text{mol}$  (Median:  $7.95\ \text{mmol}/\text{mol}$ ). The signal consists of eight maxima ( $\varnothing 8.4\ \text{mmol}/\text{mol}$ ) and nine minima ( $\varnothing 7.57\ \text{mmol}/\text{mol}$ ), where the highest amplitude is  $1.08\ \text{mmol}/\text{mol}$  and the mean amplitude  $0.82\ \text{mmol}/\text{mol}$ . Between those maxima and minima the signal is wiggled. Even if the curve is not smooth like the  $\delta^{18}\text{O}$  signal, it is possible to gain an age model referenced on Sr/Ca ratios which is used for all LA-ICP-MS data shown here and synchronized to the masterchronology ( $\delta^{18}\text{O}$ -years).

**Mg/Ca** Mg/Ca ratios were measured after a change in the Laser settings after 30 samples were already measured. Due to this, the signal is shorter than from the other measured elements. The Mg/Ca signal also shows a cyclic curve (Fig. 31). It's values spread between  $2.6 - 4.7\ \text{mmol}/\text{mol}$  and average at  $3.72 \pm 0.51\ \text{mmol}/\text{mol}$  (Median:  $3.80\ \text{mmol}/\text{mol}$ ). The signal consists of seven maxima ( $\varnothing 4.43\ \text{mmol}/\text{mol}$ ) and six minima ( $\varnothing 2.81\ \text{mmol}/\text{mol}$ ), where the highest amplitude is  $2.03\ \text{mmol}/\text{mol}$  and the mean amplitude  $1.6\ \text{mmol}/\text{mol}$ . The distinct cycles are characterized by a second maximum and a small minimum between the two maxima, while the minima are sharp and short. The Mg/Ca ratio has a significant anti-correlation with the Sr/Ca signal ( $r = -0.71$ ).

**B/Ca** The B/Ca signal shows a cyclic curve with pronounced maxima (Fig. 31). The values spread between  $0.34 - 0.54\ \text{mmol}/\text{mol}$  and average at  $0.41 \pm 0.04\ \text{mmol}/\text{mol}$  (Median:  $0.39\ \text{mmol}/\text{mol}$ ). The signal consists of nine maxima ( $\varnothing 0.49\ \text{mmol}/\text{mol}$ ) and nine minima ( $\varnothing 0.36\ \text{mmol}/\text{mol}$ ), where the highest amplitude is  $0.18\ \text{mmol}/\text{mol}$  and the mean amplitude  $0.13\ \text{mmol}/\text{mol}$ . Between the clear maxima in a cycle the areas of the



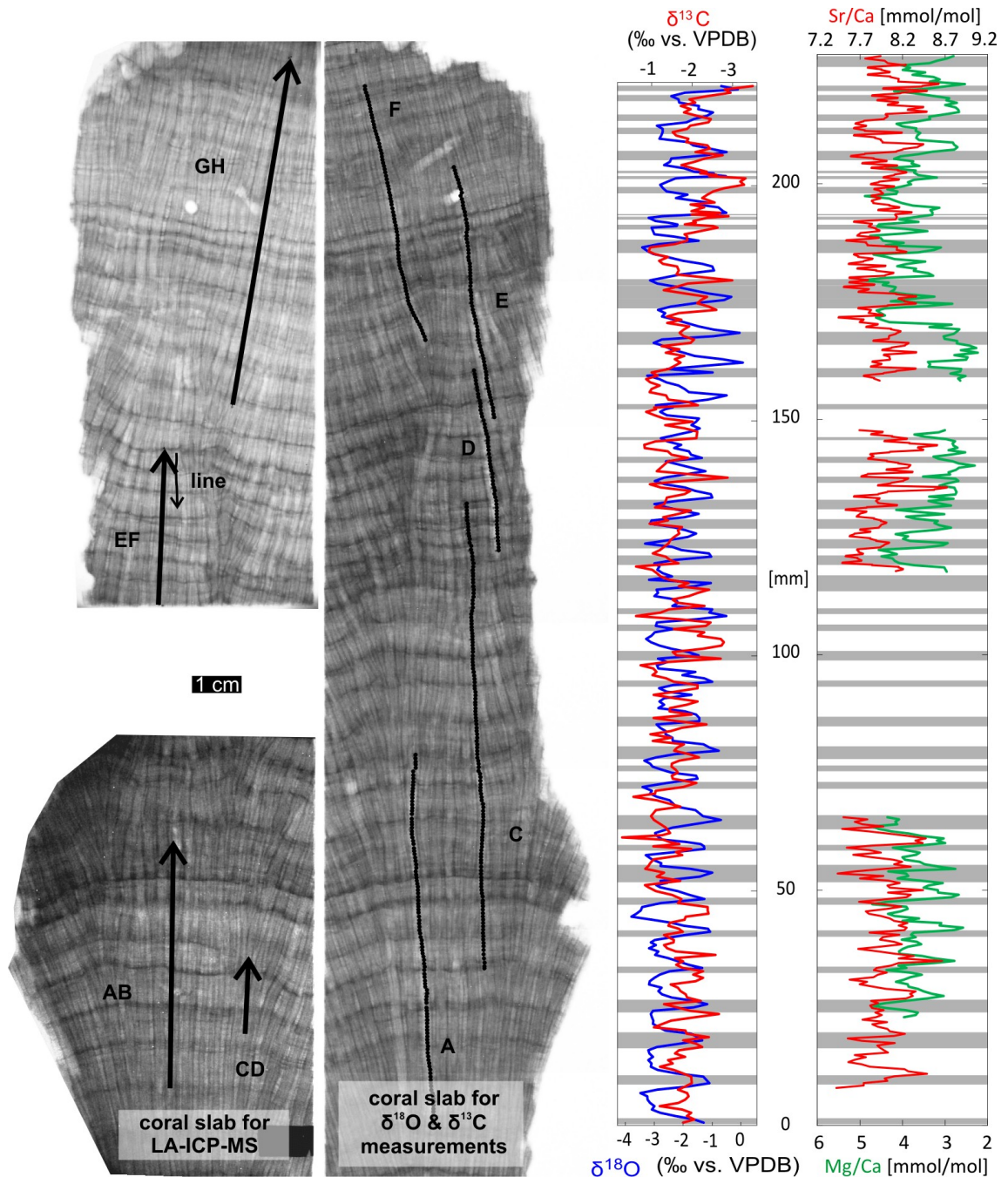


Figure 30: X-ray image of two parallel coral slabs from 452K1. The right slab (S6) was used for measurements of  $\delta^{18}O$  and  $\delta^{13}C$  isotopes (Transect A, C, D, E and F) while the left slab (S5) was used for LA-ICP-MS measurements (profiles AB and CD from 2011, EF and GH from 2013). Line-measurement was also carried out in 452K1 S5 parallel to profile EF. X-ray reveals a perfect correlation in density banding between the two slabs.

minima are shallow and broad. A weak anticorrelation to the Mg/Ca signal is observable ( $r = -0.48$ ).

**Ba/Ca** The Ba/Ca signal shows a more or less cyclic curve. The values spread between  $7.2 - 21.9 \mu\text{mol/mol}$  and average at  $12.8 \pm 3.5 \mu\text{mol/mol}$  (Median:  $12.4 \mu\text{mol/mol}$ ). The signal consists of eight maxima ( $\varnothing 19.1 \mu\text{mol/mol}$ ) and nine minima ( $\varnothing 8.6 \mu\text{mol/mol}$ ), where the highest amplitude is  $14 \mu\text{mol/mol}$  and the mean amplitude  $10.5 \mu\text{mol/mol}$  (Fig.

31). Between the maxima and minima the signal is uncalm with at least one minor minimum and maximum within one cycle.

**U/Ca** The U/Ca ratio correlates with the Ba/Ca signal ( $r = 0.86$ ). U/Ca ratios spread between  $1.0 - 3.4 \mu\text{mol/mol}$  and average at  $1.9 \pm 0.5 \mu\text{mol/mol}$  (Median:  $1.81 \mu\text{mol/mol}$ ). The signal consists of eight maxima ( $\varnothing 2.9 \mu\text{mol/mol}$ ) and nine minima ( $\varnothing 1.24 \mu\text{mol/mol}$ ), where the highest amplitude is  $2.25 \mu\text{mol/mol}$  and the mean amplitude  $1.64 \mu\text{mol/mol}$  (Fig. 31). Between the maxima and minima the signal is wiggled with at least one minor minimum and maximum within one cycle similar to the Ba/Ca ratio. Another correlation exists to the Sr/Ca ratio ( $r = 0.6$ ).

**Y/Ca** The Y/Ca ratio highly correlates to the U/Ca ratio ( $r = 0.9$ ) and to the Ba/Ca ratio ( $r = 0.8$ ). It can be described as a cyclic signal with distinct maxima and broad minima with several fluctuations and at least one minor maximum in a cycle. The values spread between  $0.12 - 0.39 \mu\text{mol/mol}$  and average at  $0.22 \pm 0.06 \mu\text{mol/mol}$  (Median:  $0.21 \mu\text{mol/mol}$ ). The signal consists of eight maxima ( $\varnothing 0.33 \mu\text{mol/mol}$ ) and nine minima ( $\varnothing 0.14 \mu\text{mol/mol}$ ), where the highest amplitude is  $0.26 \mu\text{mol/mol}$  and the mean amplitude  $0.18 \mu\text{mol/mol}$  (Fig. 31).

#### **Younger part of the Coral 452K1 (Profiles EF & GH)**

**Sr/Ca** The Sr/Ca signal in the profiles EF and GH shows a more or less cyclic pattern. The values spread between  $7.4 - 8.7 \text{mmol/mol}$  and average at  $7.96 \pm 0.24 \text{mmol/mol}$  (Median:  $7.94 \text{mmol/mol}$ ). The signal consists of 18 maxima ( $\varnothing 8.32 \pm 0.2 \text{mmol/mol}$ ) and minima ( $\varnothing 7.65 \pm 0.13 \text{mmol/mol}$ ), where the highest amplitude is  $1.0 \text{mmol/mol}$  and the mean amplitude  $0.67 \text{mmol/mol}$ . Between those maxima and minima the signal is wiggled. Even if the curve is not smooth like the  $\delta^{18}\text{O}$  signal, it is possible to gain an age model referenced on Sr/Ca ratios which is synchronized to the masterchronology ( $\delta^{18}\text{O}$ -years) (Fig. 31).

**Mg/Ca** The Mg/Ca signal in the younger part of the coral also shows a cyclic curve. It's values spread between  $2.2 - 5.0 \text{mmol/mol}$  and average at  $3.47 \pm 0.63 \text{mmol/mol}$  (Median:  $3.39 \text{mmol/mol}$ ). The signal consists of 18 maxima ( $\varnothing 4.1 \pm 0.6 \text{mmol/mol}$ ) and minima ( $\varnothing 2.8 \pm 0.29 \text{mmol/mol}$ ), where the highest amplitude is  $2.17 \text{mmol/mol}$  and the mean amplitude  $1.35 \text{mmol/mol}$ . The distinct cycles are characterized by a second maximum and a small minimum between the two maxima, while the minima are sharp and short. The Mg/Ca ratio has a significant anti-correlation with the Sr/Ca signal ( $r = -0.58$ ) (Fig. 31).

**B/Ca** The B/Ca signal shows a cyclic curve with pronounced maxima. The values spread between  $0.37 - 0.59 \text{mmol/mol}$  and average at  $0.46 \pm 0.05 \text{mmol/mol}$  (Median:  $0.45 \text{mmol/mol}$ ). The signal consists of 18 maxima ( $\varnothing 0.54 \pm 0.04 \text{mmol/mol}$ ) and minima ( $\varnothing 0.39 \pm 0.02 \text{mmol/mol}$ ), where the highest amplitude is  $0.20 \text{mmol/mol}$  and the mean amplitude  $0.15 \text{mmol/mol}$ . Between the clear maxima in a cycle the areas of the minima are shallow and broad. The correlation coefficient to the Mg/Ca signal is low ( $r = -0.13$ ) (Fig. 31).

**Ba/Ca** The Ba/Ca signal shows a more or less cyclic curve. The values spread between  $7.1 - 21.4 \mu\text{mol/mol}$  and average at  $13 \pm 2.7 \mu\text{mol/mol}$  (Median:  $12.8 \mu\text{mol/mol}$ ). The signal consists of 18 maxima ( $\varnothing 16.8 \pm 2.2 \mu\text{mol/mol}$ ) and minima ( $\varnothing 9.1 \pm 1.1 \mu\text{mol/mol}$ ),

where the highest amplitude is  $11 \mu\text{mol}/\text{mol}$  and the mean amplitude  $7.8 \mu\text{mol}/\text{mol}$ . Between the maxima and minima the signal is uncalm with at least one minor minimum and maximum within one cycle (Fig. 31).

**U/Ca** The U/Ca ratio correlates with the Ba/Ca signal ( $r = 0.81$ ). U/Ca ratios spread between  $0.88 - 3.8 \mu\text{mol}/\text{mol}$  and average at  $2.02 \pm 0.56 \mu\text{mol}/\text{mol}$  (Median:  $2.04 \mu\text{mol}/\text{mol}$ ). The signal consists of 18 maxima ( $\varnothing 2.7 \pm 0.44 \mu\text{mol}/\text{mol}$ ) and minima ( $\varnothing 1.24 \pm 0.25 \mu\text{mol}/\text{mol}$ ), where the highest amplitude is  $1.98 \mu\text{mol}/\text{mol}$  and the mean amplitude  $1.48 \mu\text{mol}/\text{mol}$ . Between the maxima and minima the signal is wiggled with at least one minor minimum and maximum within one cycle similar to the Ba/Ca ratio. The correlation coefficient between U/Ca and Sr/Ca ratio is low ( $r = 0.33$ ) (Fig. 31).

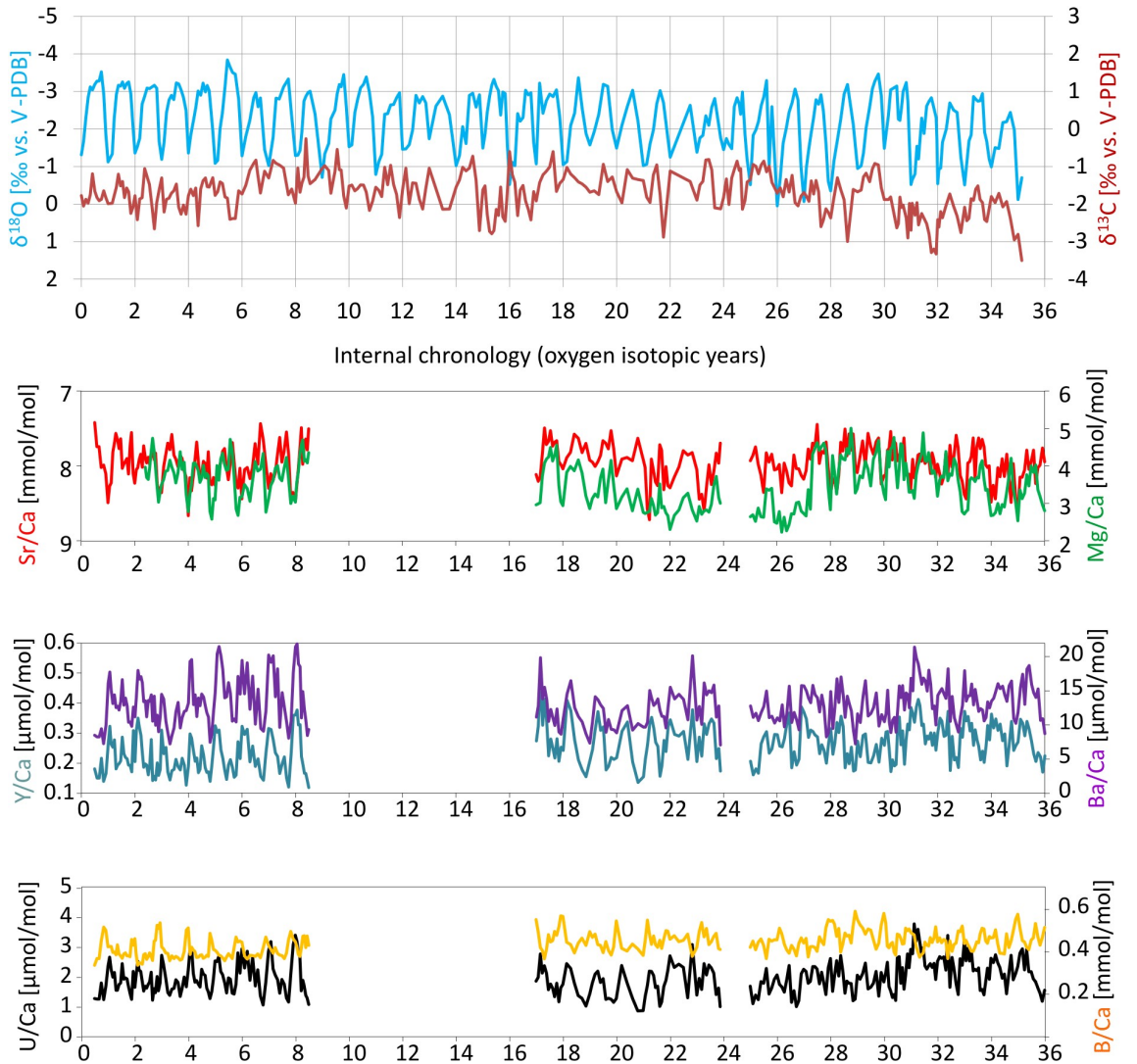


Figure 31: Comparison of selected element/calcium-ratios and stable isotope values in 452K1. All x-axis referenced on the internal masterchronology.

**Y/Ca** The Y/Ca ratio highly correlates to the U/Ca ratio ( $r = 0.85$ ) and to the Ba/Ca ratio ( $r = 0.76$ ). It can be described as a cyclic signal with distinct maxima and broad minima with several fluctuations and at least one minor maximum in a cycle. The values spread between  $0.14 - 0.48 \mu\text{mol}/\text{mol}$  and average at  $0.27 \pm 0.06 \mu\text{mol}/\text{mol}$  (Median:

0.28  $\mu\text{mol/mol}$ ). The signal consists of 18 maxima ( $\varnothing 0.37 \pm 0.04 \mu\text{mol/mol}$ ) and minima ( $\varnothing 0.18 \pm 0.03 \mu\text{mol/mol}$ ), where the highest amplitude is 0.28  $\mu\text{mol/mol}$  and the mean amplitude 0.18  $\mu\text{mol/mol}$  (Fig. 31).

**REE** The shale-normalized REE pattern shows in all four profiles an enrichment of HREE compared to LREE. A positive Eu and a negative Ce anomaly is present in all profiles. An increase in LREE in the younger profiles (EF & GH) compared to the older profiles (AB & CD) is evident. HREE in the older profiles are highly variable compared to the quite constant HREE composition of the younger profiles (Fig. 32).

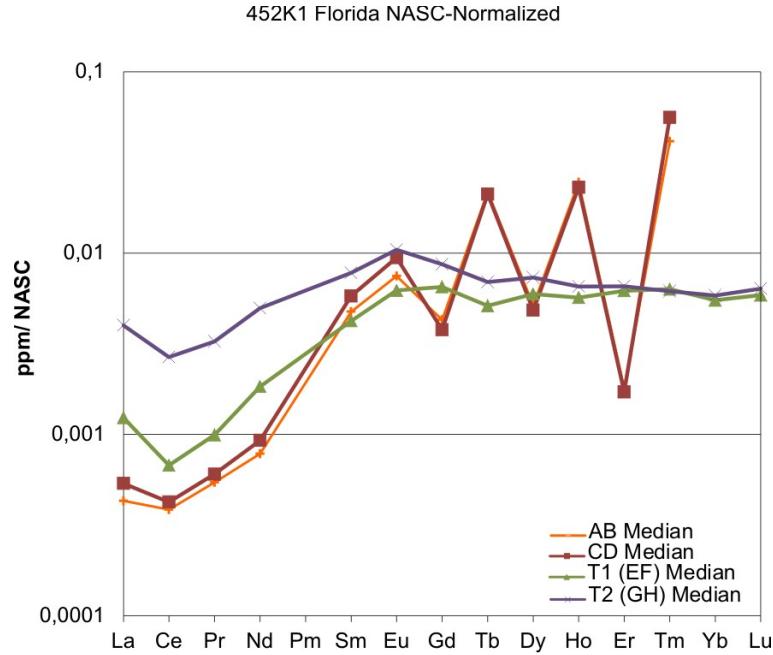


Figure 32: Shale-normalized REE patterns of the median-values of the four profiles AB, CD, EF and GH in *Solenastrea* 452K1 based on North American shale composite (NASC) (*Taylor and McLennan, 1985*).

**Line-Measurement** The measured line in *Solenastrea* 452K1 has a total length of 10.97 mm and a width of 40  $\mu\text{m}$  (Fig. 30). Scanning speed was set to 10  $\mu\text{m/s}$ . The measured elements are  $^{25}\text{Mg}$ ,  $^{43}\text{Ca}$ ,  $^{88}\text{Sr}$ ,  $^{89}\text{Y}$ ,  $^{137}\text{Ba}$  and  $^{238}\text{U}$ . The measured values show at least two superior cycles which correspond with the two HDBs crossed in the profile and the parallel running spot-profile EF (Fig. 33). The cycles are more pronounced in Ba/Ca, Mg/Ca, U/Ca and Y/Ca than in the quite constant Sr/Ca signal. All signals show an inferior cycle which is clearest in Sr/Ca and has a periodicity of approximately 5-6 repetitions (approx. 1 mm) per superior cycle. The absolute values for Sr/Ca range between 5.16 – 12.16  $\text{mmol/mol}$  and average at  $7.85 \pm 1.08 \text{mmol/mol}$  (Median: 7.77  $\text{mmol/mol}$ ), for Mg/Ca from 1.08 – 6.01  $\text{mmol/mol}$  and average at  $2.71 \pm 0.74 \text{mmol/mol}$  (Median: 2.67  $\text{mmol/mol}$ ), for Ba/Ca from 3.6 – 39.2  $\mu\text{mol/mol}$  and average at  $11.6 \pm 4.5 \mu\text{mol/mol}$  (Median: 10.7  $\mu\text{mol/mol}$ ), for Y/Ca from 0.08 – 0.86  $\mu\text{mol/mol}$  and average at  $0.27 \pm 0.12 \mu\text{mol/mol}$  (Median: 0.25  $\mu\text{mol/mol}$ ) and for U/Ca from 0.5 – 5.24  $\mu\text{mol/mol}$  and average at  $1.57 \pm 0.73 \mu\text{mol/mol}$  (Median: 1.4  $\mu\text{mol/mol}$ ).

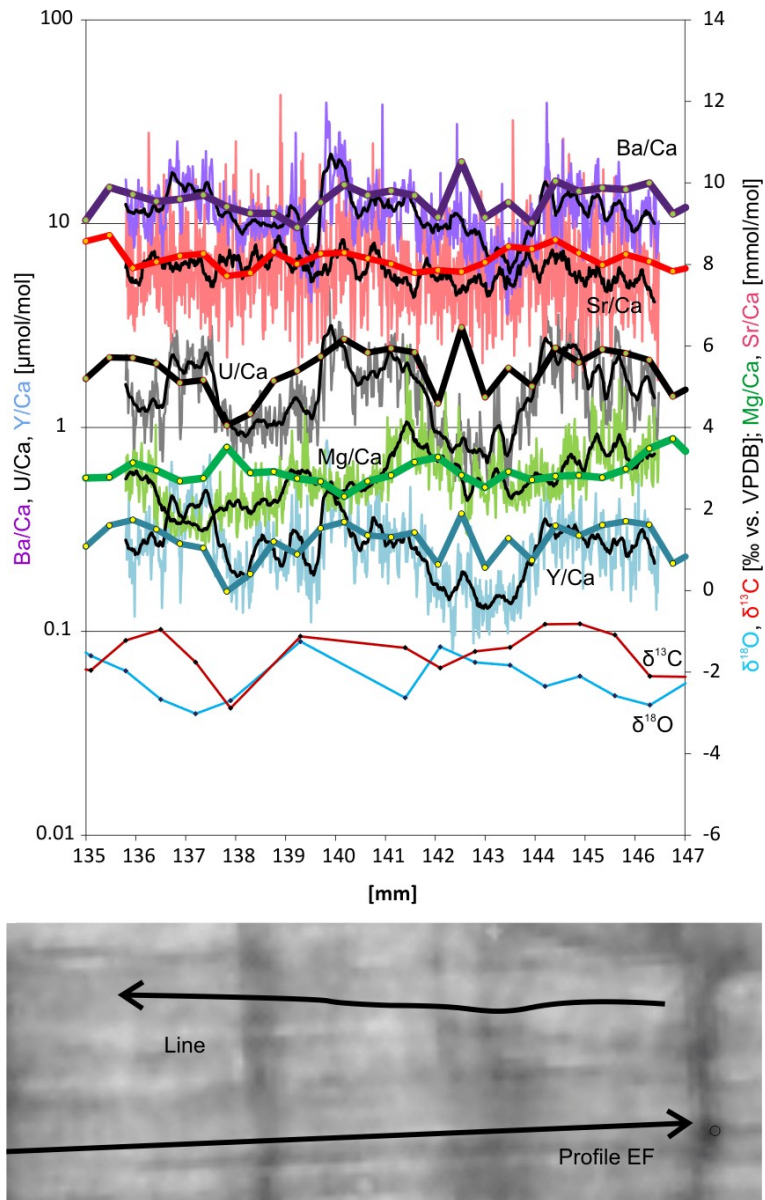


Figure 33: Line-measurement in *Solenastrea* 452K1. Metal/calcium ratios (colorful thin lines) with their running means (black thin lines) and spot-profile data (bold colorful lines) from neighboring profile EF for comparison and stable isotope data from the neighboring coral slab

### 3.1.4 X-radiography/Coral densitometry

The coral slab 452K1 S6 was radiographed with 40 KV, 800  $\mu$ A and an exposure time of 60s. Because of the length of 25 cm of the coral slab several pictures were taken under the same conditions and weld together in a graphic program. The same procedure needs to be done for the background images for density measurements. For 452K1 S6 the densities were measured for each transect close beside the drilling locations to have the highest possible correlation of density and stable isotope signal. The measured densities were resampled in the same resolution as the drilling holes for the stable isotopes and in the same way spliced to produce comparable data (Fig. 34). In total 432 samples for density were measured with the software CoralXDS (*Helmle et al., 2002*) in this coral. After resampling and splicing the transects together into one timeseries, a total of 316 recalculated sample points remained (Fig. 34). The density values range between 0.51 g/cm<sup>3</sup> and 1.0 g/cm<sup>3</sup>, which is

a range of  $0.49 \text{ g/cm}^3$ . The mean is  $0.73 \pm 0.09 \text{ g/cm}^3$  (median:  $0.71 \text{ g/cm}^3$ ). Despite two cyclic signals as density and  $\delta^{18}\text{O}$  there is no correlation between both ( $r = 0.05$ ). This is due to a change of the HDB formation within the coral slab.

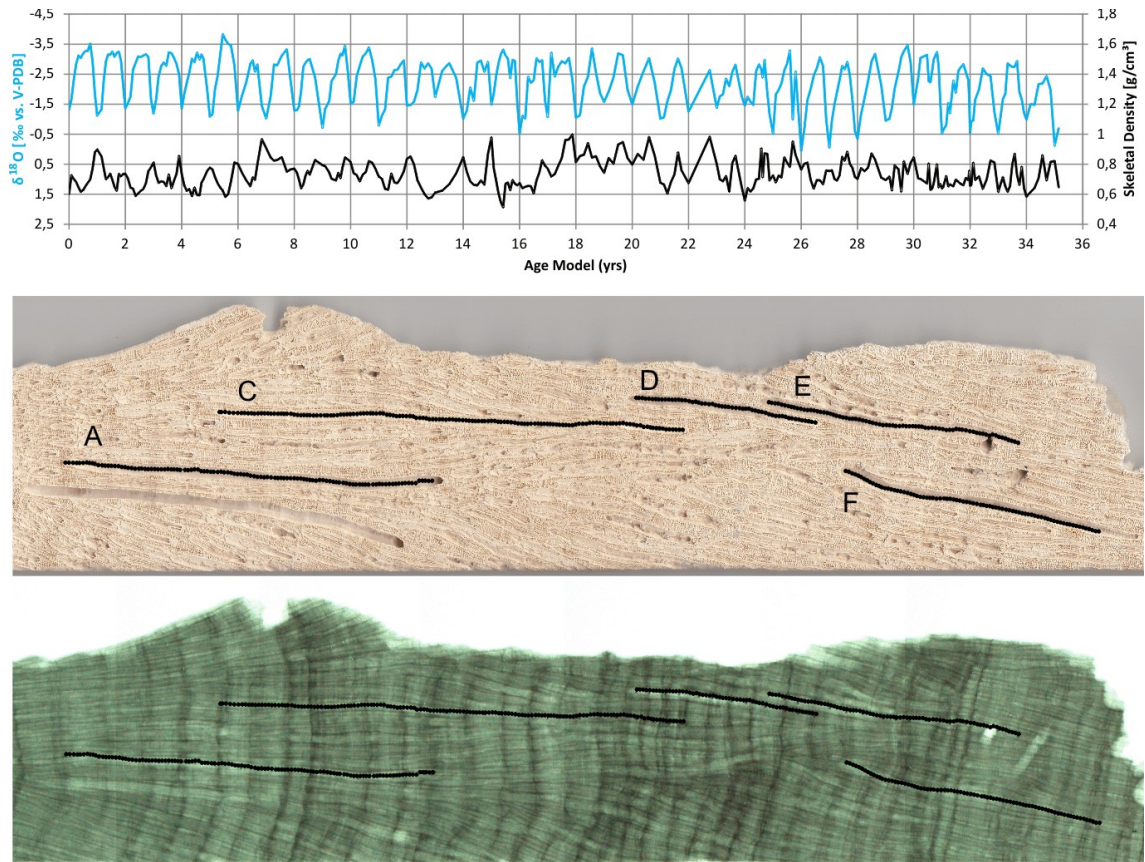


Figure 34: X-radiograph (bottom) and visible light image (middle) of *Solenastrea* 452K1 S6. Sample Transects A-F marked and the spliced  $\delta^{18}\text{O}$  and density measurements shown above. Growth direction from left to right. See text for details.

The coral slabs reveal a banding which is barely visible in visible light and well visible in the X-radiograph (Fig. 34). This banding pattern is interpreted as annual growth pattern and each HDB and the following LDB stand for one year of the corals life. For *Solenastrea* 452K1 were measured 55 couplets of HDBs and LDBs. For the X-radiograph the annual growth rate spreads ranges between  $4.78 \pm 1.88 \text{ mm/yr}$ . The values vary from 1.2–9.1 mm/yr.

### 3.2 452K14 *Solenastrea* Hennessy Airport Quarry, DeSoto, Florida

In slab 452K14 S6 eight overlapping transects were drilled with a total of 260 samples for stable isotope measurements. These samples could not be measured yet but other data as growth rate and skeletal density at the transects are available.

#### 3.2.1 Preservation

X-ray diffraction measured in one area in the coral 452K14 shows only the aragonite phase and no detectable calcite. The skeleton appears with all skeletal elements preserved and large volumes of interskeletal porosity. Along the rim of the coral head some yellow and brownish discolorations and sediment trapped inside skeletal porosity is existent (Fig. 35). In *Solenastrea* 452K14 a pristine skeleton is present and suitable for paleoclimate investigations.

#### 3.2.2 X-radiography/Coral densitometry

Along the transects several HDBs and LDBs are cut. The transect length totals 15.2 cm and encompasses 58 HDBs from which at least 20 seem to be halves of 10 dHDBs (Fig. 35). An unknown number of the other HDBs are likely also halves of dHDBs but cut in this slab not in a perfect way ( $\neq 90^\circ$  between HDBs and slabs surface) to reveal their true origin. Calculating a reliable growth rate is therefore impossible without independent age constraints and can give a range between two cases only (1) all dense bands are parts of dHDBs: 5.2 mm/yr and (2) only the visible 10 dHDBs are evaluated as such and the other HDBs are counted as years: 3.2 mm/yr.

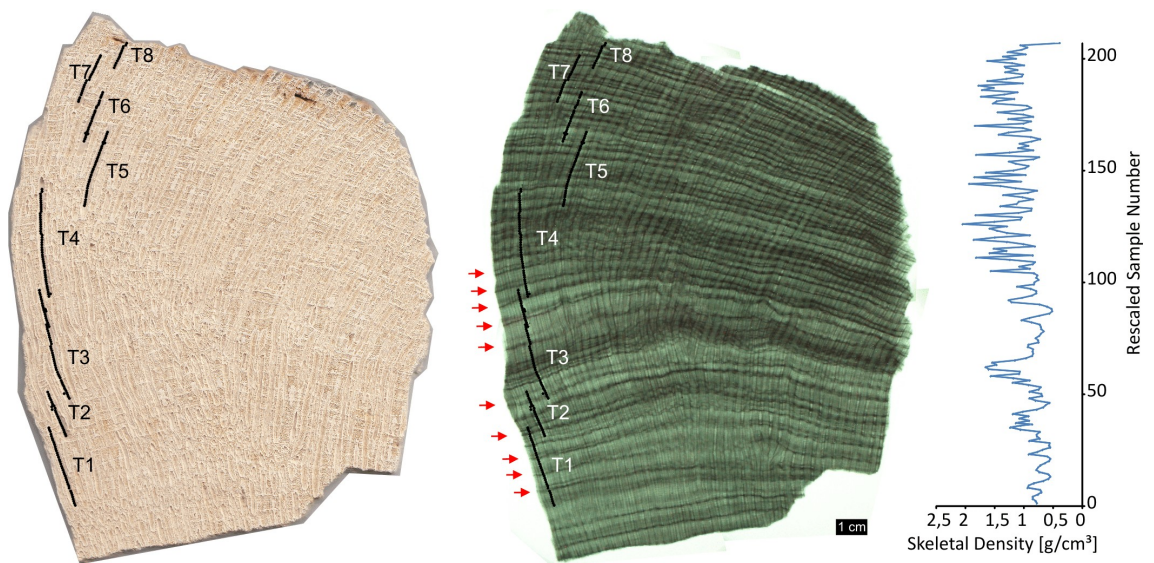


Figure 35: Visible light, X-ray and skeletal density for 452K14. In the lower part of the X-radiograph dHDBs are present (red arrows).

### 3.3 509A *Solenastrea* from an abandoned pit, Florida

The second coral of the genus *Solenastrea* from Florida was collected at outcrop 509 which consists of raised soil from an abandoned pit. It is probably the same stratigraphic unit as in locality 452 (see discussion). For both the geologic map of the state of Florida indicates shelly sediments of Plio-Pleistocene age, which is the Okeechobee Group. The sediments are part of the Pliocene fossil reef of southwest Florida and the locality is also described as a composite (Meeder, 1979). Due to the lack of direct numerical dates for this coral a finer stratigraphic classification is not possible.

#### 3.3.1 Preservation

The investigations with X-ray diffraction to test the coral slabs for diagenetic influence show in two measured areas in the coral 509A only the aragonite phase and in one sample mainly aragonite with trace of calcite ( $< 1\%$ ) at detection limit of method.

In small areas small dissolution holes with diameters not larger than  $2\ \mu\text{m}$  are observable. Samples of the somehow altered border (ca. 3 mm bleached rim) of the coral head show more diagenetic effects than samples from the central parts close to the stable isotope transect. These effects are sporadic framboidal pyrite with a diameter of  $3\ \mu\text{m}$ . EDX detects no Fe or S which is believed to be an effect of the angular orientation to the beam. Other effects are some isolated microborings in the length of several hundred  $\mu\text{m}$  which also occur close to the corals border (Fig. 36). All these are common shallow-marine reef cements (MacIntyre, 1977) (Constantz, 1986) (Nothdurft and Webb, 2009). *Solenastrea* 509A displays a skeleton in pristine preservation.



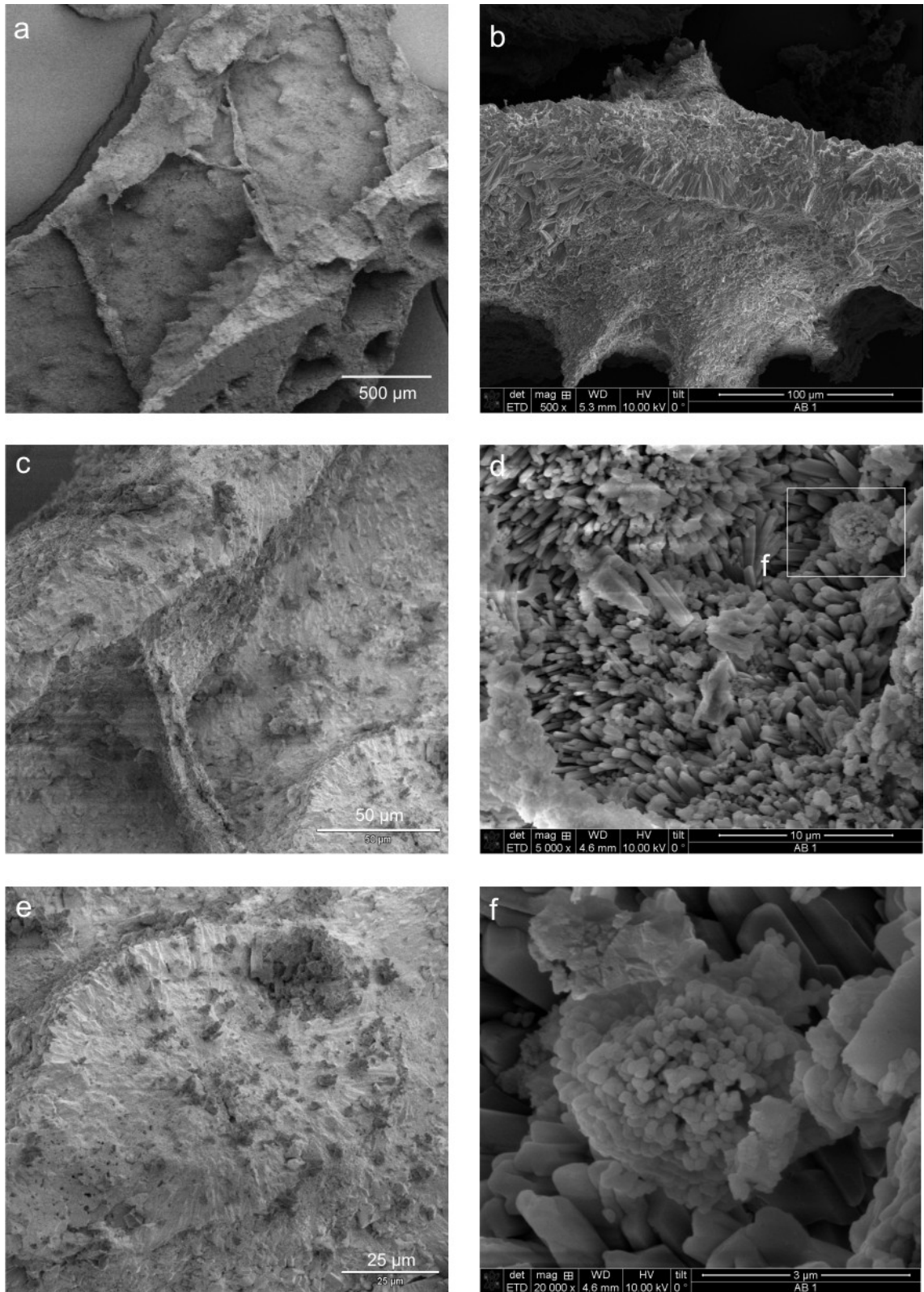


Figure 36: SEM images of coral head 509A. (a) Pore space is still open and pristine. (b) Fractured dissepiment from the bleached rim of the coral shows primary arrangement of sclerodermites (aragonite skeleton). (c) Fractured coenchym with dissepiment (d) Cover with secondary aragonitic cements (e) Primary arrangement of sclerodermites on fractured skeletal dentation with small dissolution holes (lower left). Dark "minerals" on the fracture are crumbs from the fracturing process which are lesser charged (f) Framboidal pyrite.

### 3.3.2 Oxygen and Carbon Stable Isotope Composition

In *Solenastrea* 509A S1 three transects were sampled along the direction of maximum growth of the corallites. A total of 196 samples for  $\delta^{18}\text{O}$  and  $\delta^{13}\text{C}$  was measured in this coral. The  $\delta^{18}\text{O}$  values range between  $-3.13\text{‰}$  and  $-0.48\text{‰}$ , which is a range of  $2.65\text{‰}$ . The mean is  $-2.05 \pm 0.5\text{‰}$  (*median* =  $-2.12\text{‰}$ ). The  $\delta^{13}\text{C}$  values range between  $-3.5\text{‰}$  and  $-1.61\text{‰}$ , which is a range of  $1.9\text{‰}$ . The mean is  $-2.48 \pm 0.45\text{‰}$  (*median* =  $-2.48\text{‰}$ ). After resampling and splicing the transects into one masterseries, a total of 186 recalculated sample points remain (see chapter 2 for details). The spliced  $\delta^{18}\text{O}$  signal is oscillating sharply with a more or less constant frequency and there were counted 62 different minima and maxima. The  $\delta^{18}\text{O}$  minima and maxima quite constant and are alternating in a short distance every 1-4 samples (Fig. 29, Fig. 38). The average values of these 62 distinct minima are  $-2.53 \pm 0.27\text{‰}$  (*median* =  $-2.53\text{‰}$ ). The range along the minima is  $1.2\text{‰}$  from  $-3.13$  to  $-1.91\text{‰}$ . The average values of the 62 distinct maxima are  $-1.56 \pm 0.36\text{‰}$  (*median* =  $-1.54\text{‰}$ ) and the range of the maxima is from  $-2.47\text{‰}$  to  $-0.48\text{‰}$  (range of  $2\text{‰}$ ). The  $\delta^{13}\text{C}$  signal is repeating the  $\delta^{18}\text{O}$  oscillation clearly.  $\delta^{13}\text{C}$  displays 58 couplets of minima and maxima which are in the same frequency as the  $\delta^{18}\text{O}$  variations. The  $\delta^{13}\text{C}$  maxima vary from  $-3.04\text{‰}$  to  $-1.61\text{‰}$  ( $\sigma = -2.09 \pm 0.32\text{‰}$ ) and the minima from  $-3.5\text{‰}$  to  $-2\text{‰}$  ( $\sigma = -2.91 \pm 0.26\text{‰}$ ). A cross-correlation to the  $\delta^{18}\text{O}$  signal is showing a correlation of  $r=0.42$  ( $r=-0.4$ ) at a lag of 1 (-1) sample. The cross-correlation also reveals a repetition of the correlation every four samples. Cross-correlation of the single transects (not spliced)  $\delta^{18}\text{O}$  and  $\delta^{13}\text{C}$  values, show for transect 1 the highest correlation for a lag of 1 (-1) of  $r=0.8$  ( $r = -0.71$ )(Fig. 37). Both isotope signals have a similar average difference between there maxima and minima. For all  $\delta^{13}\text{C}$  maxima and minima the difference is  $0.81\text{‰}$  and for all  $\delta^{18}\text{O}$  maxima and minima the average difference is  $0.96\text{‰}$ .

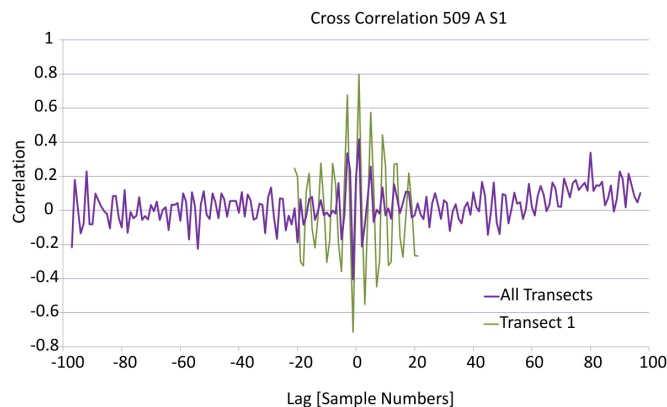


Figure 37: Cross Correlation of  $\delta^{18}\text{O}$  and  $\delta^{13}\text{C}$  in the coral 509A S1. With a lag of one sample the correlation is maximal. See text for details. Transect 1 separate shown to facilitate comparison of the cross-correlating two signals.

### 3.3.3 X-radiography/Coral densitometry

The coral slab reveals in the X-radiograph a clear banding which is in the lower and upper part very regular and closely spaced. In the middle part of the slab it becomes more diffuse and the distance between the bandings become much wider (Fig. 38). This pattern is due to a lateral slewing of the coral colony during growth and hence the X-rays do not pass through the HDBs orthogonally like in the lower part of the coral. All in all 37 HDB were counted along the three stable isotope transects. The distance between the HDBs varies from 1.5 to 7.5 mm (mean:  $3.6 \pm 1.5$  mm). The  $\delta^{18}\text{O}$  data show 62 cycles in the same

distance of 13 cm, which implies a mean annual growth rate of 2.16 mm/yr. The difference is due to the blurring HDBs in the central part at the X-radiograph because of an angle to the X-rays of not 90°. This leads to some unsharp and broad HDBs which truly consist of several more different HDBs which can not be depicted by X-radiography. This suggestion has been proved by computer tomography of this coral slice. In this case the  $\delta^{18}\text{O}$  values are more reliable for an age model.

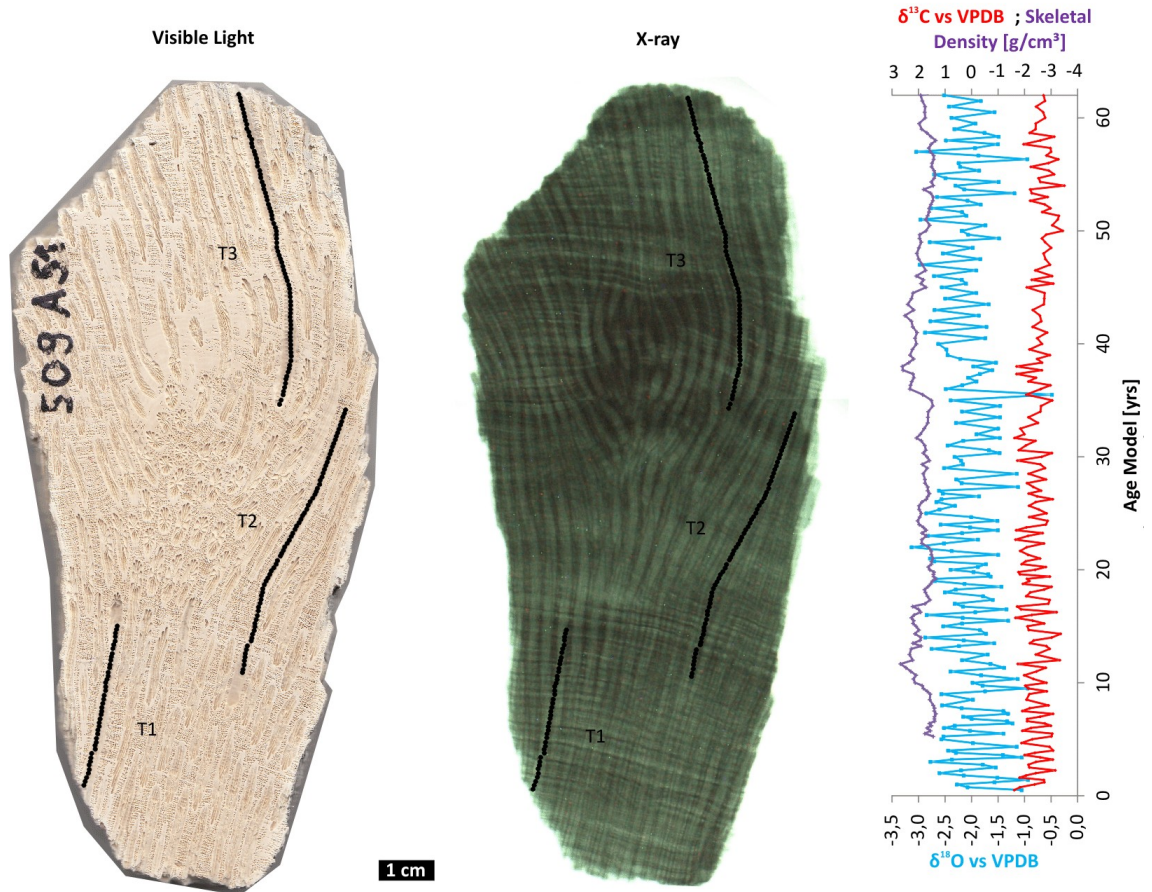


Figure 38: Visible light and X-radiograph image of 509A S1 *Solenastrea* coral slab.

The skeletal density at the three transects was measured with the following settings 7.5 mm thickness, 40 kV, 800  $\mu\text{A}$  and an exposure time of 60 s. The individual transects were resampled and spliced into a master transect in the same way as the stable isotope data. Due to the thinning of the slab, the the first 20 density values of T1 show unreliable values and were rejected for further analysis. Remaining 166 resampled and spliced density values vary between 1.2  $\text{g}/\text{cm}^3$  and 2.7  $\text{g}/\text{cm}^3$  ( $\bar{\rho} = 1.81 \pm 0.31 \text{ g}/\text{cm}^3$ ) (Fig. 38). A correlation between skeletal density and  $\delta^{18}\text{O}$  ( $r = 0.04$ ) and  $\delta^{13}\text{C}$  ( $r = 0.06$ ) is not present.

### 3.4 455C *Montastrea* Dominican Republic

Data from the coral 455C was sampled and described by *Lohmann* (2013) for his master thesis and should be also be considered herein. Additional SEM investigations were carried out by the author of this thesis.

### 3.4.1 Preservation

Eight measured samples with X-ray diffraction in the coral 455C show only the aragonite phase and no detectable calcite. The skeleton appears with all skeletal elements preserved and large volumes of interskeletal porosity. Minor features are narrow spots of brown, black and orange minerals, which never cover a larger space than a few millimeters in diameter. They are spread all over the coral skeleton covering all skeletal elements in the described areas (Fig. 40). The pore surfaces of the skeleton are covered everywhere by acicular secondary aragonite. These crystals measure some  $\mu\text{m}$  in width and  $< 50 \mu\text{m}$  in length. The crystallites forming these coatings display flattened edges, interpreted to be due to dissolution effects (Fig. 39). EDX-measurements in these areas show that no other elements except Ca, C and O are involved in mineral build-up. Narrow spots with a dark mineral coverage viewed in electron microscope show a meshwork structure with tubes of  $8 \mu\text{m}$  in diameter and a length of up to  $< 200 \mu\text{m}$ . They form a tight three dimensional meshwork with open constructional porosity (Fig. 39). For those meshwork the EDX measurements show in order of decreasing abundance the elements O, C, Fe, Ca plus 1-2% Mg and Al. For the high concentration of Fe and O these structures were interpreted as rootlets covered by ironoxides (Fig. 40). Unfortunately, the samples of the macroscopic unaltered skeletal areas for SEM are part of the somehow altered rim (ca. 3 mm distance to the bleached rim) of the coral head. Just the samples for the narrow dark areas belong to the inner part of the skeleton and show in difference to the rim-near locations more septae and dissepiments. In *Montastrea* 455C, a slightly diagenetic influenced skeleton is observable. Nevertheless the coral skeleton of 455C is in a nearly pristine conservation and suitable for paleoclimate investigations as rootlets are avoided for stable isotope sampling.

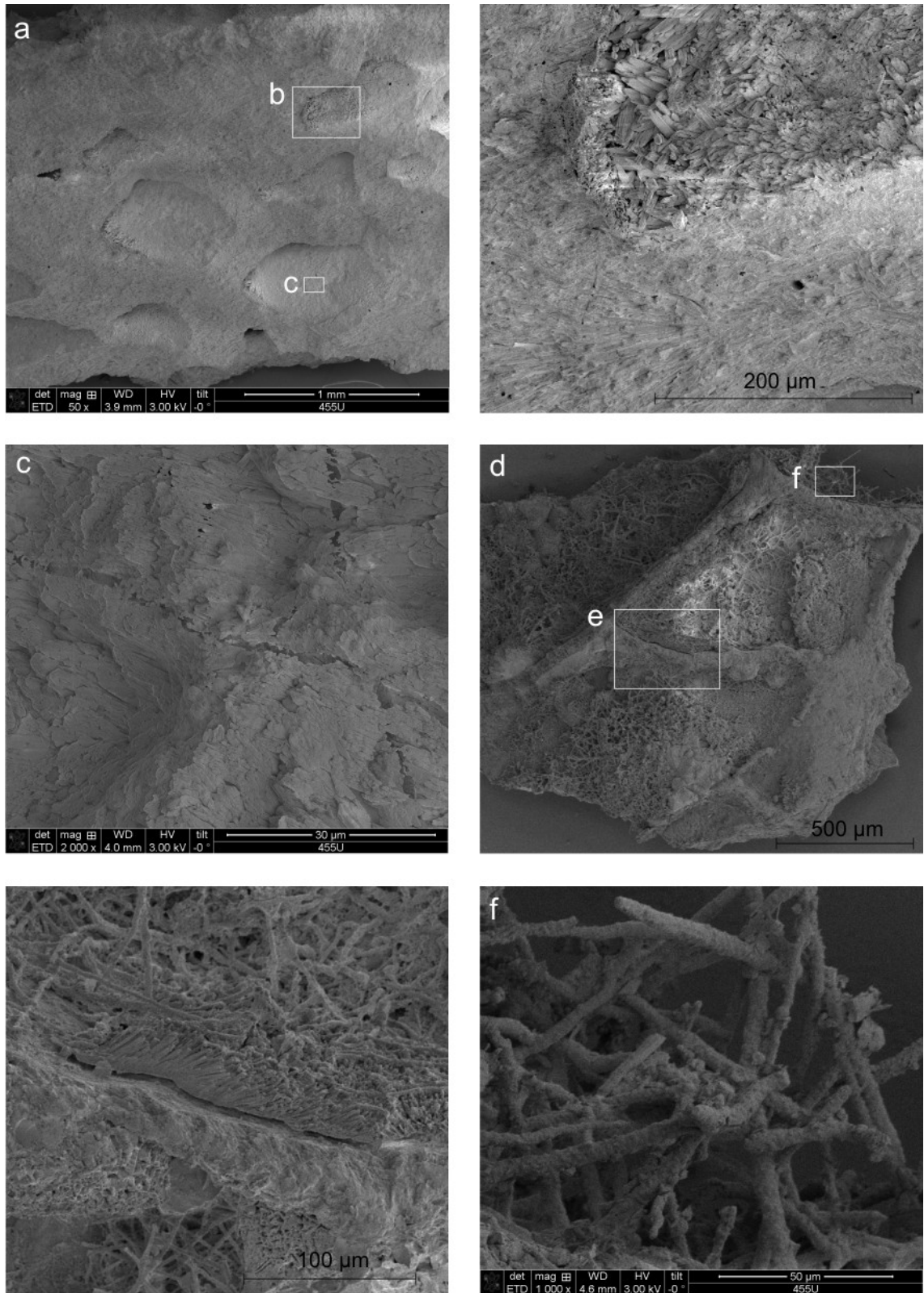


Figure 39: SEM images from two parts of *Montastrea* 455C S2. Pictures a, b and c show the altered rim of the coral head while pictures d, e and f show a narrow area which is covered by a brown/orange material that is patchy distributed inside the skeleton and probably resulting from plant roots. (a) Skeletal porosity and secondary aragonite cements covering all surfaces isopachous (b) Fractured dissepiment with arrangement of sclerodermites and skeletal porosity covered by secondary aragonite cements (c) Linear excavations from microboring organisms (d) Overview of the central part of the coral slab with coverage of brown minerals. Coralline skeleton is pristine (e) Contact of skeletal wall with secondary aragonite (f) Close-up of rootlets

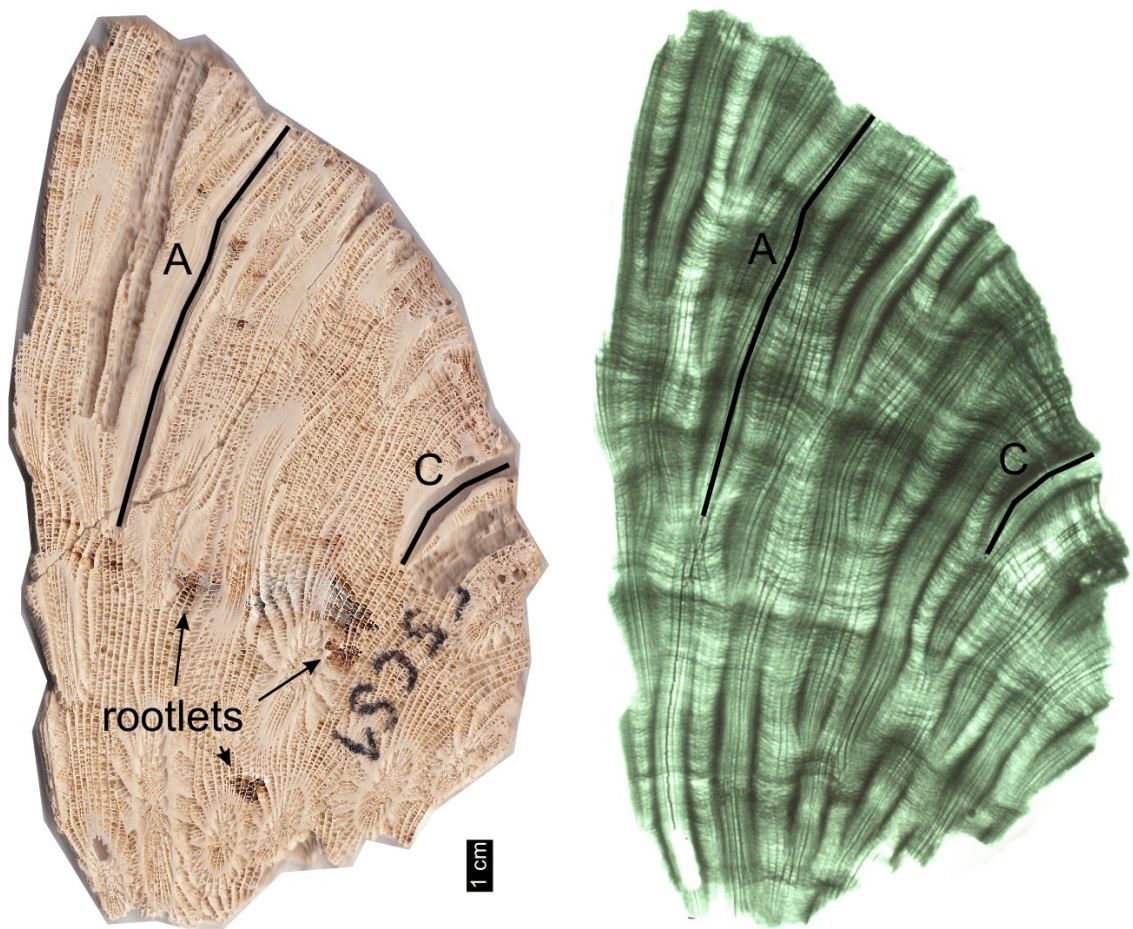


Figure 40: Overview of the coral slab from *Montastrea* 455C. Visual light and X-radiograph with the location of the sampling transects A and C are shown. Rootlets are described in text and Fig. 39.

### 3.4.2 Oxygen and Carbon Stable Isotope Composition

In *Montastrea* 455C two parallel transects were sampled. A long transect A ( $n = 286$ ) is along the direction of maximum growth and the short transect C ( $n = 60$ ) is from a coeval grown corallite but in a skeletal zone with lower extension rate. In total, 346 samples for  $\delta^{18}\text{O}$  and  $\delta^{13}\text{C}$  were measured in this coral. The  $\delta^{18}\text{O}$  values for transect A vary between  $-5.12\text{‰}$  and  $-2.94\text{‰}$ , which is a range of  $2.2\text{‰}$ . The mean is  $-3.71 \pm 0.28\text{‰}$  ( $median = -3.69\text{‰}$ ). The  $\delta^{13}\text{C}$  values range between  $-2.87\text{‰}$  and  $0.32\text{‰}$ , which is a range of  $3.2\text{‰}$ . The mean is  $-1.4 \pm 0.55\text{‰}$  ( $median = -1.42\text{‰}$ ) (Fig. 41). The  $\delta^{18}\text{O}$  values for transect C from  $-4.6\text{‰}$  to  $-2.34\text{‰}$ , which is a range of  $2.3\text{‰}$ . The mean is  $-3.17 \pm 0.45\text{‰}$  ( $median = -3.07\text{‰}$ ). The  $\delta^{13}\text{C}$  values range between  $-3.2\text{‰}$  and  $0.33\text{‰}$ , which is a range of  $3.5\text{‰}$ . The mean is  $-0.84 \pm 0.86\text{‰}$  ( $median = -0.6\text{‰}$ ) (Fig. 42). The  $\delta^{18}\text{O}$  signal in both transects is oscillating with more or less the same frequency but variable amplitude. Several different minima and maxima along this timeseries have been counted. The  $\delta^{18}\text{O}$  minima and maxima seem to be abrupt but cyclic.

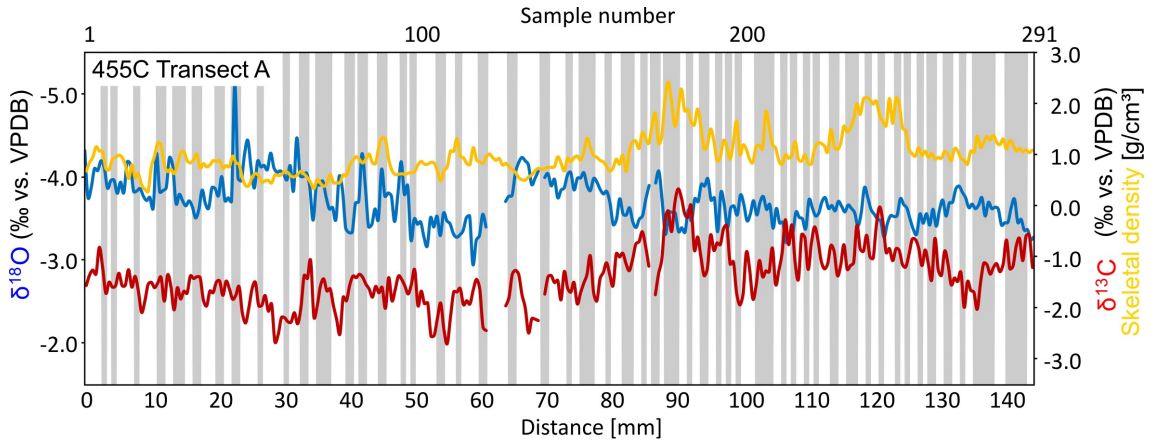


Figure 41: 455C Transect A stable isotope data and skeletal density. Grey: HDBs from X-radiograph. Data from *Lohmann* (2013).

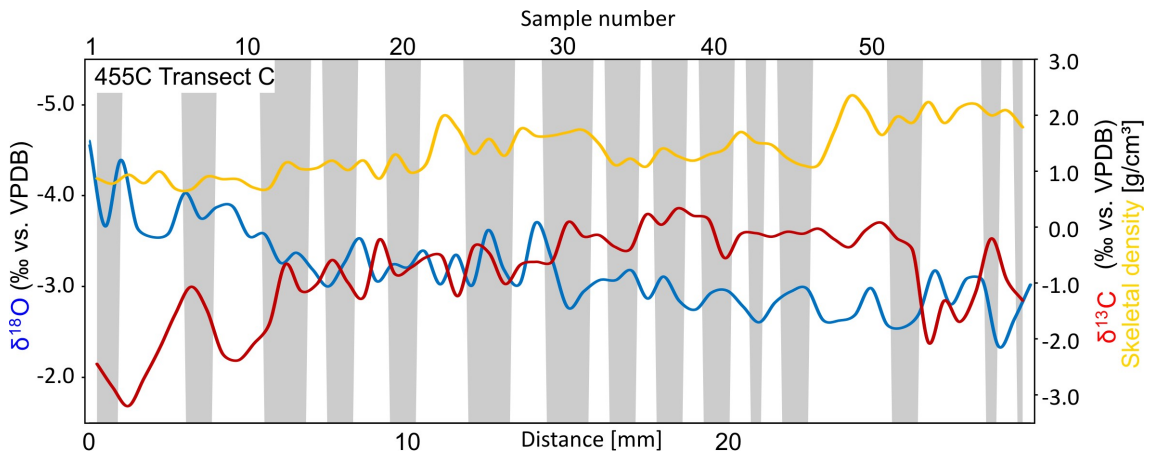


Figure 42: 455C Transect C stable isotope data and skeletal density. Grey: HDBs from X-radiograph. Data from *Lohmann* (2013).

The  $\delta^{13}C$  signal is following this oscillation in most cases and correlates in both transects different with the  $\delta^{18}O$  signal. In transect A the correlation between the both stable isotope signals is less significant ( $r=0.38$ ) than in transect C ( $r=0.75$ ). There is also a difference in correlation between the isotope data and the skeletal density in both transects. The correlation for both transects between  $\delta^{18}O$  and skeletal density is opposed to the correlation of  $\delta^{13}C$  and skeletal density in both transects (Transect A:  $\delta^{18}O$  and skeletal density have  $r=0.35$ ,  $\delta^{13}C$  and skeletal density have  $r=0.64$ ; Transect C:  $\delta^{18}O$  and skeletal density have  $r=0.60$ ,  $\delta^{13}C$  and skeletal density have  $r=0.36$ ).

### 3.4.3 X-radiography/Coral densitometry

Coral slab 455C S1 was radiographed with 40 kV, 800  $\mu$ A and an exposure time of 60 s. Several pictures were taken under the same conditions and stitched together in a graphic program. The procedure was repeated for the background images for density measurements and is the same as for the slab X-radiographs. For 455C S1 the density was measured in a transect close to the sample spots of the two transects to reach the highest possible spatial relationship of density and stable isotopes signal. The measured densities were resampled in the same resolution as the samples for the stable isotopes. In total 352 (A: 292; C: 60) samples for density were measured using the software CoralXDS (*Helmle et al.*, 2002) in

this coral. The density values for transect A range between  $0.27 \text{ g/cm}^3$  and  $2.42 \text{ g/cm}^3$ , which is a range of  $2.1 \text{ g/cm}^3$ . The mean is  $1.0 \pm 0.4 \text{ g/cm}^3$  (*median* =  $0.93 \text{ g/cm}^3$ ) (Fig. 41). For Transect C density values range between  $0.67 \text{ g/cm}^3$  and  $2.34 \text{ g/cm}^3$ , which is a range of  $1.67 \text{ g/cm}^3$ . The mean is  $1.38 \pm 0.45 \text{ g/cm}^3$  (*median* =  $1.29 \text{ g/cm}^3$ ) (Fig. 42).

### 3.5 464C *Stephanocoenia* Dominican Republic

Coral slab 464C S2 was sampled along a continuous transect with a total of 113 sampling spots.

#### 3.5.1 Preservation

X-ray diffraction measured in three areas in the coral 464C show only the aragonite phase and nearly no detectable calcite. In one sample calcite was slight above the detection limit with approximately  $< 1\text{-}2 \%$ , while the rest is aragonite. The skeleton appears with all skeletal elements preserved and large volumes of interskeletal porosity. In the X-radiograph in the upper 1-2 cm below the former surface of the coral a higher density ( $> 2 \text{ g/cm}^3$ ) than in the rest of the skeleton is visible (Fig. 45). The samples for SEM are part of the somehow altered lateral rim of the coral head, which is due to the sampling strategy to break off parts from the rim without destroying the coral slab. The pore surfaces are covered everywhere by acicular secondary aragonite. The crystals measure some  $\mu\text{m}$  in width and  $< 20 \mu\text{m}$  in length, probably shortened by dissolution. EDX-measurements in these areas show that no other elements than Ca, C and O are significantly involved in mineral build-up. Besides the secondary aragonite another authigenic phase is patchy distributed over the skeletons surface. Crystals of this phase form large isometric crystals with a size  $< 100 \mu\text{m}$  and single crystal-faces larger than  $100 \mu\text{m}^2$  (Fig. 43). EDX measurements reveal the elements O, C, Ca and S. Inferred from the bad cleavability of the crystals and the element distribution indicating gypsum. In *Stephanocoenia* 464C is a slight diagenetic influenced skeleton present. Nevertheless the coral skeleton is in the most areas in a nearly pristine conservation and suitable for paleoclimate investigations.



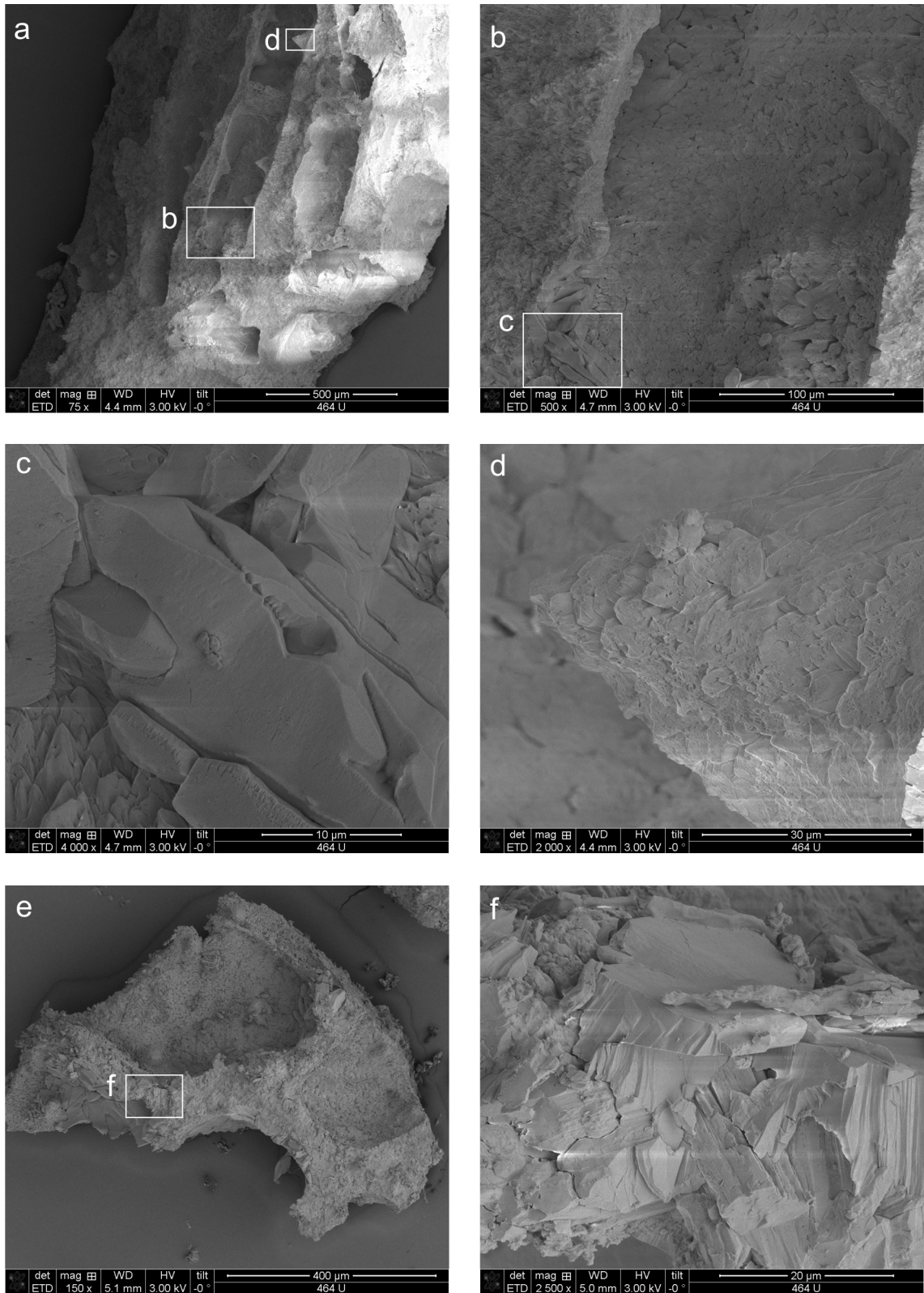


Figure 43: SEM images of *Stephanocoenia* 464C from a sample approximately 3 mm near the altered rim of the coral head. (a) Pore space is open but all surfaces show thin isopachous linings of secondary aragonitic cements (b). (c) Patches of gypsum crystals (d) Skeletal dentation with secondary aragonite overgrowth (e) Overview of a broken part from the coenosteum with open skeletal porosity but gypsum as well (f).

### 3.5.2 Oxygen and Carbon Stable Isotope Composition

The  $\delta^{18}O$  values for the samples analyzed ( $n = 111$ ) vary between  $-3.48\text{‰}$  and  $-2.47\text{‰}$ , which is a range of  $1.01\text{‰}$ . The mean is  $-3.04 \pm 0.18\text{‰}$  (*median* =  $-3.05\text{‰}$ ). The  $\delta^{13}C$  values range between  $-2.73\text{‰}$  and  $0.05\text{‰}$ , which is a range of  $2.78\text{‰}$ . The mean is  $-1.03 \pm 0.52\text{‰}$  (*median* =  $-0.98\text{‰}$ ) (Fig. 45). The calculated correlation coefficient of  $\delta^{18}O$  and  $\delta^{13}C$  is  $r = 0.42$  (Fig. 44).

Both,  $\delta^{18}O$  and  $\delta^{13}C$  are oscillating cyclically. Within the  $\delta^{18}O$  signal, 20 maxima and 20 minima are present. The  $\delta^{13}C$  signal shows 21 maxima which are coinciding with the  $\delta^{18}O$  maxima and 21  $\delta^{13}C$  minima which are coinciding with the  $\delta^{18}O$  minima. Obviously the  $\delta^{18}O$  maxima coincide with the  $\delta^{13}C$  maxima and the other way around for the minima. The  $\delta^{18}O$  and  $\delta^{13}C$  minima and maxima are constant and alternating in a distance of 4-8 samples. The values of the 20  $\delta^{18}O$  maxima vary from  $-3.12\text{‰}$  to  $-2.47\text{‰}$  (*mean* =  $-2.84 \pm 0.15\text{‰}$ ) and the  $\delta^{18}O$  minima from  $-3.48\text{‰}$  to  $-3.01\text{‰}$  (*mean* =  $-3.22 \pm 0.12\text{‰}$ ). The mean difference between the  $\delta^{18}O$  maxima and minima is  $-0.39 \pm 0.17\text{‰}$  with values between  $0.1$  and  $0.72\text{‰}$ . For the  $\delta^{13}C$  maxima values spread between  $-1.59\text{‰}$  and  $0.05\text{‰}$  (*mean* =  $-0.49 \pm 0.34\text{‰}$ ) and for the  $\delta^{13}C$  minima between  $-2.73\text{‰}$  and  $-1.00\text{‰}$  (*mean* =  $-1.64 \pm 0.34\text{‰}$ ). For  $\delta^{13}C$  the mean difference between the maxima and minima is  $1.15 \pm 0.32\text{‰}$  and takes values from  $0.51 - 1.60\text{‰}$ . Cross-correlation analysis of the  $\delta^{18}O$  and  $\delta^{13}C$  values was performed for the continuous sample sequence but ignoring two missing data points (97 and 113). Highest correlation coefficients are achieved at a lag of one sample ( $r = 0.45$ ) and a lag of -2 samples ( $r = -0.49$ ) (Fig. 44).

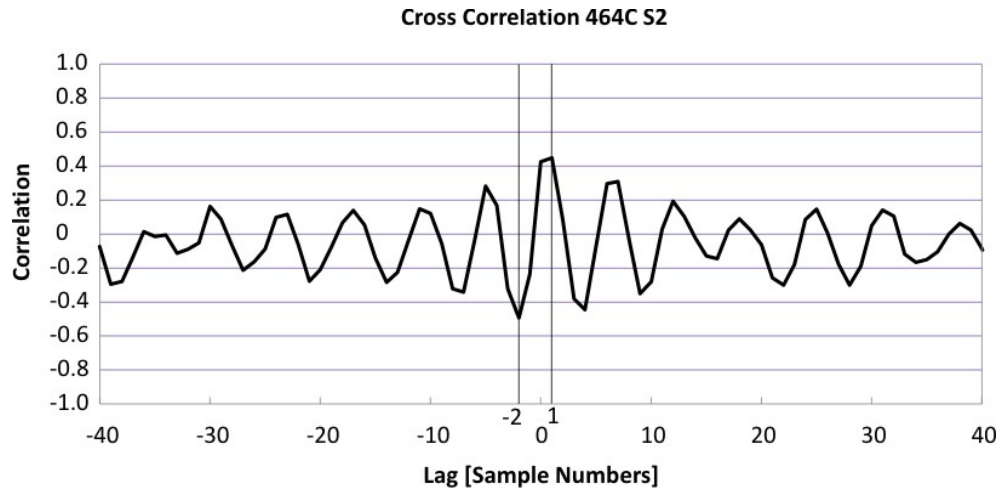


Figure 44: Cross correlation of all stable isotope data for *Stephanocoenia* 464C S2. Highest positive correlation for all data is at a lag of one sample ( $r = 0.45$ ), highest negative correlation at a lag of -2 is  $r = -0.49$ .

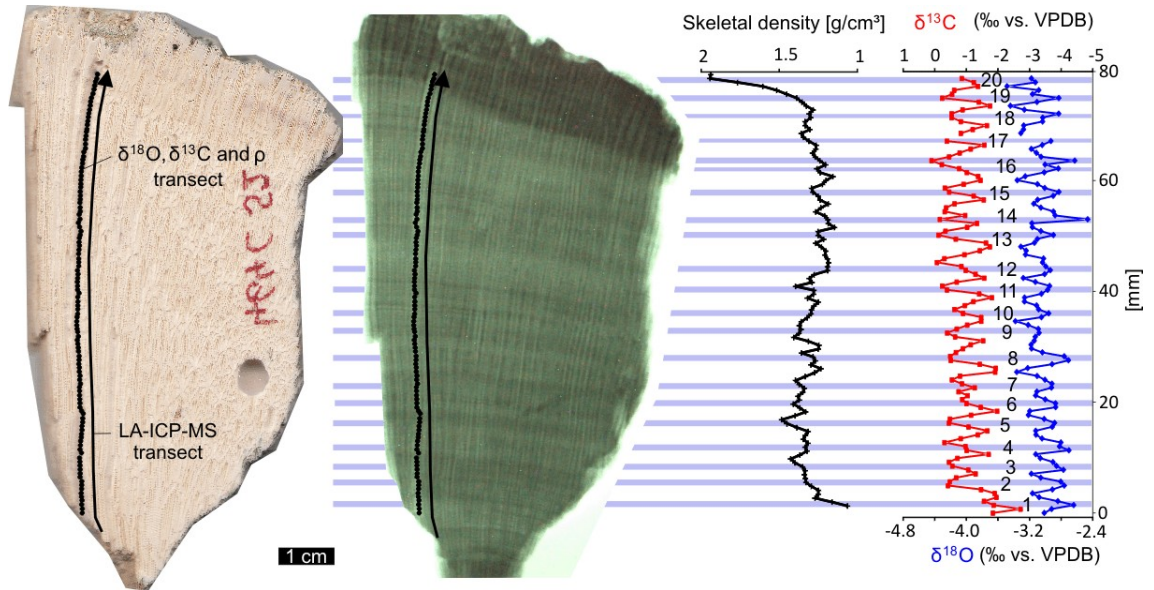


Figure 45: Visual light, X-radiograph and measured parameter (skeletal density,  $\delta^{18}O$  and  $\delta^{13}C$ ) for *Stephanocoenia* 464C S2. Blue shaded lines ( $\delta^{18}O$  maxima!) are here to facilitate comparison of the timing of the  $\delta^{18}O$ -maxima with the carbon isotopes and skeletal density.

### 3.5.3 Main and Trace Element Composition

The LA-ICP-MS track in *Stephanocoenia* 464C was oriented parallel to the  $\delta^{18}O$  sampling track in the axis of maximum growth (Fig. 45). The laser spots were aimed to hit the perpendicular cut theca wall of the truncated corallite. A full penetration of the theca wall in the coenchym beyond happened in some samples and the theca wall could not always clearly identified as such during targeting the laser spots because of the uneven slabs surface which causes a defocussation in the small section. A spatial resolution of  $500\ \mu m$  corresponds to seven to eight samples per year at an average annual growth rate of  $\sim 3.7\ mm$ . The laser ablation profile represents 166 laser spots within 20 years ( $\delta^{18}O$  internal chronology) of the coral. In total the length of this transect is 82.5 mm. An age model was created on the basis of  $\delta^{18}O$  data together with annual density banding to provide an internally consistent time series for the laser ablation element transect (Fig. 45) (Fig. 46).

**Sr/Ca** The Sr/Ca signal in the coral slab 464C shows a more or less cyclic pattern (Fig. 46). The values spread between  $6.6 - 8.0\ mmol/mol$  and average at  $7.2 \pm 0.24\ mmol/mol$  (Median:  $7.18\ mmol/mol$ ). An anticorrelation to Mg/Ca and a correlation to Ba/Ca exists (Table 2).

**Mg/Ca** The Mg/Ca signal also shows a cyclic curve (Fig. 46). It's values spread between  $2.1 - 5.7\ mmol/mol$  and average at  $3.22 \pm 0.47\ mmol/mol$  (Median:  $3.18\ mmol/mol$ ). An anticorrelation to Sr/Ca exists (Table 2).

**B/Ca** The B/Ca signal shows a cyclic curve (Fig. 46). The values spread between  $0.29 - 0.47\ mmol/mol$  and average at  $0.37 \pm 0.03\ mmol/mol$  (Median:  $0.37\ mmol/mol$ ). A weak anticorrelation to the  $\delta^{13}C$  signal is observable (Table 2).

**Ba/Ca** The Ba/Ca signal shows a more or less cyclic curve (Fig. 46). The values spread between  $6.8 - 12.5\ \mu mol/mol$  and average at  $9.4 \pm 1.2\ \mu mol/mol$  (Median:  $9.3\ \mu mol/mol$ ).

Ba/Ca correlates positive with Sr/Ca and weak with Y/Ca (Table 2).

**U/Ca** U/Ca ratios spread between  $0.37 - 2.78 \mu\text{mol/mol}$  and average at  $0.55 \pm 0.31 \mu\text{mol/mol}$  (Median:  $0.49 \mu\text{mol/mol}$ ) (Fig. 46). No correlation to other measured signals exist (Table 2).

**Y/Ca** The Y/Ca values spread between  $0.1 - 0.21 \mu\text{mol/mol}$  and average at  $0.14 \pm 0.02 \mu\text{mol/mol}$  (Median:  $0.13 \mu\text{mol/mol}$ ) (Fig. 46). Y/Ca is weak correlated with Sr/Ca and Ba/Ca ratios (Table 2).

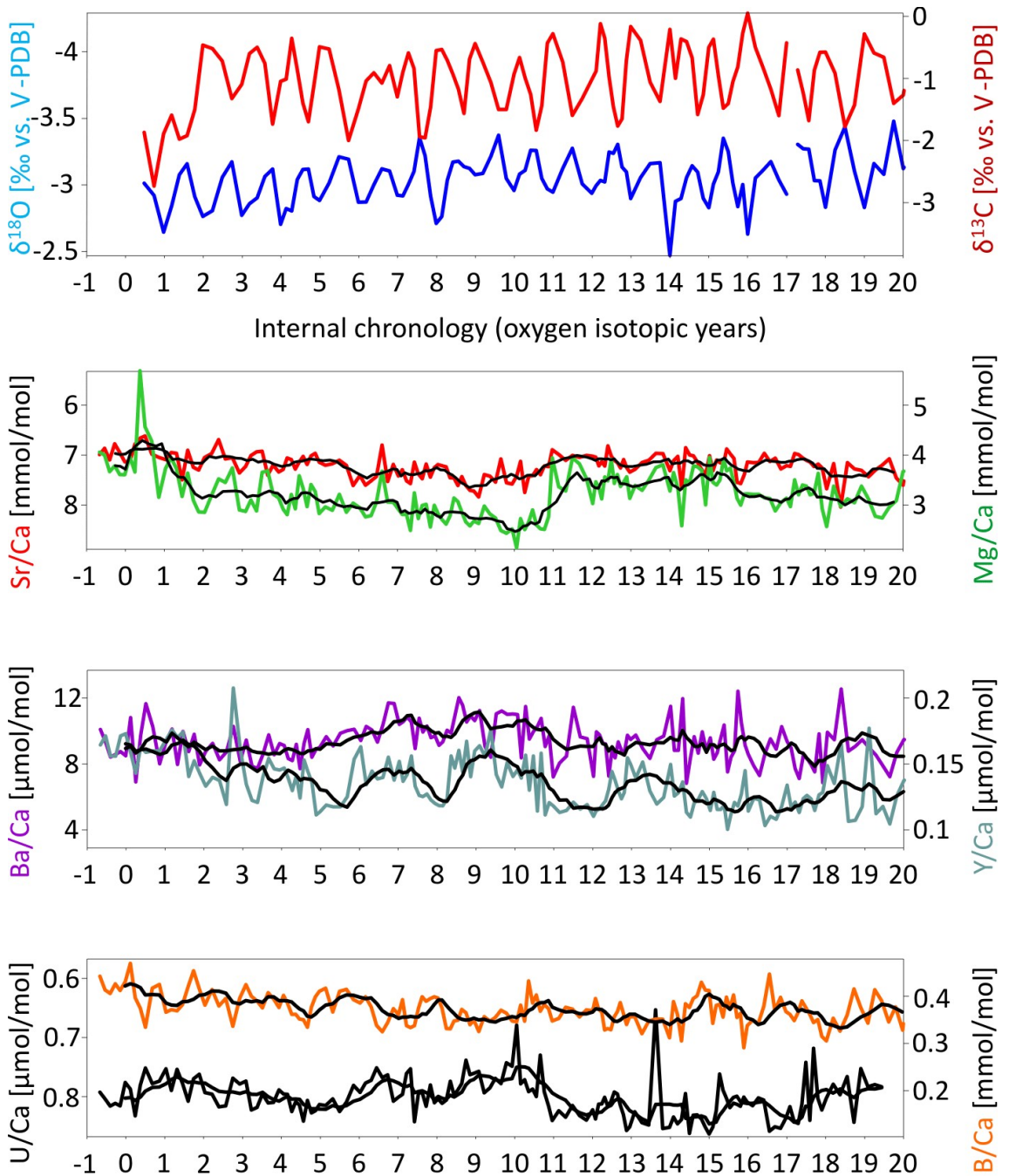


Figure 46: Comparison of selected element/calcium-ratios and stable isotope values in 464C. All x-axis referenced on the internal masterchronology.

Table 2: Correlation coefficients for selected Metall/Calcium ratios and stable isotopes for *Stephanocoenia* 464C

	Sr/Ca	Mg/Ca	Ba/Ca	Y/Ca	U/Ca	B/Ca
$\delta^{18}O$	-0.04	-0.07	-0.04	0.10	-0.20	0.07
$\delta^{13}C$	0.04	-0.17	-0.17	-0.22	-0.11	-0.34
<b>Sr/Ca</b>	1.00	-0.62	0.56	0.38	0.18	-0.21
<b>Mg/Ca</b>	-0.62	1.00	-0.23	-0.07	0.02	0.00
<b>Ba/Ca</b>	0.56	-0.23	1.00	0.38	-0.01	-0.15
<b>Y/Ca</b>	0.38	-0.07	0.38	1.00	0.05	-0.26
<b>U/Ca</b>	0.18	0.02	-0.01	0.05	1.00	-0.11

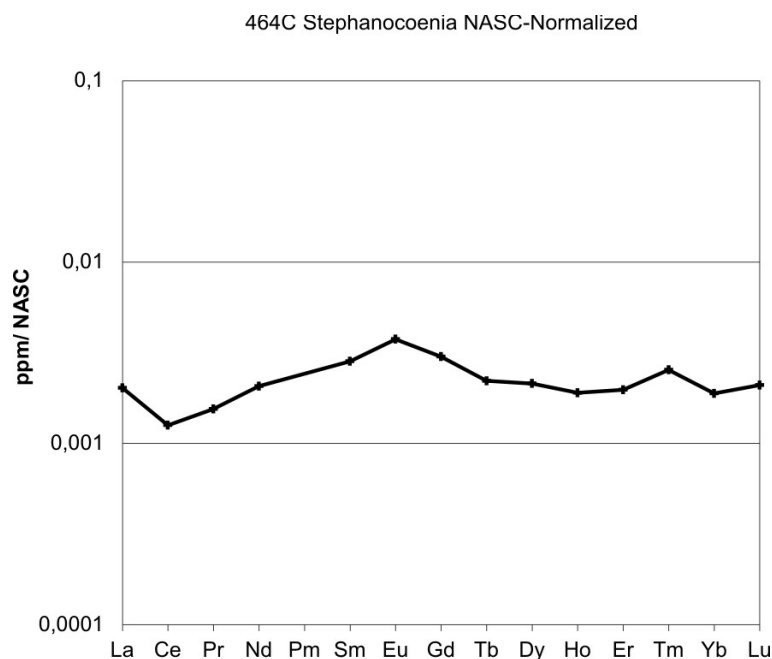


Figure 47: Shale-normalized REE patterns of the median-values of the profile along the stable isotope transect in *Stephanocoenia* 464C based on North American shale composite (NASC) (*Taylor and McLennan, 1985*).

**REE** The shale-normalized REE pattern shows a gentle enrichment of HREE compared to LREE. A positive Eu and a negative Ce anomaly is present (Fig. 47).

### 3.5.4 X-radiography/Coral densitometry

Coral slab 464C S2 was radiographed with 40 kV, 800  $\mu$ A and an exposure time of 60 s. The slab is slightly wedge-shaped but has a constant thickness of 6.5 mm along the measured transect. Density was measured prior to isotope sampling on the positions of the drilling locations to achieve the highest possible correlation of density and stable isotopes signal. Measured density was resampled in the same resolution as the drilling holes for the stable isotopes (Fig. 45). In total, 113 samples for density were measured with the software CoralXDS (*Helmle et al., 2002*) in this coral. The first two measured density values are biased because of the thinning of the coral slab at this position and not considered here. The density values of the remaining 111 measured spots range between 1.06 g/cm<sup>3</sup> and 1.94 g/cm<sup>3</sup>, which is a range of 0.88 g/cm<sup>3</sup>. The mean is  $1.32 \pm 0.13$  g/cm<sup>3</sup>

(*median* =  $1.3 \text{ g/cm}^3$ ). The measured density variation is weak because of the low contrast between HDBs and LDBs. The correlation coefficient for skeletal density and  $\delta^{18}\text{O}$  ( $r = -0.14$ ) and  $\delta^{13}\text{C}$  ( $r = 0.07$ ), respectively, is weak (no correlation). However, comparison of the X-radiograph with the isotope signal shows an explicit coincidence of  $\delta^{18}\text{O}$  maxima (grey lines in Fig. 45) with LDBs. The Age model was developed according the  $\delta^{18}\text{O}$  cycles. Along the measured transect 19 years could be distinguished, which results in a mean growth rate of  $3.7 \text{ mm/yr}$ .

### 3.6 X-radiography of other corals

Evasively density and growth rates measurements were taken out. Calculated calcification rates are presented here for coral slabs without geochemical data. For completeness the measured values of geochemically investigated corals are included also. In total 30 corals were investigated for densitometry (Table 3 and 4). The thickness of the coral slabs varies between 5–9 mm and some are wedge shaped with a thickness-difference from 0.1–3.1 mm and some even with two slopes (double wedges or tetrahedra). To achieve a mean density for slabs like those, small areas of equal thickness ( $\pm 0.1 \text{ mm}$ ) were measured for density and only average values were considered. A correlation between the thickness and density for all measured coral slabs is not present ( $r = 0.14$ ), which suggests that the systematic error is small enough to gather conclusions of the values (Fig. 48).

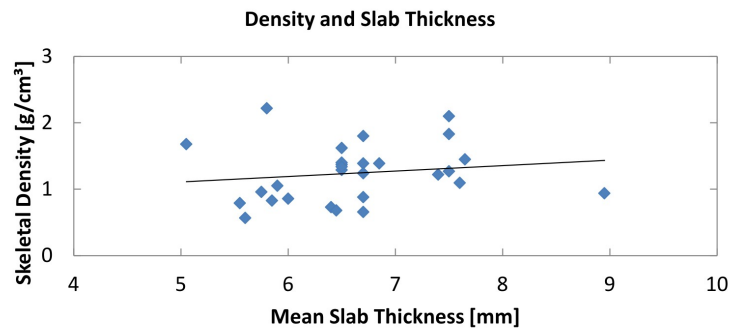


Figure 48: Relationship of coral density and thickness of the slabs ( $n = 29$ ).

Calcification rates of corals were calculated as mean calcification rates. This means, the average density calculated for the coral was multiplied with the mean annual growth rate (see equation 1). All here presented coral slabs were investigated by X-ray diffraction to reveal possible diagenetic alteration. The very most samples contain no or only traces of calcitic content (0-1 %) while the rest is aragonite. Only two samples (469M and 467K1) vary from the normal aragonitic content, they have high amounts of calcite (approximately 20-30 % calcite, rest aragonite). Another coral (461B) shows selective diagenetic alteration and precipitation of calcite and iron oxides between a well preserved aragonitic skeleton. All other coral slabs are pristine and well suited for calcification rate studies.

#### 3.6.1 Plio/Pleistocene Florida

For the Plio/Pleistocene Caloosahatchee Formation a total of 11 corals of the genus *Solenastrea* was measured for density and extension rates (Table 3) (Fig. 51).

**Extension Rates:** Skeletal extension rates were measured at 11 specimens of the genus *Solenastrea*. Mean annual extension rates range between  $2.25 - 4.8 \text{ mm/yr}$  and have a

mean of  $3.69 \pm 0.86 \text{ mm/yr}$  ( $median = 3.6 \text{ mm/yr}$ ) (Table 3). An identification of growth bands as annual growth increments was not possible in all corals because of unsharp HDBs in some areas ( $\neq 90^\circ$  between HDBs and slabs surface). Identification was also not possible when dHDBs were present and not distinguishable from normal HDBs (Fig. 51).

**Skeletal Density:** Skeletal density varies between  $0.6 - 1.8 \text{ g/cm}^3$ . The mean density of the here measured coral skeletons is  $0.91 \pm 0.34 \text{ g/cm}^3$  ( $median = 0.86 \text{ g/cm}^3$ ) (Table 3). A correlation between density and growth rate is not obvious ( $r = -0.20$ ). The correlation coefficient for all *Solenastreas* skeletal density and extension rate ignoring coral 509A S1 (difference to mean density is  $\approx 3\sigma$ ) is  $r = -0.37$  (Fig. 49).

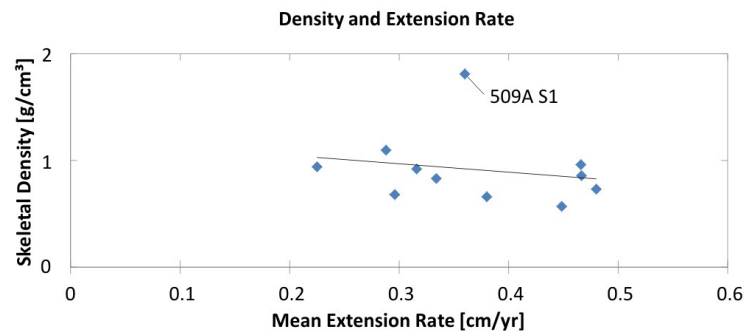


Figure 49: Scatter plot of skeletal density and extension rate for *Solenastrea* Florida. Correlation coefficient is  $r = -0.20$ . Correlation coefficient of  $r = -0.37$  (except the sample 509A S1) indicates a slightly decreasing density with increasing growth rate.

**Calcification Rates:** Mean calcification rate for all *Solenastrea* is  $0.33 \pm 0.13 \text{ g/cm}^2/\text{yr}$  ( $median = 0.29 \text{ g/cm}^2/\text{yr}$ ) and extends from  $0.2 - 0.7 \text{ g/cm}^2/\text{yr}$  (Table 3).

Table 3: Mean skeletal extension rate ( $\text{cm/yr}$ ), skeletal density ( $\text{g/cm}^3$ ) and calcification rate ( $\text{g/cm}^2/\text{yr}$ ) for corals from Florida. Recent corals from the literature for comparison in the lower part.

Sample	Genus	Density	Extension	Calcification	Form- ation
		[ $\text{g/cm}^3$ ]	Rate [ $\text{cm/yr}$ ]	Rate [ $\text{g/cm}^2/\text{yr}$ ]	
452 K1	<i>Solenastrea</i>	0.73	0.48	0.35	Caloosahatchee
452 K13	<i>Solenastrea</i>	0.68	0.30	0.20	Caloosahatchee
452 K14	<i>Solenastrea</i>	0.92	0.32	0.29	Caloosahatchee
452 K15	<i>Solenastrea</i>	0.83	0.33	0.28	Caloosahatchee
452 K17	<i>Solenastrea</i>	0.86	0.47	0.40	Caloosahatchee
452 K3	<i>Solenastrea</i>	0.57	0.45	0.25	Caloosahatchee
452 K4	<i>Solenastrea</i>	0.66	0.38	0.25	Caloosahatchee
508 A	<i>Solenastrea</i>	1.10	0.29	0.32	Caloosahatchee
508 B	<i>Solenastrea</i>	0.96	0.47	0.45	Caloosahatchee
509 A	<i>Solenastrea</i>	1.81	0.36	0.65	Caloosahatchee
452 K5	<i>Solenastrea</i>	0.94	0.23	0.21	Caloosahatchee
<b>mean</b>		<b>0.91</b>	<b>0.37</b>	<b>0.33</b>	
*	<i>S. bournoni</i>	-	0.51	-	Recent, Florida Bay
**	<i>S. bournoni</i>	-	0.89	-	Recent, Florida Bay
***	<i>S. bournoni</i>	-	0.41	-	Pinecrest Beds, Fl

Sample	Genus	Density	Extension Rate	Calcification Rate	Formation
		[ $g/cm^3$ ]	[ $cm/yr$ ]	[ $g/cm^2/yr$ ]	
* <i>Swart et al.</i> (1996), ** <i>Hudson et al.</i> (1989), *** <i>Roulier and Quinn</i> (1995)					

### 3.6.2 Miocene Cercado Formation and Mio/Pliocene Gurabo Formation, Dominican Republic

The more difficult sampling possibilities in the Cibao Valley compared to the easily accessible pillars in Florida result in a mix of different coral species. In Florida the main focus lay on the collection of *Solenastrea* and in the Dominican Republic this species was in the most outcrops absent. Within the Cibao Valley several corals (17) were sampled from the Cercado (7) (Fig. 53) and the Gurabo (10) Formation (Fig. 52 and 54). One specimen from the Holocene Lago Enriquillo Reef was also measured (Fig. 54). Outcrop Numbers for the Cercado Formation corals are 463 (n = 4) and 464 (n = 3), for the Gurabo Formation 455 (n = 1, see master thesis from *Lohmann*, 2013), 460 (n = 2), 461 (n = 2), 467 (n = 1), 469 (n = 4) and for the Lago Enriquillo 503 (n = 1). The here analyzed corals are *Montastrea* (n = 6), *Siderastrea* (n = 4), *Stephanocoenia* (n = 3), *Porites/Goniopora* (n = 3) and *Solenastrea* (n = 2).

**Extension Rates:** From the 17 corals from Cibao Valley, growth rates could be measured in 13 at X-radiographs. Four corals did not show any couplets of HDBs and LDBs and therefore no extension rate could be measured for those. Within some of the here presented growth rates a high uncertainty exists due to unclear transformation of true skeletal architecture to an X-radiograph with bright and dark bandings in some of the corals. The mean annual skeletal extension of all specimen is  $5.05 \pm 2.33 \text{ mm/a}$  (*median* =  $4 \text{ mm/a}$ ) and ranges for the individual corals in mean between  $2.12 - 9.15 \text{ mm/a}$ . Divided into corals from the Cercado Formation ( $n = 6$ , range:  $3.2 - 9.15 \text{ mm/a}$ , mean:  $5.6 \pm 2.5 \text{ mm/a}$ ) and Gurabo Formation ( $n = 7$ , range:  $2.12 - 8.73 \text{ mm/a}$ , mean:  $4.6 \pm 2.3 \text{ mm/a}$ ) slight differences are likely to exist. A one way random effects analyses of variance (ANOVA) shows that the null hypothesis stating no difference in extension rates between the formations exist could not be rejected (Table 4).

**Skeletal Density:** All mean skeletal density varies between  $0.88 - 2.22 \text{ g/cm}^3$ . The mean density of all measured coral skeletons from Cibao Valley is  $1.45 \pm 0.35 \text{ g/cm}^3$  (*median* =  $1.39 \text{ g/cm}^3$ ). Mean skeletal densities from corals of the Cercado Formation ( $n = 7$ ) range from  $0.9 - 1.45 \text{ g/cm}^3$  (*mean* :  $1.28 \pm 0.19 \text{ g/cm}^3$ ). For the Gurabo Formation ( $n = 10$ ) the mean densities of the individual corals range from  $1.0 - 2.2 \text{ g/cm}^3$  (*mean* :  $1.57 \pm 0.39 \text{ g/cm}^3$ ) (Table 4).

Extension rates and skeletal densities display no obvious relationship. High growth rates seem to accompany with high skeletal densities (correlation coefficient for all Dominican Republic corals:  $r = 0.29$ ) which increases dramatically when ignoring coral 469A S1 with the highest skeletal density ( $\rho = 2.22 \text{ g/cm}^3$ ): correlation coefficient between mean growth rate and mean skeletal density for all specimen  $r = 0.63$  (Fig. 50).



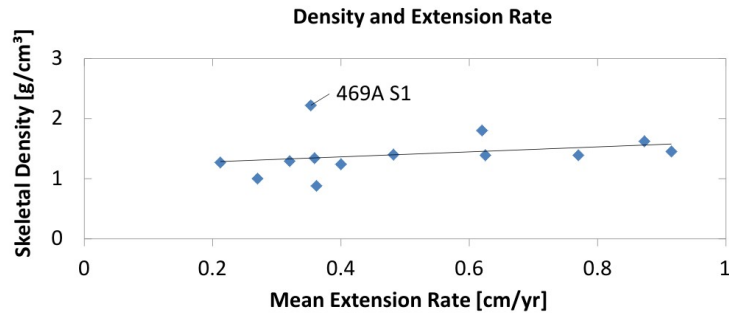


Figure 50: Density and growth rates of corals from the Cibao Valley, Dominican Republic. Correlation coefficient is low ( $r = 0.29$ ) but high when ignoring the coral with the highest skeletal density ( $r = 0.63$ ).

**Calcification Rates:** Calcification rates were calculated for corals with measured growth rate and skeletal density. Since the annual skeletal extension in four specimen could not be quantified, no calcification rates were calculated for those four corals. For the other 13 corals from the Cibao Valley the mean calcification rate is  $0.73 \pm 0.4 \text{ g/cm}^2/\text{yr}$  (*median* =  $0.67 \text{ g/cm}^2/\text{yr}$ ). Split into Cercado Formation ( $n = 6$ ) the values spread between  $0.32 - 1.33 \text{ g/cm}^2/\text{yr}$  ( $\bar{\sigma} = 0.75 \pm 0.41 \text{ g/cm}^2/\text{yr}$ ) and Gurabo Formation ( $n = 7$ ) values range within  $0.27 - 1.41 \text{ g/cm}^2/\text{yr}$  ( $\bar{\sigma} = 0.72 \pm 0.43 \text{ g/cm}^2/\text{yr}$ )(Table 4).

Table 4: Mean skeletal extension rate ( $\text{cm/yr}$ ), skeletal density ( $\text{g/cm}^3$ ) and calcification rate ( $\text{g/cm}^2/\text{yr}$ ) for corals from the Dominican Republic. Mean for Mio/Pliocene Gurabo Formation, Miocene Cercado Formation and both Formations (mean Cibao Valley). Samples from Holocene Lago Enriquillo not included in the means. Recent corals from the literature for comparison in the lower part.

Sample	Genus	Density [ $\text{g/cm}^3$ ]	Extension Rate [ $\text{cm/yr}$ ]	Calcification Rate [ $\text{g/cm}^2/\text{yr}$ ]	Formation
455 C	<i>Montastrea</i>	1.00	0.27	0.27	Gurabo
460 B	<i>Siderastrea?</i>	1.37	-	-	Gurabo
460 A	<i>Stephanocoenia</i>	1.27	0.21	0.27	Gurabo
461 B	<i>Siderastrea?</i>	1.40	0.48	0.67	Gurabo
461 A	<i>Solenastrea</i>	1.80	0.62	1.12	Gurabo
467 K1	<i>Porites?</i>	1.68	-	-	Gurabo
469 M	<i>Montastrea</i>	1.24	0.40	0.50	Gurabo
469 N	<i>Montastrea</i>	1.62	0.87	1.41	Gurabo
469 A	<i>Siderastrea</i>	2.22	0.35	0.78	Gurabo
469 R	<i>Siderastrea</i>	2.10	-	-	Gurabo
463 K1	<i>Montastrea?</i>	0.88	0.36	0.32	Cercado
463 K3	<i>Montastrea?</i>	1.29	0.32	0.41	Cercado
463 K4	<i>Porites/Goniopora?</i>	1.22	-	-	Cercado
463 K2	<i>Solenastrea</i> or <i>Montastrea</i>	1.39	0.63	0.87	Cercado
464 E	<i>Goniopora?</i>	1.39	0.77	1.07	Cercado
464 A	<i>Montastrea</i>	1.45	0.92	1.33	Cercado
464 C	<i>Stephanocoenia</i>	1.34	0.36	0.48	Cercado
503	<i>Stephanocoenia?</i>	2.50	0.13	0.31	L. En- riquillo

Sample	Genus	Density [g/cm <sup>3</sup> ]	Extension Rate [cm/yr]	Calcification Rate [g/cm <sup>2</sup> /yr]	Formation
<b>mean</b>					
<b>Gurabo</b>		<b>1.57</b>	<b>0.46</b>	<b>0.72</b>	
<b>mean</b>					
<b>Cercado</b>		<b>1.28</b>	<b>0.56</b>	<b>0.75</b>	
<b>mean</b>					
<b>Cibao Valley</b>		<b>1.45</b>	<b>0.51</b>	<b>0.73</b>	
1	<i>M.annularis</i>	1.73	0.91	1.57	USVI
2	<i>M.annularis</i>	1.71	0.38	0.65	Jamaica
3	<i>M.annularis</i>	1.8	0.76	1.35	Belize
4	<i>M.annularis</i>	1.28	0.98	1.23	USVI
5	<i>M.annularis</i>	1.74	0.87	1.5	Mexican Caribbean
6	<i>Porites</i>	0.95	0.7	0.65	Gulf of Cal- ifornia
7	<i>S.sidera</i>	1.60	-	-	Jamaica
8	<i>S.sidera</i>	1.61	0.41	-	Barbados

1 *Baker and Weber* (1975), 2 *Dustan* (1975), 3 *Graus, RR and MacIntyre, IG* (1982),  
4 *Dodge and Brass* (1984), 5 *Carricart-Ganivet et al.* (2000), 6 *Cabral-Tena et al.* (2013),  
7 *Mallela* (2004), 8 *Stearn et al.* (1977),

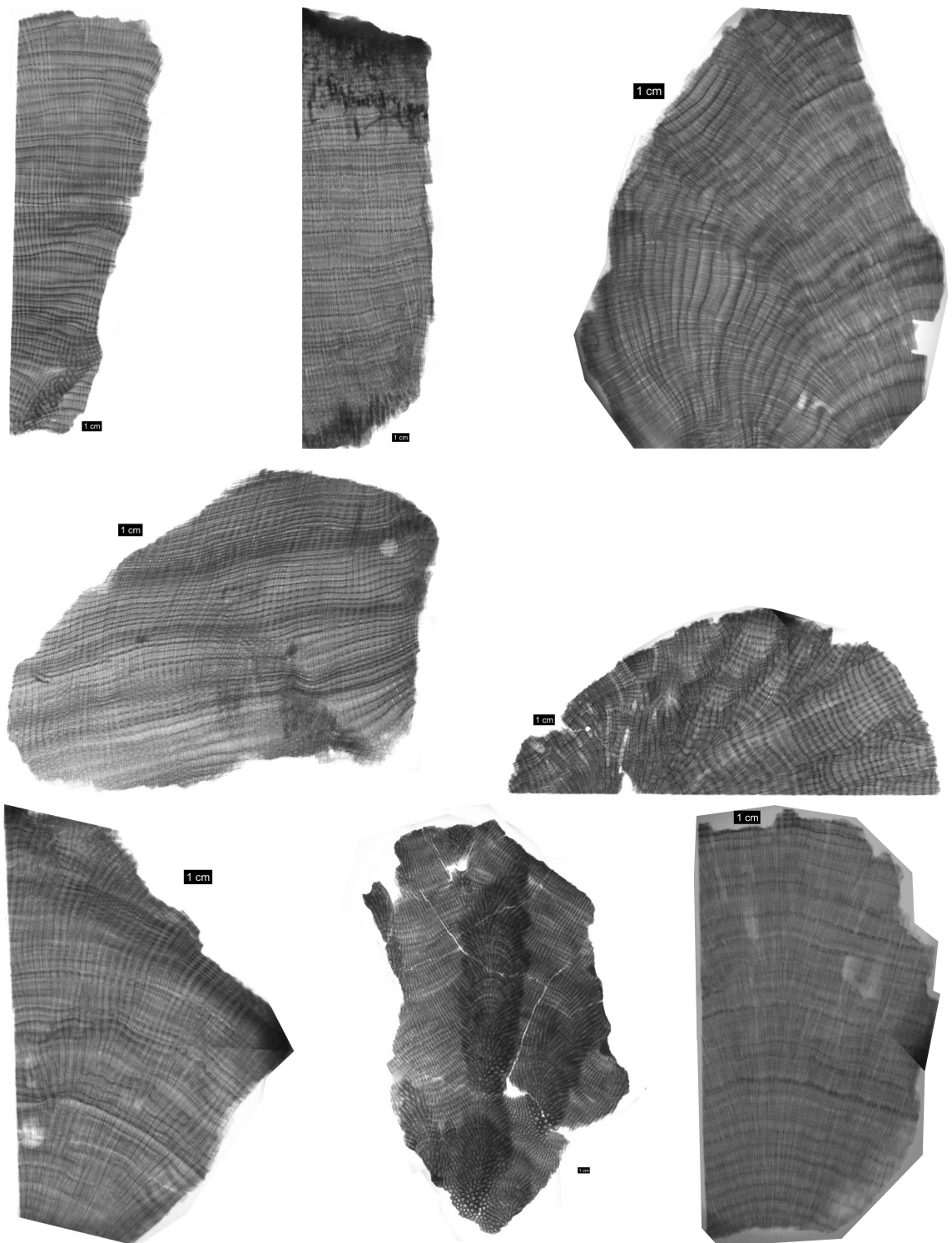


Figure 51: X-radiographs of coral slabs 452K13, 452K15, 452K17, 452K5, 452K4, 508A, 508B and 452K3 from upper left to lower right. All from Plio/Pleistocene of South Florida.

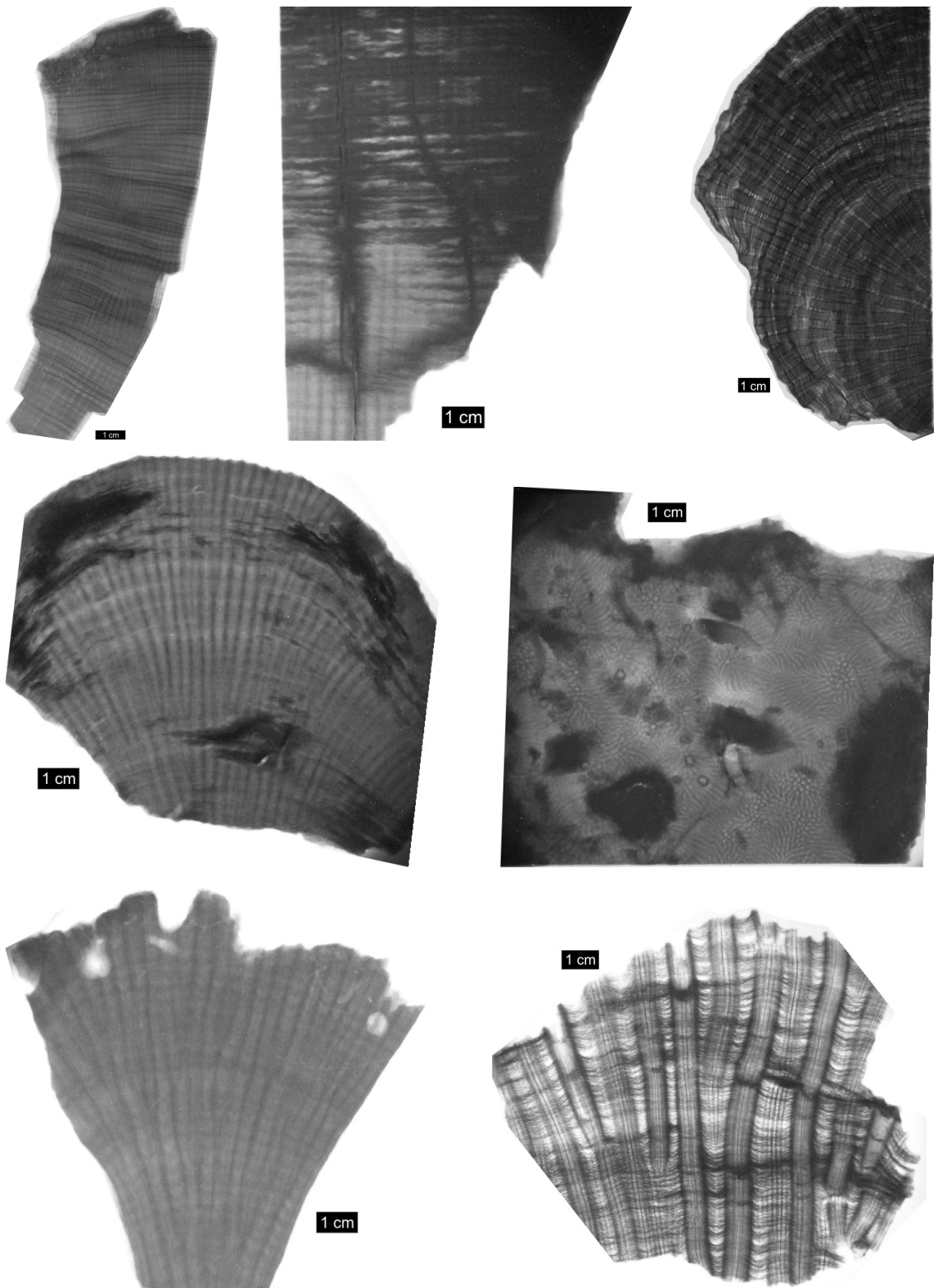


Figure 52: X-radiographs of coral slabs 460AS1, 460BS1, 461AS1, 461BS1, 467K1, 469AS1 and 469MS1 from upper left to lower right. All from Gurabo Formation, Dominican Republic

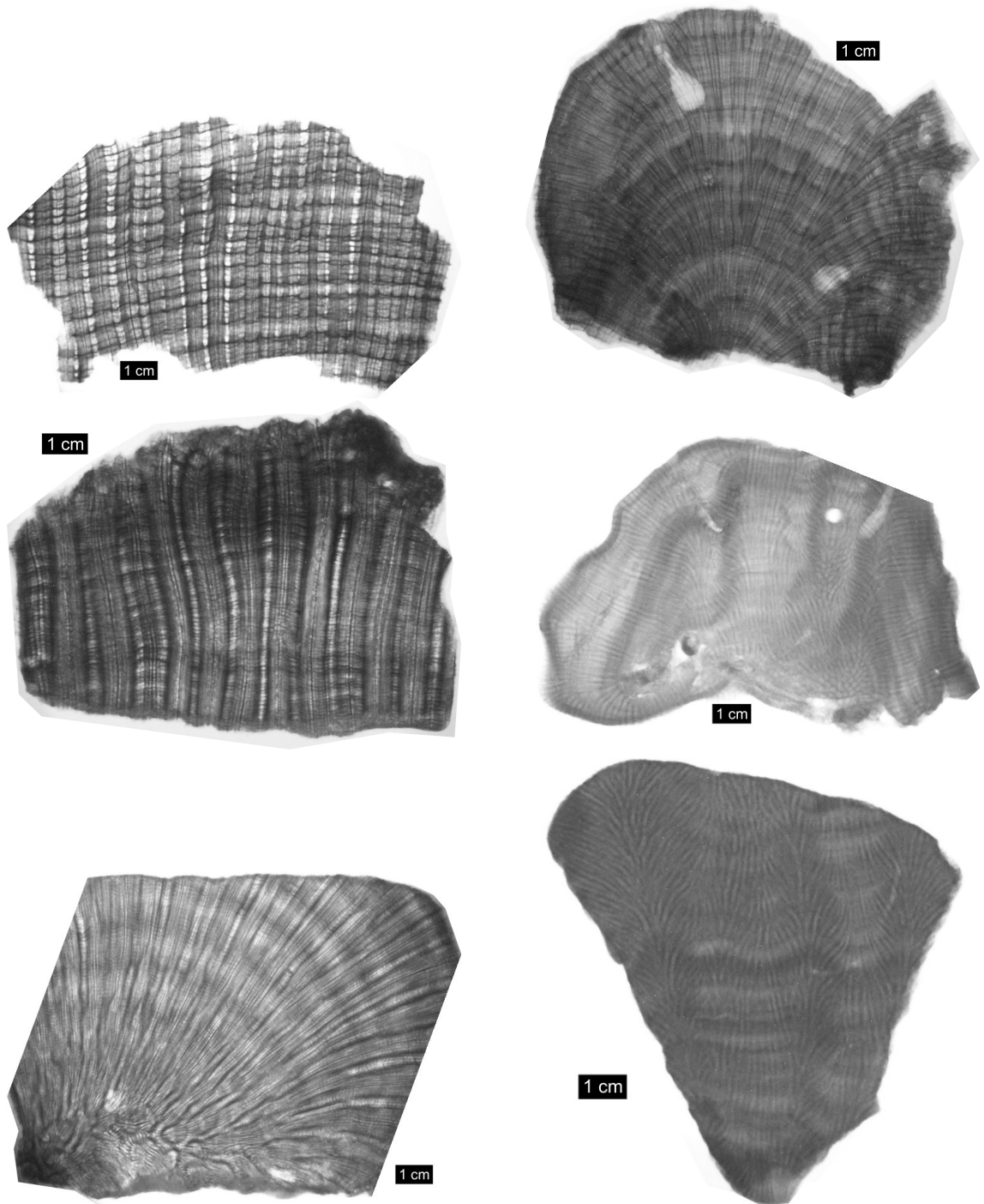


Figure 53: X-radiographs of coral slabs 463K1S1, 463K2S1, 463K3S1, 463K4S1, 464AS3 and 464ES3 from upper left to lower right. All from Cercado Formation, Dominican Republic

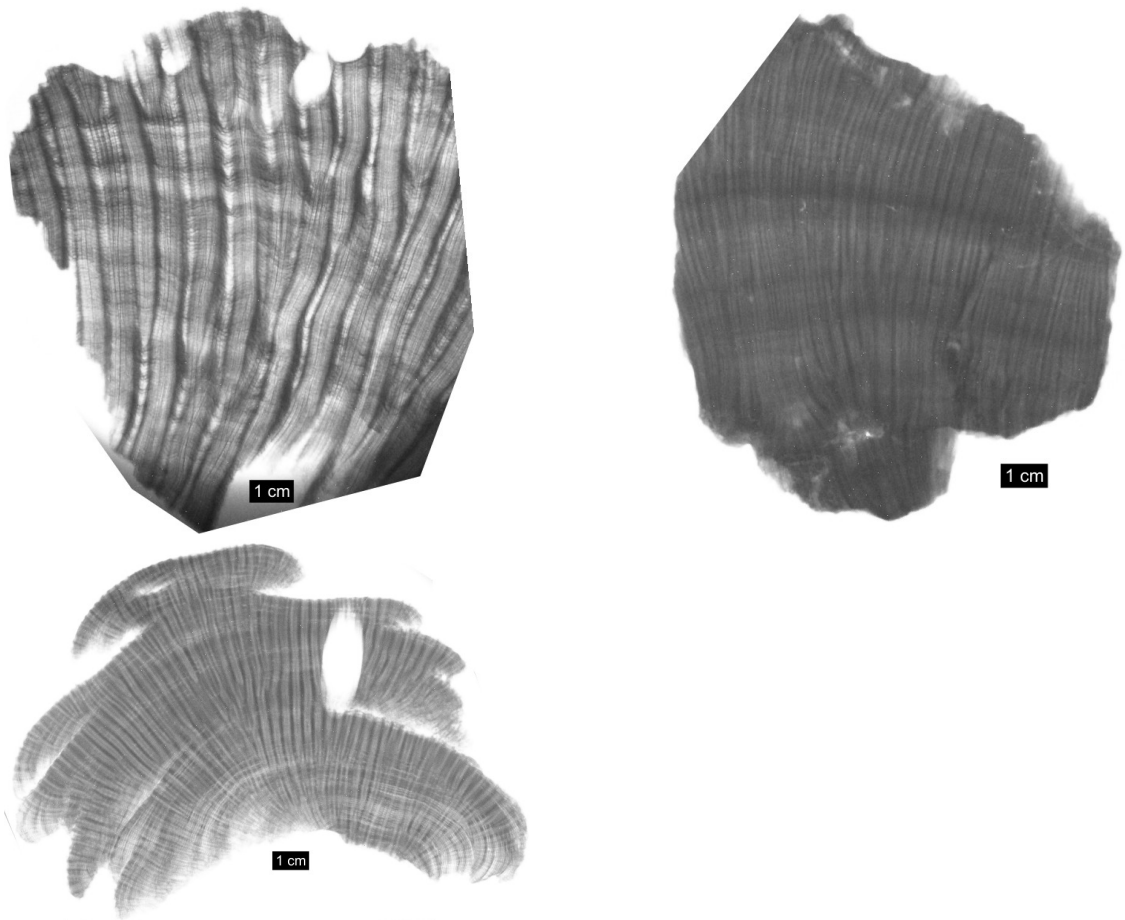


Figure 54: X-radiographs of coral slabs 469NS1, 469RS1 and 503 from upper left to lower right. 469NS1 and 469RS1 are from Gurabo Formation, 503 is from Holocene Lago Enriquillo, Dominican Republic

## 4 Discussion

### 4.1 Florida

#### 4.1.1 Outcrop 452

**Age** The geologic map of the state of Florida suggests for the surface Plio/Pleistocene Caloosahatchee Formation (*Scott et al.*, 2001). The pit has a depth of 60 ft (18.3 m), for this reason the surface map is not indicating without fail the age of the samples. However, local experts evaluate the sediments in this outcrop as Plio/Pleistocene Caloosahatchee Formation (E. Petuch, oral communication). Direct numerical data for this outcrop are not existent, so a finer stratigraphic classification is not possible. The samples from outcrop 452 are highly probable material from the Plio/Pleistocene Caloosahatchee Formation. The age of the Caloosahatchee Formation is located in the late Pliocene and early Pleistocene with age estimations of 2.1-1.6 Ma (*Petuch*, 1982; *Lyons*, 1990; *Petuch*, 2007).

**Preservation** The skeleton of coral 452K1 is in a pristine state of conservation. It displays all skeletal elements (septae, columnella and theca walls). Between these a high porosity and no visible secondary mineral growth causes a low density below 1 g/cm<sup>3</sup>. Submerged in water, this coral is even floating. Also no hints for minerals other than aragonite are found via X-ray diffraction and only a few pore spaces show in SEM pictures some mineral overgrowth, mainly secondary aragonitic fiber bundles, which is typical for early marine diagenesis and also exists in live coral colonies (*Schroeder and Purser*, 1986; *Nothdurft and Webb*, 2009). No correlation between both signals,  $\delta^{18}O$  and  $\delta^{13}C$ , exists. Finally the U/Ca and the Sr/Ca ratios are in a positive correlation which is also a clear sign for pristine preservation as found in modern diagenetically unaffected corals (*Fallon et al.*, 1999).

**Skeletal Growth Rhythmic and Stable Isotope Data** 6-7 samples for stable isotopes within a typical year ( $\emptyset$  growth rate = 4.8 mm/yr) are placed in average. This average sampling frequency depicts the seasonal isotopic variability in the Plio/Pleistocene rather well. The stable Isotope data suggest an annual cycle within each HDB in the X-radiograph. Annual  $\delta^{18}O$  variability ranges from 1.13 ‰ to 3.11 ‰, the mean seasonality is 2.08 ‰. After literature data (SST: -0.22 ‰/1°C, *Druffel*, 1997) and the assumption, that the  $\delta^{18}O$  signal is modulated only by SST, the mean seasonal temperature difference is 9.5 °C (5.1 - 14.1 °C). A control of  $\delta^{18}O$  values only by SST is unlikely due to groundwater and riverwater runoff from Florida which is isotopically fractionated in the modern Florida Bay, which has a comparable environment for corals as the Okeechobee subsea during the Plio/Pleistocene (*Swart et al.*, 1989, 1996; *Petuch*, 2007). *Jones and Allmon* (1995) could restore Pliocene seasonality with the help of oxygen and carbon isotope profiles in mollusk shells in the Pinecrest Beds near Sarasota, Florida which averages 9°C, which is close to here presented results. *Solenastrea* 452K1's Sr/Ca ratios (visual anticorrelating to  $\delta^{18}O$ ) and Mg/Ca ratios (visual correlating to  $\delta^{18}O$ ), both in antiphase/phase with the  $\delta^{18}O$  signal and the density pattern, suggest a mean seasonality for Sr/Ca of 14.4 °C (slope: *Marshall and McCulloch*, 2002) and for Mg/Ca of 12.7°C (slope: *Mitsuguchi et al.*, 1996), which is quite similar to the  $\delta^{18}O$  seasonality. The difference of 3-5 degrees from the mean  $\delta^{18}O$  seasonality can either be explained as a higher resolution of the laser ablation samples (and so a lesser mixing of skeletal material from several “months” as within the drilled powder samples for stable isotopes) which shows a less dampened signal. Only traces of calcite are found within the coral skeleton, which excludes a possible diagenetic overprint with secondary calcite, which would show up with a twenty times elevated Sr/Ca-SST

compared to  $\delta^{18}\text{O}$ -SST (Dalbeck *et al.*, 2011). Indeed the Sr/Ca-SST are higher than the  $\delta^{18}\text{O}$ -SST but the seasonal differences are one magnitude lower than for a significantly altered coral. Most probably the influence of other factors onto the  $\delta^{18}\text{O}$  signal than SST is depicted here, e.g. groundwater inflow or river discharge. Higher Ba/Ca ratios correlates with a higher river discharge, which seems to increase in the *Solenastrea* 452K1 approximately 3 months after the SST-Minima (winter) in the spring. Combined with the higher resolution of the laser ablation samples the difference is explainable by this.

We classified HDBs in two ways:

(1) The first way to classify the HDBs was to describe its characteristic in the X-radiograph. Here is distinguished between HDBs with a regular spacing and a smooth development with a gradual transition to the LDB, which seems to be the “normal” form (violet). Another form of HDB is dark and well visible but also sharp delimited (orange). Some of the HDBs are barely visible and are marked yellow (Fig. 55). In this characterization is also a trend from the usual type of smooth and regular HDBs (violet) to the sharp and dark HDBs (orange).

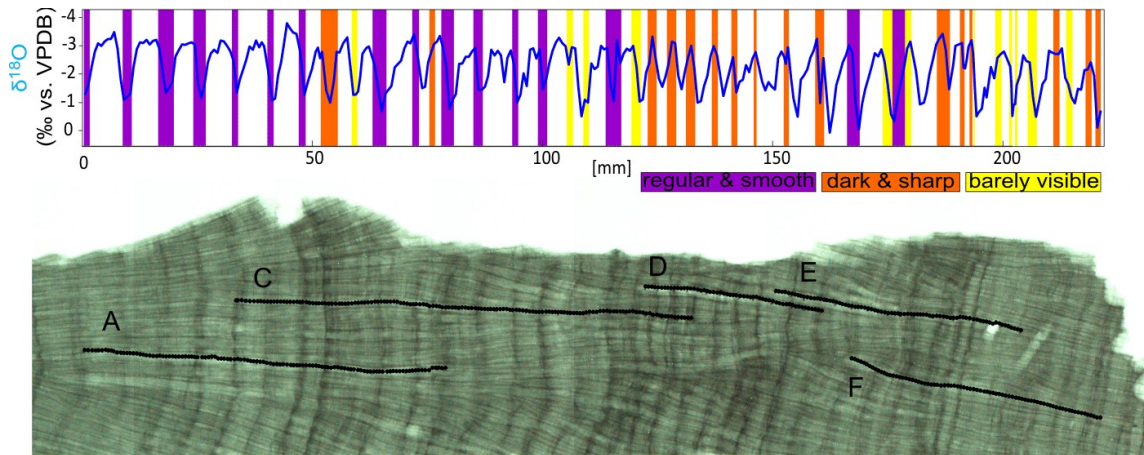


Figure 55: HDBs classified after their subjective appearance in the X-radiograph of *Solenastrea* 452K1. HDBs regular and smooth (violet), HDBs dark and sharp (orange) and HDBs barely visible (yellow).

(2) The second way was to discriminate by the position of the HDBs in relation to the  $\delta^{18}\text{O}$  cycle. The grey marked HDBs coincide with the  $\delta^{18}\text{O}$  maxima and are present mostly in the lower segment of the slab. In the upper segment of the coral HDBs dominate, which coincide with  $\delta^{18}\text{O}$  minima (orange) and somewhere between (yellow) (Fig. 56).

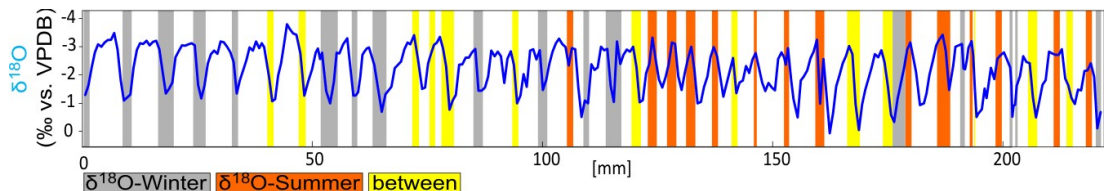


Figure 56: HDBs in *Solenastrea* 452K1 classified after the position of the  $\delta^{18}\text{O}$  maxima and minima: HDB in correlation with  $\delta^{18}\text{O}$  maximum (grey), HDB in correlation with  $\delta^{18}\text{O}$  minimum (orange) and HDB somewhere in between (yellow). The scale is the same as in Fig. 55.

As stable isotopes and laser ablation geochemistry show in accordance with X-radiography



a clear annual cycle for the Plio/Pleistocene in this coral, the density pattern in the coral adds another feature here: interannual variability.

To investigate the effects of extreme SSTs on coral and bivalve calcification, systematical analyses of skeletal accretion patterns were carried out on this *Solenastrea* 452K1 and the bivalve *Mercenaria* from the Caloosahatchee Formation (Hansmann, 2011). The main clue behind this is to find out why recent *Mercenaria* have the same seasonal rhythm of shell accretion as fossil specimen, while recent and Mid-Pliocene *Solenastrea* (Roulier and Quinn, 1995) differ from the here observed calcification pattern.

The Plio/Pleistocene *Solenastrea* 452K1 shows a clear annual cycle in the  $\delta^{18}O$  values too. But different to recent and Mid-Pliocene *Solenastrea*, the  $\delta^{18}O$  maxima does not belong to just one season for the coral record (either summer or winter). Supposed that the  $\delta^{18}O$  maxima in the Plio/Pleistocene *Solenastrea* represent the winter and the  $\delta^{18}O$  minima represent the summer, in *Solenastrea* 452K1 a mixture of HDBs formed in winter (44%), summer (39%) or spring/fall (17%) along the coralline record (36 yrs).

Since each genus has a different ecological niche with a temperature range ( $T_{min} - T_{max}$ ) in between it can live and find an optimum temperature ( $T_{opt}$ ), *Solenastrea* and *Mercenaria* are unequal. The  $T_{opt}$  for recent *Solenastrea* is assumed to be approximately 30°C, which is the modern summer SST where HDBs are formed. Temperate *Mercenaria mercenaria* lives recently all along the eastcoast of North America until a northern latitude of 45°N, which is overlapping partly with the modern distribution of tropical *Solenastrea hyades*. The southern limit of *Mercenaria mercenaria* environmental tolerance is defined by too high summer SSTs ( $T_{max}$ ) while *Solenastrea hyades* northern limit defined by cold winter SSTs ( $T_{min}$ ). The conclusion of this is, that both species in the same area have at different seasons their  $T_{opt}$ , hence more calcification in a given time than in other seasons of the year. Adapted to the Worum-model of calcification (see chapter coral calcification, Fig. 2), *Mercenaria* and *Solenastrea* have their highest calcification rate during their  $T_{opt}$  which occurs for *Mercenaria* during the winter because the summer SSTs are above this value and for *Solenastrea* in some of the cases in the summer, the winter and in spring/fall. Some years had high winter SSTs close to *Solenastrea* 452K1  $T_{opt}$  and even higher summer SSTs which lead *Solenastrea* 452K1 to form its HDB during the winter (e.g. the first 5 years in Fig. 56). Other years recorded by *Solenastrea* 452K1 were characterized by low winter SSTs and summer SSTs close to  $T_{opt}$ , where the coral formed its HDB during the summer (e.g. the years between 110 and 140 mm in Fig. 56). Under the assumption, that Mid-Pliocene SSTs were 3-4°C warmer than today (Haywood and Valdes, 2004), the  $T_{opt}$  for Mid-Pliocene *Solenastrea* was exceeded during summer and the formation of HDB took part during the cold season (winter). The modern setting is the opposite case - HDB formation during summer. In consideration of the skeletal records of the Mid-Pliocene and recent *Solenastrea* (Roulier and Quinn, 1995; Swart et al., 1996), the interannual variability during the Early Pleistocene (*Solenastrea* 452K1) was enhanced (Fig. 57) A high interannual variability of temperatures which oscillates the summer SSTs in the Plio/Pleistocene around the  $T_{opt}$  for *Solenastrea* cause also an interannual variability of the HDB formation in *Solenastrea* (Fig. 57). The formation of the HDB in *Solenastrea* can be in winter (as recent when  $T_{opt}$  is reached in August, Fig. 8), in summer (as in Mid-Pliocene) or in spring and fall as dHDBs in this  $\delta^{18}O$  data. *Mercenaria*  $T_{opt}$  is lower than *Solenastrea*  $T_{opt}$  and only hit or approached in winter so that the HDB formation in all investigated specimen is consistent only during winter (Hansmann, 2011). However, the  $\delta^{18}O$  signal shows no trend or high variability between it's maxima and minima, respectively. Clearly dHDBs as observed in *Solenastrea* 452K14 (same outcrop and epoch as 452K1) argue for this pattern too, but could unfortunately not been measured for stable isotopes yet (Fig. 35).

On the other hand, the timing of density band formation varies in recent *Solenastrea* as

well. *Swart et al.* (1996) observed in Florida Bay that HDBs form mainly coincident with low skeletal  $\delta^{18}O$  values (summer), but in some years during highest  $\delta^{18}O$  values. Within 20 years of coralline record, they found 5 years in which dense band and high  $\delta^{18}O$  value coincide. Their conclusion was either a higher salinity during the summer associated with HDB formation or that the HDB formed at another time than summer. For the latter case, HDB formation during another season than summer, a time shift in order of some months would be enough (*Swart et al.*, 1996). Despite the recent HDB formation during different  $\delta^{18}O$  "times", *Solenastrea* 452K1 shows a more excessive switching in HDB-formation and also seems to have lived in an environment closer to the Florida Keys than Florida Bay (*Brachert et al.*, 2013b). An environment like the modern Florida Keys is less influenced by SSS changes due to groundwater and river input than the Florida Bay (Fig. 9), supporting the assumption that SST is the main driver of  $\delta^{18}O$  variability. Between the coral  $\delta^{18}O$  and  $\delta^{13}C$  signal is no correlation. This is not surprising since in recent *Solenastrea* from Florida Bay also no relationship between either temperature or salinity could be found and the  $\delta^{13}C$  signal is more related to hurricane and storm frequency and not to any seasonal parameter (*Swart et al.*, 1996)

**Main and Trace Element Composition** Ba/Ca ratios seem to be a good proxy for river discharge in *Montastrea annularis* in the Caribbean (*Horta-Puga and Carrquiry*, 2012). They found a clear correlation for high coral Ba/Ca ratios and high precipitation rates in the hinterland. Regarding the Ba/Ca ratios measured in *Solenastrea* 452K1, peak Ba/Ca coincides with peak  $\delta^{18}O$  values (winter). Somehow this is contrasting the modern situation of precipitation maxima in southeast Florida, where a minor maximum happens in early summer is followed by a major maximum in the late summer/autumn. As figured out, the *Solenastrea* 452K1 must have lived in an environment similar to the modern Florida Keys. The Florida Keys are bordering Florida Bay, a semi-enclosed marine environment which strongly depends from the riverine input of the Everglades area. Waters from the Everglades area is strongly enriched in  $\delta^{18}O$  as a result of evaporation during a long residence time of up to two years (*Swart et al.*, 1989, 1996). Possibly, the Ba/Ca ratio in *Solenastrea* 452K1 could be influenced by such lagged freshwater inputs mimic high winter precipitation. Also possible is a really different precipitation pattern to modern times. Since not only the Everglades freshwater runoff influences an environment similar to the Florida Keys, a higher winter/spring precipitation in the southeastern North American continent could have been. This was suggested with a Pliocene *Siderastrea* sp in a condition of a permanent El Nino like state (*Slika and Herbert*, 2009).

U/Ca ratios change contemporaneously with Sr/Ca, Ba/Ca and  $\delta^{18}O$ . Sr/Ca and  $\delta^{18}O$  are supposed to be temperature driven and this correlation in recent hermatypic corals from

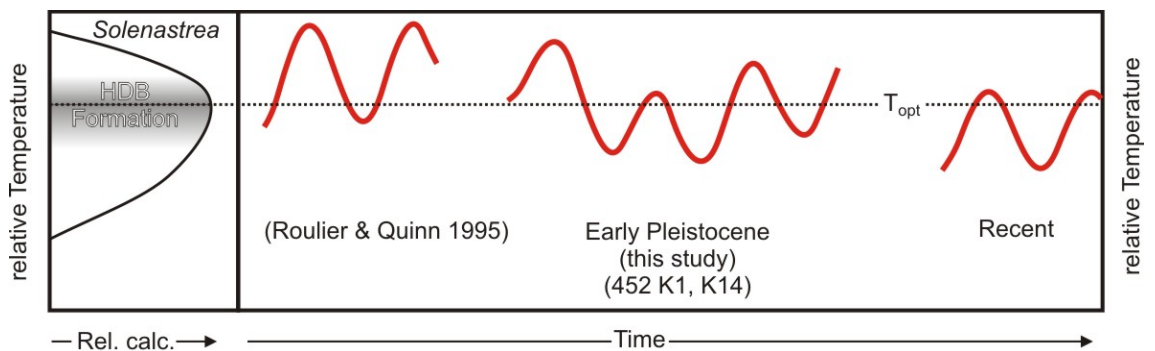


Figure 57: Schematic representation of SST changes in the younger Neogene of Florida inferred from growth rhythms in *Solenastrea* and *Mercenaria*,  $\delta^{18}O$  variability, and modern distributions.

Galapagos is also interpreted as mostly SST controlled (*Shen and Dunbar, 1995*). The change in U/Ca ratios (mean amplitude:  $1.64 \mu\text{mol/mol}$ ) calculated as relative SST changes (slope:  $-0.05 \mu\text{mol/mol}$  per  $1^\circ\text{C}$ ; (*Shen and Dunbar, 1995*)) results in an unrealistic  $32.8^\circ\text{C}$  SST change. The mean uranium concentration in the profiles (3.7-5 ppm) ranges slightly above the literature values for fossil coral reefs (1.5-4 ppm, *Min et al., 1995*, and references cited therein). A similar unrealistic seasonal temperature change is calculated using the calibration of *Min et al. (1995)*:  $26.9^\circ\text{C}$ . Highly likely other factors than temperature affect the U/Ca ratios. U/Ca ratio is correlating with Ba/Ca and Y/Ca, which are derived by riverine input. The U/Ca seasonal temperature change using the calibration of *Sinclair et al. (1998)* is  $11.7^\circ\text{C}$ , which is much more realistic regarding the here calculated Sr/Ca, Mg/Ca and  $\delta^{18}\text{O}$  relative temperature changes.

The B/Ca signal with it's annual minimum values is predating the Sr/Ca signal by approximately 2 months. Calculating seasonal SST differences with boron (slope: *Sinclair et al., 1998*) results in a lower seasonality ( $6.4^\circ\text{C}$ ) than strontium, magnesium or oxygen temperatures. This is not reliable and no SST record compared with B/Ca data is available in the literature. The incorporation of B into coral skeletons is different to Sr and temperature not the only controlling factor, as pH and secondary aragonite growth can also affect boron incorporation (*Gaillardet and Allegre, 1995*). Cementation processes (diagenesis) also decrease the B/Ca content, because coral porewaters have a lower pH (7.5-7.7) than coral calcifying fluid (8-9, *Allison et al., 2007*).

**REE** The nonflat pattern of the shale-normalized rare earth element composition is typical for water with riverine input (*Nozaki, 2001*). Nothing else can be expected here, since most of the carbonates of the Caloosahatchee Formation are deposited in a very shallow marine environment with also restricted conditions (*Lloyd, 1969*).

The comparison of the shale-normalized REE profiles from the upper part of the coral (profile AB & CD) and those of the lower part (Profiles EF & GH) reveals two characteristic differences. The first and more obvious difference is the saw-toothed shape of the HREE in the upper profiles, which does not repeat in the lower profiles (Fig. 32). In unnormalized profiles this could be the Oddo-Harkins effect (*North, 2008*), but at first this profile is normalized and second the Oddo-Harkins rule is just working for elements with even atomic number (more common) and odd atomic number (less common). All, the higher concentrated elements ( $^{159}\text{Tb}$ ,  $^{165}\text{Ho}$ ,  $^{169}\text{Tm}$ ) and the lesser concentrated elements ( $^{157}\text{Gd}$ ,  $^{163}\text{Dy}$ ,  $^{167}\text{Er}$ ) of these profiles have odd atomic numbers. The second difference is a higher concentration of LREE in the upper profiles. Since the REE are mostly transported by rivers into the oceans (*Nozaki, 2001*), an increasing riverine input, caused by higher or changed precipitation patterns, could lead to this pattern in the upper part of the coral (e.g. *Kasper-Zubillaga et al., 2010*). This is interesting because the HDB-formation during the lifetime of this coral changed significantly. It is suggested that lower summer SSTs lead to a formation of the HDB during the summer ( $T_{opt}$ ), which is accompanied by an increased precipitation, as REE pattern show in the upper profiles of coral 452K1.

**Spectral Analyses** The spectral analyses of the three time series of *Solenastrea* 452K1 (skeletal density,  $\delta^{13}\text{C}$  and  $\delta^{18}\text{O}$ ) show mostly the annual peak which is in all frequency/power plots significantly above the 99% confidence interval (see chapter 2 for description of method). This is not surprising since there is a clear rhythm in all signals which accord with seasonal growth patterns. Within both isotopic records ( $\delta^{18}\text{O}$  and  $\delta^{13}\text{C}$ ) a small peak at the period of 0.5 years appears, which is visualized in a Fourier transform of  $\delta^{18}\text{O}$  over the lifetime of the coral (Fig. 58). Interestingly, the  $\delta^{18}\text{O}$ -signal shows no other significant peaks than the 1 yr and 0.5 yr peaks.  $\delta^{13}\text{C}$  and skeletal density show peaks with

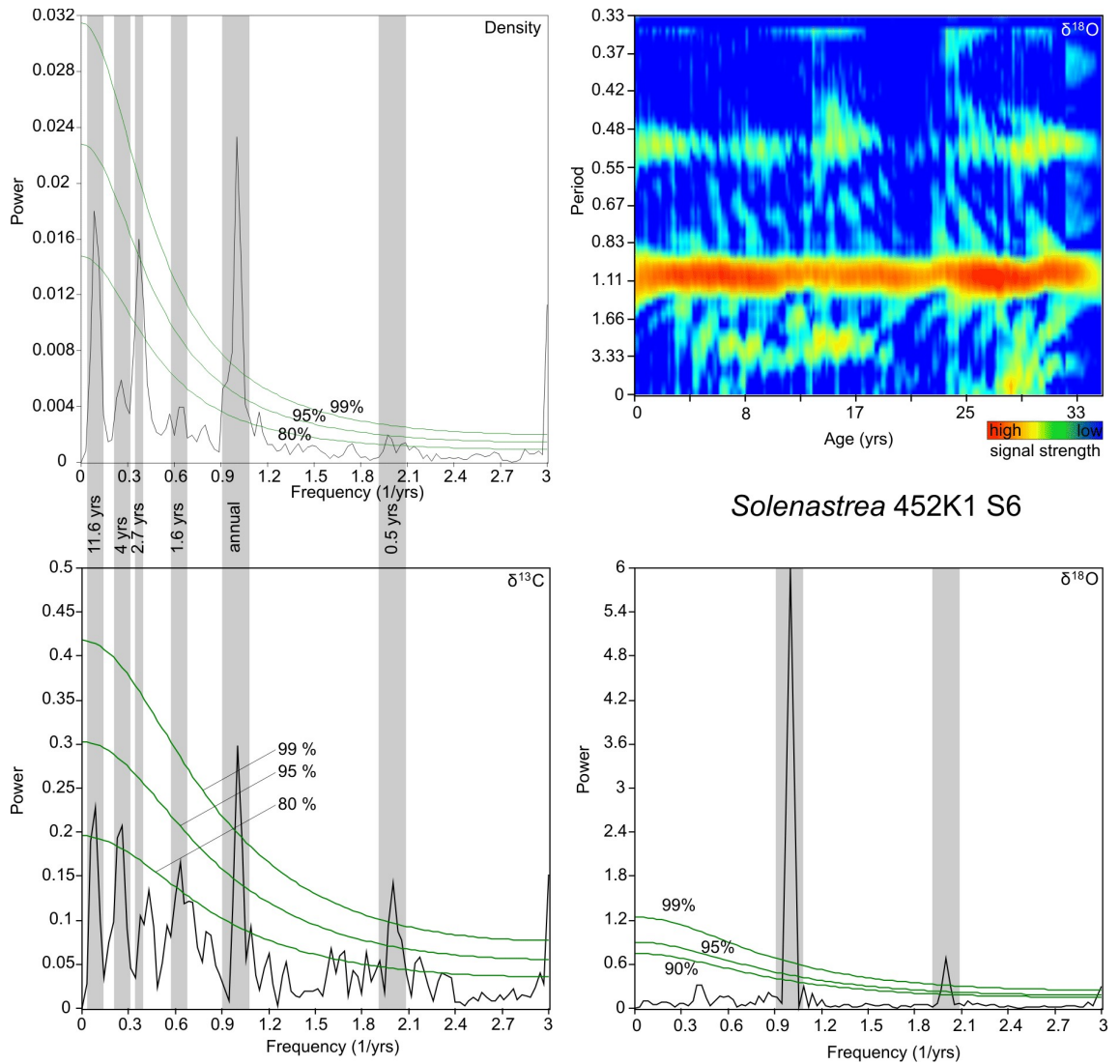


Figure 58: Spectral analyses of skeletal density (top left),  $\delta^{13}C$  (bottom left) and  $\delta^{18}O$  (bottom right) from coral 452K1. All analyses were done with a rectangular window. Grey bars show where spectral peaks cross the confidence intervals. Additional short-time Fourier transform with window Multitaper 5 (top right). Since  $\delta^{18}O$  signal shows the expected annual peak, additional a 0.5-yr peak is significant but appears not during the whole timeseries. Density and  $\delta^{13}C$  show also this peak of  $\delta^{18}O$  and one common spectral peaks above the 80% confidence interval with a period of 11.6 yrs.

larger periods but only the 11.6 yr peak is in both signals above the 80% confidence interval. Other peaks in  $\delta^{13}C$  (1.6 yr, 4 yr) and skeletal density (2.7 yr) above the 80% confidence interval are just single appearances and therefore doubtful in significance, because they are not shown by skeletal density and  $\delta^{13}C$ , respectively. However, the 2.7-4 yr periodicities detected could belong to ENSO, which impacts with a 4-5 months delay in the tropical North Atlantic and the Caribbean (*Enfield and Mayer, 1997*). This ENSO pattern in this region is not very intense, but was also described by other studies (*Gischler and Oschmann, 2005; Gischler et al., 2009*) and therefore present in a weak form in *Solenastrea 452K1* (with uncertainties).

### 4.1.2 Outcrop 509

**Age** In 2012 outcrop 509 was encountered as abandoned mining and quarry lakes with more or less remaining boulders. The *Solenastrea* 509A was sampled in a spoil pile from this abandoned pit. The geologic map of the state of Florida indicates shelly sediments of Plio-Pleistocene age, which is the Okeechobee Group (probably the same stratigraphic unit as in locality 452)(*Scott et al.*, 2001). The outcrop 509 is highly probable the stop 11 from J.F. Meeders fieldtrip guide (*Meeder*, 1979). East of the US 41 at Alico Road is described a location (Stop 11) which exists of quarry lakes with large boulders and active mining. The author of the fieldtrip guide described the deposits as part of the Pliocene fossil reef of south Florida (*Meeder*, 1979). This reef was first reported as part of the Plio/Pleistocene Caloosahatchee formation (*Wilson*, 1976) and later as part of the Upper Tamiami Formation (Pinecrest Beds)(*Meeder*, 1979). The age of the Pinecrest Beds between the Tamiami formation and Caloosahatchee Formation is dated as Late Pliocene (*Meeder*, 1982; *Allmon*, 1993). Due to the lack of direct numerical dates for this coral a fine stratigraphic classification is not possible.

**Preservation** The skeleton of the coral 509A is in a pristine conservation. Perfect preservation with finely developed skeletal elements as septae, columnella and theca walls are obvious. A high original porosity and no visible secondary mineral growth is present. Also no hints for minerals other than aragonite are found via X-ray diffraction. SEM analyses with EDX show tight secondary aragonitic fiber bundles growth on many surfaces with an increasing concentration towards the corals bleached rim (approx. 3 mm). A more intense aragonite needle cement compared to pore space of coral 452K1 is observed here and in the central parts of the coral head the pristine skeleton is much lesser influenced. This pattern was also found in coral 452K1. *Solenastrea* 509A the correlation between  $\delta^{18}O$  and  $\delta^{13}C$  is lagging 1 and -1 sample position (Fig. 37), which is interpreted as absence of diagenetic leveling.

**Skeletal Growth Rhythmic and Stable Isotope Data** Within a typical year ( $\emptyset$  growth rate = 2.2 mm/yr according to  $\delta^{18}O$ -data) 3 samples in average were taken for stable isotopes. This average sampling resolution is insufficient for the seasonal isotopic variability of this coral. However, the stable isotope data suggest clear annual cycles within the sampled area. Due to blurring of HDBs in the central part of the coral slab isotope data and density were compared only in transect 1 which is near the margin of the coral slab (Fig. 59). Here, the  $\delta^{18}O$  maxima (winter) have average distances of  $2.9 \pm 0.4$  mm which is slightly above the average  $\delta^{18}O$ -based growth rate. The density pattern of the coral skeleton is formed by two different kinds of HDB alternating with LDBs. The first kind is dark, thin and very sharp developed and in the most cases coincident with a  $\delta^{18}O$ -maximum, interpreted here as winter, while the second kind of HDB is indistinct and has a lesser contrast (to the LDB) compared to the first kind of HDB. There is an unambiguous chronology in the formation of the different kinds of HDBs. This means, the coral is supposed to form a sharp HDB, after this an LDB, after this an indistinct HDB, again a LDB and the cycle reoccurs. The delimiter for this cycle is the  $\delta^{18}O$ -maximum (winter), which implies that one year consists of two HDBs and two LDBs – dHDBs (Fig. 59). In the classification after the Worum-model for temperature-dependent calcification (see chapter coral calcification, Fig. 2), the SST for *Solenastrea* 509A oscillates around its optimum calcification temperature (*Worum et al.*, 2007). A mean growth rate of  $3.6 \pm 1.5$  mm/yr is not just because of the blurring of HDBs in the central part of the coral skeleton unlikely, it is also masked by dHDBs and therefor pretending wrong growth rates

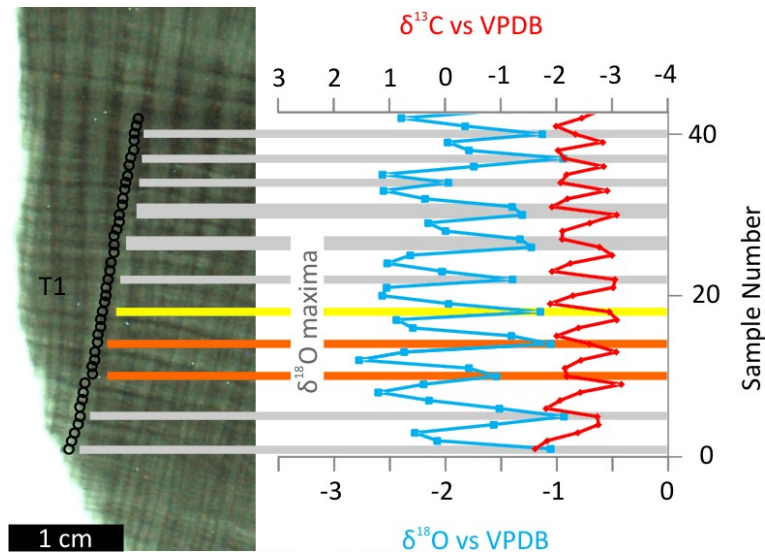


Figure 59: Correlation of X-radiograph and stable isotope data in 509A S1 only in transect 1.  $\delta^{18}\text{O}$ -maxima (winter) coincide in the most cases with sharp HDBs (grey lines). Note the unarticulated HDBs between the sharp dense bandings which together are interpreted as dHDBs. Orange and yellow lines indicate HDBs in summer/transitional seasons.

(Fig. 59). Growth rate measured from X-radiographs for this *Solenastrea* is to interpret carefully as the analysis of transect 1 shows.

The mean seasonality is in average 0.96 ‰ but it varies between 0.15 ‰ and 2.09 ‰. Quite the same annual variation in  $\delta^{18}\text{O}$  was found in another fossil *Solenastrea* (0.7 to 2.27 ‰, *Roulier and Quinn*, 1995), while a modern *Solenastrea* has a higher annual  $\delta^{18}\text{O}$  range of 0.17 ‰ to 4.42 ‰ (*Swart et al.*, 1996, Fig. 60). Application of the coral temperature slope ( $-0.22\text{‰}/1^\circ\text{C}$ , *Druffel*, 1997) to estimate annual temperature ranges produces variations from 0.7-9.5°C (Mid-Pliocene *Solenastrea*: 3-10°C from *Roulier and Quinn* (1995); modern *Solenastrea*: 7.5-13.5°C from *Swart et al.* (1996)). This seasonality recorded by 509A is in average 4.4°C, which is compared to 452K1 from the same Formation unrealistic. Possible diagenetic influences on isotopic composition of the coral skeleton should be considered too since it is the *Solenastrea* with the highest mean skeletal density and secondary overgrowths from the Plio/Pleistocene of Florida. The amount of calcite in this coral is 1%, which can affect the calculated SSTs. In recent and Holocene corals amounts of 10% secondary calcite changed the calculated  $\delta^{18}\text{O}$  derived SSTs just by 0.6°C, which means a negligible effect on *Solenastrea* 509A  $\delta^{18}\text{O}$ -SST (*Dalbeck et al.*, 2011). Most likely the  $\delta^{18}\text{O}$  signal is dampened by the insufficient number of samples within one year which can explain the low  $\delta^{18}\text{O}$  seasonality (*Leder et al.*, 1991; *Swart et al.*, 1996). Under the assumption the mean seasonal SST change is equal to coral 452K1 ( $\sim 12^\circ\text{C}$ ), the calculated  $\delta^{18}\text{O}$ -SST-seasonality with 3 samples/year would be in the worst case 7°C (Table 5). Furthermore a control of  $\delta^{18}\text{O}$  values only by SST is unlikely too and the same environmental conditions as in 452K1 can be expected here. The difference between fossil and modern corals is explained as different environmental conditions during growth and (1) either the coral grew close to the seasonal thermocline and the Mid-Pliocene seasonality was similar to modern or (2) the coral grew near the sea surface and the Mid-Pliocene seasonality was dampened (*Roulier and Quinn*, 1995). The modern thermocline off Sarasota, FL, reaches a maximum depth of 40-70 m in August (*Roulier and Quinn*, 1995), which is an unimaginable depth for reef coral *Solenastrea* 509A.

In difference to 452K1 a high cross-correlation between  $\delta^{18}\text{O}$  and  $\delta^{13}\text{C}$  at lag 1 and -1 along all 62 years sampled in this coral (509A) exists ( $r = 0.4$  and  $r = -0.42$ ). To figure out

Table 5: Theoretical dampened SST seasonality (worst case) when only 3 samples/year for stable isotopes are taken but the true SST seasonality is 12°C.

Month	1	2	3	4	5	6	7	8	9	10	11	12
rel. SST (°C)	0	2	4	6	8	10	12	10	8	6	4	2
	Sample 1			Sample 2			Sample 3					
mean (°C)	3			10			5					

which one of the signals predates the other,  $\delta^{18}O$  (Transect 1) was shifted 1 sample position towards younger and the correlation become  $r = 0.8$ . The contrary case that  $\delta^{18}O$  is shifted 1 sample position (approx. 4 months) towards older produced a correlation of  $r = -0.71$ . Using this, the annually peak  $\delta^{18}O$  values precede the peak  $\delta^{13}C$  values by approximately 4 months. A predating of peak  $\delta^{18}O$  values to peak  $\delta^{13}C$  of 2 months was also observed in the Mid-Pliocene *Solenastrea* (Roulier and Quinn, 1995). The four-monthly resolution of the samples is too low to decide if the time delay is really bigger than the 2 months of the Mid-Pliocene *Solenastrea*, but in general a similar pattern exists.

Average annual range of  $\delta^{13}C$  is  $0.81 \pm 0.34$ ‰ and spreads between 0.18 and 1.59‰. Compared to  $\delta^{13}C$  seasonal changes in a modern *Solenastrea* (0.15 – 2.66‰,  $\sigma = 0.98$ ‰, Swart *et al.*, 1996) and a Mid-Pliocene *Solenastrea* (0.31 – 2.21‰, Roulier and Quinn, 1995) the values of *Solenastrea* 509A have a similar scale but are somehow smoothed. Assuming a higher interannual variability during the Plio/Pleistocene in Florida as found in *Solenastrea* 452K1 from the same Formation, the signal in *Solenastrea* 509A seems to be dampened by the insufficient number of samples per year. However, the carbon isotope record shows in most of the years a clear annual cycle following the oxygen records with a lag of approximately four months (one sample distance).  $\delta^{13}C$  values in zooxanthellate scleractinian corals are controlled dominantly by the photosymbionts (zooxanthae) activity, recording the seasonal number of sunshine hours (Fairbanks and Dodge, 1979; Pätzold, 1984). This time lag in between periods of high sunshine and periods of low SST is similar with today (hot/rainy summers and cool/dry winters, Roulier and Quinn, 1995). Thereafter, the Plio/Pleistocene corals record a climatic pattern which is transitional to the modern situation, as HDB formation in Caloosahatchee Formation corals and the isotope records thereof reveal. Reconstructed paleotemperatures of gastropod shells from the Pliocene Pinecrest Beds and the Caloosahatchee Formation yield that the Mid-Pliocene SST ( $25.1 \pm 1.4$ °C) were slightly above those in the late Pliocene/Pleistocene ( $22.4 \pm 0.5$ °C), which is in agreement with the late Pliocene cooling event (Crowley, 1991; Lisiecki and Raymo, 2005; Tao and Grossman, 2010). The paleoenvironmental conditions for the Caloosahatchee Formation at outcrop 451 were investigated by Hansmann (2011) with the help of oxygen and carbon isotope records in the bivalve *Mercenaria mercenaria*. An open-marine milieu and a similar climate as recent as well as a situation compared to the modern Florida Bay is discussed herein. All isotopic values plot within the area for an open-marine environment within the Florida Bay Model from Halley and Roulier (1999, Fig. 60). This is somehow contradictory, since intrinsic to the Florida Bay Model everglades runoff is highly evaporated and thus enriched in  $\delta^{18}O$ . However, within the Florida Bay some regions are more restricted and some are better circulated by marine waters (Lloyd, 1969; Halley and Roulier, 1999; Tao and Grossman, 2010). Possibly, the  $\delta^{18}O$  enrichment by evaporation has only a little influence on *Mercenaria* due to a better circulation in a more open-marine milieu than today (Hansmann, 2011). The changing environmental conditions within the different members of the Caloosahatchee Formation

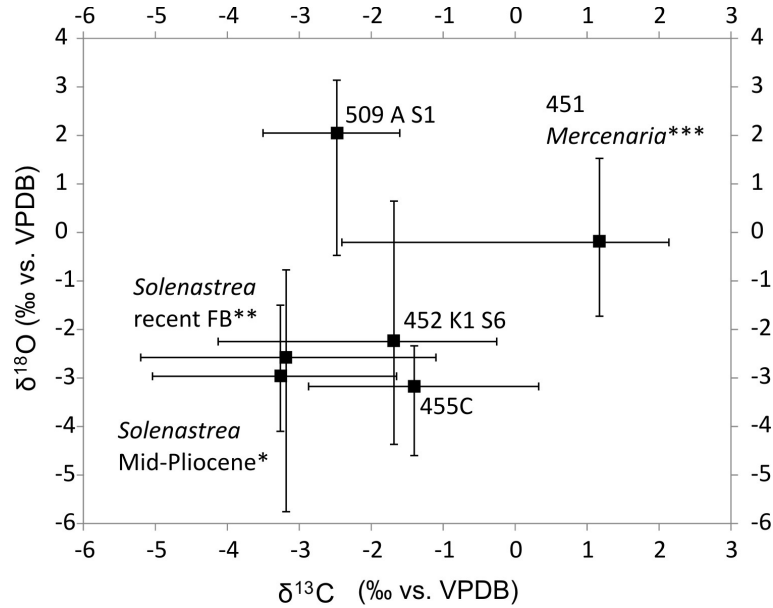


Figure 60: Comparison of isotopic ranges from *Solenastrea* 452K1 and 509A with a recent *Solenastrea* from Florida Bay\*\* and a *Solenastrea* from the Mid-Pliocene\* and *Mercenaria*\*\*\* from outcrop 451. \*Roulier and Quinn (1995), \*\*Swart et al. (1996), \*\*\*Hansmann (2011). 455C is a *Montastrea* from the Miocene Gurabo Formation, Dominican Republic (Lohmann, 2013).

and the paleogeographic position of the Caloosahatchee Strait allows the suggestion, that the Caloosahatchee Formation imaged by the *Mercenarias* in 451 was in a well mixed open-marine setting (DuBar, 1958; Lloyd, 1969; Petuch, 2007; Hansmann, 2011). Oxygen and carbon isotope data for *Solenastrea* 452K1 plot between specimen from the Florida Bay and the Florida Keys, which indicates a habitat closer to the Florida Keys than the Florida Bay (Swart et al., 1996)

During the Pliocene, a higher productivity off western Florida is observed in the Pinecrest Beds, underlying the Caloosahatchee Formation (Jones and Allmon, 1995; Tao and Grossman, 2010). The source of this productivity has been interpreted as the reflection of terrigenous input (delivered by increased riverine input due to a higher precipitation in the hinterland) (Weinlein et al., 2008; Sliko and Herbert, 2009) or as a result of nearshore upwelling (Jones and Allmon, 1995). Isotopic signatures differ for upwelling (negative  $\delta^{13}C$ - $\delta^{18}O$  correlation) and freshwater input (positive  $\delta^{13}C$ - $\delta^{18}O$  correlation) (Tao and Grossman, 2010). As discussed above, the  $\delta^{18}O$ -signal is interpreted as predating the  $\delta^{13}C$  signal in *Solenastrea* 509A and the cross-correlation with a lag of 1 sample results in a correlation for  $\delta^{18}O$  and  $\delta^{13}C$  of  $r=0.8$ . It was interpreted that the Caloosahatchee Formation and the Pinecrest Beds had similar conditions with excessive rainy seasons during winter/spring seasons. Such a situation is typical for an (modern) El Nino event in the southeastern North American continent (Sliko and Herbert, 2009). Sliko and Herbert (2009) and Weinlein et al. (2008) are going further to interpret this as an indication for a permanent El Nino-like state in the Pliocene. For Pleistocene *Mercenaria campechensis* the opposite pattern was found with high summer precipitation and no dominance of El Nino-like conditions (Weinlein et al., 2008). Following the idea that coral 509A lived in SST conditions around its  $T_{opt}$  and a higher precipitation during winter (HDB-Formation) decreases the  $\delta^{18}O$  value in the surrounding waters, the El Nino-like conditions continued to exist during the lifetime of *Solenastrea* 509A. At least this marks a salinity influence on the  $\delta^{18}O$ -signal and could explain in part the dampening of the  $\delta^{18}O$ -signal.



**Spectral Analyses** The spectral analyses of *Solenastrea* 509A stable isotope signals highlight a clear annual peak (Fig. 61). Beside this peak no other significant period is present. Spectral data based on skeletal density need to be carefully treated, as the problem with the radiographs true annual resolution in the central part of the coral slab could not be excluded for spectral analyses ("blurred HDBs", see chapter 3). Within the skeletal density pattern the annual peak is not formed clearly, probably due to this "blurred-HDBs" effect. Instead a 2 yrs, 6.4 yrs, 11.5 yrs and 19 yrs spectral peaks show up. The 19 yrs peak is very slightly above the 80% confidence interval and therefore probably an artefact. It is unlikely, that it belongs to a multi-decadal cyclicity as the AMO. For the 11.5 yrs and the 6.4 yrs spectral peaks the 95% confidence interval is exceed and both have periods similar to known climatic oscillations in this region (*Gischler and Oschmann, 2005; Greer and Swart, 2006; Gischler et al., 2009*). The 11.5 yrs peak seems to correlate with a spectral analysis of the ENSO index Nino 3.4 and an SST dataset (gridded ERSST dataset from 1890-2005) for Florida Keys (*Gischler et al., 2009*). Even if these spectral peaks were found in recent climate data, in the Caribbean a multi-decadal pattern in the precipitation at the Holocene was also found (*Greer and Swart, 2006*). The 6.4 yrs spectral peak was found in a Pleistocene coral record from Windley Key, Florida (*Gischler et al., 2009*) and in a recent coral in Belize (*Gischler and Oschmann, 2005*).

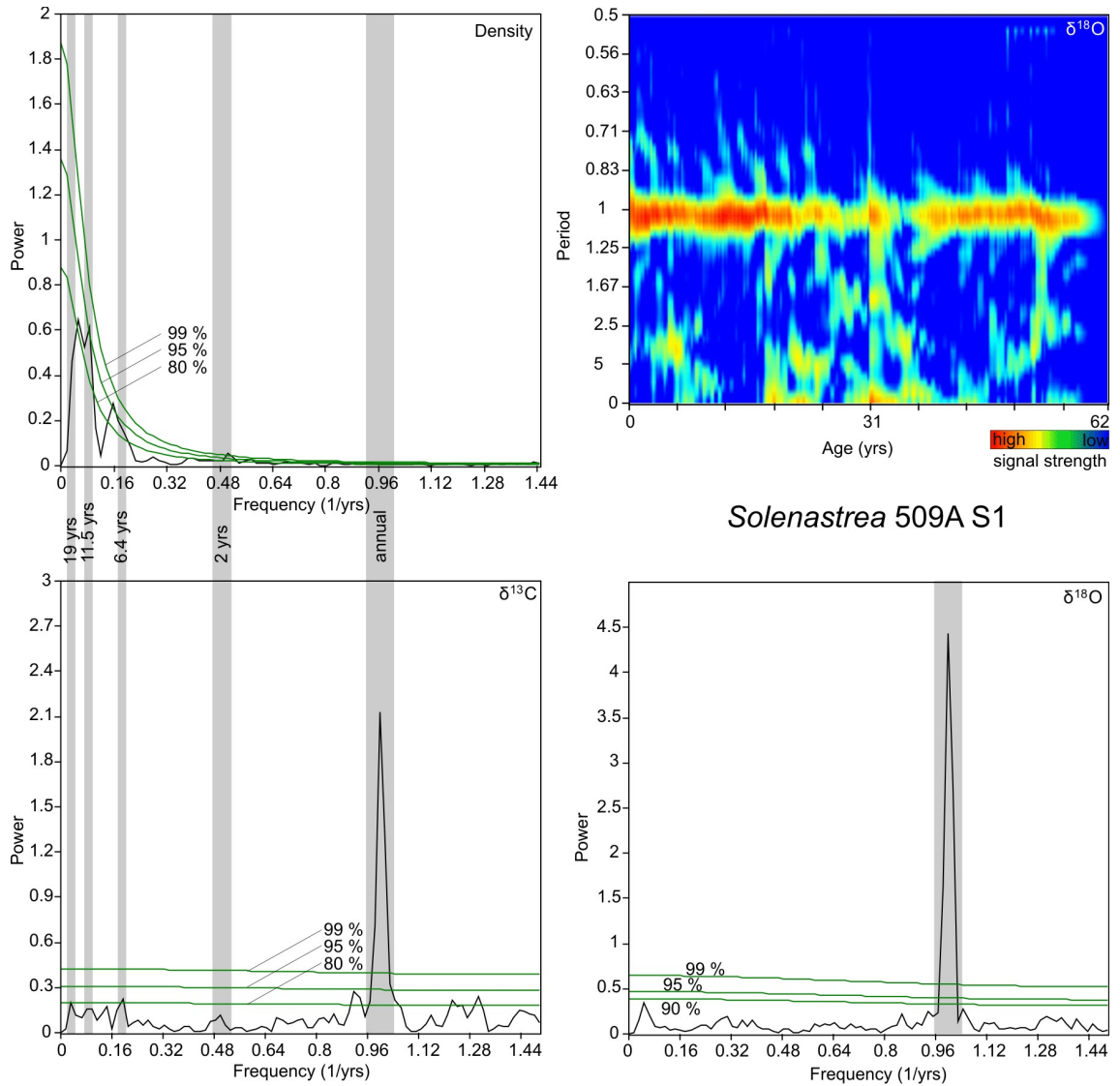


Figure 61: Spectral analyses of skeletal density (top left),  $\delta^{13}C$  (bottom left) and  $\delta^{18}O$  (bottom right) from coral 509A. All analyses were done with a rectangular window. Grey bars show spectral peaks crossing the confidence intervals. Short-time Fourier transform with window Multitaper 5 (top right).  $\delta^{18}O$  signal shows the expected annual peak. Density and  $\delta^{13}C$  show also this peak of  $\delta^{18}O$  and two common spectral peaks above the 80 % confidence interval with periods of 11.5 yrs and 19 yrs.

#### 4.1.3 Skeletal growth parameters of Plio/Pleistocene Corals from Florida

From the Plio/Pleistocene Caloosahatchee Formation a total of 11 *Solenastrea* were investigated for linear extension rate and bulk density. Mean linear skeletal extension rates of the here investigated fossil *Solenastrea* are low ( $\bar{\varnothing} = 3.7 \pm 0.9 \text{ mm/a}$ ) but comparable with recent ( $5.1 \text{ mm/a}$ ) and Mid-Pliocene ( $4.1 \text{ mm/a}$ ) growth rates of *Solenastrea* from Florida Bay (Roulier and Quinn, 1995; Swart et al., 1996) (Table 3). A weak positive correlation ( $r = 0.34$ ) between the two growth parameters linear skeletal extension rate and calcification rate in all Florida corals exists (Fig. 62). If one coral (509A) is treated as outlier because the calcification rate is  $2.5 \sigma$  above the mean calcification rate of all *Solenastrea* from Florida, the correlation coefficient between skeletal extension rate and calcification rate becomes  $r = 0.7$ . The same correlation is found in modern *Porites* from the Gulf of California and the Great Barrier Reef (Lough and Barnes, 2000; Cabral-Tena

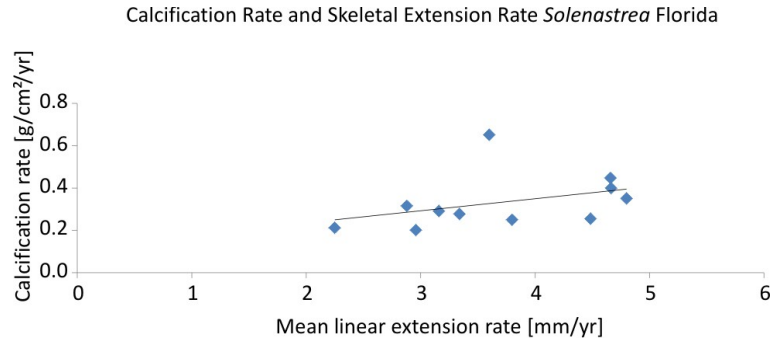


Figure 62: Calcification Rate and Growth Rate *Solenastrea* Florida. Correlation between both parameters is  $r = 0.34$ , without coral 509A (highest calcification rate in diagram)  $r = 0.7$ .

*et al.*, 2013). A weak inverse correlation between skeletal density and extension rate exists ( $r = -0.2$  for all;  $r = -0.37$  without 509A). Between skeletal density and calcification rate the correlation is  $r = 0.83$  and becomes  $r = 0.39$  if coral 509A is not considered. Skeletal density in this study varies in a range from  $0.6 - 1.8 \text{ g/cm}^3$ , which is a higher variability than in skeletal extension rates ( $2.25 - 4.8 \text{ mm/yr}$ ). Recent reef corals from Florida reach skeletal extension rates up to  $12 \text{ mm/yr}$ , recent Caribbean corals up to  $17 \text{ mm/yr}$  (Johnson and Perez, 2006), which is about a magnitude higher than extension rates in this study. This illustrates, that the linear extension rate is the main source of variability in calcification rate, comparable to modern *Porites* from Great Barrier Reef (Lough and Barnes, 2000; Lough, 2008). In the modern *Porites*, these changes in growth parameters are linearly related to average SSTs from  $23\text{-}30^\circ\text{C}$  (Lough, 2008). It is likely valid for the Plio/Pleistocene *Solenastrea* as well. Lough and Barnes (2000) showed that for each  $1^\circ\text{C}$  rise in SST the average annual calcification rate increases in *Porites* in GBR by  $0.33 \text{ g/cm}^2/\text{yr}$  and the annual extension rate by  $3.1 \text{ mm/yr}$ . Certainly the mean skeletal extension rate of the GBR corals is much higher than from *Solenastrea* (this study), but this pattern adopted to Plio/Pleistocene *Solenastrea* could either indicate to too cool or too warm SSTs with respect to  $T_{opt}$ . A too low SST in the high variable Plio/Pleistocene is unlikely, as found out with the comparison of HDB formation in *Solenastrea* and *Mercenaria* and shown in other studies (Petuch, 1982; Willard *et al.*, 1993; Petuch, 2007).

Calcification rates of *Solenastrea* sp within the literature are not existent. For *Montastrea annularis* and *Porites* sp many data in the literature exist (e.g. Johnson and Perez, 2006). However, the calcification rates for these corals are 2-5 times higher than for the Plio/Pleistocene mean in *Solenastrea* (this study; Table 3). Experiments with scleractinian corals under environmental stress in the Gulf of California showed a decrease of calcification rates in the corals in relation to unstressful times (Cabral-Tena *et al.*, 2013). Despite the corals used there were of the genus *Porites*, here investigated Florida corals were stressed by a high interannual variability, which is possibly a cause for the low calcification rates. It should also be considered, that in Recent reefs growth rates vary significantly between coral taxa (Johnson and Perez, 2006). This is also a problem since the Caribbean reef coral fauna has not been constant in the last millions of years and the end-Pliocene extinction took place (Budd, 2000; Jackson and Johnson, 2000). All here presented corals have a more or less wide range of environmental growth conditions.

## 4.2 Dominican Republic

### 4.2.1 Outcrop 455

The main discussion about the results in *Montastrea* 455C are to find in *Lohmann* (2013). For completeness of the oxygen and carbon isotope records, this coral should be considered here and compared with coral *Stephanocoenia* 464C from the Dominican Republic.

**Age** *Montastrea* 455C stratigraphic position is at 278 m (height in section above basal contact) between the samples taken and allocated by *Saunders et al.* (1986). The bedded siltstone outcropping is one of the main lithofacies of the Gurabo Formation. Its depositional environment is interpreted as low angle clinoforms of the lower part of the Gurabo Formation (*McNeill et al.*, 2012).

**Preservation** The skeleton of *Montastrea* 455C was surrounded by a fine grained silty sediment. Small fissures and cavities at the corals surface are filled with this sediment. The slabbed coral head is, except for brownish rootlets, unaffected by macroscopic dissolution or recrystallization. The rootlets show up as brownish areas, which are located on the surface of the skeletal porosity. Radiographs of the coral slabs reveal an undoubtful well preserved coral skeleton with all skeletal elements visible (Fig. 40). Several XRD measurements at the pristine skeleton are free of other minerals than aragonite. Additional SEM investigations show a pristine aragonitic skeleton which is covered in large areas by secondary aragonite in a volume of approximately a few percent. The rootlets are pictured in SEM as branched meshwork with single diameters of 3- 10  $\mu\text{m}$  and therefore identified as roots covered by ironoxides (brownish color). These structures are invisible in the radiograph, which is surprising since a high density for iron oxides was expected. This is explainable because the rootlets cover only the surfaces of the coral skeleton and consist of a meshwork with a high porosity. However, rootlets were never sampled for stable isotopes and therefore their impact on stable isotope values is negligible. Prior to microsampling of the corallites, the septae were removed using a driller (see chapter 2). The main part of the secondary aragonite overgrowth was removed during this procedure. At least in Transect A the correlation between  $\delta^{18}\text{O}$  and  $\delta^{13}\text{C}$  is not significant ( $r = 0.38$ ) (Fig. 41), while in transect C the correlation is high ( $r = 0.75$ ) (Fig. 42). A high correlation between both stable isotope signals is usually an indicator for a diagenetic alteration of the coral skeleton, but this should affect both transects equally. The high correlation is probably due to the kinetic effect during slow growth of *Montastrea* 455C's transect C (*McConnaughey*, 1989a). All in all *Montastrea* 455C shows no disablement for the use as paleoclimate archive (*Lohmann*, 2013).

**Skeletal Growth Rhythmic and Stable Isotope Data** The mean  $\delta^{18}\text{O}$  values for Transect A in *Montastrea* 455C is  $-3.7 \pm 0.3\text{‰}$ . This values are very similar to modern *Montastrea* from Tobago (Atlantic Ocean off Venezuela) where mean  $\delta^{18}\text{O}$  values for three *Montastrea faveolata* are  $-4 \pm 0.29\text{‰}$ ,  $-4 \pm 0.34\text{‰}$  and  $-3.8 \pm 0.15\text{‰}$  were measured (*Moses et al.*, 2006). The Tobago corals have an average  $\delta^{18}\text{O}$  seasonality of  $0.22\text{‰}$  (*Moses et al.*, 2006). Radiography of *Montastrea* 455C shows a fine density banding perpendicular to the axis of maximum growth. Amounts of small (sub-mm) and intercalating HDBs and LDBs are present but were not possible to be grouped into clear annual cycles (Fig.40). Within the skeleton, condensed sub-mm HDBs occur more or less periodic, but the delimitation against LDBs is fluent and too variable. An undoubtful annual skeletal extension rate within *Montastrea* 455C is not to be delivered here. A correlation of HDBs and  $\delta^{18}\text{O}$  cannot clear out this problem too. This also leads to the fact that no reliable

calcification rate can be estimated, even if the skeletal density was measured. Possible annual extension rates vary between < 1 mm and 2-3 cm. The possible calcification rate in transect A and transect C as product of mean annual skeletal extension and mean skeletal density would range from < 0.1 – 3.0  $g/cm^2/yr$  and < 0.14 – 4.1  $g/cm^2/yr$ , respectively. Recent *Montastrea* from the Caribbean (USVI) exhibit mean annual extension rates of  $0.98 \pm 0.28 cm/yr$  (n=607, *Dodge and Brass*, 1984). Other studies on recent Caribbean *Montastrea annularis* from Jamaica, Barbados and Bermuda estimate mean extension rates of  $0.87 \pm 0.12 cm/yr$  (n=6),  $1.04 \pm 0.14 cm/yr$  (n=8) and  $0.39 \pm 0.05 cm/yr$  (n=1), respectively (*Fairbanks and Dodge*, 1979) and for recent Mexican reefs  $0.87 cm/yr$  (*Carricart-Ganivet et al.*, 2000, also *Montastrea annularis*). *Dodge and Brass* (1984) also calculated the mean calcification rate of 607 *Montastrea annularis*, which is  $1.23 \pm 0.33 g/cm^2/yr$ . This literature values and the possible values for *Montastrea* 455C differ in a magnitude, so that the lacking skeletal growth rate also inhibits an estimation about the mean annual calcification. Correlation between skeletal density and stable oxygen signal in transect A is weak (r=0.35) and between skeletal density and stable carbon is significant (r=0.64). According to the observations of *Fairbanks and Dodge* (1979) that HDB formation in *Montastrea annularis* corresponds to the periods of warm water, lowest  $\delta^{18}O$  and highest  $\delta^{13}C$  values (summer), the correlation of stable isotopes and skeletal density in *Montastrea* 455C is likely due to similar environmental conditions (Fig. 41,42).

#### 4.2.2 Outcrop 464

**Age** Outcrop 464 is located in the incised valley of the Arroyo Bellaco, a tributary of the Rio Cana (Fig. 24). The height within the stratigraphic section of *Saunders et al.* (1986) is 150-175 m above basal contact. The outcropping reef was first dated with the use of planktic foraminifera and nannofossil zones to an age of 7.5-8.3 Ma (*Klaus and Budd*, 2003) and later refined by *Maier et al.* (2007) with the use of  $^{87}Sr/^{86}Sr$  ratios to an age of 6.2 Ma to the late Miocene Cercado Formation.

**Preservation** Perfect preservation with finely developed skeletal elements as septae, columnella and theca walls are obvious in *Stephanocoenia* 464C. A high porosity and no visible macroscopic secondary mineral growth is present. Also no hints for minerals other than aragonite were found via X-ray diffraction and only in one sample calcite seems to appear around the detection limit of 1-2%. SEM analyses with EDX show secondary aragonitic fiber bundles growth on all surfaces and also gypsum precipitation. The portion of other minerals versus pristine skeletal aragonite found in SEM is estimated to amount a few percent. Coral 464C has a relatively pristine conservation, at least in the measured areas of the skeleton. *Klaus and Budd* (2003) described the reef unit (here outcrop 464) as preserved perfect with an intact, original reef-zonation pattern and pristine specimens.

**Skeletal Growth Rhythmic and Stable Isotope Data**  $\delta^{18}O$  and  $\delta^{13}C$  labels a lagging correlation with a shift of 1 and -2 sample positions. This is also an indication for no diagenetic leveling. From the radiograph is visible, that the upper 1.5 cm of the coral are much denser than the lower part of the skeleton. This dense part has an internal banding similar to the skeletal structure of the lighter part where the isotope transect is situated (Fig. 63). The contrast within the skeleton is low compared to other specimens with similar slab thickness in this work, especially those from Florida. From all 113 measured values for skeletal density, 80% of the values vary between 1.2 and 1.4  $g/cm^3$  and the range of the density values along the profile except the first (bottom) 4 values and the last (top) 6 values ranges only from 1.15 to 1.49  $g/cm^3$  (*median* =  $1.3 \pm 0.07 g/cm^3$ ). These first and last values of the transect were not considered due to excursions of the signal related

to thinning of the coral slab at the beginning and diagenetic precipitation at the top, respectively. This low contrast in skeletal density could be an effect of lower seasonality in temperature as this is forced by the lower latitude of the Dominican Republic. Bleaching as a consequence of high solar irradiation but not increased SSTs has been observed in a recent Caribbean *Stephanocoenia* and should be considered as a possible explanation for a negative influenced skeleton build-up due to tissue loss (*Fournie et al.*, 2012). No available literature data for fossil or recent growth parameters of *Stephanocoenia* exist.

Recent *Stephanocoenia mitchelinii* from the Florida Keys were mainly found in a water depth of 15 m or below, on the Cuban shelf in depths between 15-24 m but never on the reef-crest (*Rice and Hunter*, 1992; *Gonzalez-Diaz et al.*, 2010). Fossil *Stephanocoenia* 464C lived also in a shallow, warm-water marine environment. Other authors also interpreted the depositional environment of the Cercado Formation as the shallow inner-shelf (*McNeill et al.*, 2012). The average skeletal extension rate of 3.7 mm per year specifies an average sampling frequency of 4-5 samples per year. This is a better frequency than for *Solenastrea* 509A (Florida) but still not the optimum as probably hit in *Solenastrea* 452K1 (also Florida). Stable isotope data describe a clear annual cycle according to the density banding of the coral. The mean seasonal difference in  $\delta^{18}O$  is  $-0.39 \pm 0.17 \text{‰}$  and takes values between  $0.1 - 0.72 \text{‰}$ . Adopted the coral paleotemperature slope (*Druffel*, 1997, :  $-0.22 \text{‰}/1^\circ\text{C}$ ) and ignoring possible other effects than temperature on  $\delta^{18}O$  composition,  $\delta^{18}O$  values reflect a mean SST seasonality of  $1.8 \pm 0.8^\circ\text{C}$  ( $0.4 - 3.3^\circ\text{C}$ ). A low SST seasonality has been found by other studies for southern Caribbean corals as recent *Diploria strigosa* in Bonaire, where the Sr/Ca-seasonality is  $2.8 \pm 0.2^\circ\text{C}$  ( $2.4 - 3.0^\circ\text{C}$ ) and in the mid- to late Holocene  $3.1 \pm 0.2^\circ\text{C}$ , imaging the true SST seasonality in Bonaire very well ( $2.9 \pm 0.1^\circ\text{C}$ ) (*Giry et al.*, 2012). A seasonality of less than  $2^\circ\text{C}$  has also been reconstructed for the last century for offshore southern Hispaniola (*Greer and Swart*, 2006). Temperature seems to be in coral 464C the most important driver of  $\delta^{18}O$  signal, as mean SST seasonality and no covariance in  $\delta^{13}C$  and  $\delta^{18}O$  signals show. The measured (modern) SST variation within a year in Hispaniola is less than  $5.5^\circ\text{C}$  (*Horst*, 1992) and if a lower seasonality for the Mio/Pliocene is expected (*Zubakov and Borzenkova*, 1988), a mean seasonality in coral 464C of  $1.8 \pm 0.8^\circ\text{C}$  seems to be reliable. Comparing the stable isotope signals in *Stephanocoenia* 464C with those of *Montastrea* 455C, noticeably the standard deviations of the isotopic ratios are nearly identical (464C mean  $\delta^{18}O = -3.04 \pm 0.18 \text{‰}$ , range =  $1.01 \text{‰}$ , mean  $\delta^{13}C = -1.03 \pm 0.52 \text{‰}$ , range =  $2.78 \text{‰}$ ; 455C (transect A) mean  $\delta^{18}O = -3.71 \pm 0.28 \text{‰}$ , range =  $2.2 \text{‰}$ , mean  $\delta^{13}C = -1.4 \pm 0.55 \text{‰}$ , range =  $3.2 \text{‰}$ ). Similar values were also measured for a *Goniopora hilli* by *Denniston et al.* (2008) with mean  $\delta^{18}O$  of  $-3.2 \text{‰}$  and mean  $\delta^{13}C$  of  $-0.2 \text{‰}$  and seasonal ranges of  $0.4 \text{‰}$  ( $\delta^{18}O$ ) and  $0.9 \text{‰}$  ( $\delta^{13}C$ ). *McNeill et al.* (2012) reinterpreted and revised the three Neogene Formations of the Cibao Valley and proposed a new sequence stratigraphic framework, within each formation was deposited on the marginal shelf during one individual depositional sequence with material delivered by the Cordillera Central.

HDB-formation in *Stephanocoenia* 464C took place during times of low  $\delta^{18}O$  values, interpreted as summer. From 20  $\delta^{18}O$  maxima (winter), 15 are located in a LDB, 2 in a HDB and 3 cannot be located (Fig. 63). *Lutz et al.* (2008) found out that during the early Pliocene of the Cibao Basin the mean annual SST increased to more than  $28-29^\circ\text{C}$ , related to a tectonic event during the partial closure of the CAS. Considering a temperature in the late Miocene which is a little bit lower when *Stephanocoenia* 464C grew, the mean SST is oscillating approximately around  $27^\circ\text{C}$  and it is likely that during summers the HDB formation occurred ( $T_{opt}$ ) and during winter the LDB formation. The true  $T_{opt}$  for *Stephanocoenia* is not known but a recent *Stephanocoenia* from a patch reef off Florida lived in  $24-26^\circ\text{C}$  and is supposed to live at or near its physiological limits (*Rice and Hunter*,

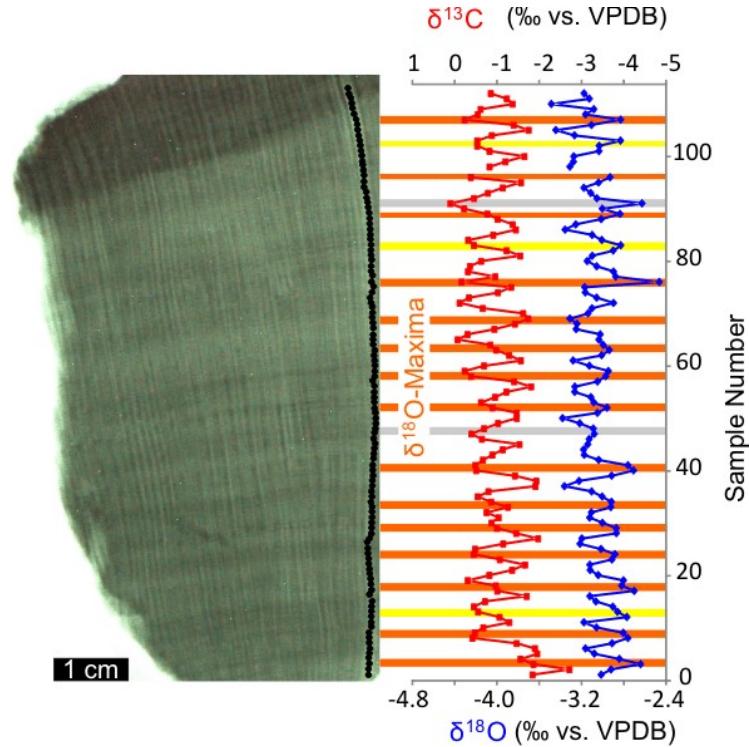


Figure 63: *Stephanocoenia* 464C, skeletal density banding compared to stable isotope data. Note the prevailing coincidence of  $\delta^{18}O$ -maxima (orange lines) with LDBs. Only some  $\delta^{18}O$ -maxima seem to represent a HDB (grey lines) or cannot be related (yellow lines).

1992). For the tropic late Miocene *Stephanocoenia* 464C a higher SST than in modern Florida sounds more realistic and it is therefore interpreted that  $T_{opt}$  (HDB formation) is achieved during summer in *Stephanocoenia* 464C.

Optical comparison and cross correlation show that  $\delta^{13}C$  peak values are shifted from the  $\delta^{18}O$  peak values. Lowest  $\delta^{13}C$  values always appear within a  $^{18}O$ -defined year between the  $\delta^{18}O$  maxima. To decide which signal predates the other, again the highest correlation or anticorrelation should be considered. If the  $\delta^{13}C$  signal is predating the  $\delta^{18}O$  signal by 2 samples, the correlation becomes -0.49 which is the highest anticorrelation in this record. Shifting the  $\delta^{18}O$  signal to predate the  $\delta^{13}C$  signal by 1 sample, correlation becomes 0.4, the highest correlation within this record. Regarding the sampling frequency of 4-5 samples per year, a shift of 1 sample seems to be more likely than a shift of 2 samples, which would be approximately a half year. Sample shift of 1 implies a time shift of 2-3 months which is more realistic for signals which are seasonally influenced. The  $\delta^{18}O$  signal predates the  $\delta^{13}C$  signal in this coral like coral 509A. Hence it can be concluded that high  $\delta^{13}C$  values (e.g. higher zooxanthellae productivity) follow shortly after  $\delta^{18}O$ -maxima (winter) in all cases where the  $\delta^{18}O$  maxima coincide with the LDB-formation. In the two cases where the  $\delta^{18}O$  maxima coincide with the HDB, no lag in  $\delta^{13}C$  peak values exists (Fig. 63). Unfortunately, two cases of coincidence of HDB and  $\delta^{18}O$  maxima is not a vast fundament, but at least a hint for an interannual variability where the mean SST in winter is higher (and probably closer to  $T_{opt}$ ) than in the other years and allows a HDB formation in winter.

**Main and Trace Element Composition** No correlation between  $\delta^{18}O$  and Sr/Ca or Mg/Ca signals ( $r = 0.04$  and  $-0.07$  respectively) in *Stephanocoenia* 464C is existent, but a high anticorrelation between Sr/Ca and Mg/Ca ( $r = -0.62$ ), which is surprising. From a comparison of the X-radiograph,  $\delta^{18}O$ -maxima and trace element composition at least

Mg/Ca reproduces the stable isotope pattern - in most  $\delta^{18}\text{O}$ -maxima (grey lines) is also located a Mg/Ca-minimum (or nearby; Fig. 64). This annual pattern is interpreted as an alternation of HDBs and LDBs every 3-4 mm, supported by the seasonality of the  $\delta^{18}\text{O}$  and  $\delta^{13}\text{C}$  signals. Here it is shown, that the  $\delta^{18}\text{O}$  values achieve maxima during the LDB formation (Fig. 63). Sr/Ca ratios ( $7.21 \pm 0.24 \text{ mmol/mol}$ ) are lower than those for a recent Caribbean *Siderastrea* from Venezuela ( $8.72 \pm 0.26 \text{ mmol/mol}$ ) and two Miocene (16 Ma) *Montastrea* ( $\varnothing 8.59 \pm 0.18 \text{ mmol/mol}$ ) and *Siderastrea* ( $\varnothing 8.61 \pm 0.18 \text{ mmol/mol}$ ) from Venezuela (Griffiths et al., 2013). Griffiths et al. (2013) also found in all secondary aragonite precipitations higher values (9.07-13.53 mmol/mol) than in *Stephanocoenia* 464C. This likely indicates a reliable Sr/Ca signal in Miocene *Stephanocoenia* and SST calculations based on Sr/Ca SST-relationship after Marshall and McCulloch (2002) produce values of 21.2°C temperature difference within the lifetime of this coral (without outliers). SST calculations using Mg/Ca range after Mitsuguchi et al. (1996) produces 19.7°C temperature difference respectively. This is not the seasonality, but still an unlikely high value for this latitude. A calculation of trace-element based SST seasonalities produces no reliable values, which is because the masterchronology (from  $\delta^{18}\text{O}$ ) and the trace-element measurements have originally different x-scales. This is due to different lengths of the profiles, different spatial resolution (stable isotopes: 0.7 mm sample distance and 0.8 mm in diameter; trace elements: 0.5 mm sample distance and 0.08 mm in diameter) and not exact the same positions for trace-elements as for stable isotopes could be sampled (stable isotope measurements consumes magnitudes more volume in skeletal material than LA-ICP-MS measurements). The correlation between both signals is not from maximum to maximum but in the mm-scale, which produces a visual correlation (Fig. 64) but no mathematical correlation. The discussed annual pattern, visualized by  $\delta^{18}\text{O}$  and  $\delta^{13}\text{C}$  cycles, is probably accompanied by a higher order pattern in *Stephanocoenia* 464C. This pattern can be observed as grouped HDBs in equal distances interrupted by less denser skeletal areas (light green boxes in Fig. 64). By visual judgement, a correlation from these skeletal areas to Ba/Ca, Y/Ca, U/Ca and B/Ca ratios are given. A mathematical correlation between measured skeletal density (along the sampling transect) and trace element data results in weak (no) correlations, except for U/Ca where  $r = 0.74$ . Probably the density contrast is too small for reliable correlations. However, typical riverine proxies as Ba/Ca and Y/Ca depicts the superimposed pattern in the X-radiograph and therefore two scenarios come in consideration. (1) the supposed annual pattern shown by stable isotopes in combination with X-radiograph is not such and the superior pattern is probably the annual cycle. (2) the stable isotope signal depicts the annual frequency and trace elements are influenced by some other factor in a periodicity of approximately 4 years. Especially the riverine delivered (precipitation dependent) trace elements Ba/Ca (McCulloch et al., 2003), Y/Ca and U/Ca (Cochran, 1992) suggest the second pattern, while the temperature dependent trace elements Sr/Ca and Mg/Ca show nearly no correlation to the superimposed cyclicality. The cyclic pattern of  $\delta^{18}\text{O}$  and  $\delta^{13}\text{C}$  signals also suggests the scenario of two overlain pattern, which is not depicted by  $\delta^{18}\text{O}$  and  $\delta^{13}\text{C}$ . Under the assumption that  $\delta^{18}\text{O}$  is only controlled by SST, the calculated SST seasonality of  $1.8 \pm 0.8^\circ\text{C}$  ( $0.4 - 3.3^\circ\text{C}$ ) sounds realistic. The higher order pattern shown by Ba/Ca, B/Ca, Y/Ca and U/Ca is likely influencing the precipitation but not the temperature.

**Spectral Analyses** The analyzed stable isotope spectra in *Stephanocoenia* 464C show a clear annual spectral peak in  $\delta^{18}\text{O}$  and  $\delta^{13}\text{C}$  signals (Fig. 65). Other peaks, except one minor peak with a period of 1.1 years which is probably an artefact of the annual peak, are not significant in the  $\delta^{18}\text{O}$  and  $\delta^{13}\text{C}$  signals. Skeletal density includes some weak peaks, which exceed the 80 % confidence interval (annual, 1.1 yrs, 1.7 yrs, 2.1 yrs and 9.5 yrs), from



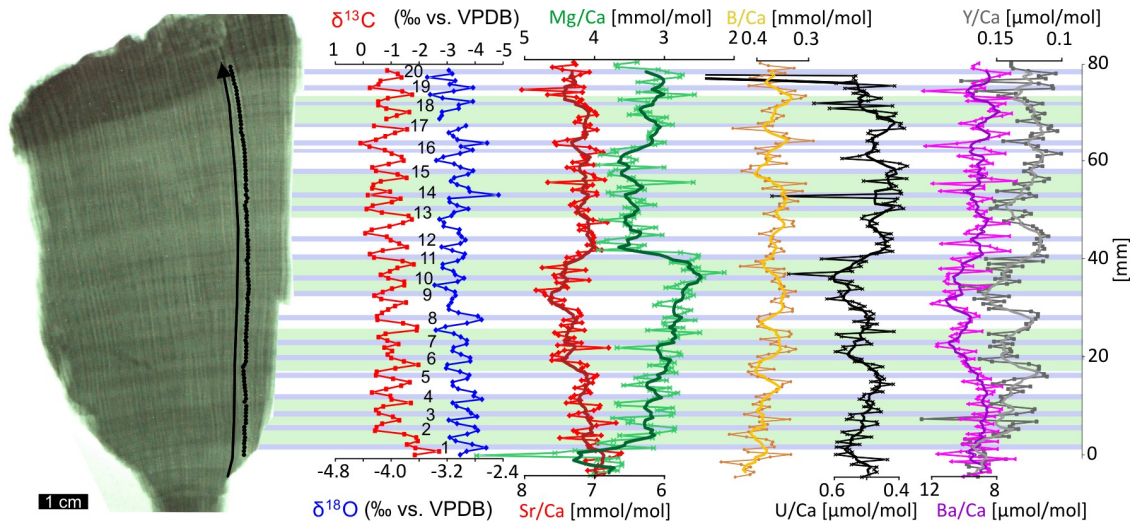


Figure 64: Comparison of X-radiograph from *Stephanocoenia* 464C with geochemical data. Green lines show combined areas of higher skeletal density (probably several HDBs), blue lines mark  $\delta^{18}\text{O}$ -maxima (annual signal). The trace elements (especially the river-proxies Y/Ca and Ba/Ca) seem to correspond with the superior areas of skeletal density, illustrated by the green lines (see text). Thick lines along trace elements are sixfold running means.

which the annual, 2.1 yrs and 1.7 yrs peaks also exceed the 95 % confidence interval. Peaks with smaller periodicities than one year are interpreted as artefacts (Fig. 65). The weak appearance of the peaks in the skeletal density is not surprising, since the general SST seasonality is very low ( $\delta^{18}\text{O}$ :  $1.8 \pm 0.8^\circ\text{C}$ ) in this coral and therefore the calcium carbonate precipitation of the corals skeleton is not changed as strong as corals in higher latitudes with higher SST seasonalities (e.g. *Solenastrea* 452, Florida). The remaining peaks in skeletal density (beside the annual one), 1.7-2.1 years and 9.5 years are probably realistic. The decadal peak can be caused by decadal-scale patterns in the tropical North Atlantic SST, as found as driver of multidecadal precipitation fluctuations due to an movement of the ITCZ during the Holocene in Dominican Republic corals (*Greer and Swart*, 2006) and Recent in Belize (*Gischler and Oschmann*, 2005). Also possible is, that the 9.5 yr spectral peak belongs to the sunspot cycle. To differ between a possible multidecadal fluctuation and the sunspot cycle a longer record is required, subject to future works in this project.

#### 4.2.3 Skeletal growth parameters of all Mio/Pliocene Corals from Dominican Republic

The broad mixture of different species in different formations makes it difficult to compare the results. The genus *Montastrea* is found in both investigated formations from the Cibao Valley and delivers data to compare. Studies from recent coral growth parameters show a significant correlation between increasing SSTs and decline in calcification rate (*Helmle and Dodge*, 2011; *Lough and Cooper*, 2011). In general the X-radiographs of corals from the Dominican Republic have lower density contrasts than specimen from Florida. This reflects, assuming a calcification rate and density mostly driven by SST, a lower seasonal temperature contrast in the Mio/Pliocene of the Dominican Republic than in the Plio/Pleistocene of Florida. This is also visible in lower seasonal isotopic contrasts from the corals investigated. The mean density and the mean calcification rate of all Mio/Pliocene Dominican Corals is higher than the mean density and the mean calcification rate of the Plio/Pleistocene Florida corals. Together with the lower density contrasts, here observed corals from Hispaniola grew in a more optimal environment than those corals from Florida.

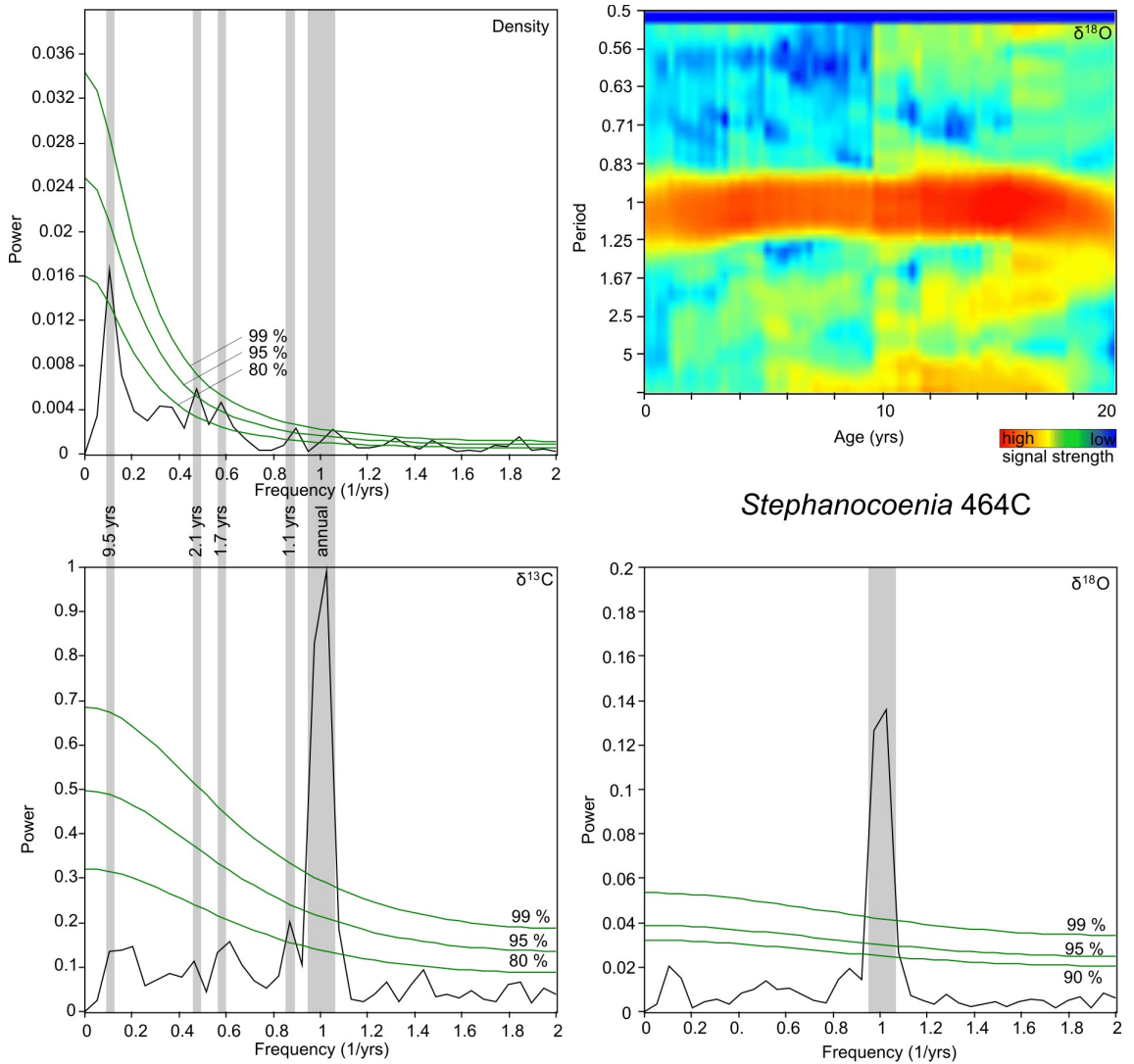


Figure 65: Spectral analyses of skeletal density (top left),  $\delta^{13}C$  (bottom left) and  $\delta^{18}O$  (bottom right) from coral *Stephanocoenia* 464C. All analyses were done with a rectangular window. Grey bars show where spectral peaks cross the confidence intervals. Additional short-time Fourier transform with window Multitaper 5 (top right).  $\delta^{18}O$  signal shows the expected annual peak. Density and  $\delta^{13}C$  show also this peak of  $\delta^{18}O$  but no common spectral peaks above the 80% confidence interval. Just within the density three spectral peaks occur with periods of 1.7 yrs, 2.1 yrs and 9.5 yrs.

## 5 Conclusion

### 5.1 Growth rates

Coral growth rates can be compared with taking into consideration different factors modulating those. In general, the recent reefs on earth show significant higher growth rates in the tropical Indo-Pacific regions than in the Atlantic and Caribbean regions (*Johnson and Perez* (2006) and literature cited therein). Additionally, growth rates in recent reefs differ significantly along latitudes in the Atlantic and Pacific. High-latitude reefs, such these of Bermuda, have an order of magnitude lower than growth rates from more tropical regions (*Johnson and Perez*, 2006). Further, significant variations in growth rates are present along different genera. Published skeletal extension rates for fossil corals show also a significant difference along different stratigraphic units. Relatively slow-growing

colonies from the Late Miocene were recovered from the Cercado and Gurabo Formation (mean = 3.8 mm/yr) while all other Cenozoic coral growth rates median is 6.25 mm/yr (Johnson and Perez, 2006).

The different growth rates for different regions, latitudes, genera and stratigraphic units are for this reason difficult to interpret and other controlling mechanisms as discussed above should be respected.

The comparison of skeletal parameters between both investigated areas Florida and Dominican Republic is not possible without limitations. The different regions have different latitudes and are also in different periods. Coral genera during time changed significant in the last 30 million years in the Caribbean due to rapid taxonomic turnovers (Budd, 2000; Jackson and Johnson, 2000; Klaus and Budd, 2003). Neither individual coral species nor genera existed continuously, which may explain some variation in the growth rates Also the environmental conditions of the Florida platform are not easy to compare with the stack of fine-grained sediments in shelf and slope facies from the Cibao Valley (Mann et al., 1991; Johnson and Perez, 2006). Climatic influencing features, like the southward movement of the ITCZ since the early Pliocene (Flohn, 1981; Steph et al., 2006) have also an unknown possible influence on the growth rates presented here.

Nevertheless, the mean densities of the Plio/Pleistocene corals from Florida are much smaller than those of the Mio/Pliocene Caribbean corals investigated here, which results probably from more stress during fast environmental changes, as a high interannual SST variability.

Coral records for all three growth parameter extension, density and calcification are rare in the literature. More often only the extension rate is measured, especially for long-term records (Helmle and Dodge, 2011). It were measured in this study all three parameters wherever it was possible, but real long-term records in century scales were not available.

## 5.2 Proxies Florida, 452 and 509

Screening for diagenetic alterations in the coral skeletons indicates both corals as suitable for stable isotope analysis. Both specimens were found in different locations, but the same formation and are of the genus *Solenastrea*. 452K1 has a mean growth rate of 4.8 mm/yr (36 yrs), which results with a mean skeletal density of  $0.73 \pm 0.09 \text{ g/cm}^3$  in a mean calcification rate of  $0.35 \text{ g/cm}^2/\text{yr}$ . Mean  $\delta^{18}\text{O}$  is  $-2.24 \pm 0.84 \text{ ‰}$  (range = 5.01 ‰) with a mean seasonality of 2.08 ‰ and mean  $\delta^{13}\text{C}$  is  $-1.69 \pm 0.56 \text{ ‰}$  (range of 3.9 ‰). Calculated SST seasonalities are 9.5 °C ( $\delta^{18}\text{O}$ ), 12.7 °C (Mg/Ca) and 14.4 °C (Sr/Ca). HDBs were formed either during winter or summer or in between (according to  $\delta^{18}\text{O}$ ), implicating a higher interannual SST variability during the Plio/Pleistocene compared to Mid-Pliocene or modern climatic situation.

509 has a mean linear extension rate of 3.6 mm/yr (62 yrs), a mean skeletal density of  $1.81 \text{ g/cm}^3$  and a mean calcification rate of  $0.65 \text{ g/cm}^2/\text{yr}$ . Mean  $\delta^{18}\text{O}$  is  $-2.05 \pm 0.5 \text{ ‰}$  (range = 2.65 ‰) with a mean seasonality of 0.96 ‰ and a mean  $\delta^{13}\text{C}$  is  $-2.48 \pm 0.45 \text{ ‰}$  (range of 1.9 ‰).  $\delta^{18}\text{O}$  based SST variability is 4.4 °C, which is unrealistic due to low sampling resolution. HDBs were built-up during winter ( $\delta^{18}\text{O}$ ) and show for each  $\delta^{18}\text{O}$ -cycle a double high density band. Both specimen from Florida indicate SSTs oscillating around the optimal temperature for coral growth in the Plio/Pleistocene, with SSTs between higher SSTs in the Mid-Pliocene and lower SSTs today.

## 5.3 Proxies Dominican Republic, 455 and 464 (and 503)

Screening for diagenetic alterations in the coral skeletons indicates both corals as suitable for stable isotope analysis. Interestingly both corals from the Dominican Republic show

similar stable isotope values, regarding means, seasonalities and standard deviations. Both specimens were found in different locations, different formations with different ages and 455C is the genus *Montastrea* while 464C is a *Stephanocoenia*. The mean linear extension rate in *Stephanocoenia* 464C is  $3.7 \text{ mm/yr}$  (62 years). Skeletal density is in average  $1.32 \pm 0.13 \text{ g/cm}^3$  and the calcification rate is  $0.48 \text{ g/cm}^2/\text{yr}$ . 464C has a mean  $\delta^{18}\text{O}$  of  $-3.04 \pm 0.18 \text{ ‰}$  (range =  $1.01 \text{ ‰}$ ) and a mean  $\delta^{13}\text{C}$  of  $-1.03 \pm 0.52 \text{ ‰}$  (range =  $2.78 \text{ ‰}$ ). Mean seasonality ( $\delta^{18}\text{O}$ ) is  $1.8 \pm 0.8^\circ\text{C}$ , similar to modern seasonality. In *Stephanocoenia* 464C the HDB formation takes place during the warm season (summer). A higher order cycle with a periodicity of 4 years is influencing *Stephanocoenia* 464C riverine delivered trace elements (Ba, U, Y, B). Spectral analysis of skeletal density shows a 9.5 yr spectral peak, which is possibly related to the sunspot cycle.

*Montastrea* 455C's annual extension rate remains unclear and could take possible values between  $< 1 \text{ mm}$  and  $2\text{-}3 \text{ cm}$ . A mean skeletal density of  $1.0 \pm 0.4 \text{ g/cm}^3$  leads to possible calcification rates from  $< 0.1 - 3.0 \text{ g/cm}^2/\text{yr}$ . 455C (transect A) has a mean  $\delta^{18}\text{O}$  of  $-3.71 \pm 0.28 \text{ ‰}$  (range =  $2.2 \text{ ‰}$ ) and a mean  $\delta^{13}\text{C}$  of  $-1.4 \pm 0.55 \text{ ‰}$  (range =  $3.2 \text{ ‰}$ ). The variations (or homogenities) of stable isotopes in both corals seem to reflect environmental perturbations which did not change significantly during the deposition of both formations. Notably in Holocene corals from Lago Enriquillo similar values were also found (close to the outcrop 503) (*Greer and Swart, 2006*).

## Acknowledgements

I thank Prof. Dr. Thomas Brachert for the great opportunity to work and research under his supervision. Further I want to thank him for the support and discussion within this interesting theme during my time in Leipzig.

Also I want to thank Dr. Walter Etter and Olivier Schmidt, Naturhistorisches Museum Basel, for providing samples from former field trips to the Dominican Republic for comparison.

James Klaus and Donald McNeill, University of Miami, are gratefully thanked for their active help and providing of maps and local informations about the outcrop situation in the Dominican Republic.

Dr. Santiago Muñoz from Servicio Geologico de la Republica Dominicana, Santiago, Dominican Republic is gratefully thanked for his support and providing of maps.

Special thanks belong to Jörg Lenzner, Institut für Experimentelle Physik II, Universität Leipzig, for his patience during the scanning electron microscopy sessions.

For their selfless support and help during laser ablation measurements I want to thank very much Prof. Dr. Klaus Peter Jochum, Ulrike Weiss and Brigitte Stoll, Max-Planck-Institut für Chemie, Mainz and also Dr. Gerhard Brüggemann, Universität Mainz, for his help during analysis of the laser ablation data.

Prof Dr. Michael Joachimski, FAU Erlangen, and Prof. Dr. Michael Staubwasser, Universität Köln, need to be thanked for stable isotope measurements during downtimes of our spectrometer.

I also thank Roel Nagtegaal, Royal Netherlands Institute for Sea Research, for the discussion and experiments with UV-luminescence at my corals.

Dr. Markus Reuter, Universität Graz, Austria, should be thanked especially for his indispensable help during the field trips and for discussion.

I thank Hans Lohmann for his support in the laboratories and during the field trip 2012. Oliver Sturm is thanked for his support in the laboratories too.

Thanks for the preparation of different aluminium wedges in a high precise way to Andre Schollbach, Institut für Geophysik und Geologie.

For the preparation of pure aluminium plates I want to thank the workshop-team of the Fakultät für Physik und Geowissenschaften, Universität Leipzig.

The pathology-team of the Universitätsklinikum Leipzig is thanked for the abrasive belt grinding of very large coral heads in their institute.

I thank Dr. Alexander Heidrich, Hans-Knöll-Institut Jena, for supporting computer tomography of corals to clear out questions concerning three dimensional effects.

Last but not least I appreciate the intense support of my wife Agnes and my daughter Ida in the ups and downs of the last years, which is representative for all my families benefit. Funding by the Deutsche Forschungsgemeinschaft (Br 1153/13-1) is gratefully acknowledged.

## References

- Aharon, P., Recorders of reef environment histories - stable isotopes in corals, giant clams, and calcareous algae, *Coral Reefs*, *10*, 71–90, 1991. (Cited on page 13)
- Allison, N., A. A. Finch, J. M. Webster, and D. A. Clague, Palaeoenvironmental records from fossil corals: the effects of submarine diagenesis on temperature and climate estimates, *Geochimica et Cosmochimica Acta*, *71*, 4693–4703, 2007. (Cited on page 82)
- Allmon, W., Age, environment and mode of deposition of the densely fossiliferous pinecrest sand (pliocene of florida) - implications for the role of biological productivity in shell bed formation, *Palaaios*, *8*, 183–201, 1993. (Cited on pages 15 and 84)
- Allmon, W., S. Emslie, D. Jones, and G. Morgan, Late neogene oceanographic change along Florida's west coast: Evidence and mechanisms, *Journal Of Geology*, *104*, 143–162, 1996. (Cited on page 15)
- Baker, P., and J. Weber, Coral growth rate: Variation with depth, *Earth and Planetary Science Letters*, *27*, 57–61, 1975. (Cited on page 73)
- Barnes, D., and J. Lough, On the nature and causes of density banding in massive coral skeletons, *Journal Of Experimental Marine Biology And Ecology*, *167*, 91–108, 1993. (Cited on page 9)
- Barnston, A., and R. Livezey, Classification, seasonality and persistence of low-frequency atmospheric circulation patterns, *Monthly Weather Review*, *115*, 1083–1126, 1987. (Cited on page 20)
- Bartoli, G., M. Sarnthein, M. Weinelt, H. Erlenkeuser, D. Garbe-Schonberg, and D. Lea, Final closure of Panama and the onset of northern hemisphere glaciation, *Earth And Planetary Science Letters*, *237*, 33–44, 2005. (Cited on pages 17 and 23)
- Bosscher, H., Computerized tomography and skeletal density of coral skeletons, *Coral Reefs*, *12*, 97–103, 1993. (Cited on page 9)
- Brachert, T., M. Reuter, S. Krüger, A. Böcker, H. Lohmann, R. Mertz-Kraus, and C. Fassoulas, Density banding in corals: barcodes of past and current climate change, *Coral Reefs*, pp. 1–11, 2013a. (Cited on page 10)
- Brachert, T. C., A. Boecker, K. Hansmann, S. Krüger, H. Lohmann, M. Reuter, and J. S. Klaus, Changing growth rhythms of south Florida marine invertebrates during Plio-Pleistocene climatic change, *Geology*, *submitted*, 2013b. (Cited on page 81)
- Budd, A., Diversity and extinction in the Cenozoic history of Caribbean reefs, *Coral Reefs*, *19*, 25–35, 2000. (Cited on pages 90 and 98)
- Budd, A., and K. Johnson, Coral reef community dynamics over 8 myr of evolutionary time: Stasis and turnover, in *Proceedings of the 8th International Coral Reef Symposium*, vol. 1, p. 423–428, 1997. (Cited on page 23)
- Budd, A., and K. Johnson, Origination preceding extinction during late Cenozoic turnover of Caribbean reefs, *Paleobiology*, *25*, 188–200, 1999. (Cited on page 23)
- Budd, A., and K. Johnson, *Neogene Paleontology in the Northern Dominican Republic - 19. The family Faviidae (Anthozoa: Scleractinia) Part II. The genera Caulastraea, Favia, Diploria, Thysanus, Hadrophyllia, Manicina, and Colpophyllia*, *Bulletins of American Paleontology*, 1999. (Cited on page 16)

- Budd, A., K. Johnson, and T. Stemann, Plio-pleistocene turnover and extinctions in the caribbean reef coral fauna, in *Evolution and Environment in Tropical America*, edited by A. G. C. Jeremy B. Jackson, Ann F. Budd, pp. 168–204, University of Chicago Press, 1996. (Cited on page 23)
- Buddemeier, R., J. Maragos, and D. Knutson, Radiographic studies of reef coral exoskeletons: Rates and patterns of coral growth, *Journal of Experimental Marine Biology and Ecology*, *14*, 179 – 199, 1974. (Cited on page 38)
- Cabral-Tena, R. A., H. Reyes-Bonilla, S. Lluch-Cota, D. A. Paz-Garcia, L. E. Calderon-Aguilera, O. Norzagaray-Lopez, and E. F. Balart, Different calcification rates in males and females of the coral *Porites panamensis* in the Gulf of California, *Marine Ecology Progress Series*, *476*, 1–8, 2013. (Cited on pages 73, 89 and 90)
- Carricart-Ganivet, J. P., Sea surface temperature and the growth of the West Atlantic reef-building coral *Montastraea annularis*, *Journal of Experimental Marine Biology and Ecology*, *302*, 249 – 260, 2004. (Cited on page 9)
- Carricart-Ganivet, J. P., A. U. Beltran-Torres, M. Merino, and M. A. Ruiz-Zarate, Skeletal extension, density and calcification rate of the reef building coral *Montastraea annularis* (Ellis and Solander) in the Mexican Caribbean, *Bulletin of Marine Science*, *66*, 215–224, 2000. (Cited on pages 73 and 92)
- Cochran, J., The oceanic chemistry of the uranium and thorium series nuclides., in *Uranium-series Disequilibrium: Applications to Earth, Marine, and Environmental Sciences*, edited by M. Ivanovich and R. Harmon, Oxford Science Publications, Clarendon Press, 1992. (Cited on page 95)
- Constantz, B., The primary surface area of corals and variations in their susceptibility to diagenesis, in *Reef Diagenesis*, edited by J. Schroeder and B. Purser, pp. 53–76, Springer Berlin Heidelberg, 1986. (Cited on page 55)
- Craig, H., The geochemistry of the stable carbon isotopes, *Geochimica et Cosmochimica Acta*, *3*, 53 – 92, 1953. (Cited on page 40)
- Cronin, T., Pliocene shallow-water paleoceanography of the north-atlantic ocean based on marine ostracodes, *Quaternary Science Reviews*, *10*, 175–188, 1991. (Cited on page 15)
- Crowley, T., Modeling Pliocene warmth, *Quaternary Science Reviews*, *10*, 275–282, 1991. (Cited on pages 15, 23 and 86)
- Dalbeck, P., M. Cusack, P. S. Dobson, N. Allison, A. E. Fallick, A. W. Tudhope, and EIMF, Identification and composition of secondary meniscus calcite in fossil coral and the effect on predicted sea surface temperature, *Chemical Geology*, *280*, 314–322, 2011. (Cited on pages 79 and 85)
- Denniston, R. F., Y. Asmerom, V. Y. Polyalk, D. F. McNeill, J. S. Klaus, P. Cole, and A. F. Budd, Caribbean chronostratigraphy refined with U-Pb dating of a Miocene coral, *Geology*, *36*, 151–154, 2008. (Cited on pages 28, 29, 30 and 93)
- Dodge, R., R. Aller, and J. Thomson, Coral growth related to resuspension of bottom sediments, *Nature*, *247*, 574–576, 1974. (Cited on pages 8 and 9)
- Dodge, R. E., and G. W. Brass, Skeletal extension, density and calcification of the reef coral *Montastrea annularis*: St. Croix, U.S. Virgin Islands, *Bulletin of Marine Science*, *34*, 288–307, 1984. (Cited on pages 9, 73 and 92)

- Dowsett, H., J. Barron, and R. Poore, Middle Pliocene sea surface temperatures: a global reconstruction, *Marine Micropaleontology*, *27*, 13 – 25, 1996. (Cited on page 23)
- Draper, G., and J. Lewis, Geology and tectonic evolution of the northern margin of the Caribbean, in *The Caribbean Region (The Geology of North America, Vol. H)*, edited by J. C. G. Dengo, pp. 77–140, Geological Society of America, 1990. (Cited on page 27)
- Draper, G., and F. Nagle, Geology, structure and tectonic development of the Rio San Juan Complex, northern Dominican Republic, in *Geologic and Tectonic Development of the North American–Caribbean Plate Boundary in Hispaniola*, edited by J. L. P Mann, D Grenville, Geological Society of America, 1991. (Cited on page 27)
- Draper, G., P. Mann, and J. Lewis, Hispaniola, in *Caribbean Geology*, edited by T. J. S.K. Donovan, pp. 129–150, The University of the West Indies Publishers' Association, 1994. (Cited on page 26)
- Druffel, E., Geochemistry of corals: Proxies of past ocean chemistry, ocean circulation, and climate, *Proceedings Of The National Academy Of Sciences Of The United States Of America*, *94*, 8354–8361, 1997, Colloquium on Carbon Dioxide and Climate Change, Natl Acad Sci, Irvine, CA, Nov 13-15, 1995. (Cited on pages 8, 14, 15, 78, 85 and 93)
- DuBar, J. R., *Stratigraphy and paleontology of the late Neogene strata of the Caloosahatchee River area of southern Florida*, Florida Geological Survey Bulletin, 1958. (Cited on pages 25 and 87)
- Dullo, W.-C., Coral growth and reef growth: A brief review, *Facies*, *51*, 33–48, 2005. (Cited on page 8)
- Duque-Caro, H., Neogene stratigraphy, paleoceanography and paleobiogeography in north-west South-America and the evolution of the Panama Seaway, *Palaeogeography Palaeoclimatology Palaeoecology*, *77*, 203–234, 1990. (Cited on page 17)
- Dustan, P., Growth and form in the reef-building coral *Montastrea annularis*, *Marine Biology*, *33*, 101–107, 1975. (Cited on page 73)
- Enfield, D. B., and D. A. Mayer, Tropical Atlantic sea surface temperature variability and its relation to El Niño-Southern Oscillation, *Journal of Geophysical Research*, *102*, 929–945, 1997. (Cited on page 83)
- Epstein, S., and T. Mayeda, Variation of O18 content of waters from natural sources, *Geochimica et Cosmochimica Acta*, *4*, 213 – 224, 1953. (Cited on pages 8, 14 and 15)
- Erikson, J., J. Pindell, G. Karner, L. Sonder, E. Fuller, and L. Dent, Neogene sedimentation and tectonics in the Cibao basin and northern Hispaniola: An example of basin evolution near a strike-slip-dominated plate boundary, *Journal Of Geology*, *106*, 473–494, 1998. (Cited on pages 27, 28 and 30)
- Evans, C., Facies Evolution in a Neogene Transpressional Basin: Cibao Valley, Dominican Republic , Ph.D. thesis, University of Miami, Coral Gables, Florida, 1986. (Cited on pages 30 and 31)
- Evans, C., A field guide to the mixed reefs and siliciclastics of the Neogene Yaque Group, Cibao Valley, Dominican Republic, Miami, University of Miami, Rosenstiel School of Marine and Atmospheric Science, 1986. (Cited on page 31)



- Fairbanks, R., and R. Dodge, Annual periodicity of the O18-O16 and C13-C12 ratios in the coral *Montastrea annularis*, *Geochimica Et Cosmochimica Acta*, *43*, 1009–1020, 1979. (Cited on pages 86 and 92)
- Fallon, S. J., M. T. McCulloch, R. van Woesik, and D. J. Sinclair, Corals at their latitudinal limits: laser ablation trace element systematics in *Porites* from Shirigai Bay, Japan, *Earth and Planetary Science Letters*, *172*, 221 – 238, 1999. (Cited on page 78)
- Fedorov, A., P. Dekens, M. McCarthy, A. Ravelo, P. deMenocal, M. Barreiro, R. Pacanowski, and S. Philander, The Pliocene paradox (mechanisms for a permanent El Nino), *Science*, *312*, 1485–1489, 2006. (Cited on page 17)
- Flohn, H., A hemispheric circulation asymmetry during late Tertiary, *Geol. Rundsch.*, *70*, 725–736, 1981. (Cited on pages 23 and 98)
- Fournie, J. W., D. N. Vivian, S. H. Yee, L. A. Courtney, and M. G. Barron, Comparative sensitivity of six scleractinian corals to temperature and solar radiation, *Diseases Of Aquatic Organisms*, *99*, 85–93, 2012. (Cited on page 93)
- Fratantoni, D. M., North Atlantic surface circulation during the 1990's observed with satellite-tracked drifters, *Journal of Geophysical Research: Oceans*, *106*, 22,067–22,093, 2001. (Cited on pages 15 and 16)
- Gagan, M., L. Ayliffe, J. Beck, J. Cole, E. Druffel, R. Dunbar, and D. Schrag, New views of tropical paleoclimates from corals, *Quaternary Science Reviews*, *19*, 45–64, 2000. (Cited on page 14)
- Gaillardet, J., and C. Allegre, Boron isotopic compositions of corals: Seawater or diagenesis record?, *Earth and Planetary Science Letters*, *136*, 665–676, 1995. (Cited on page 82)
- Giannini, A., Y. Kushnir, and M. A. Cane, Interannual Variability of Caribbean Rainfall, ENSO, and the Atlantic Ocean, *Journal of Climate*, *13*, 297–311, 2000. (Cited on pages 17 and 23)
- Giry, C., T. Felis, M. Kölling, D. Scholz, W. Wei, G. Lohmann, and S. Scheffers, Mid- to late Holocene changes in tropical Atlantic temperature seasonality and interannual to multidecadal variability documented in southern Caribbean corals, *Earth and Planetary Science Letters*, *331–332*, 187 – 200, 2012. (Cited on pages 17 and 93)
- Gischler, E., and W. Oschmann, Historical climate variation in Belize (Central America) as recorded in scleractinian coral skeletons, *Palaios*, *20*, 159–174, 2005. (Cited on pages 83, 88 and 96)
- Gischler, E., J. Hudson, and D. Storz, Growth of Pleistocene massive corals in south Florida: low skeletal extension-rates and possible ENSO, decadal, and multi-decadal cyclicities, *Coral reefs*, *28*, 823–830, 2009. (Cited on pages 83 and 88)
- Gonzalez-Diaz, P., G. Gonzalez-Sanson, S. Alvarez Fernandez, and O. Perera Perez, High spatial variability of coral, sponges and gorgonian assemblages in a well preserved reef, *Revista De Biologia Tropical*, *58*, 621–634, 2010. (Cited on page 93)
- Gordon, A. L., Circulation of the Caribbean Sea, *Journal of Geophysical Research*, *72*, 6207–6223, 1967. (Cited on page 16)

- Graus, RR and MacIntyre, IG, Variation in growth forms of the reef coral *Montastrea annularis* (Ellis and Solander): A quantitative evaluation of growth response to light distribution using computer simulation, in *The Atlantic Barrier Reef Ecosystem at Carrie Bow Cay, Belize*, edited by K. Rutzler and I.G. MacIntyre, pp. 441–464, Smithsonian Institution, Washington, D.C., 1982. (Cited on page 73)
- Greer, L., and P. K. Swart, Decadal cyclicality of regional mid-Holocene precipitation: Evidence from Dominican coral proxies, *Paleoceanography*, *21*, PA2020, 2006. (Cited on pages 88, 93, 96 and 99)
- Greer, L., J. E. Jackson, H. A. Curran, T. Guilderson, and L. Teneva, How vulnerable is *Acropora cervicornis* to environmental change? Lessons from the early to middle Holocene, *Geology*, *37*, 263–266, 2009. (Cited on page 34)
- Griffiths, N., W. Müller, K. G. Johnson, and O. A. Aguilera, Evaluation of the effect of diagenetic cements on element/Ca ratios in aragonitic Early Miocene (16 Ma) Caribbean corals: Implications for ‘deep-time’ palaeo-environmental reconstructions, *Palaeogeography, Palaeoclimatology, Palaeoecology*, *369*, 185 – 200, 2013. (Cited on pages 38 and 95)
- Halley, R., and L. Roulier, Reconstructing the history of eastern and central Florida Bay using mollusk-shell isotope records, *Estuaries*, *22*, 358–368, 1999. (Cited on pages 26 and 86)
- Hammer, Ø., D. A. Harper, and P. D. Ryan, PAST: paleontological statistics software package for education and data analysis, *Palaeontologia electronica*, *4*, 9, 2001. (Cited on page 43)
- Hansmann, K., Stabile Isotope zur Rekonstruktion des Paläoklimas: Das Potenzial der Bivalve *Mercenaria* (Plio-/Pleistozän, SW-Florida), Master’s thesis, Institut für Geophysik und Geologie, Universität Leipzig, 2011. (Cited on pages 80, 86 and 87)
- Hastenrath, S., M. Wu, and P. Chu, Towards the monitoring and prediction of northeast Brazil droughts, *Quarterly Journal Of The Royal Meteorological Society*, *110*, 411–425, 1984. (Cited on page 17)
- Haug, G., and R. Tiedemann, Effect of the formation of the Isthmus of Panama on Atlantic Ocean thermohaline circulation, *Nature*, *393*, 673–676, 1998. (Cited on pages 17 and 23)
- Haywood, A. M., and P. J. Valdes, Modelling Pliocene warmth: contribution of atmosphere, oceans and cryosphere, *Earth and Planetary Science Letters*, *218*, 363–377, 2004. (Cited on page 80)
- Helmle, K., and R. Dodge, Sclerochronology, in *Encyclopedia of Modern Coral Reefs*, edited by D. Hopley, Encyclopedia of Earth Sciences Series, pp. 958–966, Springer Netherlands, 2011. (Cited on pages 96 and 98)
- Helmle, K., K. Kohler, and R. Dodge, Relative optical densitometry and the coral X-radiograph densitometry system: CoralXDS, in *Int. Soc. Reef Studies 2002 European Meeting*, Cambridge, England, 2002. (Cited on pages 40, 52, 62 and 68)
- Hetzinger, S., Stable oxygen isotopes and Sr-Ca-ratios in modern *Diploria strigosa* corals from different sites in the Caribbean Sea - evaluation of a new climate archive for the tropical Atlantic, Ph.D. thesis, Mathematisch-Naturwissenschaftliche Fakultät der Christian-Albrechts-Universität zu Kiel, 2007. (Cited on pages 13 and 14)

- Highsmith, R., Coral growth-rates and environmental-control of density banding, *Journal Of Experimental Marine Biology And Ecology*, *37*, 105–125, 1979. (Cited on pages 8 and 9)
- Horst, O. H., Climate and the “Encounter” in the Dominican Republic, *Journal of Geography*, *91*, 205–210, 1992. (Cited on pages 23 and 93)
- Horta-Puga, G., and J. D. Carriquiry, Coral Ba/Ca molar ratios as a proxy of precipitation in the northern Yucatan Peninsula, Mexico, *Applied Geochemistry*, *27*, 1579 – 1586, 2012. (Cited on page 81)
- Huber, M., and R. Caballero, Eocene El Nino: Evidence for robust tropical dynamics in the “hothouse”, *Science*, *299*, 877–881, 2003. (Cited on page 23)
- Hudson, J., E. Shinn, R. Halley, and B. Lidz, Sclerochronology - tool for interpreting past environments, *Geology*, *4*, 361–364, 1976. (Cited on page 9)
- Hudson, J., G. Powell, M. Robblee, and T. Smith, A 107-year-old coral from Florida Bay - barometer of natural and man-induced catastrophes, *Bulletin Of Marine Science*, *44*, 283–291, 1989. (Cited on pages 26 and 71)
- Hurrell, J. W., and C. Deser, North Atlantic climate variability: The role of the North Atlantic Oscillation, *Journal Of Marine Systems*, *78*, 28–41, 2009. (Cited on page 20)
- Jackson, J., and A. Budd, Evolution and environment : Introduction and overview, in *Evolution and Environment in Tropical America*, edited by A. G. C. Jeremy B. Jackson, Ann F. Budd, pp. 1–20, University of Chicago Press, 1996. (Cited on page 23)
- Jackson, J., and K. Johnson, Life in the last few million years, in *Deep Time: Paleobiology’s Perspective*, edited by S. W. D.H. Erwin, vol. 26, pp. 221–235, Paleobiology, 2000. (Cited on pages 23, 90 and 98)
- Jochum, K. P., et al., Determination of reference values for NIST SRM 610-617 glasses following ISO guidelines, *Geostandards And Geoanalytical Research*, *35*, 397–429, 2011. (Cited on page 43)
- Johnson, K., and M. Perez, Skeletal extension rates of Cenozoic Caribbean reef corals, *Palaios*, *21*, 262–271, 2006. (Cited on pages 90, 97 and 98)
- Johnston, I. S., The ultrastructure of skeletogenesis in hermatypic corals, in *International Review of Cytology*, edited by G. Bourne and J. Danielli, vol. 67, pp. 171 – 214, Academic Press, 1980. (Cited on page 8)
- Jokiel, P., and S. Coles, Effects of temperature on the mortality and growth of Hawaiian reef corals, *Marine Biology*, *43*, 201–208, 1977. (Cited on page 8)
- Jones, D., and W. Allmon, Records of upwelling, seasonality and growth in stable-isotope profiles of Pliocene mollusk shells from Florida, *Lethaia*, *28*, 61–74, 1995. (Cited on pages 15, 78 and 87)
- Kasper-Zubillaga, J., L. Rosales-Hoz, and J. Bernal, Rare earth elements in corals from the Isla de Sacrificios Reef, Veracruz, Mexico, *Chemie der Erde - Geochemistry*, *70*, 55 – 60, 2010. (Cited on page 82)
- Kelble, C. R., E. M. Johns, W. K. Nuttle, T. N. Lee, R. H. Smith, and P. B. Ortner, Salinity patterns of Florida Bay, *Estuarine Coastal And Shelf Science*, *71*, 318–334, 2007. (Cited on page 26)

- Kennedy, L. M., S. P. Horn, and K. H. Orvis, A 4000-year record of fire and forest history from Valle de Bao, Cordillera Central, Dominican Republic, *Palaeogeography, Palaeoclimatology, Palaeoecology*, *231*, 279 – 290, 2006. (Cited on page 23)
- Klaus, J., and A. Budd, Comparison of Caribbean coral reef communities before and after Plio-Pleistocene faunal turnover: Analyses of two Dominican Republic reef sequences, *Palaios*, *18*, 3–21, 2003. (Cited on pages 26, 92 and 98)
- Klaus, J. S., B. P. Lutz, D. F. McNeill, A. F. Budd, K. G. Johnson, and S. E. Ishman, Rise and fall of Pliocene free-living corals in the Caribbean, *Geology*, *39*, 375–378, 2011. (Cited on page 16)
- Knutson, D., S. Smith, and R. Buddemeier, Coral chronometers - seasonal growth bands in reef corals, *Science*, *177*, 270–&, 1972. (Cited on pages 8, 9 and 38)
- Kottek, M., J. Grieser, C. Beck, B. Rudolf, and F. Rubel, World map of the Koppen-Geiger climate classification updated, *Meteorologische Zeitschrift*, *15*, 259–263, 2006. (Cited on page 22)
- Lane, C. S., S. P. Horn, C. I. Mora, and K. H. Orvis, Late-Holocene paleoenvironmental change at mid-elevation on the Caribbean slope of the Cordillera Central, Dominican Republic: a multi-site, multi-proxy analysis, *Quaternary Science Reviews*, *28*, 2239 – 2260, 2009. (Cited on page 23)
- Leder, J., A. Szmant, and P. Swart, The effect of prolonged “bleaching” on skeletal banding and stable isotopic composition in *Montastrea annularis*, *Coral Reefs*, *10*, 19–27, 1991. (Cited on page 85)
- Levitus, S., and T. Boyer, World Ocean Atlas 1994, Vol. 3: Salinity, *NOAA Atlas NESDIS 3*, *3*, 1994a. (Cited on page 19)
- Levitus, S., and T. Boyer, World Ocean Atlas 1994, Vol. 4: Temperature, *NOAA Atlas NESDIS 4*, *4*, 1994b. (Cited on page 18)
- Lewis, J., Resume of the geology of Hispaniola : Field Guide, in *9th Caribbean Geol. Conf*, pp. 5–31, Santo Domingo, Dominican Republic, 1980. (Cited on page 27)
- Lisiecki, L., and M. Raymo, A Pliocene-Pleistocene stack of 57 globally distributed benthic delta O-18 records, *Paleoceanography*, *20*, 2005. (Cited on page 86)
- Lloyd, R., A paleoecological interpretation of Caloosahatchee Formation using stable isotope methods, *Journal Of Geology*, *77*, 1–25, 1969. (Cited on pages 25, 26, 82, 86 and 87)
- Lohmann, H., *Scleractinia als spätmiozäne Klimafenster der Karibik*, Master’s thesis, Institut für Geophysik und Geologie, Universität Leipzig, 2013. (Cited on pages 58, 62, 71, 87 and 91)
- Lough, J., and D. Barnes, Intraannual timing of density band formation of *Porites* coral from the central Great-Barrier-Reef , *Journal Of Experimental Marine Biology And Ecology*, *135*, 35–57, 1990. (Cited on page 9)
- Lough, J., and D. Barnes, Environmental controls on growth of the massive coral *Porites*, *Journal Of Experimental Marine Biology And Ecology*, *245*, 225–243, 2000. (Cited on pages 89 and 90)

- Lough, J. M., Coral calcification from skeletal records revisited, *Marine Ecology Progress Series*, 373, 257–264, 2008. (Cited on page 90)
- Lough, J. M., and T. F. Cooper, New insights from coral growth band studies in an era of rapid environmental change, *Earth-Science Reviews*, 108, 170–184, 2011. (Cited on pages 9 and 96)
- Lunt, D. J., P. J. Valdes, A. Haywood, and I. C. Rutt, Closure of the Panama Seaway during the Pliocene: implications for climate and Northern Hemisphere glaciation, *Climate Dynamics*, 30, 1–18, 2008. (Cited on page 17)
- Lutz, B., S. Ishman, D. McNeill, J. Klaus, and A. Budd, Late Neogene planktonic foraminifera of the Cibao Valley (northern Dominican Republic): Biostratigraphy and paleoceanography, *Marine Micropaleontology*, 69, 282 – 296, 2008. (Cited on pages 16, 17, 28, 31 and 93)
- Lyons, W., A Caloosahatchee-Age Fauna at APAC Mine, Sarasota County, Florida, in *Plio-Pleistocene Stratigraphy and Paleontology of South Florida*, edited by W. Allmon and T. Scott, p. unpaginated, Southeastern Geological Society Annual Fieldtrip Guidebook, 1990. (Cited on page 78)
- MacIntyre, I., Distribution of submarine cements in a modern Caribbean fringing reef, Galeta Point, Panama, *Journal Of Sedimentary Petrology*, 47, 503–516, 1977. (Cited on pages 44 and 55)
- Maier, K., J. Klaus, D. McNeill, and A. F. Budd, A late Miocene low-nutrient window for Caribbean reef formation?, *Coral Reefs*, 26, 635–639, 2007. (Cited on pages 31 and 92)
- Mallela, J., Coral reef communities and carbonate production in a fluvially-influenced embayment, Rio Bueno, Jamaica., Ph.D. thesis, Manchester Metropolitan University, 2004. (Cited on page 73)
- Mann, P., C. Schubert, and K. Burke, Review of Caribbean neotectonics, in *The Caribbean Region (The Geology of North America, Vol. H)*, edited by J. C. G. Dengo, pp. 307–338, Geological Society of America, 1990. (Cited on pages 27 and 29)
- Mann, P., D. Grenville, and J. Lewis, An overview of the geologic and tectonic development of Hispaniola, in *Geologic and Tectonic Development of the North American–Caribbean Plate Boundary in Hispaniola*, edited by J. L. P. Mann, D. Grenville, pp. 152–176, Geological Society of America, 1991. (Cited on pages 26 and 98)
- Mann, P., F. Taylor, K. Burke, and R. Kulstad, Subaerially exposed Holocene coral-reef, Enriquillo Valley, Dominican Republic, *Geological Society Of America Bulletin*, 95, 1084–1092, 1984. (Cited on page 34)
- Marshall, A., Calcification in hermatypic and ahermatypic corals, *Science*, 271, 637–639, 1996. (Cited on page 9)
- Marshall, A., and P. Clode, Calcification rate and the effect of temperature in a zooxanthellate and an azooxanthellate scleractinian reef coral, *Coral Reefs*, 23, 218–224, 2004. (Cited on pages 9 and 10)
- Marshall, J. F., and M. T. McCulloch, An assessment of the Sr/Ca ratio in shallow water hermatypic corals as a proxy for sea surface temperature, *Geochimica et Cosmochimica Acta*, 66, 3263 – 3280, 2002. (Cited on pages 78 and 95)

- McConnaughey, T., C-13 and O-18 isotopic disequilibrium in biological carbonates .1. Patterns, *Geochimica Et Cosmochimica Acta*, *53*, 151–162, 1989a. (Cited on pages 12, 13, 14 and 91)
- McConnaughey, T., C-13 and O-18 isotopic disequilibrium in biological carbonates .2. *In vitro* simulation of kinetic isotope effects, *Geochimica Et Cosmochimica Acta*, *53*, 163–171, 1989b. (Cited on pages 12, 13 and 14)
- McCrea, J., On the isotopic chemistry of carbonates and a paleotemperature scale, *Journal Of Chemical Physics*, *18*, 849–857, 1950. (Cited on page 13)
- McCulloch, M., S. Fallon, T. Wyndham, E. Hendy, J. Lough, and D. Barnes, Coral record of increased sediment flux to the inner Great Barrier Reef since European settlement, *Nature*, *421*, 727–730, 2003. (Cited on page 95)
- McGregor, H. V., and N. J. Abram, Images of diagenetic textures in *Porites* corals from Papua New Guinea and Indonesia, *Geochemistry Geophysics Geosystems*, *9*, 2008. (Cited on pages 38 and 44)
- McNeill, D. F., J. S. Klaus, A. F. Budd, B. P. Lutz, and S. E. Ishman, Late Neogene chronology and sequence stratigraphy of mixed carbonatesiliciclastic deposits of the Cibao Basin, Dominican Republic, *Geological Society Of America Bulletin*, *124*, 35–58, 2012. (Cited on pages 16, 26, 27, 28, 29, 30, 31, 91 and 93)
- Meeder, J. F., Pliocene fossil reef of southwest florida, Miami Geol. Society Field Trip, 1979. (Cited on pages 33, 34, 55 and 84)
- Meeder, J. F., Coralline and associated carbonates from Florida Bank (Pliocene), Lee and Collier Counties, Florida: ABSTRACT, *AAPG Bulletin*, *66*, 1982. (Cited on page 84)
- Min, G., R. Edwards, F. Taylor, J. Recy, C. Gallup, and J. Beck, Annual cycles of U/Ca in coral skeletons and U/Ca thermometry, *Geochimica et Cosmochimica Acta*, *59*, 2025–2042, 1995. (Cited on page 82)
- Mitsuguchi, T., E. Matsumoto, O. Abe, T. Uchida, and P. J. Isdale, Mg/Ca thermometry in coral skeletons, *Science*, *274*, 961–963, 1996. (Cited on pages 78 and 95)
- Molnar, P., and M. A. Cane, El Niño’s tropical climate and teleconnections as a blueprint for pre-Ice Age climates, *Paleoceanography*, *17*, 11–1–11–11, 2002. (Cited on pages 17 and 23)
- Montes, C., et al., Evidence for middle Eocene and younger land emergence in central Panama: Implications for Isthmus closure, *Geological Society Of America Bulletin*, *124*, 780–799, 2012. (Cited on page 17)
- Moses, C. S., P. K. Swart, and R. E. Dodge, Calibration of stable oxygen isotopes in *Siderastrea radians* (Cnidaria : Scleractinia): Implications for slow-growing corals, *Geochemistry Geophysics Geosystems*, *7*, 2006. (Cited on page 91)
- Nagle, F., Blueschist, eclogite, paired metamorphic belts, and the early tectonic history of Hispaniola, *Geological Society of America Bulletin*, *85*, 1461–1466, 1974. (Cited on page 27)
- Nehm, R., Patterns and processes of evolutionary stasis and change in Eratoidea (Gastropoda : Marginellidae) from the Dominican Republic Neogene, *Caribbean Journal Of Science*, *41*, 189–214, 2005. (Cited on page 27)

- Nof, D., and S. Van Gorder, Did an open Panama Isthmus correspond to an invasion of Pacific water into the Atlantic?, *Journal Of Physical Oceanography*, *33*, 1324–1336, 2003. (Cited on page 17)
- North, J., *Cosmos: an illustrated history of astronomy and cosmology*, University of Chicago Press, 2008. (Cited on page 82)
- Nothdurft, L., and G. Webb, Earliest diagenesis in scleractinian coral skeletons: implications for palaeoclimate-sensitive geochemical archives, *Facies*, *55*, 161–201, 2009. (Cited on pages 38, 44, 55 and 78)
- Nozaki, Y., Rare earth elements and their isotopes in the ocean, in *Encyclopedia of Ocean Sciences*, edited by J. H. Steele, pp. 2354 – 2366, Academic Press, Oxford, 2001. (Cited on page 82)
- O’Neil, J. R., R. N. Clayton, and T. K. Mayeda, Oxygen isotope fractionation in divalent metal carbonates, *The Journal of Chemical Physics*, *51*, 5547–5558, 1969. (Cited on pages 11 and 12)
- Paillard, D., L. Labeyrie, and P. Yiou, Macintosh program performs time-series analysis, *Eos, Transactions American Geophysical Union*, *77*, 379–379, 1996. (Cited on page 42)
- Pätzold, J., Growth rhythms recorded in stable isotopes and density bands in the reef coral *Porites lobata* (Cebu, Philippines), *Coral Reefs*, *3*, 87–90, 1984. (Cited on page 86)
- Petuch, E. J., Notes on the molluscan paleoecology of the Pinecrest Beds at Sarasota, Florida with the description of *Pyruella*, a stratigraphically important new genus (Gastropoda: Melongenidae), *Proceedings of the Academy of Natural Sciences of Philadelphia*, *134*, 12–30, 1982. (Cited on pages 78 and 90)
- Petuch, E. J., *Cenozoic Seas: The View From Eastern North America.*, CRC Press, London, 2003. (Cited on page 15)
- Petuch, E. J., *The Geology of the Everglades and Adjacent Areas*, CRC Press, Hoboken, 2007. (Cited on pages 15, 21, 22, 24, 25, 26, 78, 87 and 90)
- Philander, S. G., and A. V. Fedorov, Role of tropics in changing the response to Milankovich forcing some three million years ago, *Paleoceanography*, *18*, 23–1–23–11, 2003. (Cited on page 23)
- Reuter, M., T. Brachert, A. Böcker, and J. Klaus, An unusual Pocillopora reef from the Late Miocene of Hispaniola, *Coral Reefs*, *30*, 307–307, 2011. (Cited on page 37)
- Reuter, M., A. Böcker, H. Lohmann, and T. Brachert, The Lago Enriquillo fringing reef (Dominican Republic): a unique window into Holocene coral reef ecosystems of the Caribbean Sea, *International Journal of Earth Sciences*, *102*, 781–782, 2013. (Cited on page 34)
- Rice, S. A., and C. L. Hunter, Effects of suspended sediment and burial on scleractinian corals from west central Florida patch reefs, *Bulletin Of Marine Science*, *51*, 429–442, 1992. (Cited on page 93)
- Ross, R. S., A. Chakraborty, A. Chen, L. Stefanova, S. Sirdas, and T. N. Krishnamurti, Improved seasonal climate forecasts for the Caribbean region using the Florida State University Synthetic Superensemble, *Meteorology and Atmospheric Physics*, *98*, 137–174, 2007. (Cited on page 23)

- Roulier, L. M., and T. M. Quinn, Seasonal- to decadal-scale climatic variability in southwest Florida during the Middle Pliocene: Inferences from a coralline stable isotope record, *Paleoceanography*, *10*, 429–443, 1995. (Cited on pages 71, 80, 85, 86, 87 and 89)
- Saunders, J., P. Jung, and B. Biju-Duval, *Neogene Paleontology in the Northern Dominican Republic - 1. Field Surveys, Lithology, Environment, and Age*, Paleontological Research Institution, 1986. (Cited on pages 16, 26, 27, 28, 29, 30, 31, 34, 35, 37, 91 and 92)
- Sayani, H. R., K. M. Cobb, A. L. Cohen, W. C. Elliott, I. S. Nurhati, R. B. Dunbar, K. A. Rose, and L. K. Zaunbrecher, Effects of diagenesis on paleoclimate reconstructions from modern and young fossil corals, *Geochimica Et Cosmochimica Acta*, *75*, 6361–6373, 2011. (Cited on page 44)
- Schlager, W., Benthic carbonate factories of the Phanerozoic, *International Journal of Earth Sciences*, *92*, 445–464, 2003. (Cited on page 8)
- Schott, F. A., T. N. Lee, and R. Zantopp, Variability of structure and transport of the Florida Current in the period range of days to seasonal, *Journal Of Physical Oceanography*, *18*, 1209–1230, 1988. (Cited on page 15)
- Schroeder, J., and B. Purser, *Reef diagenesis*, Springer, Berlin, Heidelberg, 1986. (Cited on pages 44 and 78)
- Scott, T., K. Campbell, F. Rupert, J. Arthur, T. Missimer, J. Lloyd, J. Yon, and J. Duncan (Eds.), *Geologic Map of the State of Florida*, Open-File Report 80, Florida Geological Survey and Florida Department of Environmental Protection, 2001. (Cited on pages 78 and 84)
- Shen, G. T., and R. B. Dunbar, Environmental controls on uranium in reef corals, *Geochimica et Cosmochimica Acta*, *59*, 2009–2024, 1995. (Cited on page 82)
- Sinclair, D. J., L. P. Kinsley, and M. T. McCulloch, High resolution analysis of trace elements in corals by laser ablation ICP-MS, *Geochimica et Cosmochimica Acta*, *62*, 1889 – 1901, 1998. (Cited on page 82)
- Sliko, J., and G. Herbert, Nutrient decline, rainfall patterns, and the end-Pliocene regional mass extinction in Florida, in *Annual Meeting*, Geological Society of America, 2009. (Cited on pages 81 and 87)
- Stearn, C., T. Scoffin, and W. Martindale, Calcium carbonate budget of a fringing reef on the west coast of Barbados. Part I: Zonation and productivity, *Bulletin of Marine Science*, *27*, 479–510, 1977. (Cited on pages 9 and 73)
- Steph, S., R. Tiedemann, M. Prange, J. Groeneveld, D. Nürnberg, L. Reuning, M. Schulz, and G. H. Haug, Changes in caribbean surface hydrography during the pliocene shoaling of the central american seaway, *Paleoceanography*, *21*, 2006. (Cited on pages 16, 17, 23 and 98)
- Swart, P., G. Healy, R. Dodge, P. Kramer, J. Hudson, R. Halley, and M. Robblee, The stable oxygen and carbon isotopic record from a coral growing in Florida Bay: A 160 year record of climatic and anthropogenic influence, *Palaeogeography Palaeoclimatology Palaeoecology*, *123*, 219–237, 1996. (Cited on pages 26, 71, 78, 80, 81, 85, 86, 87 and 89)
- Swart, P., G. Healy, L. Greer, M. Lutz, A. Saied, D. Anderegg, R. Dodge, and D. Rudnick, The use of proxy chemical records in coral skeletons to ascertain past environmental conditions in Florida Bay, *Estuaries*, *22*, 384–397, 1999. (Cited on page 26)



- Swart, P. K., Carbon and oxygen isotope fractionation in scleractinian corals: a review, *Earth-Science Reviews*, *19*, 51–80, 1983. (Cited on pages 8, 9, 12 and 13)
- Swart, P. K., L. D. Sternberg, R. Steinen, and S. A. Harrison, Controls on the oxygen and hydrogen isotopic composition of the waters of Florida Bay, USA, *Chemical Geology: Isotope Geoscience section*, *79*, 113–123, 1989. (Cited on pages 26, 78 and 81)
- Sykes, L. R., W. R. McCann, and A. L. Kafka, Motion of Caribbean plate during last 7 million years and implications for earlier Cenozoic movements, *Journal of Geophysical Research*, *87*, 10,656–10,676, 1982. (Cited on page 27)
- Tao, K., and E. L. Grossman, Origin of high productivity in the Pliocene of the Florida Platform: Evidence from stable isotopes and trace elements, *Palaios*, *25*, 796–806, 2010. (Cited on pages 16, 25, 26, 86 and 87)
- Taylor, S. R., and S. M. McLennan, *The continental crust: its composition and evolution : an examination of the geochemical record preserved in sedimentary rocks*, Blackwell Scientific, Oxford, 1985. (Cited on pages 51 and 68)
- van den Bold, W., Distribution of the *Radimella confragosa* group (Ostracoda, Hemi-cytherinae) in the late Neogene of the Caribbean, *Journal of Paleontology*, *49*, 692–701, 1975. (Cited on page 30)
- Vaughan, T. W., C. W. Cooke, D. D. Condit, C. P. Ross, W. P. Woodring, and F. C. Calkins, *Geological Survey of the Dominican Republic - A geological reconnaissance of the Dominican Republic*, vol. 1, Press of Gibson Brothers, Inc., Washington, 1921. (Cited on pages 16 and 26)
- Wang, C., and D. Enfield, A further study of the tropical Western Hemisphere warm pool, *Journal Of Climate*, *16*, 1476–1493, 2003. (Cited on page 17)
- Wang, C., D. B. Enfield, S.-k. Lee, and C. W. Landsea, Influences of the Atlantic warm pool on Western Hemisphere summer rainfall and Atlantic hurricanes, *Journal Of Climate*, *19*, 3011–3028, 2006. (Cited on page 17)
- Wang, C., S.-K. Lee, and D. B. Enfield, Impact of the Atlantic warm pool on the summer climate of the Western Hemisphere, *Journal Of Climate*, *20*, 5021–5040, 2007. (Cited on page 17)
- Wang, C., S.-K. Lee, and D. B. Enfield, Climate response to anomalously large and small Atlantic warm pools during the summer, *Journal Of Climate*, *21*, 2437–2450, 2008a. (Cited on page 17)
- Wang, C., S.-K. Lee, and D. B. Enfield, Atlantic Warm Pool acting as a link between Atlantic Multidecadal Oscillation and Atlantic tropical cyclone activity, *Geochemistry Geophysics Geosystems*, *9*, 2008b. (Cited on page 17)
- Weber, J. N., and P. M. Woodhead, Carbon and oxygen isotope fractionation in the skeletal carbonate of reef-building corals, *Chemical Geology*, *6*, 93 – 117, 1970. (Cited on pages 8, 9 and 12)
- Weber, J. N., and P. M. J. Woodhead, Temperature dependence of oxygen-18 concentration in reef coral carbonates, *Journal of Geophysical Research*, *77*, 463–473, 1972. (Cited on pages 12, 13 and 15)

- Weinlein, W., A. Kasprak, J. Sliko, P. J. Harries, G. S. Herbert, E. A. Oches, R. W. Portell, and M. C. Coe, The role of trace-metal proxies as upwelling indicators on the Florida Platform during the Plio-Pleistocene, in *Geological Society of America Abstracts with Programs*, vol. 40, p. 72, 2008. (Cited on page 87)
- Wells, J., Scleractinia, in *Treatise on invertebrate paleontology, Part F*, edited by R. Moore, pp. 328–444, Geological Society of America, 1956. (Cited on pages 8 and 9)
- Willard, D. A., T. M. Cronin, S. E. Ishman, and R. J. Litwin, Terrestrial and marine records of climatic and environmental changes during the Pliocene in subtropical Florida, *Geology*, 21, 679–682, 1993. (Cited on page 90)
- Wilson, D., *A reef in the Caloosahatchee Marl of southwest Florida*, U.S. Geological Survey Professional Paper, Geological Survey (U.S.), 1976. (Cited on page 84)
- Worum, F. P., J. P. Carricart-Ganivet, L. Benson, and D. Golicher, Simulation and observations of annual density banding in skeletons of *Montastraea* (Cnidaria : Scleractinia) growing under thermal stress associated with ocean warming, *Limnology And Oceanography*, 52, 2317–2323, 2007. (Cited on pages 9, 10, 11 and 84)
- Wüst, G., On the stratification and the circulation in the cold water sphere of the Antillean-Caribbean basins, in *Deep Sea Research*, vol. 10, pp. 165–187, Elsevier, 1963. (Cited on page 16)
- Wyatt, M., S. Kravtsov, and A. Tsonis, Atlantic Multidecadal Oscillation and Northern Hemisphere's climate variability, *Climate Dynamics*, 38, 929–949, 2012. (Cited on page 19)
- Yonge, C., Coral Reef Project - Papers in Memory of Dr. Thomas F. Goreau. 1. The nature of reef-building (hermatypic) corals, *Bulletin of Marine Science*, 23, 1–15, 1973. (Cited on page 8)
- Zubakov, V., and I. Borzenkova, Pliocene palaeoclimates: Past climates as possible analogues of mid-twenty-first century climate, *Palaeogeography, Palaeoclimatology, Palaeoecology*, 65, 35 – 49, 1988. (Cited on pages 23 and 93)

Appendix A1 Stable isotope data 452K1 S6

Sample Number (rescaled)	Age [yrs]	$\delta^{18}O$ [‰] vs. VPDB	$\delta^{13}C$ [‰] vs. VPDB	density [g/cm <sup>3</sup> ]	distance [mm]
1.0	0.00	-1.31	-1.78	0.60	0.7
2.0	0.08	-1.66	-2.05	0.73	1.4
3.0	0.17	-2.31	-1.87	0.70	2.1
4.0	0.25	-2.83	-1.98	0.68	2.8
5.0	0.33	-3.12	-1.76	0.65	3.5
6.0	0.42	-3.04	-1.20	0.62	4.2
7.0	0.50	-3.19	-1.66	0.63	4.9
8.0	0.58	-3.27	-1.83	0.65	5.6
9.0	0.67	-3.28	-1.91	0.68	6.3
10.0	0.75	-3.52	-1.88	0.70	7.0
11.0	0.83	-2.93	-1.65	0.77	7.7
12.0	0.92	-1.84	-1.83	0.88	8.4
13.0	1.00	-1.12	-1.99	0.90	9.1
15.0	1.15	-1.33	-1.98	0.85	10.5
16.0	1.23	-2.28	-1.77	0.77	11.2
17.0	1.31	-2.92	-1.55	0.70	11.9
18.0	1.38	-3.16	-1.21	0.71	12.6
19.0	1.46	-3.14	-1.52	0.74	13.3
20.0	1.54	-3.25	-1.40	0.70	14.0
21.0	1.62	-3.08	-1.83	0.65	14.7
22.0	1.69	-3.21	-1.58	0.62	15.4
23.0	1.77	-3.25	-1.68	0.74	16.1
24.0	1.85	-2.94	-2.25	0.72	16.8
25.0	1.92	-2.13	-2.10	0.74	17.5
26.0	2.00	-1.36	-1.78	0.74	18.2
27.0	2.09	-1.53	-2.42	0.71	18.9
28.0	2.18	-1.75	-1.86	0.64	19.6
29.0	2.27	-2.66	-1.83	0.64	20.3
30.0	2.36	-2.87	-1.05	0.59	21.0
31.0	2.45	-3.09	-1.27	0.61	21.7
32.0	2.55	-3.07	-1.48	0.62	22.4
33.0	2.64	-3.12	-2.07	0.63	23.1
34.0	2.73	-3.16	-2.66	0.67	23.8
35.0	2.82	-3.08	-1.96	0.75	24.5
36.0	2.91	-1.67	-1.63	0.78	25.2
37.0	3.00	-1.19	-1.30	0.81	25.9
38.0	3.09	-1.64	-2.21	0.73	26.6
39.0	3.18	-2.43	-1.87	0.68	27.3
40.0	3.27	-2.77	-1.84	0.69	28.0
41.0	3.36	-2.89	-1.71	0.68	28.7
42.0	3.45	-2.78	-1.65	0.65	29.4
43.0	3.55	-3.23	-1.47	0.73	30.1
44.0	3.64	-3.20	-2.09	0.64	30.8
45.0	3.73	-3.04	-2.27	0.69	31.5
46.0	3.82	-2.84	-2.03	0.74	32.2
47.0	3.91	-2.49	-2.27	0.86	32.9

—*Solenastrea* 452K1 S6 Florida—

Sample Number	Age	$\delta^{18}O$	$\delta^{13}C$	density	distance
48.0	4.00	-1.36	-1.77	0.74	33.6
49.0	4.09	-1.84	-1.61	0.66	34.3
50.0	4.18	-2.21	-1.77	0.62	35.0
51.0	4.27	-2.56	-1.57	0.63	35.7
52.0	4.36	-3.01	-2.58	0.59	36.4
53.0	4.45	-2.90	-1.60	0.65	37.1
54.0	4.55	-3.22	-1.38	0.59	37.8
55.0	4.64	-2.99	-1.31	0.59	38.5
55.8	4.70	-3.16	-1.54	0.68	39.0
56.5	4.77	-3.02	-1.55	0.70	39.6
58.0	4.91	-1.96	-1.30	0.76	40.6
59.0	5.00	-1.09	-1.77	0.78	41.3
59.9	5.09	-1.17	-1.67	0.77	41.9
60.8	5.18	-2.01	-1.41	0.71	42.6
61.8	5.28	-2.44	-1.45	0.67	43.2
62.7	5.37	-3.13	-1.81	0.65	43.9
63.6	5.46	-3.84	-1.84	0.62	44.5
64.5	5.55	-3.66	-2.41	0.58	45.2
65.5	5.65	-3.51	-2.39	0.60	45.9
66.5	5.75	-3.46	-2.39	0.68	46.6
67.8	5.88	-2.80	-1.65	0.81	47.4
69.0	6.00	-1.29	-1.73	0.80	48.3
70.2	6.15	-1.80	-1.50	0.74	49.1
71.3	6.29	-2.22	-1.11	0.69	49.9
72.5	6.44	-2.83	-0.92	0.65	50.8
73.2	6.52	-2.97	-0.83	0.71	51.2
73.8	6.60	-2.59	-1.27	0.70	51.7
74.5	6.69	-2.83	-1.71	0.80	52.2
75.8	6.84	-1.45	-1.13	0.97	53.0
77.0	7.00	-1.02	-1.31	0.91	53.9
78.2	7.16	-1.78	-0.84	0.84	54.7
79.0	7.28	-2.82	-0.92	0.82	55.3
79.8	7.39	-2.80	-0.96	0.83	55.9
81.0	7.56	-3.12	-1.04	0.85	56.7
82.3	7.74	-3.33	-1.76	0.75	57.6
83.2	7.86	-2.33	-1.60	0.77	58.2
84.2	8.00	-1.29	-1.98	0.77	58.9
85.0	8.09	-1.30	-1.04	0.74	59.5
85.7	8.17	-1.42	-1.69	0.70	60.0
86.3	8.24	-1.95	-1.44	0.64	60.4
87.0	8.32	-2.74	-1.28	0.66	60.9
87.7	8.39	-2.87	-0.26	0.72	61.4
88.3	8.47	-2.97	-1.25	0.76	61.8
89.0	8.55	-3.01	-1.46	0.73	62.3
90.7	8.73	-2.40	-1.35	0.83	63.5
93.0	9.00	-0.71	-1.05	0.79	65.1
94.2	9.09	-1.34	-0.98	0.79	65.9
96.0	9.24	-1.61	-1.10	0.74	67.2

—*Solenastrea* 452K1 S6 Florida—

Sample Number	Age	$\delta^{18}O$	$\delta^{13}C$	density	distance
97.0	9.32	-2.27	-1.71	0.70	67.9
99.0	9.48	-2.51	-1.12	0.69	69.3
100.0	9.56	-2.94	-0.55	0.74	70.0
101.0	9.64	-3.18	-1.08	0.71	70.7
101.8	9.71	-3.13	-1.10	0.78	71.3
103.0	9.80	-3.45	-1.78	0.85	72.1
104.3	9.90	-2.59	-2.11	0.83	73.0
105.5	10.00	-1.53	-1.52	0.81	73.9
106.4	10.11	-1.58	-1.49	0.74	74.5
107.3	10.22	-2.43	-1.65	0.73	75.1
108.3	10.32	-2.78	-1.59	0.69	75.8
109.2	10.43	-3.10	-1.49	0.73	76.4
110.1	10.54	-3.19	-1.49	0.75	77.1
111.0	10.65	-3.39	-1.69	0.82	77.7
112.0	10.76	-2.97	-2.17	0.81	78.4
113.0	10.88	-2.32	-1.92	0.77	79.1
114.0	11.00	-0.79	-1.55	0.72	79.8
115.0	11.11	-1.12	-1.63	0.70	80.5
116.0	11.22	-1.32	-1.80	0.64	81.2
117.0	11.33	-2.39	-1.02	0.63	81.9
118.0	11.44	-2.41	-1.49	0.74	82.6
119.0	11.56	-2.64	-0.97	0.68	83.3
120.0	11.67	-2.65	-1.48	0.67	84.0
121.0	11.78	-2.83	-1.74	0.71	84.7
122.0	11.89	-2.96	-2.36	0.75	85.4
123.0	12.00	-1.46	-1.63	0.84	86.1
124.0	12.13	-1.47	-1.05	0.85	86.8
125.0	12.25	-1.58	-1.99	0.80	87.5
126.0	12.38	-1.97	-1.44	0.69	88.2
127.0	12.50	-2.89	-1.45	0.64	88.9
128.0	12.63	-2.69	-1.87	0.60	89.6
129.0	12.75	-2.86	-2.13	0.57	90.3
130.0	12.88	-2.69	-1.58	0.58	91.0
131.0	13.00	-1.74	-1.05	0.61	91.7
132.0	13.25	-2.61	-1.59	0.62	92.4
133.0	13.50	-2.87	-2.14	0.67	93.1
134.0	13.75	-2.38	-2.13	0.74	93.8
135.0	14.00	-1.02	-1.55	0.85	94.5
136.0	14.13	-1.29	-1.36	0.75	95.2
137.0	14.25	-2.06	-1.02	0.68	95.9
138.0	14.38	-1.61	-1.11	0.66	96.6
139.0	14.50	-2.89	-1.04	0.66	97.3
140.0	14.63	-2.95	-0.72	0.69	98.0
141.0	14.75	-2.58	-1.37	0.66	98.7
142.0	14.88	-2.91	-2.71	0.87	99.4
143.0	15.00	-1.49	-1.62	0.98	100.1
144.0	15.08	-1.85	-1.52	0.77	100.8
145.0	15.17	-2.43	-2.26	0.69	101.5

—*Solenastrea* 452K1 S6 Florida—

Sample Number	Age	$\delta^{18}O$	$\delta^{13}C$	density	distance
146.0	15.25	-2.86	-2.73	0.61	102.2
147.0	15.33	-3.16	-2.79	0.55	102.9
148.0	15.42	-3.32	-2.71	0.51	103.6
149.0	15.50	-3.13	-2.14	0.67	104.3
150.0	15.58	-3.02	-2.30	0.68	105.0
151.0	15.67	-2.37	-1.55	0.63	105.7
152.0	15.75	-2.98	-2.35	0.69	106.4
153.0	15.83	-2.94	-2.46	0.67	107.1
154.0	15.92	-1.56	-1.67	0.66	107.8
155.0	16.00	-0.52	-0.61	0.67	108.5
156.0	16.10	-1.11	-1.22	0.64	109.2
157.0	16.20	-1.02	-1.42	0.65	109.9
158.0	16.30	-2.41	-2.31	0.66	110.6
159.0	16.40	-2.21	-1.63	0.65	111.3
160.0	16.50	-2.30	-1.51	0.61	112.0
161.0	16.60	-3.03	-1.92	0.69	112.7
162.0	16.70	-2.91	-2.14	0.75	113.4
163.0	16.80	-2.96	-2.42	0.83	114.1
164.0	16.90	-1.64	-1.67	0.79	114.8
165.0	17.00	-1.07	-1.91	0.77	115.5
166.0	17.13	-3.22	-1.43	0.72	116.2
167.0	17.25	-2.42	-1.22	0.73	116.9
168.0	17.38	-2.75	-1.13	0.79	117.6
169.0	17.50	-2.93	-1.01	0.84	118.3
170.0	17.63	-2.86	-0.61	0.96	119.0
171.0	17.75	-3.04	-1.66	0.96	119.7
172.0	17.88	-2.31	-1.45	1.00	120.4
173.0	18.00	-1.05	-1.35	0.81	121.1
174.0	18.14	-1.13	-1.02	0.85	121.8
175.0	18.29	-2.09	-1.20	0.86	122.5
176.0	18.43	-2.43	-1.30	0.94	123.2
177.0	18.57	-3.36	-1.41	0.84	123.9
178.0	18.71	-2.55	-1.46	0.85	124.6
179.0	18.86	-1.87	-1.55	0.79	125.3
180.0	19.00	-1.58	-1.69	0.74	126.0
181.0	19.17	-1.93	-1.65	0.84	126.7
182.0	19.33	-2.39	-1.75	0.80	127.4
183.0	19.50	-3.19	-0.94	0.93	128.1
184.0	19.67	-3.14	-1.40	0.95	128.8
185.0	19.83	-1.98	-1.28	0.84	129.5
186.0	20.00	-1.49	-1.67	0.80	130.2
187.0	20.20	-2.10	-1.97	0.87	130.9
188.0	20.40	-2.59	-1.08	0.83	131.6
189.0	20.60	-3.03	-1.31	0.98	132.3
190.0	20.80	-2.21	-1.35	0.86	133.0
191.0	21.00	-1.02	-1.38	0.68	133.7
192.0	21.13	-1.06	-1.81	0.66	134.4
193.0	21.25	-1.60	-1.96	0.60	135.1

—*Solenastrea* 452K1 S6 Florida—

Sample Number	Age	$\delta^{18}O$	$\delta^{13}C$	density	distance
194.0	21.38	-1.97	-1.22	0.68	135.8
195.0	21.50	-2.67	-0.96	0.73	136.5
196.0	21.63	-3.02	-1.76	0.88	137.2
197.0	21.75	-2.70	-2.88	0.76	137.9
199.0	22.00	-1.25	-1.12	0.67	139.3
202.0	22.75	-2.63	-1.40	0.98	141.4
203.0	23.00	-1.38	-1.90	0.80	142.1
204.0	23.11	-1.76	-1.49	0.70	142.8
205.0	23.22	-1.83	-1.40	0.69	143.5
206.0	23.33	-2.35	-0.83	0.72	144.2
207.0	23.44	-2.10	-0.82	0.62	144.9
208.0	23.56	-2.58	-1.09	0.81	145.6
209.0	23.67	-2.81	-2.10	0.86	146.3
211.0	23.89	-1.76	-2.13	0.65	147.7
212.0	24.00	-1.45	-1.82	0.56	148.4
213.0	24.10	-1.75	-1.33	0.64	149.1
214.0	24.20	-1.59	-2.01	0.62	149.8
215.0	24.30	-1.48	-1.31	0.64	150.5
216.0	24.40	-2.60	-1.08	0.70	151.2
217.0	24.50	-2.83	-0.86	0.70	151.9
217.8	24.58	-2.66	-1.11	0.91	152.5
218.3	24.63	-2.39	-1.06	0.71	152.8
219.0	24.70	-2.98	-2.14	0.87	153.3
220.0	24.80	-1.85	-1.90	0.87	154.0
220.8	24.88	-1.17	-1.41	0.69	154.5
222.0	25.00	-0.52	-1.35	0.73	155.4
223.0	25.10	-1.83	-0.95	0.68	156.1
224.0	25.20	-1.98	-1.00	0.72	156.8
225.0	25.30	-2.20	-1.19	0.71	157.5
226.0	25.40	-2.63	-0.96	0.85	158.2
227.0	25.50	-2.86	-0.86	0.81	158.9
228.0	25.60	-3.29	-1.14	0.78	159.6
229.0	25.70	-1.00	-1.00	0.95	160.3
230.0	25.80	-2.59	-1.42	0.86	161.0
232.0	26.00	0.05	-1.71	0.76	162.4
233.0	26.11	-0.68	-1.57	0.80	163.1
234.0	26.22	-1.63	-1.81	0.81	163.8
235.0	26.33	-2.00	-1.35	0.70	164.5
236.0	26.44	-2.45	-1.68	0.64	165.2
237.0	26.56	-2.70	-1.24	0.69	165.9
238.0	26.67	-3.06	-1.97	0.69	166.6
239.0	26.78	-2.77	-2.05	0.67	167.3
240.0	26.89	-1.00	-1.79	0.76	168.0
241.0	27.00	-0.07	-1.69	0.75	168.7
242.0	27.09	-0.97	-1.79	0.76	169.4
243.0	27.18	-1.49	-1.93	0.70	170.1
244.0	27.27	-1.91	-1.39	0.69	170.8
245.0	27.36	-2.31	-1.73	0.73	171.5

—*Solenastrea* 452K1 S6 Florida—

Sample Number	Age	$\delta^{18}O$	$\delta^{13}C$	density	distance
246.0	27.45	-2.78	-1.38	0.85	172.2
247.0	27.55	-2.66	-1.67	0.82	172.9
248.0	27.64	-2.91	-2.60	0.88	173.6
249.0	27.73	-2.48	-2.43	0.80	174.3
250.0	27.82	-1.63	-2.13	0.77	175.0
251.0	27.91	-0.60	-2.22	0.71	175.7
252.0	28.00	-0.35	-2.37	0.70	176.4
253.0	28.13	-1.17	-1.81	0.77	177.1
254.0	28.25	-1.71	-1.30	0.75	177.8
255.0	28.38	-2.27	-1.62	0.78	178.5
256.0	28.50	-2.93	-1.89	0.87	179.2
257.0	28.63	-3.18	-3.00	0.83	179.9
258.8	28.84	-2.13	-1.61	0.71	181.1
260.0	29.00	-0.95	-1.67	0.69	182.0
261.2	29.13	-1.02	-1.62	0.72	182.8
262.0	29.22	-1.37	-1.27	0.63	183.4
262.9	29.32	-2.03	-1.18	0.79	184.0
264.1	29.46	-2.58	-1.40	0.77	184.9
265.0	29.56	-3.07	-1.07	0.62	185.5
265.8	29.64	-3.27	-0.92	0.82	186.1
267.0	29.78	-3.46	-0.96	0.74	186.9
268.0	29.89	-2.88	-1.57	0.81	187.6
269.0	30.00	-1.49	-1.88	0.84	188.3
270.3	30.16	-2.37	-1.88	0.70	189.2
271.0	30.24	-3.04	-1.81	0.70	189.7
273.0	30.47	-3.14	-2.63	0.67	191.1
273.5	30.53	-2.26	-2.52	0.80	191.5
274.0	30.59	-2.23	-1.82	0.63	191.8
274.5	30.65	-2.57	-2.09	0.64	192.2
275.0	30.71	-3.00	-2.03	0.67	192.5
276.0	30.82	-3.24	-2.38	0.80	193.2
276.5	30.88	-2.74	-2.90	0.65	193.6
277.0	30.94	-1.61	-1.99	0.67	193.9
277.5	31.00	-0.52	-2.70	0.64	194.3
278.0	31.04	-0.64	-1.98	0.65	194.6
279.2	31.15	-0.80	-2.30	0.72	195.4
280.0	31.22	-1.54	-1.97	0.65	196.0
280.7	31.28	-1.20	-2.56	0.67	196.5
282.0	31.40	-2.29	-2.25	0.65	197.4
283.0	31.49	-1.88	-2.38	0.70	198.1
284.0	31.58	-2.61	-2.52	0.68	198.8
285.0	31.67	-2.74	-2.79	0.67	199.5
286.0	31.76	-2.83	-3.29	0.66	200.2
287.0	31.85	-2.57	-3.20	0.71	200.9
288.0	31.94	-2.30	-3.33	0.69	201.6
288.3	31.97	-1.71	-2.87	0.76	201.8
288.7	32.00	-0.54	-2.42	0.66	202.1
289.0	32.04	-0.93	-2.61	0.66	202.3

—*Solenastrea* 452K1 S6 Florida—



Sample Number	Age	$\delta^{18}O$	$\delta^{13}C$	density	distance
289.5	32.11	-0.96	-2.20	0.81	202.7
290.0	32.18	-1.65	-2.36	0.70	203.0
291.0	32.32	-1.99	-2.02	0.72	203.7
292.0	32.45	-2.69	-1.73	0.64	204.4
293.0	32.59	-2.50	-2.05	0.70	205.1
294.0	32.73	-2.44	-2.32	0.82	205.8
295.0	32.86	-1.24	-2.76	0.81	206.5
296.0	33.00	-0.51	-2.09	0.62	207.2
297.0	33.08	-1.10	-2.44	0.67	207.9
298.0	33.17	-1.68	-2.38	0.71	208.6
299.0	33.25	-1.84	-1.86	0.65	209.3
300.0	33.33	-2.86	-1.90	0.62	210.0
301.0	33.42	-2.79	-1.60	0.65	210.7
302.0	33.50	-2.74	-1.52	0.80	211.4
303.0	33.58	-2.75	-1.88	0.87	212.1
304.0	33.67	-2.94	-1.96	0.73	212.8
305.0	33.75	-1.91	-2.41	0.66	213.5
306.0	33.83	-1.66	-2.47	0.78	214.2
307.0	33.92	-1.20	-2.12	0.64	214.9
308.0	34.00	-0.99	-1.80	0.58	215.6
309.0	34.14	-1.50	-1.96	0.61	216.3
310.0	34.29	-1.48	-1.72	0.64	217.0
311.0	34.43	-2.17	-2.07	0.71	217.7
312.0	34.57	-2.19	-1.93	0.86	218.4
313.0	34.71	-2.44	-2.38	0.69	219.1
314.0	34.86	-1.97	-2.96	0.82	219.8
315.0	35.00	-0.12	-2.81	0.82	220.5
316.0	35.14	-0.70	-3.50	0.65	221.2
— <i>Solenastrea</i> 452K1 S6 Florida—					

Appendix A2 Stable isotope data 509A S1

Sample Number (rescaled)	Age [yrs]	$\delta^{18}O$ [‰] vs. VPDB	$\delta^{13}C$ [‰] vs. VPDB	density [g/cm <sup>3</sup> ]	distance [mm]
1	0.5	-1.05	-1.61	0.48	0.7
2	0.8	-2.07	-1.83	0.60	1.4
3	1.0	-2.28	-2.38	0.70	2.1
4	1.2	-1.57	-2.75	0.70	2.8
5	1.4	-0.94	-2.73	0.80	3.5
6	1.6	-1.51	-1.81	0.72	4.2
7	1.8	-2.15	-2.06	0.85	4.9
8	2.0	-2.60	-2.42	0.81	5.6
9	2.3	-2.20	-3.16	0.82	6.3
10	2.5	-1.54	-2.18	0.96	7
11	2.8	-1.79	-2.14	1.02	7.7
12	3.0	-2.78	-2.43	1.02	8.4
13	3.2	-2.37	-3.07	1.08	9.1
14	3.4	-1.05	-2.59	1.09	9.8
15	3.6	-1.41	-2.00	1.06	10.5
16	3.8	-2.29	-2.39	1.35	11.2
17	4.0	-2.44	-3.08	1.28	11.9
18	4.3	-1.15	-2.94	1.34	12.6
19	4.7	-1.97	-1.88	1.34	13.3
20	5.0	-2.57	-2.29	1.56	14
21	5.3	-2.53	-3.01	1.44	14.7
22	5.5	-1.40	-3.05	1.76	15.4
23	5.8	-2.03	-1.91	1.55	16.1
24	6.0	-2.52	-2.25	1.68	16.8
25	6.2	-2.32	-3.00	1.51	17.5
26	6.4	-1.23	-2.77	1.59	18.2
27	6.6	-1.33	-2.10	1.39	18.9
28	6.8	-2.00	-2.10	1.40	19.6
29	7.0	-2.16	-2.59	1.40	20.3
30	7.3	-1.31	-3.08	1.34	21
31	7.5	-1.40	-1.91	1.41	21.7
32	7.8	-2.18	-2.19	1.40	22.4
33	8.0	-2.56	-2.91	1.44	23.1
34	8.5	-1.97	-2.07	1.58	23.8
35	9.0	-2.57	-2.18	1.56	24.5
36	9.3	-1.75	-2.84	1.67	25.2
37	9.5	-0.94	-2.14	1.82	25.9
38	9.8	-1.79	-2.02	1.86	26.6
39	10.0	-1.98	-2.83	2.12	27.3
40	10.3	-1.13	-2.33	2.20	28
41	10.7	-1.82	-1.99	2.09	28.7
42	11.0	-2.40	-2.45	2.29	29.4
43	11.3	-1.39	-2.80	2.47	30.1
44	11.7	-1.64	-1.74	2.68	30.8
45	12.0	-2.18	-3.33	2.22	31.5
46	12.5	-1.70	-2.42	2.34	32.2

—*Solenastrea* 509A S1 Florida—

Sample Number	Age	$\delta^{18}O$	$\delta^{13}C$	density	distance
47	13.0	-2.75	-2.95	2.28	32.9
48	13.3	-2.24	-2.82	1.90	33.6
49	13.5	-1.57	-2.20	2.21	34.3
50	13.8	-2.15	-2.35	1.94	35
51	14.0	-2.87	-3.02	1.91	35.7
52	14.3	-1.73	-3.36	2.13	36.4
53	14.7	-1.84	-2.16	1.99	37.1
54	15.0	-2.53	-2.11	2.09	37.8
55	15.3	-2.18	-2.74	2.21	38.5
56	15.5	-1.31	-2.30	2.18	39.2
57	15.8	-2.17	-1.66	2.27	39.9
58	16.0	-2.84	-2.27	2.16	40.6
59	16.3	-1.93	-3.22	1.92	41.3
60	16.5	-1.34	-1.87	2.00	42
61	16.8	-2.16	-1.72	2.22	42.7
62	17.0	-2.32	-2.90	1.75	43.4
63	17.3	-1.60	-2.95	1.57	44.1
64	17.7	-1.78	-2.06	1.67	44.8
65	18.0	-2.50	-2.21	1.74	45.5
66	18.3	-2.30	-2.74	1.77	46.2
67	18.5	-1.44	-3.02	1.64	46.9
68	18.8	-2.13	-1.94	1.54	47.6
69	19.0	-2.69	-2.18	1.48	48.3
70	19.2	-2.68	-2.09	1.35	49
71	19.4	-1.64	-2.96	1.43	49.7
72	19.6	-1.68	-1.83	1.44	50.4
73	19.8	-1.96	-1.77	1.41	51.1
74	20.0	-2.39	-2.40	1.57	51.8
75	20.3	-1.88	-2.81	1.63	52.5
76	20.5	-1.73	-1.89	1.51	53.2
77	20.8	-2.70	-2.04	1.51	53.9
78	21.0	-2.78	-2.59	1.45	54.6
79	21.3	-1.50	-2.13	1.52	55.3
80	21.7	-2.38	-1.83	1.52	56
81	22.0	-3.13	-2.08	1.63	56.7
82	22.3	-2.52	-2.74	1.87	57.4
83	22.7	-1.88	-1.66	1.88	58.1
84	23.0	-2.82	-2.13	1.70	58.8
85	23.3	-2.18	-2.69	1.87	59.5
86	23.5	-1.50	-1.68	1.71	60.2
87	23.8	-2.03	-2.07	1.82	60.9
88	24.0	-2.58	-2.80	1.97	61.6
89	24.3	-1.51	-2.87	2.03	62.3
90	24.7	-2.01	-2.17	1.95	63
91	25.0	-2.86	-2.83	1.89	63.7
92	25.3	-2.60	-2.54	1.98	64.4
93	25.7	-2.31	-2.17	1.98	65.1
94	26.0	-2.66	-2.42	1.87	65.8

—*Solenastrea* 509A S1 Florida—

Sample Number	Age	$\delta^{18}O$	$\delta^{13}C$	density	distance
95	26.3	-2.56	-3.07	1.70	66.5
96	26.5	-1.86	-2.47	1.65	67.2
97	26.8	-2.54	-2.15	1.58	67.9
98	27.0	-2.61	-2.62	1.66	68.6
99	27.3	-1.12	-2.33	1.65	69.3
100	27.7	-2.18	-2.09	1.75	70
101	28.0	-2.29	-2.81	1.76	70.7
102	28.5	-1.15	-2.15	1.82	71.4
103	29.0	-2.52	-2.77	1.67	72.1
104	29.3	-2.16	-2.60	1.86	72.8
105	29.7	-2.20	-1.73	1.59	73.5
106	30.0	-2.32	-2.65	1.68	74.2
107	30.3	-1.47	-3.03	1.82	
108	30.6	-1.67	-1.78	1.72	74.9
109	31.0	-2.45	-2.04	1.76	75.6
110	31.4	-2.16	-2.42	1.89	76.3
111	31.7	-1.47	-1.62	2.08	77
112	32.0	-1.91	-2.00	1.93	77.7
113	32.5	-1.50	-1.84	1.78	78.4
114	33.0	-2.29	-2.51	1.65	79.1
115	33.5	-1.46	-2.14	1.64	79.8
116	34.0	-2.18	-2.60	1.63	80.5
117	34.5	-1.46	-2.62	1.46	81.2
118	35.0	-2.39	-3.05	1.51	81.9
119	35.5	-0.48	-2.07	1.84	82.6
120	36.0	-2.48	-2.61	2.33	83.3
121	36.3	-2.18	-2.98	2.30	84
122	36.7	-1.91	-2.15	2.25	84.7
123	37.0	-2.06	-2.43	2.17	85.4
124	37.3	-1.84	-1.70	2.21	86.1
125	37.7	-1.61	-2.66	2.59	86.8
126	38.0	-1.97	-1.70	2.61	87.5
127	38.3	-1.54	-2.66	2.37	88.2
128	38.7	-2.21	-2.47	2.18	88.9
129	39.0	-2.45	-2.96	2.32	89.6
130	39.5	-2.47	-2.18	2.23	90.3
131	40.0	-2.63	-2.66	2.08	91
132	40.5	-1.74	-2.47	2.13	91.7
133	41.0	-2.88	-2.85	2.05	92.4
134	41.5	-1.72	-2.30	2.22	93.1
135	42.0	-2.77	-2.63	2.27	93.8
136	42.5	-1.86	-2.58	2.51	94.5
137	43.0	-2.70	-2.31	2.18	95.2
138	43.5	-1.68	-2.73	2.41	95.9
139	44.0	-2.50	-2.74	2.27	96.6
140	44.5	-1.91	-2.76	2.21	97.3
141	45.0	-2.56	-2.09	1.72	98
142	45.3	-2.11	-3.08	1.91	98.7

—*Solenastrea* 509A S1 Florida—

Sample Number	Age	$\delta^{18}O$	$\delta^{13}C$	density	distance
143	45.7	-2.19	-2.27	1.81	99.4
144	46.0	-2.71	-3.04	2.09	100.1
145	46.5	-1.91	-2.40	1.73	100.8
146	47.0	-2.98	-2.96	1.86	101.5
147	47.5	-1.83	-2.79	1.99	102.2
148	48.0	-2.54	-2.72	2.06	102.9
149	48.5	-1.98	-3.01	1.98	103.6
150	49.0	-2.79	-2.77	1.90	104.3
151	49.3	-1.48	-2.65	1.96	105
152	49.7	-2.07	-2.81	1.96	105.7
153	50.0	-2.18	-3.44	1.72	106.4
154	50.5	-1.74	-3.04	1.58	107.1
155	51.0	-2.96	-3.25	1.73	107.8
156	51.3	-2.10	-3.29	1.66	108.5
157	51.7	-2.18	-2.66	1.60	109.2
158	52.0	-2.76	-2.98	1.60	109.9
159	52.3	-1.83	-2.77	1.53	110.6
160	52.7	-2.08	-2.21	1.46	111.3
161	53.0	-2.65	-2.88	1.45	112
162	53.3	-1.19	-2.27	1.54	112.7
163	53.7	-2.14	-2.21	1.81	113.4
164	54.0	-2.30	-3.50	1.44	114.1
165	54.3	-1.49	-2.59	1.52	114.8
166	54.7	-2.49	-2.53	1.41	115.5
167	55.0	-2.70	-3.12	1.36	116.2
168	55.3	-1.85	-2.92	1.41	116.9
169	55.7	-2.21	-2.24	1.51	117.6
170	56.0	-2.24	-2.90	1.49	118.3
171	56.3	-0.95	-3.28	1.43	119
172	56.7	-1.87	-2.82	1.43	119.7
173	57.0	-3.04	-3.00	1.55	120.4
174	57.3	-1.93	-2.98	1.61	121.1
175	57.7	-1.50	-1.96	1.52	121.8
176	58.0	-2.48	-2.60	1.35	122.5
177	58.3	-1.49	-3.12	1.53	123.2
178	58.7	-1.76	-2.19	1.68	123.9
179	59.0	-2.32	-2.42	1.88	124.6
180	59.5	-1.93	-2.42	1.98	125.3
181	60.0	-2.38	-2.78	1.75	126
182	60.5	-1.57	-2.70	1.77	126.7
183	61.0	-2.43	-2.44	1.75	127.4
184	61.5	-1.82	-2.77	1.86	128.1
185	62.0	-2.52	-2.72	1.92	128.8
186	62.3	-2.42	-2.71	1.18	129.5

—*Solenastrea* 509A S1 Florida—

Appendix A3 Stable isotope data 455C Transect A

Sample Number	Age [ <i>yrs</i> ]	$\delta^{18}O$ [‰] vs. VPDB	$\delta^{13}C$ [‰] vs. VPDB	density [ <i>g/cm</i> <sup>3</sup> ]	distance [ <i>mm</i> ]
1	0.0	-4.33	-1.57	0.67	0
2	0.1	-3.75	-1.36	0.84	0.5
3	0.3	-3.87	-1.27	0.95	1
4	0.4	-4.10	-1.34	1.15	1.5
5	0.6	-4.07	-0.82	1.07	2
6	0.7	-4.19	-1.20	1.06	2.5
7	0.9	-4.11	-1.72	0.72	3
8	1.0	-3.86	-1.50	0.70	3.5
9	1.3	-3.95	-1.60	0.90	4
10	1.7	-3.96	-1.57	0.94	4.5
11	2.0	-3.80	-1.33	0.99	5
12	2.1	-3.94	-1.57	0.94	5.5
13	2.3	-3.81	-1.56	0.80	6
14	2.4	-4.18	-1.26	0.53	6.5
15	2.6	-4.15	-1.60	0.80	7
16	2.7	-3.82	-1.39	0.55	7.5
17	2.9	-3.83	-1.68	0.62	8
18	3.0	-3.86	-2.09	0.40	8.5
19	3.1	-3.77	-1.87	0.32	9
20	3.3	-3.71	-1.55	0.27	9.5
21	3.4	-3.75	-1.51	0.76	10
22	3.5	-3.62	-1.61	0.97	10.5
23	3.6	-4.28	-1.52	1.23	11
24	3.8	-3.82	-1.41	1.18	11.5
25	3.9	-3.83	-1.87	0.79	12
26	4.0	-3.87	-1.36	0.67	12.5
27	4.2	-4.23	-1.58	0.71	13
28	4.3	-4.13	-2.05	0.63	13.5
29	4.5	-3.68	-1.61	0.80	14
30	4.7	-3.79	-1.83	1.03	14.5
31	4.8	-3.71	-1.68	1.06	15
32	5.0	-3.65	-1.72	0.88	15.5
33	5.2	-3.71	-1.38	0.83	16
34	5.4	-3.64	-1.43	0.90	16.5
35	5.6	-3.50	-1.40	1.01	17
36	5.8	-3.61	-1.41	0.73	17.5
37	6.0	-3.84	-1.85	0.82	18
38	6.1	-3.67	-1.97	0.76	18.5
39	6.3	-3.62	-1.68	0.79	19
40	6.4	-3.87	-1.71	0.88	19.5
41	6.6	-3.86	-1.50	0.86	20
42	6.7	-3.77	-1.48	0.88	20.5
43	6.9	-4.00	-1.76	0.73	21
44	7.0	-3.71	-1.48	0.78	21.5
45	7.2	-3.75	-1.63	0.76	22
46	7.4	-3.70	-1.84	0.97	22.5

—*Montastrea* 455C Transect A Dominican Republic—

Sample Number	Age	$\delta^{18}O$	$\delta^{13}C$	density	distance
47	7.6	-5.12	-1.75	0.84	23
48	7.8	-3.99	-1.59	0.80	23.5
49	8.0	-3.95	-2.11	0.53	24
50	8.1	-4.27	-2.30	0.39	24.5
51	8.3	-4.44	-2.00	0.39	25
52	8.4	-4.11	-1.63	0.56	25.5
53	8.6	-3.87	-1.51	0.63	26
54	8.7	-4.19	-1.96	0.58	26.5
55	8.9	-4.12	-1.96	0.46	27
56	9.0	-4.14	-1.76	0.49	27.5
57	9.1	-4.09	-2.07	0.49	28
58	9.3	-4.28	-1.93	0.44	28.5
59	9.4	-4.11	-2.67	0.60	29
60	9.5	-4.06	-2.53	0.59	29.5
61	9.6	-4.07	-2.20	0.60	30
62	9.8	-4.03	-2.20	0.67	30.5
63	9.9	-3.96	-2.28	0.64	31
64	10.0	-4.13	-2.28	0.58	31.5
65	10.2	-3.83	-2.10	0.56	32
66	10.3	-4.47	-2.32	0.61	32.5
67	10.5	-4.02	-2.00	0.67	33
68	10.7	-4.00	-1.37	0.62	33.5
69	10.8	-4.04	-1.43	0.55	34
70	11.0	-3.87	-1.08	0.45	34.5
71	11.1	-3.48	-2.18	0.33	35
72	11.1	-3.89	-1.97	0.51	35.5
73	11.2	-3.90	-1.58	0.44	36
74	11.3	-3.95	-1.44	0.38	36.5
75	11.4	-3.76	-1.67	0.44	37
76	11.4	-3.61	-1.63	0.61	37.5
77	11.5	-3.63	-1.96	0.45	38
78	11.6	-3.49	-2.23	0.45	38.5
79	11.6	-4.00	-2.52	0.45	39
80	11.7	-3.84	-1.80	0.60	39.5
81	11.8	-3.38	-1.87	0.59	40
82	11.9	-3.33	-1.56	0.79	40.5
83	11.9	-3.33	-1.38	0.89	41
84	12.0	-3.68	-1.41	0.95	41.5
85	12.3	-3.70	-1.35	0.90	42
86	12.5	-4.28	-1.41	0.83	42.5
87	12.8	-3.90	-1.54	0.91	43
88	13.0	-3.40	-1.64	1.01	43.5
89	13.1	-3.42	-1.80	0.84	44
90	13.2	-3.61	-1.58	0.83	44.5
91	13.3	-3.48	-1.71	1.17	45
92	13.3	-4.09	-1.61	1.33	45.5
93	13.4	-3.77	-2.01	1.30	46
94	13.5	-3.80	-1.41	0.90	46.5

—*Montastrea* 455C Transect A Dominican Republic—

Sample Number	Age	$\delta^{18}O$	$\delta^{13}C$	density	distance
95	13.6	-3.77	-1.87	0.69	47
96	13.7	-3.46	-1.65	0.61	47.5
97	13.8	-3.79	-1.38	0.61	48
98	13.8	-4.18	-1.45	0.62	48.5
99	13.9	-3.79	-1.58	0.61	49
100	14.0	-3.89	-1.73	0.63	49.5
101	14.3	-3.24	-1.54	0.65	50
102	14.7	-3.49	-1.26	0.66	50.5
103	15.0	-3.43	-1.96	0.80	51
104	15.1	-3.45	-1.68	0.86	51.5
105	15.2	-3.27	-1.92	0.81	52
106	15.3	-3.17	-1.91	0.81	52.5
107	15.4	-3.51	-2.55	0.85	53
108	15.6	-3.39	-2.55	0.83	53.5
109	15.7	-3.53	-2.21	0.68	54
110	15.8	-3.29	-1.91	0.48	54.5
111	15.9	-3.56	-2.44	0.68	55
112	16.0	-3.47	-2.71	0.76	55.5
113	16.2	-3.43	-2.19	1.06	56
114	16.4	-3.31	-1.70	1.06	56.5
115	16.6	-3.27	-1.70	1.31	57
116	16.8	-3.30	-1.63	0.97	57.5
117	17.0	-3.35	-1.94	0.94	58
118	17.1	-3.51	-1.87	0.82	58.5
119	17.3	-3.53	-1.93	0.81	59
120	17.4	-2.94	-1.66	1.14	59.5
121	17.5	-3.23	-1.45	0.90	60
122	17.6	-3.29	-1.63	0.85	60.5
123	17.8	-3.55	-2.38	0.83	61
124	17.9	-3.39	-2.45	0.95	61.5
125	18.0			1.01	62
126	18.1			0.94	62.5
127	18.2	-3.73	-2.87	0.88	63
128	18.3			0.92	63.5
129	18.4			0.79	64
130	18.6	-3.70	-1.97	0.83	64.5
131	18.7	-3.77	-1.80	0.76	65
132	18.8	-3.78	-1.35	0.71	65.5
133	18.9	-4.04	-1.27	0.65	66
134	19.0	-4.17	-1.36	0.55	66.5
135	19.1	-4.23	-1.75	0.50	67
136	19.2	-4.19	-2.01	0.50	67.5
137	19.3	-4.14	-2.50	0.56	68
138	19.4	-3.91	-2.22	0.60	68.5
139	19.5	-3.98	-2.23	0.68	69
140	19.6	-4.07	-2.25	0.73	69.5
141	19.7			0.71	70
142	19.8	-3.99	-1.74	0.72	70.5

—*Montastrea* 455C Transect A Dominican Republic—



Sample Number	Age	$\delta^{18}O$	$\delta^{13}C$	density	distance
143	19.9	-4.04	-1.40	0.75	71
144	20.0	-3.89	-1.37	0.75	71.5
145	20.1	-3.97	-1.51	0.76	72
146	20.1	-3.75	-1.47	0.95	72.5
147	20.2	-3.84	-1.85	0.83	73
148	20.3	-3.87	-1.29	0.68	73.5
149	20.4	-4.02	-1.61	0.93	74
150	20.4	-4.05	-1.70	0.86	74.5
151	20.5	-3.84	-1.51	0.94	75
152	20.6	-3.98	-1.93	0.97	75.5
153	20.6	-3.99	-1.71	0.89	76
154	20.7	-4.05	-1.52	1.04	76.5
155	20.8	-3.89	-1.35	1.32	77
156	20.9	-3.83	-0.99	1.14	77.5
157	20.9	-3.98	-1.70	0.98	78
158	21.0	-3.94	-1.87	0.95	78.5
159	21.2	-3.85	-1.44	0.88	79
160	21.4	-3.79	-1.31	0.86	79.5
161	21.6	-3.82	-1.12	0.77	80
162	21.8	-3.69	-1.36	0.67	80.5
163	22.0	-3.43	-1.57	0.74	81
164	22.1	-3.49	-0.95	0.91	81.5
165	22.3	-3.74	-1.01	0.81	82
166	22.4	-3.55	-0.94	0.99	82.5
167	22.6	-3.54	-1.14	0.67	83
168	22.7	-3.63	-1.28	1.06	83.5
169	22.9	-3.46	-1.06	1.24	84
170	23.0	-3.39	-0.76	1.26	84.5
171	23.1	-3.49	-0.71	1.12	85
172	23.3	-3.53	-0.51	1.43	85.5
173	23.4	-3.73	-0.80	1.32	86
174	23.5	-3.90	-1.19	1.22	86.5
175	23.6			1.57	87
176	23.8	-3.93	-1.75	1.80	87.5
177	23.9	-4.07	-1.33	1.21	88
178	24.0	-3.71	-1.05	1.36	88.5
179	24.2	-3.31	-0.27	2.09	89
180	24.3	-3.57	-0.10	2.42	89.5
181	24.5	-3.57	-0.51	2.03	90
182	24.7	-3.56	0.05	1.55	90.5
183	24.8	-3.34	0.32	1.86	91
184	25.0	-3.39	0.16	2.28	91.5
185	25.3	-3.33	-0.16	1.86	92
186	25.5	-3.60	-0.23	1.88	92.5
187	25.8	-3.47	-0.01	1.64	93
188	26.0	-3.74	-0.87	1.58	93.5
189	26.2	-3.70	-0.62	1.89	94
190	26.4	-3.91	-1.00	1.56	94.5

—*Montastrea* 455C Transect A Dominican Republic—

Sample Number	Age	$\delta^{18}O$	$\delta^{13}C$	density	distance
191	26.6	-3.89	-1.37	1.11	95
192	26.8	-3.98	-1.24	1.18	95.5
193	27.0	-3.72	-0.58	1.50	96
194	27.3	-3.75	-0.88	1.27	96.5
195	27.5	-3.34	-0.73	0.88	97
196	27.8	-3.81	-0.76	0.95	97.5
197	28.0	-3.67	-0.45	1.27	98
198	28.2	-3.39	-0.39	1.15	98.5
199	28.3	-3.62	-1.14	0.91	99
200	28.5	-3.65	-1.10	1.23	99.5
201	28.7	-3.54	-1.72	1.66	100
202	28.8	-3.78	-1.95	1.00	100.5
203	29.0	-3.67	-1.73	1.19	101
204	29.1	-3.47	-0.91	1.10	101.5
205	29.2	-3.55	-1.25	0.90	102
206	29.3	-3.71	-1.83	0.84	102.5
207	29.4	-3.54	-1.57	1.16	103
208	29.5	-3.69	-1.08	1.18	103.5
209	29.6	-3.76	-1.40	1.11	104
210	29.7	-3.61	-1.28	1.84	104.5
211	29.8	-3.67	-1.30	1.55	105
212	29.9	-3.38	-0.83	1.20	105.5
213	30.0	-3.62	-1.55	1.13	106
214	30.3	-3.44	-1.27	0.88	106.5
215	30.5	-3.45	-0.93	0.80	107
216	30.8	-3.21	-0.28	0.99	107.5
217	31.0	-3.26	-0.77	0.93	108
218	31.3	-3.31	-0.38	0.99	108.5
219	31.7	-3.57	-1.12	1.25	109
220	32.0	-3.51	-1.45	0.91	109.5
221	32.3	-3.49	-0.57	0.87	110
222	32.5	-3.37	-0.63	1.00	110.5
223	32.8	-3.72	-1.25	0.83	111
224	33.0	-3.63	-0.74	0.82	111.5
225	33.3	-3.53	-0.42	1.12	112
226	33.7	-3.56	-0.67	1.23	112.5
227	34.0	-3.70	-1.08	1.22	113
228	34.1	-3.75	-1.24	1.17	113.5
229	34.2	-3.62	-1.14	1.05	114
230	34.3	-3.65	-0.78	1.49	114.5
231	34.3	-3.59	-0.90	1.17	115
232	34.4	-3.70	-1.37	1.09	115.5
233	34.5	-3.64	-1.17	1.22	116
234	34.6	-3.58	-0.77	1.55	116.5
235	34.7	-3.66	-1.25	1.44	117
236	34.8	-3.62	-1.18	1.52	117.5
237	34.8	-3.57	-1.12	1.69	118
238	34.9	-3.41	-0.39	2.00	118.5

—*Montastrea* 455C Transect A Dominican Republic—

Sample Number	Age	$\delta^{18}O$	$\delta^{13}C$	density	distance
239	35.0	-3.57	-0.85	1.78	119
240	35.1	-3.87	-0.90	2.08	119.5
241	35.3	-3.75	-0.58	2.12	120
242	35.4	-3.61	-1.00	2.07	120.5
243	35.5	-3.55	-1.03	1.99	121
244	35.6	-3.49	-0.38	2.04	121.5
245	35.8	-3.47	-0.03	1.77	122
246	35.9	-3.27	-0.33	1.64	122.5
247	36.0	-3.43	-0.92	1.56	123
248	36.2	-3.53	-0.84	2.10	123.5
249	36.4	-3.52	-1.08	1.61	124
250	36.6	-3.53	-0.85	2.11	124.5
251	36.8	-3.74	-0.88	1.99	125
252	37.0	-3.67	-1.15	1.53	125.5
253	37.3	-3.62	-1.21	1.46	126
254	37.7	-3.49	-0.96	1.11	126.5
255	38.0	-3.36	-0.66	1.02	127
256	38.1	-3.31	-0.67	0.97	127.5
257	38.3	-3.55	-0.84	1.13	128
258	38.4	-3.44	-1.18	0.98	128.5
259	38.5	-3.56	-0.87	1.06	129
260	38.6	-3.42	-1.16	0.95	129.5
261	38.8	-3.61	-1.46	1.02	130
262	38.9	-3.41	-0.64	0.91	130.5
263	39.0	-3.60	-1.26	0.94	131
264	39.2	-3.72	-1.37	0.93	131.5
265	39.4	-3.53	-0.89	1.06	132
266	39.6	-3.68	-1.14	1.01	132.5
267	39.8	-3.69	-1.55	0.87	133
268	40.0	-3.85	-1.42	1.11	133.5
269	40.3	-3.89	-1.49	1.07	134
270	40.5	-3.81	-1.31	0.93	134.5
271	40.8	-3.75	-2.00	0.88	135
272	41.0	-3.63	-1.49	0.81	135.5
273	41.1	-3.67	-1.66	1.07	136
274	41.2	-3.62	-1.70	1.04	136.5
275	41.3	-3.66	-2.03	1.36	137
276	41.4	-3.75	-1.52	1.13	137.5
277	41.6	-3.53	-1.13	1.24	138
278	41.7	-3.69	-1.16	1.35	138.5
279	41.8	-3.62	-1.34	1.28	139
280	41.9	-3.63	-1.21	1.37	139.5
281	42.0	-3.61	-1.14	1.23	140
282	42.1	-3.42	-1.30	1.19	140.5
283	42.2	-3.45	-1.14	1.30	141
284	42.3	-3.45	-0.68	1.11	141.5
285	42.4	-3.63	-1.23	1.27	142
286	42.5	-3.73	-1.19	1.19	142.5

—*Montastrea* 455C Transect A Dominican Republic—

Sample Number	Age	$\delta^{18}O$	$\delta^{13}C$	density	distance
287	42.6	-3.45	-0.79	1.06	143
288	42.7	-3.49	-0.64	1.12	143.5
289	42.8	-3.36	-1.08	1.06	144
290	42.9	-3.36	-0.60	1.09	144.5
291	43.0	-3.24	-0.58	1.04	145
292	43.1	-3.28	-1.22	1.08	145.5
— <i>Montastrea</i> 455C S2 Transect A Dominican Republic—					

Stable isotope data 455C Transect C

Sample Number	$\delta^{18}O$ [‰] vs. VPDB	$\delta^{13}C$ [‰] vs. VPDB	density [g/cm <sup>3</sup> ]	distance [mm]
1	-4.60	-2.45	0.87	0
2	-3.66	-2.86	0.78	0.5
3	-4.39	-3.20	0.94	1
4	-3.65	-2.70	0.79	1.5
5	-3.54	-2.16	0.99	2
6	-3.59	-1.55	0.69	2.5
7	-4.03	-1.07	0.67	3
8	-3.75	-1.48	0.90	3.5
9	-3.87	-2.26	0.86	4
10	-3.88	-2.38	0.85	4.5
11	-3.55	-2.09	0.70	5
12	-3.58	-1.72	0.70	5.5
13	-3.26	-0.67	1.15	6
14	-3.37	-1.14	1.04	6.5
15	-3.19	-1.02	1.05	7
16	-3.00	-0.59	1.19	7.5
17	-3.26	-0.99	1.02	8
18	-3.53	-1.25	1.19	8.5
19	-3.06	-0.22	0.87	9
20	-3.24	-0.84	1.30	9.5
21	-3.21	-0.73	0.97	10
22	-3.39	-0.54	1.14	10.5
23	-3.02	-0.52	1.97	11
24	-3.35	-1.23	1.76	11.5
25	-3.01	-0.35	1.31	12
26	-3.62	-0.47	1.58	12.5
27	-3.19	-1.02	1.28	13
28	-3.03	-0.67	1.76	13.5
29	-3.70	-0.62	1.63	14
30	-3.30	-0.62	1.63	14.5
31	-2.77	0.09	1.69	15
32	-2.95	-0.17	1.73	15.5
33	-3.07	-0.14	1.49	16
34	-3.07	-0.35	1.11	16.5
35	-3.18	-0.39	1.22	17
36	-2.87	0.22	1.08	17.5
37	-3.11	0.04	1.40	18
— <i>Montastrea</i> 455C Transect C Dominican Republic—				

Sample Number	$\delta^{18}O$	$\delta^{13}C$	density	distance
38	-2.84	0.33	1.27	18.5
39	-2.75	0.20	1.19	19
40	-2.93	0.13	1.30	19.5
41	-2.95	-0.55	1.39	20
42	-2.78	-0.13	1.70	20.5
43	-2.61	-0.11	1.52	21
44	-2.83	-0.17	1.47	21.5
45	-2.95	-0.08	1.23	22
46	-2.97	-0.12	1.10	22.5
47	-2.63	-0.03	1.12	23
48	-2.62	-0.22	1.72	23.5
49	-2.69	-0.36	2.34	24
50	-2.98	-0.05	2.11	24.5
51	-2.58	0.08	1.65	25
52	-2.55	-0.21	1.98	25.5
53	-2.70	-0.42	1.87	26
54	-3.18	-2.07	2.24	26.5
55	-2.80	-1.32	1.86	27
56	-3.09	-1.69	2.14	27.5
57	-3.07	-1.17	2.20	28
58	-2.34	-0.20	2.00	28.5
59	-2.64	-0.95	2.09	29
60	-3.02	-1.31	1.79	29.5
— <i>Montastrea</i> 455C Transect C Dominican Republic—				

Appendix A4 Stable isotope data 464C S2

Sample Number	Age [yrs]	$\delta^{18}O$ [‰] vs. VPDB	$\delta^{13}C$ [‰] vs. VPDB	density [g/cm <sup>3</sup> ]	distance [mm]
1	0.5	-3.01	-1.87	3.51	0
2	0.8	-2.92	-2.73	2.76	0.7
3	1.0	-2.65	-1.89	1.06	1.4
4	1.2	-2.84	-1.59	1.16	2.1
5	1.4	-3.08	-1.98	1.27	2.8
6	1.6	-3.16	-1.92	1.25	3.5
7	1.8	-2.91	-1.50	1.25	4.2
8	2.0	-2.76	-0.46	1.29	4.9
9	2.3	-2.81	-0.52	1.33	5.6
10	2.5	-3.06	-0.72	1.33	6.3
11	2.8	-3.17	-1.32	1.34	7
12	3.0	-2.77	-1.10	1.33	7.7
13	3.2	-2.86	-0.60	1.35	8.4
14	3.4	-2.90	-0.50	1.40	9.1
15	3.6	-3.06	-0.76	1.43	9.8
16	3.8	-3.12	-1.73	1.37	10.5
17	4.0	-2.70	-1.05	1.32	11.2
18	4.1	-2.82	-1.01	1.33	11.9
19	4.3	-2.80	-0.35	1.32	12.6
20	4.4	-3.04	-0.86	1.35	13.3
21	4.6	-3.12	-1.39	1.33	14
22	4.7	-3.12	-1.70	1.32	14.7
23	4.9	-2.91	-1.11	1.39	15.4
24	5.0	-2.88	-0.49	1.45	16.1
25	5.3	-3.01	-0.53	1.49	16.8
26	5.5	-3.21	-1.18	1.40	17.5
27	5.8	-3.19	-2.00	1.33	18.2
28	6.0	-2.87	-1.49	1.37	18.9
29	6.2	-2.87	-1.04	1.41	19.6
30	6.4	-3.00	-0.91	1.37	20.3
31	6.6	-3.12	-1.07	1.38	21
32	6.8	-3.11	-0.79	1.35	21.7
33	7.0	-2.92	-1.30	1.34	22.4
34	7.1	-2.92	-0.90	1.37	23.1
35	7.3	-3.00	-0.59	1.40	23.8
36	7.4	-3.10	-0.84	1.33	24.5
37	7.6	-3.36	-1.94	1.27	25.2
38	7.7	-3.22	-1.95	1.23	25.9
39	7.9	-2.92	-1.46	1.30	26.6
40	8.0	-2.71	-0.55	1.27	27.3
41	8.1	-2.76	-0.53	1.28	28
42	8.3	-3.04	-0.71	1.36	28.7
43	8.4	-3.17	-0.93	1.25	29.4
44	8.6	-3.18	-1.17	1.25	30.1
45	8.7	-3.14	-1.56	1.31	30.8
46	8.9	-3.12	-0.69	1.41	31.5

—*Stephanocoenia* 464C S2 Dominican Republic—

Sample Number	Age	$\delta^{18}O$	$\delta^{13}C$	density	distance
47	9.0	-3.08	-0.44	1.37	32.2
48	9.2	-3.09	-0.74	1.36	32.9
49	9.4	-3.21	-1.07	1.37	33.6
50	9.6	-3.37	-1.50	1.36	34.3
51	9.8	-3.05	-1.50	1.32	35
52	10.0	-2.96	-0.93	1.30	35.7
53	10.1	-3.08	-0.67	1.29	36.4
54	10.3	-3.11	-0.99	1.28	37.1
55	10.4	-3.26	-1.26	1.25	37.8
56	10.6	-3.26	-1.83	1.32	38.5
57	10.7	-3.05	-1.44	1.28	39.2
58	10.9	-2.97	-0.43	1.28	39.9
59	11.0	-2.95	-0.28	1.40	40.6
60	11.3	-3.12	-0.74	1.29	41.3
61	11.5	-3.27	-1.59	1.31	42
62	11.8	-3.01	-1.32	1.28	42.7
63	12.0	-2.94	-1.02	1.19	43.4
64	12.1	-2.99	-0.88	1.19	44.1
65	12.2	-3.03	-0.12	1.18	44.8
66	12.3	-3.02	-0.35	1.19	45.5
67	12.4	-3.25	-0.98	1.21	46.2
68	12.6	-3.24	-1.46	1.20	46.9
69	12.7	-3.30	-1.77	1.23	47.6
70	12.8	-3.13	-1.65	1.27	48.3
71	12.9	-3.10	-0.71	1.22	49
72	13.0	-2.90	-0.17	1.25	49.7
73	13.3	-3.06	-0.38	1.25	50.4
74	13.5	-3.16	-1.06	1.15	51.1
75	13.8	-3.17	-1.37	1.19	51.8
76	14.0	-2.47	-0.21	1.19	52.5
77	14.1	-2.88	-1.00	1.21	53.2
78	14.3	-2.90	-0.36	1.27	53.9
79	14.4	-3.05	-0.41	1.23	54.6
80	14.6	-3.14	-0.67	1.19	55.3
81	14.7	-3.10	-1.58	1.24	56
82	14.9	-2.90	-1.27	1.25	56.7
83	15.0	-2.83	-0.50	1.28	57.4
84	15.1	-3.01	-0.37	1.29	58.1
85	15.3	-3.10	-0.95	1.22	58.8
86	15.4	-3.35	-1.48	1.20	59.5
87	15.5	-3.25	-1.41	1.16	60.2
88	15.6	-3.01	-1.05	1.24	60.9
89	15.8	-2.84	-0.81	1.26	61.6
90	15.9	-3.00	-0.27	1.20	62.3
91	16.0	-2.63	0.05	1.24	63
92	16.2	-3.05	-0.50	1.27	63.7
93	16.4	-3.11	-0.83	1.29	64.4
94	16.6	-3.18	-1.17	1.27	65.1

—*Stephanocoenia* 464C S2 Dominican Republic—

Sample Number	Age	$\delta^{18}O$	$\delta^{13}C$	density	distance
95	16.8	-3.04	-1.60	1.26	65.8
96	17.0	-2.93	-0.43	1.31	66.5
97	17.1			1.34	67.2
98	17.3	-3.31	-0.86	1.36	67.9
99	17.4	-3.27	-1.23	1.30	68.6
100	17.6	-3.27	-1.68	1.33	69.3
101	17.7	-3.03	-0.87	1.33	70
102	17.9	-3.03	-0.58	1.30	70.7
103	18.0	-2.83	-0.58	1.31	71.4
104	18.3	-3.26	-0.92	1.28	72.1
105	18.5	-3.44	-1.78	1.33	72.8
106	18.8	-3.10	-1.43	1.36	73.5
107	19.0	-2.83	-0.28	1.39	74.2
108	19.3	-3.16	-0.59	1.45	74.9
109	19.5	-3.08	-0.66	1.52	75.6
110	19.8	-3.48	-1.40	1.61	76.3
111	20.0	-3.12	-1.27	1.77	77
112	20.1	-3.17	-0.89	1.94	77.7
113				1.94	78.4

—*Stephanocoenia* 464C S2 Dominican Republic—



Appendix B1 LA-ICP-MS Values *Solenastrea* 452K1 Profile AB

Element	Min	Max	$\sigma$	Median	$1\sigma$	Range
(ppm)						
<sup>85</sup> Rb	0.005	0.045	0.021	0.019	0.007	0.040
<sup>88</sup> Sr	6378	7443	6847	6852	209	1066
<sup>89</sup> Y	0.103	0.329	0.191	0.179	0.053	0.226
<sup>90</sup> Zr	0.092	0.394	0.197	0.179	0.068	0.302
<sup>137</sup> Ba	9.7	29.5	18.0	17.4	4.8	19.7
<sup>139</sup> La	0.005	0.037	0.015	0.013	0.007	0.032
<sup>140</sup> Ce	0.010	0.061	0.026	0.026	0.011	0.052
<sup>141</sup> Pr	0.002	0.012	0.005	0.005	0.002	0.010
<sup>146</sup> Nd	0.002	0.042	0.022	0.021	0.008	0.040
<sup>147</sup> Sm	0.013	0.061	0.029	0.027	0.010	0.048
<sup>151</sup> Eu	0.004	0.021	0.010	0.009	0.003	0.017
<sup>157</sup> Gd	0.007	0.044	0.024	0.022	0.008	0.037
<sup>159</sup> Tb	0.008	0.047	0.020	0.019	0.007	0.040
<sup>163</sup> Dy	0.010	0.051	0.025	0.023	0.009	0.042
<sup>165</sup> Ho	0.006	0.054	0.026	0.025	0.009	0.048
<sup>167</sup> Er	0.003	0.010	0.006	0.005	0.002	0.008
<sup>169</sup> Tm	0.009	0.038	0.018	0.017	0.006	0.029
<sup>173</sup> Yb	0.010	0.029	0.022	0.025	0.006	0.019
<sup>175</sup> Lu						
<sup>208</sup> Pb	0.01	0.60	0.04	0.03	0.06	0.60
<sup>232</sup> Th	0.001	0.027	0.010	0.010	0.006	0.026
<sup>238</sup> U	2.51	7.98	4.56	4.36	1.20	5.47
<sup>63</sup> Cu	0.278	9.277	1.810	1.592	1.205	8.999
<sup>95</sup> Mo	0.008	0.062	0.034	0.033	0.011	0.054
<sup>111</sup> Cd	0.049	0.126	0.084	0.074	0.028	0.076
<sup>66</sup> Zn	0.058	1.322	0.316	0.283	0.206	1.264
<sup>67</sup> Zn	615	1128	890	910	116	514
<sup>11</sup> B	36	57	43	42	5	21
<sup>29</sup> Si	48	459	137	128	57	411
(mmol/mol)						
Mg/Ca	2.6	4.7	3.7	3.8	0.5	2.2
Sr/Ca	7.4	8.7	8.0	8.0	0.2	1.2
B/Ca	0.34	0.54	0.41	0.39	0.04	0.20
Y/Ca	0.00012	0.00038	0.00022	0.00021	0.00006	0.00026
(μmol/mol)						
Ba/Ca	7.2	21.9	13.4	12.9	3.5	14.6
Ce/Ca	0.007	0.045	0.019	0.019	0.008	0.038
La/Ca	0.004	0.027	0.011	0.010	0.005	0.024
Si/Ca	35	337	101	94	42	302
U/Ca	1.1	3.4	2.0	1.9	0.5	2.3
— <i>Solenastrea</i> 452K1 Florida Profile AB—						

LA-ICP-MS Values 452K1 Profile CD

Element	Min	Max	$\emptyset$	Median	$1\sigma$	Range
(ppm)						
<sup>85</sup> Rb	0.006	0.033	0.014	0.011	0.007	0.027
<sup>88</sup> Sr	6280	7247	6725	6727	275	966
<sup>89</sup> Y	0.131	0.341	0.196	0.184	0.056	0.211
<sup>90</sup> Zr	0.095	0.324	0.183	0.172	0.066	0.229
<sup>137</sup> Ba	9.7	23.1	14.5	13.5	3.1	13.4
<sup>139</sup> La	0.009	0.042	0.019	0.017	0.008	0.033
<sup>140</sup> Ce	0.014	0.073	0.031	0.028	0.013	0.060
<sup>141</sup> Pr	0.003	0.011	0.006	0.005	0.002	0.008
<sup>146</sup> Nd	0.012	0.060	0.027	0.025	0.010	0.048
<sup>147</sup> Sm	0.014	0.085	0.034	0.032	0.015	0.071
<sup>151</sup> Eu	0.007	0.024	0.012	0.011	0.004	0.016
<sup>157</sup> Gd	0.013	0.040	0.022	0.020	0.007	0.027
<sup>159</sup> Tb	0.008	0.042	0.020	0.018	0.008	0.034
<sup>163</sup> Dy	0.009	0.050	0.024	0.021	0.010	0.040
<sup>165</sup> Ho	0.007	0.045	0.024	0.023	0.009	0.038
<sup>167</sup> Er	0.003	0.012	0.005	0.005	0.002	0.009
<sup>169</sup> Tm	0.015	0.029	0.023	0.022	0.005	0.014
<sup>173</sup> Yb						
<sup>175</sup> Lu						
<sup>208</sup> Pb	0.01	3.70	0.16	0.04	0.67	3.68
<sup>232</sup> Th	0.004	0.022	0.010	0.008	0.005	0.018
<sup>238</sup> U	2.36	6.15	3.73	3.74	0.83	3.79
<sup>63</sup> Cu	0.457	2.675	1.018	0.807	0.563	2.218
<sup>95</sup> Mo	0.018	0.055	0.031	0.031	0.008	0.037
<sup>111</sup> Cd						
<sup>66</sup> Zn	0.112	1.685	0.827	0.760	0.507	1.574
<sup>25</sup> Mg	643	1114	875	860	133	472
<sup>11</sup> B	36	52	44	43	5	16
<sup>29</sup> Si	37	134	74	74	23	97
(mmol/mol)						
Mg/Ca	2.7	4.7	3.7	3.6	0.6	2.0
Sr/Ca	7.3	8.4	7.8	7.8	0.3	1.1
B/Ca	0.34	0.49	0.42	0.41	0.04	0.15
Y/Ca	0.00015	0.00039	0.00022	0.00021	0.00006	0.00024
(μmol/mol)						
Ba/Ca	7.2	17.1	10.7	10.1	2.3	9.9
Ce/Ca	0.010	0.053	0.023	0.021	0.010	0.043
La/Ca	0.007	0.031	0.014	0.012	0.006	0.024
Si/Ca	27	98	54	54	17	71
U/Ca	1.0	2.6	1.6	1.6	0.4	1.6
— <i>Solenastrea</i> 452K1 Florida Profile CD—						

LA-ICP-MS Values 452K1 Profile EF

Element	Min	Max	$\emptyset$	Median	$1\sigma$	Range
(ppm)						
<sup>85</sup> Rb	0.009	0.068	0.023	0.019	0.012	0.059
— <i>Solenastrea</i> 452K1 Florida Profile EF—						

Element	Min	Max	$\emptyset$	Median	$1\sigma$	Range
<sup>88</sup> Sr	6437	7491	6834	6806	228	1054
<sup>89</sup> Y	0.118	0.422	0.237	0.239	0.062	0.303
<sup>90</sup> Zr	0.107	0.447	0.221	0.220	0.069	0.341
<sup>137</sup> Ba	9.5	27.1	16.4	16.5	3.5	17.6
<sup>139</sup> La	0.014	0.107	0.041	0.038	0.019	0.092
<sup>140</sup> Ce	0.018	0.121	0.051	0.045	0.026	0.103
<sup>141</sup> Pr	0.004	0.026	0.010	0.009	0.005	0.021
<sup>146</sup> Nd	0.021	0.134	0.054	0.050	0.024	0.114
<sup>147</sup> Sm	0.011	0.067	0.026	0.024	0.011	0.056
<sup>151</sup> Eu	0.002	0.016	0.008	0.007	0.003	0.014
<sup>157</sup> Gd	0.013	0.079	0.037	0.034	0.015	0.065
<sup>159</sup> Tb	0.002	0.011	0.005	0.004	0.002	0.009
<sup>163</sup> Dy	0.009	0.061	0.028	0.026	0.012	0.052
<sup>165</sup> Ho	0.002	0.014	0.006	0.006	0.002	0.011
<sup>167</sup> Er	0.008	0.035	0.018	0.018	0.007	0.028
<sup>169</sup> Tm	0.001	0.005	0.003	0.003	0.001	0.004
<sup>173</sup> Yb	0.008	0.040	0.018	0.017	0.007	0.032
<sup>175</sup> Lu	0.001	0.007	0.003	0.003	0.001	0.006
<sup>208</sup> Pb	0.007	0.294	0.050	0.031	0.052	0.287
<sup>232</sup> Th	0.002	0.034	0.013	0.011	0.008	0.032
<sup>238</sup> U	2.05	7.24	4.20	4.21	1.16	5.19
<sup>63</sup> Cu	0.35	4.25	1.43	1.26	0.80	3.90
<sup>95</sup> Mo	0.10	0.19	0.13	0.12	0.02	0.09
<sup>111</sup> Cd	0.03	0.20	0.07	0.06	0.03	0.17
<sup>66</sup> Zn	0.10	3.83	0.72	0.37	0.77	3.73
<sup>67</sup> Zn	550	1087	778	747	129	537
<sup>11</sup> B	39	60	48	48	5	22
<sup>29</sup> Si	50	227	128	112	38	178
(mmol/mol)						
Sr/Ca	7.49	8.72	7.95	7.92	0.27	1.23
Mg/Ca	2.31	4.56	3.26	3.13	0.54	2.25
B/Ca	0.37	0.57	0.46	0.45	0.05	0.20
(μmol/mol)						
Y/Ca	0.14	0.48	0.27	0.27	0.07	0.35
Ba/Ca	7.06	20.13	12.19	12.25	2.62	13.07
U/Ca	0.88	3.10	1.80	1.80	0.50	2.23
— <i>Solenastrea</i> 452K1 Florida Profile EF—						

LA-ICP-MS Values 452K1 Profile GH

Element	Min	Max	$\emptyset$	Median	$1\sigma$	Range
(ppm)						
<sup>85</sup> Rb	0.008	0.137	0.026	0.022	0.019	0.129
<sup>88</sup> Sr	6399	7406	6844	6841	196	1007
<sup>89</sup> Y	0.140	0.359	0.240	0.243	0.051	0.218
<sup>90</sup> Zr	0.117	0.375	0.219	0.212	0.057	0.258
<sup>137</sup> Ba	9.7	28.8	17.9	17.9	3.6	19.1
<sup>139</sup> La	0.021	0.560	0.153	0.124	0.109	0.539
<sup>140</sup> Ce	0.024	0.805	0.210	0.179	0.154	0.781
— <i>Solenastrea</i> 452K1 Florida Profile GH—						

Element	Min	Max	$\emptyset$	Median	$1\sigma$	Range
<sup>141</sup> Pr	0.006	0.102	0.032	0.029	0.020	0.096
<sup>146</sup> Nd	0.022	0.468	0.155	0.136	0.089	0.447
<sup>147</sup> Sm	0.009	0.112	0.048	0.044	0.020	0.103
<sup>151</sup> Eu	0.004	0.026	0.013	0.013	0.005	0.023
<sup>157</sup> Gd	0.017	0.089	0.046	0.045	0.015	0.072
<sup>159</sup> Tb	0.002	0.011	0.006	0.006	0.002	0.009
<sup>163</sup> Dy	0.012	0.075	0.032	0.032	0.011	0.063
<sup>165</sup> Ho	0.003	0.012	0.007	0.007	0.002	0.009
<sup>167</sup> Er	0.006	0.037	0.019	0.019	0.006	0.032
<sup>169</sup> Tm	0.001	0.006	0.003	0.002	0.001	0.006
<sup>173</sup> Yb	0.008	0.034	0.018	0.018	0.005	0.025
<sup>175</sup> Lu	0.001	0.006	0.003	0.003	0.001	0.005
<sup>208</sup> Pb	0.008	0.595	0.083	0.048	0.095	0.587
<sup>232</sup> Th	0.003	0.055	0.020	0.019	0.010	0.053
<sup>238</sup> U	2.37	8.86	4.96	5.02	1.28	6.50
<sup>63</sup> Cu	0.45	8.53	1.64	1.32	1.21	8.07
<sup>95</sup> Mo	0.10	0.34	0.14	0.13	0.03	0.24
<sup>111</sup> Cd	0.04	0.12	0.07	0.07	0.02	0.09
<sup>66</sup> Zn	0.08	1.09	0.36	0.28	0.24	1.01
<sup>25</sup> Mg	532	1193	849	865	154	661
<sup>11</sup> B	39	63	49	48	5	24
<sup>29</sup> Si	82	422	166	150	64	340
(mmol/mol)						
Sr/Ca	7.45	8.62	7.97	7.96	0.23	1.17
Mg/Ca	2.23	5.01	3.56	3.63	0.65	2.77
B/Ca	0.37	0.59	0.46	0.45	0.05	0.22
(μmol/mol)						
Y/Ca	0.16	0.41	0.28	0.28	0.06	0.25
Ba/Ca	7.23	21.39	13.31	13.27	2.64	14.16
U/Ca	1.01	3.80	2.12	2.15	0.55	2.78
— <i>Solenastrea</i> 452K1 Florida Profile GH—						

LA-ICP-MS Values 452K1 Line measurement

Element	Min	Max	$\emptyset$	Median	$1\sigma$	Range
(mmol/mol)						
Sr/Ca	5.16	12.16	7.85	7.77	1.08	7.00
Mg/Ca	1.08	6.01	2.71	2.67	0.74	4.93
(μmol/mol)						
Y/Ca	0.08	0.86	0.27	0.25	0.12	0.78
Ba/Ca	3.6	39.2	11.6	10.7	4.5	35.6
U/Ca	0.50	5.24	1.57	1.40	0.73	4.73
— <i>Solenastrea</i> 452K1 Florida Line—						

## Appendix B2 LA-ICP-MS Values 464C

Element	Min	Max	$\emptyset$	Median	$1\sigma$	Range
(ppm)						
<sup>85</sup> Rb	0.008	0.122	0.023	0.018	0.016	0.114
<sup>88</sup> Sr	5683	6909	6194	6170	204	1226
<sup>89</sup> Y	0.088	0.181	0.118	0.116	0.017	0.093
<sup>90</sup> Zr	0.055	0.130	0.076	0.074	0.011	0.076
<sup>137</sup> Ba	9.2	16.9	12.6	12.6	1.6	7.7
<sup>139</sup> La	0.026	0.202	0.069	0.063	0.024	0.176
<sup>140</sup> Ce	0.030	0.257	0.095	0.085	0.038	0.227
<sup>141</sup> Pr	0.007	0.038	0.015	0.014	0.005	0.031
<sup>146</sup> Nd	0.024	0.141	0.061	0.057	0.019	0.117
<sup>147</sup> Sm	0.006	0.040	0.017	0.016	0.005	0.034
<sup>151</sup> Eu	0.002	0.009	0.005	0.005	0.001	0.006
<sup>157</sup> Gd	0.007	0.031	0.016	0.016	0.004	0.024
<sup>159</sup> Tb	0.001	0.004	0.002	0.002	0.001	0.003
<sup>163</sup> Dy	0.004	0.020	0.010	0.009	0.003	0.016
<sup>165</sup> Ho	0.001	0.004	0.002	0.002	0.001	0.003
<sup>167</sup> Er	0.003	0.012	0.006	0.006	0.002	0.010
<sup>169</sup> Tm	0.000	0.002	0.001	0.001	0.000	0.002
<sup>173</sup> Yb	0.003	0.012	0.006	0.006	0.002	0.009
<sup>175</sup> Lu	0.000	0.002	0.001	0.001	0.000	0.001
<sup>208</sup> Pb	0.002	0.078	0.011	0.008	0.011	0.076
<sup>232</sup> Th	0.000	0.005	0.001	0.001	0.001	0.005
<sup>238</sup> U	0.87	1.85	1.16	1.14	0.16	0.98
<sup>63</sup> Cu	0.3	137.3	2.6	1.1	11.3	137.0
<sup>95</sup> Mo	0.09	0.21	0.13	0.13	0.02	0.11
<sup>111</sup> Cd	0.04	0.12	0.07	0.07	0.02	0.08
<sup>66</sup> Zn	0.05	3.51	0.50	0.27	0.60	3.46
<sup>67</sup> Zn	510	1356	769	758	111	845
<sup>11</sup> B	31	50	40	39	3	19
<sup>29</sup> Si	90	383	174	160	59	293
(mmol/mol)						
Sr/Ca	6.61	8.04	7.21	7.18	0.24	1.43
Mg/Ca	2.14	5.69	3.22	3.18	0.46	3.55
B/Ca	0.29	0.47	0.37	0.37	0.03	0.18
(μmol/mol)						
Y/Ca	0.10	0.21	0.14	0.13	0.02	0.11
Ba/Ca	6.8	12.5	9.4	9.3	1.2	5.7
U/Ca	0.4	2.8	0.6	0.5	0.3	2.4
— <i>Stephanocoenia</i> 464C Dominican Republic—						